The Role of TASK-3 Two-Pore Domain Potassium Channels in the Entrainment of Mammalian Circadian Rhythms

Lynsey A. Atkinson

Submitted for the degree of Ph.D.

September 2014

Medway School of Pharmacy

Universities of Kent and Greenwich at Medway

Anson Building

Central Avenue

Chatham Maritime

Kent

ME4 4TB

"All we have to decide is what to do with the time that is given us."

J.R.R. Tolkien

Acknowledgements

There are many people who have proven themselves invaluable to me over the past three years and I will thank each of you personally. However, it is customary at this time to acknowledge in words, so here are those special people who have made an enormous difference to my PhD journey:

Gurprit Lall: Your drive and determination is unrelenting, as is your support and patience. You have been both a remarkable supervisor and a trusted friend. Thank you for giving me the opportunity to study in your research group and for always having confidence in my ability. Above all you have shown me that true success is built on hard work and integrity – values I hope to uphold throughout my academic career.

Alistair Mathie: Throughout my PhD I have benefitted from your vast knowledge and experience and feel privileged to have worked under your supervision. Thank you for your continued help and advice and for encouraging me to see the bigger picture.

David Bonsall, Emma Veale, and Helen Leech: What you guys do not know between you is clearly not worth knowing! You have provided tips, advice and technical assistance that will never be found in any books, manuals or blogs. Thank you for everything, especially your honesty and friendship.

Fellow PhD students (past and present): Thanks to all who have shared office space, lab benches, meetings, lunches, and socials – your support and camaraderie has made the long days of research just that little bit easier, and a whole lot more enjoyable. Thanks especially to Danielle Newby and Tracey Yip who have soldiered along with me, sharing the highs, lows, trials and tribulations that constitutes PhD research.

My extensive family: My Dad (Albert), Ruth and Barrie, Alan and Dee, Cheryl and Ian, Kevin and Jenny, Claire, Karen and Richard. Thank you all for taking such an interest in my work whilst also providing quality 'down time' away from it all – your love and affection means a great deal to me. And special thanks to my Mum (Sylvia) who, although unable to share this time, remains an inspiration.

Finally, my wonderful husband and children: Jon, Chloe, Lucy and Matthew. You have been the driving force behind every step of my PhD – the very reason I work to better myself. You praise me when I succeed, hug me when I'm down and make me laugh when (all too often) I take life too seriously. Thank you so much for your endless love, support, and understanding; and also for giving me the time and space in which to pursue my goals. You guys are truly amazing!

Abstract

In mammals light is the principal timing cue for alignment of physiology to the external environment. Illumination from the unrelenting 24-hour day-night cycle enters the biological system and is communicated to the master pacemaker, the suprachiasmatic nucleus (SCN) to drive circadian entrainment.

The decoding of light by the retina and the signalling pathways to and from the SCN rely on neural excitation mechanisms, achieved through changes in membrane potential from a resting state stabilised by K_{2P} channels. With TASK-3 being the most abundant K_{2P} channel in the rodent SCN it is feasible this channel has a crucial role in regulating SCN neural transmission for effective circadian entrainment. This study investigates this role through the use of transgenic TASK-3 KO mice.

In the first experimental chapter I demonstrate the presence of *TASK-3* mRNA in the SCN and retina of wild type mice. Further, I reveal a circadian pattern in *TASK-3* mRNA expression with significant midday nadir which feasibly influences resting membrane potential (RMP) supporting increased neuronal excitation reported at this time.

The following three chapters explore TASK-3 conductance in behavioural output rhythms via locomotor activity studies under light-dark cycles and in constant darkness. This series of experiments highlights how TASK-3 is essential for effective adjustment to changing light and how loss of this channel reduces light-driven and endogenous activity intensity and rhythm amplitude.

With light entering the circadian system exclusively via the eyes, the role of TASK-3 at the level of the retina is of upmost importance to entrainment. This is investigated in chapter 6 using pupillary light reflex as a measure of retinal sensitivity and decoding capacity. Through manipulation of intensity and wavelength specific classes of photoreceptor are studied for their contribution to this non-image forming response. These experiments show TASK-3 ablation significantly attenuates retinal sensitivity to sub-saturating light in a mechanism likely to be melanopsin-independent.

Finally examination of mRNA expression of core clock genes reveals the role of TASK-3 at the level of the SCN. Here, loss of TASK-3 conductance is shown to alter daily rhythms in several key genes thereby linking the properties of this background leakage channel to the molecular clockwork.

Overall these experiments demonstrate some of the roles TASK-3 conductance plays within the SCN and in output rhythms; and the requirement of this channel within the retina for effective retinal decoding across the visible spectrum over a range of light intensities.

Total Word Count: 38,579

Declaration

I declare that this is my own work, carried out under the normal term of supervision.

Table of Contents

List of Figures

List of Tables

1. General Introduction

1.1 Circadian rhythms

1.1.1 Biological rhythms

Living organisms exhibit numerous physiological and behavioural patterns which cycle with robust time periods. The length of cycle may be many months such as the annual flowering of plants or the growing of a winter coat. Equally, events may repeat within a substantially shorter time frame as in oestrous cycles for instance, or even cycle several times per minute, such as breathing. When self-sustained episodes occur with a time period of approximately 24 hours, they are said to exhibit circadian rhythm (formed irregularly from Latin circa 'about', dies 'day').

1.1.2 Mammalian circadian rhythms

Through time mammals have evolved to be active (or indeed, inactive) at particular times of day and night, to suit their needs. Success in the essential roles of hunting, prey avoidance and raising offspring are key determinates in species survival. Optimal timing of behaviour leads to distinct activity-sleep patterns emerging such as nocturnal, diurnal or crepuscular which may progress over time into physiological adaptation.

With life on Earth centred on the celestial day, many biological episodes occur with a circadian time period, close to 24 hours in length (Herzog, 2007). These include relatively simple biological cycles such as hormone release through to complex mechanisms of metabolism and physiological traits of alertness and reaction time. These cycles are driven by the planetary day-night cycle and yet have been shown

to persist in the absence of light, confirming the presence of a biological pace-maker within the organism to maintain time-keeping.

1.1.3 Synchronising rhythms to environmental light

Light has the greatest influence on circadian rhythms, driving temporal changes in behaviour and physiology daily to synchronise with environmental illuminance. Natural light transitions at dawn and dusk are particularly potent cues for clock adjustment (Daan, 2000).

In circadian biology timing cues are referred to as 'zeitgebers' and under any controlled regime, time is referred to as Zeitgeber Time (ZT). Each ZT unit is equal to one conventional hour with the timing of the cue, zeitgeber, set according to the physical day. The usual convention has ZT12 as the time of lights off or, under non-light paradigms, the expected time when nocturnal animals will be driven by the cue to become active. For diurnal models the onset of activity will coincide with ZT0.

Laboratory rodent behaviour is often studied through observation of patterns in locomotor activity and rest, with activity onset providing a marker of cycle length. The mechanism of synchronisation could be described as successive, discrete daily shifts in activity onset as the presence of light drives the clock towards the external light-dark cycle (Pittendrigh and Daan, 1976a). This non-parametric theory has been described in detail over a number of years and is widely accepted. However, an alternative theory has long been held that entrainment occurs parametrically with a continuous process of adjustment in clock velocity producing alignment of intrinsic and extrinsic timing (Daan, 2000).

Recorded locomotor activity may be plotted graphically as an actogram to demonstrate timing of daily activity onsets and offsets relative to the external day along with the intensity and duration of activity bouts. By convention the duration of the active state (from onset to offset) is referred to as alpha, α, with the length of inactive state referred to as rho, ρ. In order to demonstrate the whole circadian cycle actograms are frequently double-plotted thereby displaying two circadian cycles per horizontal line, with the second cycle plotted again, beneath the first.

A standard regime of 12 hours light/12 hours dark results in a nocturnal rodent becoming entrained to the cycle with episodes of activity largely confined to the dark hours with an absence of activity during the light. Within a few days the behaviour fully takes on the 24-hour cycle with a stable pattern of activity onset and offset becoming evident on the actogram. See Figure 1.1.

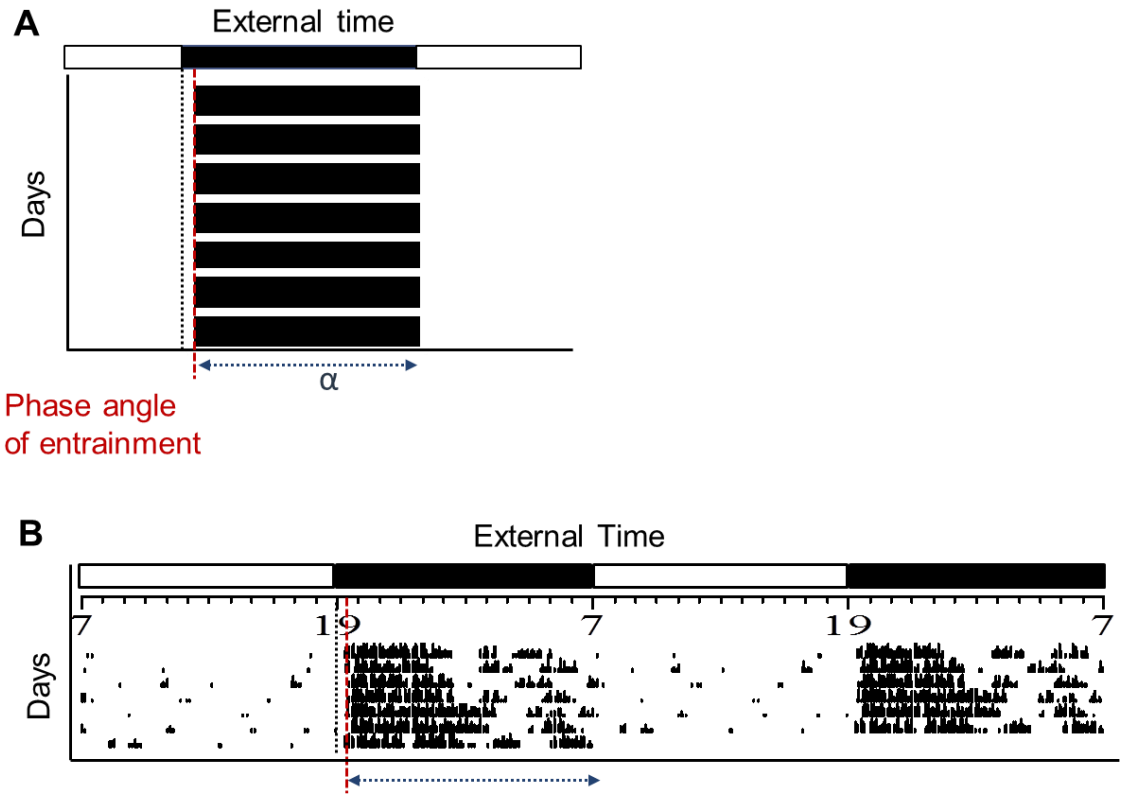

Figure 1.1: Schematic and representative actograms displaying synchronised nocturnal activity.

A: Schematic figure illustrating synchronisation to 12:12 hour light-dark (LD) cycle in nocturnal rodents. Broad dark bars within the body of the graph represent periods of activity daily over 7 days.

B: Representative double-plotted actogram of nocturnal activity in a mouse demonstrating successful synchronisation to the environmental 12:12 hour LD cycle. Dark vertical plots represent percentile distribution of wheel-running activity bouts.

Note in A and B activity is largely confined to dark hours with activity onset occurring just after the dusk transition. Elapsed time between lights off (black dotted line) and activity onset (red dashed line) is the phase angle. Measurement from activity onset to offset (dotted blue arrow) allows measurement of active state alpha, α.

Black/White bar at top of graphs A and B denotes LD cycle.

1.1.4 Endogenous rhythms

In the absence of light and indeed, all other environmental timing cues, daily behavioural and physiological cycles are determined solely by the endogenous circadian clock. In this state the subject is described as 'free-running'. Examination of the overt circadian rhythm under constant conditions by observation of locomotor activity and rest cycles reveals the natural, endogenous period of the biological clock. The rate of this natural rhythm is referred to as the 'free-running period' or tau (τ) of the organism, and will have a value close to, but not exactly 24 hours in length (Pittendrigh and Daan, 1976a, Dunlap, 1999). The actual value is species-specific with a small degree of biological variation within mammals.

Measurement of tau, τ, in an experimental rodent can be performed through assessment of locomotor activity by actigraphy. Identification of daily activity onset allows rate of drift from 24 hours exhibited daily to be calculated. See Figure 1.2.

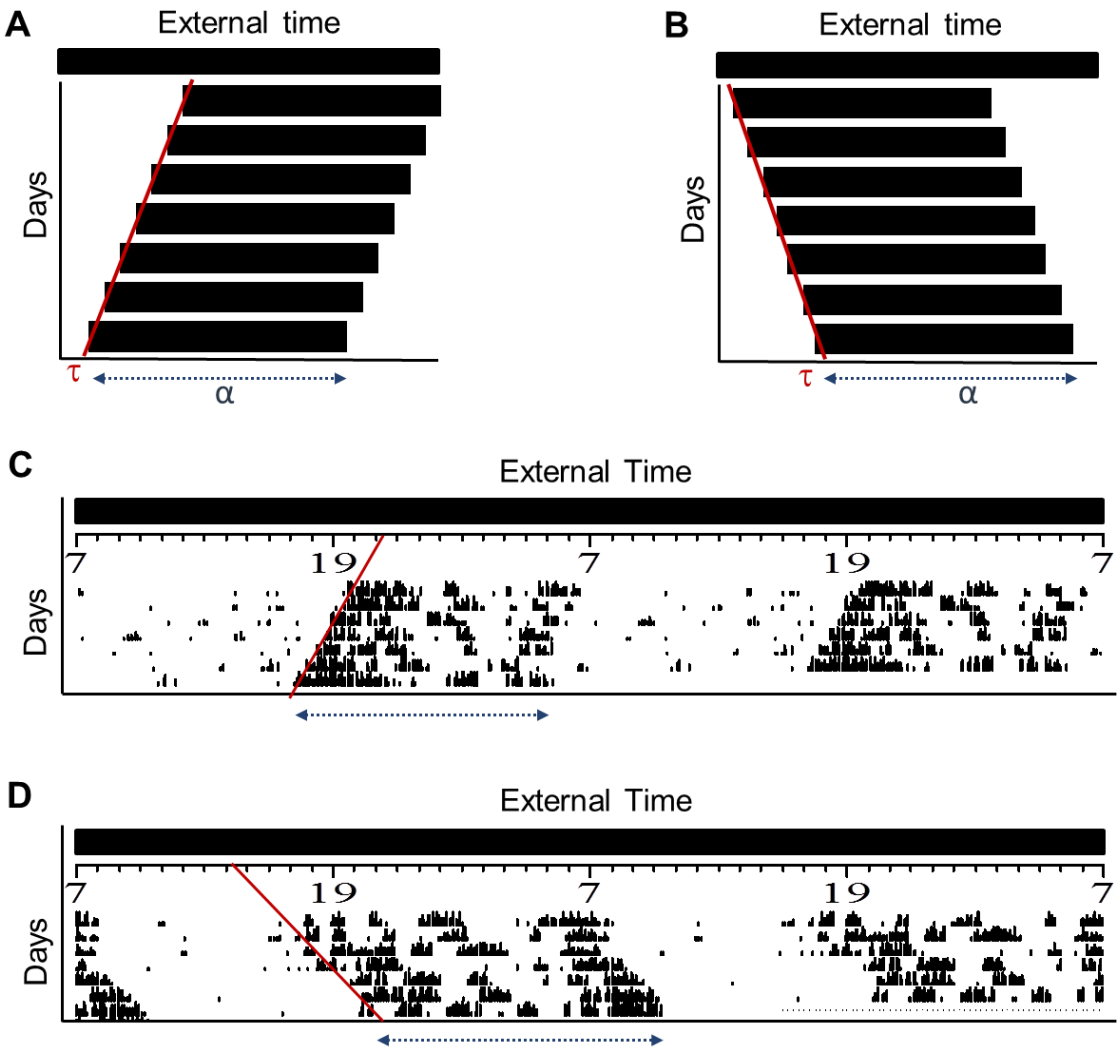

Figure 1.2: Schematic and representative actograms displaying free-running activity rhythms in two species of nocturnal rodent

A, B: Schematic figures illustrating tau, τ, being less than, and greater than, 24 hours respectively. Broad dark bars within the body of the graph represent periods of activity daily over 7 days.

C, D: Representative double-plotted actograms in a species where tau, τ, is less than, and greater than, 24 hours respectively. Dark vertical plots represent percentile distribution of wheel-running activity bouts.

Note in A and C there is a constant drift to the left as the animal begins activity earlier each day by a set amount, whilst in B and D there is a constant drift to the right as activity is delayed. Gradient of line placed through daily activity onsets (red line) provides measurement of tau, τ. Measurement from activity onset to offset (dotted blue arrow) allows measurement of active state alpha, α (as described previously). Solid black bar at top of all graphs A-D denotes Dark: Dark (DD) cycle.

By convention, under constant conditions time is referred to as Circadian Time (CT). Where no external stimulus is influencing the intrinsic time-keeping mechanism the endogenous clock-driven period of the animal dictates daily sleep-wake cycles. Therefore timing taken from the animal's daily activity onset is a reliable marker for cycle length. For nocturnal animals the start of activity is considered to be the start of the 'subjective night' and is given the value of CT12, with 'subjective day' given as CT 0. In contrast, activity onset in diurnal species marks the start of subjective day, and is denoted CT0.

As the endogenous cycle is not exactly equal to 24 hours, the circadian 'hours' are in fact units diving up the whole circadian day into 24 divisions (Pittendrigh and Daan, 1976a). For instance; mice with a period length of approximately 23.7 hours, will have each CT unit equal to 59.25 minutes, calculated as follows:

Circadian unit: *23.7 x 60 / 24 = 59.25 minutes*

Thus in mice, each circadian unit of CT is marginally less than a conventional hour.

1.2 The Master Circadian Clock

1.2.1 Evidence for a master pacemaker

The location and confirmation of a master circadian pace-maker in mammals was established over 40 years ago through lesion experiments in rats. Bilateral electrolytic destruction of the SCN (and closely associated tissue) was demonstrated to permanently eliminate the previously observed circadian behavioural rhythms in drinking and locomotor activity. In contrast, unilateral SCN lesions merely disrupted the pattern of behaviour, whilst lesions of the medial preoptic area, rather than the SCN, showed no change in free-running behavioural rhythms (Stephan and Zucker, 1972). This seminal work led on to further studies to investigate the autonomous actions of the SCN. Surgical interposition to produce isolated 'islands' of hypothalamic brain tissue containing the intact SCN allowed multiple electrode recording of the circadian clock in the absence of afferent projections. On recovery, robust circadian rhythmicity was shown to persist in brain tissue within the island, whilst circadian rhythms in additional brain regions and locomotor activity were eliminated (Inouye and Kawamura, 1979). This study clearly confirms both the role of the SCN as the master pace-maker but also the ability to maintain time-keeping autonomously.

More recent research has focussed on SCN tissue transplantation to restore rhythmicity in arrhythmic hamsters. The intact host with a stable locomotor activity pattern becomes totally arrhythmic following ablation of the SCN. Then, on implantation of a donor clock, becomes rhythmic once more. Moreover, by transplanting SCN tissue from a transgenic hamster strain (tau mutant) with a significantly shorter natural period length, the characteristics of the restored

rhythm was shown to correspond to the donor phenotype rather than the host (Ralph and Lehman, 1991). This finding demonstrates that grafted SCN tissue is able to both elicit and drive the overt rhythm of the host.

Further clock transplant studies have considered the induction of circadian rhythms in genetically arrhythmic mice through allograft of foetal SCN tissue. Once again the circadian phenotype post-allograft reflected that of the donor and interestingly, this study demonstrates that robust rhythms are able to be restored in mice previously lacking key circadian components (Sujino et al., 2003).

1.2.2 The suprachiasmatic nucleus

In mammals, the master circadian pacemaker resides within the suprachiasmatic nucleus (SCN) (Ralph and Lehman, 1991). Anatomically, this is a paired structure located in the anterior hypothalamus, just above the optic chiasm and below the third ventricle. See Figure 1.3. The two densely-packed nuclei contain around 20,000 neurons and receive direct and indirect signalling from a number of neural pathways (Reppert and Weaver, 2001). The location of the SCN, in close proximity to the optic chiasm, allows for optimal retinal innervation from environmental light (Reppert and Weaver, 2001).

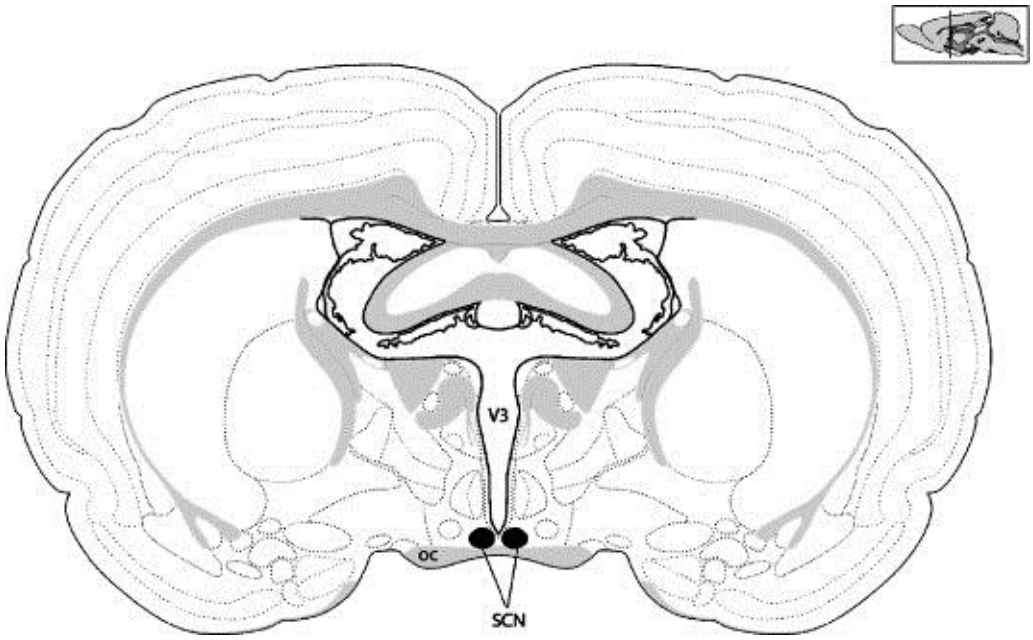

Figure 1.3 Graphic representation of a coronal slice of rodent brain depicting location of the suprachiasmatic nuclei (SCN).

The location of the SCN is directly above the optic chiasm (oc), each side of the base of the third ventricle (V3). The small additional schematic, top right, shows a sagittal plane for rostral-caudal location. [Adapted from The regulation of neuroendocrine function: Timing is everything (Kriegsfeld and Silver, 2006)].

The nuclei are considered to have two distinct zones - a dorsomedial shell and ventrolateral core with distinct differences in afferent projection and neurotransmitter release (Morin et al., 2006, Reghunandanan and Reghunandanan, 2006). See Figure 1.4.

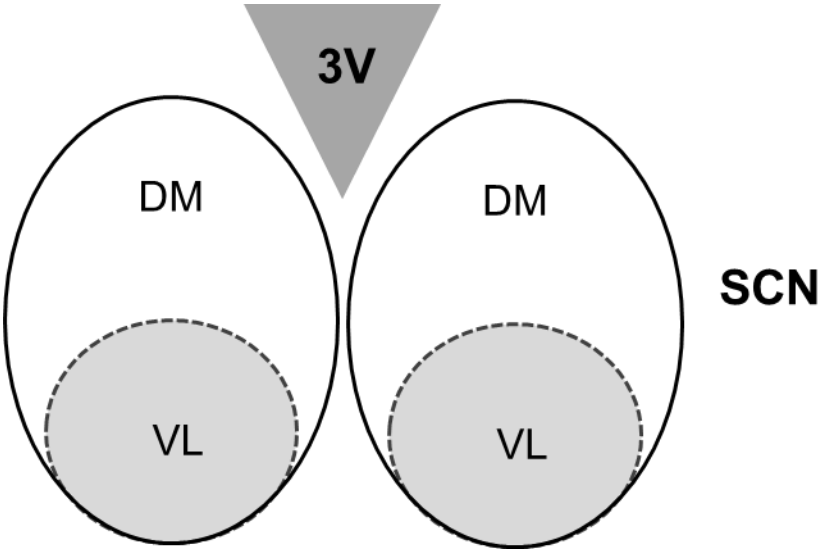

Figure 1.4: Diagram depicting the two major regions of the suprachiasmatic nuclei (SCN). The upper, region known as the dorsomedial area (DM) and the lower, region known as the ventrolateral area (VL) comprise the two major divisions of the SCN. Directly above, centrally, is the third ventricle (3V).

Communication between regions occur predominantly from core to shell with numerous projections, yet very few efferent projections from the shell innervate the core region (Mohawk and Takahashi, 2011). However, the SCN is infinitely more complex than two cooperating regions and is dependent on communication at a cellular level (Morin, 2007, Morin et al., 2006).

1.2.3 Electrical properties of the SCN

The SCN is densely populated with excitable cells which, through changes in neural activity, drive the internal time keeping mechanism. The use of electrophysiology recording techniques has provided an invaluable method of studying the electrical properties of SCN neurons. Examination of electrical properties in SCN neurons *in vitro* and *in vivo* has brought about greater understanding of SCN afferent

innervation, as well as efferent projections and importantly, communication between neurons within the clock itself. Previously the SCN was reported to consist of a monophasic cell population producing a single output rhythm (Liu et al., 1997). However additional studies have shown the thousands of neurons within the SCN to have individual rhythms. Together, through intercellular coupling, they contribute to the production of the single overt rhythm (Bernard et al., 2007). This mechanism of cellular coupling creates a stable and robust rhythm, resistant to perturbation (Mohawk and Takahashi, 2011).

The rhythmic firing of SCN neurons and associated changes in membrane potential regulates cytoplasmic intracellular pathways. These in turn drive gene expression within the molecular clock to ultimately produce the clock output firing rhythm (Colwell, 2011). Numerous SCN efferent pathways innervate tissues and organ systems within the brain and periphery, which respond according to their specific physiological role.

Electrophysiology performed *in vivo* over 30 years ago demonstrated neurons of the nocturnal rodent SCN to have a diurnal pattern of firing with higher spontaneous activity occurring during lights on compared to lights off. This pattern in electrical activity was shown to persist in the absence of a light-dark cycle, under constant conditions, thereby indicating a clock-driven rhythm as opposed to a passive response to light (Inouye and Kawamura, 1979). Later research using an in vitro hypothalamic brain slice preparation was able to provide more information on the timing of SCN activity. The peak spontaneous firing in the SCN was recorded around the middle of the projected day with a nadir occurring approximately 12 hours later. This pattern of activity continued for the full three days of recording in a consistent manner, thereby demonstrating the ability of the

clock to maintain time keeping in vitro (Brown and Piggins, 2007, Green and Gillette, 1982).

1.2.4 Principal circadian neurotransmitters

Innervation of the SCN occurs by three major afferent pathways, allowing both photic and non-photic information to be conveyed to the central biological clock for integration. This information may include food availability, social interaction and novel environmental stimuli in addition to irradiance.

The retino-hypothalamic tract (RHT) is the principal afferent projection to the SCN delivering photic information directly from the retina. A secondary branch of this tract extends to the intergeniculate leaflet (IGL) of the thalamus where photic and non-photic information interact for communication to the SCN via the geniculo-hypothalamic tract (GHT). Both the RHT and GHT pathways terminate in the ventrolateral zones of the SCN (Morin et al., 2006, Abrahamson and Moore, 2001). Additional non-photic information from behavioural stimuli is delivered to the central clock from the dorsal and median raphe nuclei of the mid-brain (Abrahamson and Moore, 2001). See Figure 1.5.

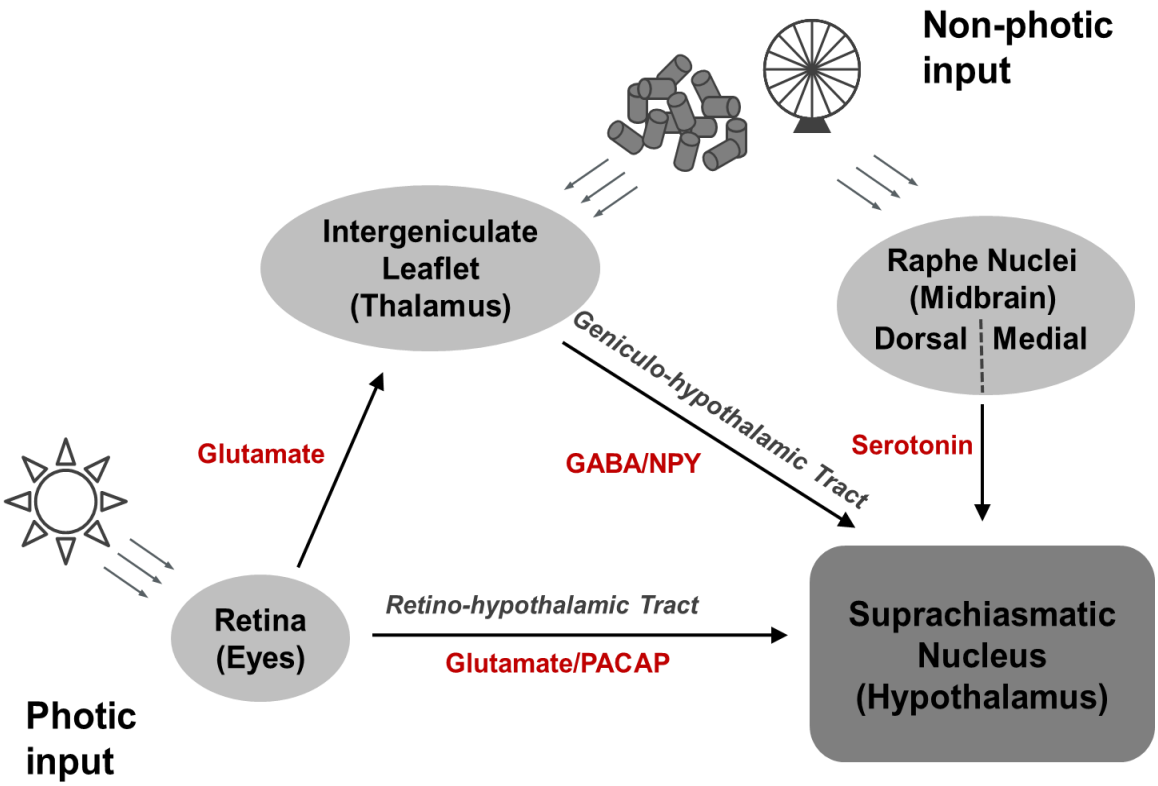

Figure 1.5: Major innervation pathways of the SCN.

Photic information from the retina is directly signalled to the SCN via the retino-hypothalamic tract (RHT) whilst photic and non-photic information is delivered from the intergeniculate leaflet via the geniculo-hypothalamic tract (GHT). Additional behavioural information is conveyed from the dorsal and median raphe nuclei. Major neural pathways are shown in italics, with key neurotransmitters highlighted in red.

Many different neurotransmitters have been described for their role in biological rhythm regulation. Within the circadian system, neurotransmitters act in either an excitatory or inhibitory manner for afferent projection to the master clock for entrainment, intra-SCN communication for integration, and in efferent projections from the clock to the periphery to produce coherent circadian rhythms (Reghunandanan and Reghunandanan, 2006). Further, neurotransmitters are not

produced in isolation but co-localised within single neuronal nuclei to afford additional signalling properties.

Signalling from the retino-hypothalamic tract (RHT) to the SCN and IGL is primarily mediated by excitory neurotransmitter glutamate. This abundant amino acid acts in conjunction with pituitary adenylate cyclase-activating polypeptide (PACAP) to deliver the essential photic information decoded by the retina directly to the master circadian clock. Exogenous application of specific agonists/antagonists of glutamate and PACAP have confirmed their roles as photic neurotransmitters as not only are they located in nerve terminals of the RHT, they have also been shown to be released by light stimulation and phase shift the clock in a similar fashion to light (Hannibal, 2002, Harrington et al., 1999).

During light exposure, co-stored glutamate and PACAP are released from nerve terminals of a sub population of retinal ganglion cells (RGCs) whose axons make up the RHT (Reghunandanan and Reghunandanan, 2006). This tract terminates directly in the ventrolateral area of the SCN with a subset of vasoactive intestinal polypeptide (VIP) containing cells propagating photic information to neighbouring cells for clock resetting (Albrecht, 2012, Morin et al., 2006).

The release of glutamate from presynaptic vesicles activates postsynaptic ionotropic (ligand-gated) receptors to provide a fast route of synaptic transmission. These include N-methyl-D-aspartate (NMDA), Alpha-Amino-3-Hydroxy-5-Methyl-4-Isoxazole Propionic Acid (AMPA) and kainate receptor groups. Additionally, metabotropic (G-protein coupled) receptors, referred to as mGluRs, are activated which modulate the presynaptic release and post-synaptic response of this amino acid transmitter (Acher, 2006). PACAP receptors are also

subject to G-protein coupled action and fall into two distinct classes: PAC1 is widely distributed in nerve terminals of the RHT and activates adenylate cyclase and phospholipase C with higher affinity than VIP. In contrast VPAC1 and VPAC2 receptors have a limited distribution, coupling to adenylate cyclase with similar affinity to VIP (Hannibal, 2002). It has been suggested that the cooperative role of PACAP in RHT projection is to generate prolonged postsynaptic activity as opposed to the more rapid release action of glutamate (Morin and Allen, 2006). PACAP is also considered to have a modulatory role in glutamatergic signalling in the early night when light has the greatest phase shifting capability (Michel et al., 2006).

Communication of non-photic information from the IGL to the SCN via the GHT, primarily utilises neuropeptide Y (NPY) in conjunction with neurotransmitter gamma amino butyric acid (GABA) (Lall and Biello, 2003). As this non-photic information is subject to photic interaction, the GHT terminates in a similar area of the SCN to the RHT, with some overlap (Morin et al., 2006). Integration of photic and non-photic information is critical for normal clock function where all entraining stimuli need to be taken into account for effective synchronisation of the clock.

The third input to the SCN from the raphe nuclei utilises serotonin in communicating information from the mid-brain. It is thought that the major role of this projection is in modulating the actions of the pace-maker in response to extrinsic stimuli (Morin, 2007).

However, the most common neurotransmitter found in almost all SCN neurons, is GABA (Reghunandanan and Reghunandanan, 2006). The role of this key transmitter has been researched extensively, with recent findings suggesting that

GABA is capable of dual effects on the SCN – excitory during the day and inhibitory during the night through having both depolarising and hyperpolarising abilities (Reghunandanan and Reghunandanan, 2006).

Communication within the clock is achieved through a combination of neurotransmitters acting to both propagate signals and modulate neurophysiology. Glutamate has been shown to play a major role in bilateral communication between left and right SCN in association with GABA, VIP and arginine vasopressin (AVP) (Michel et al., 2013). However, it is VIP mediated signalling which is responsible for cell to cell communication within SCN neurons via the VPAC2 receptor. This neurotransmitter and receptor are essential for rhythm maintenance as confirmed by transgenic studies revealing genetic ablation of the VPAC2 receptor results in arrhythmia of the clock at all levels (Cutler et al., 2003).

The synchrony and amplitude of the SCN are also subject to neurotransmitter governance, largely by AVP containing cells of the dorsomedial SCN. Studies have shown a high proportion of SCN neurons express AVP receptor V1a, with a majority responding during projected night and a minority during projected day. Genetic ablation of the V1a receptor has a consequence of low amplitude locomotor activity rhythms (Kalsbeek et al., 2010).

The overall expression of any neurotransmitter comes as a result of concentration in conjunction with receptor availability/specificity in a given cell or tissue. Both the neurotransmitter itself and the associated receptors are subject to post-transcriptional modification, providing further mechanisms for regulation and governance.

1.3 Environmental Stimuli for Entrainment

1.3.1 The process of entrainment

Entrainment is the process by which the endogenous biological clock aligns phase and cycle length with the external day. For successful entrainment all stimuli - photic and non-photic - must be integrated by the clock to ensure true alignment of daily rhythms to the environment.

The process of entrainment is not the same as synchronisation, which may occur as a result of alignment to a single timing cue. Moreover, the entrained endogenous clock may drive rhythms with different phases throughout the 24 hour cycle. For instance, an entraining cue indicating dawn will be perceived differently by nocturnal and diurnal species. Due to the variation in sleep-wake cycle, these groups will be in opposing stages of their day - diurnal species becoming active, nocturnal species preparing for sleep. Both of these examples show entrainment if they occur at the same time daily, relative to the solar day, but in opposite phase. Due to the process of entrainment they have each adopted a cycle length similar to the external physical day, and so will cycle at the same rate (period) as the external celestial day.

With mammals having a natural period close to, but not exactly 24 hours, there is a need for frequent clock adjustment in order to maintain alignment to the daily solar cycle. Thus, under an entrained system the observed rhythms in activity will reflect the external day rather than the endogenous rhythm of the clock.

1.3.2 Photic stimuli

Photic stimuli are the principal cues for circadian entrainment, whether from natural or artificial light sources. The daily solar cycle provides the most potent signal to the biological clock with immense changes in light intensity occurring daily in the range of 10 orders of magnitude (Cameron et al., 2008). This huge variability in illumination has such profound effects on physiology making detection of environmental light intensity changes at dawn and dusk key to central time-keeping.

In mammals, light can only enter the biological clock via the eyes. Previous studies to investigate extra-ocular photoreception have been strongly refuted by other researchers thereby affirming photoentrainment to occur exclusively through retinal signalling. (Campbell and Murphy, 1998, Foster, 1998). This retinal innervation serves only to entrain the clock, with time-keeping remaining an autonomous property of the master clock (Hastings et al., 2014).

Once detected and decoded by the retina, light information is communicated directly to the central clock via the RHT resulting in glutamate and PACAP release to the SCN (Reghunandanan and Reghunandanan, 2006). In this way transmission of light information is brought about through changes in neurotransmitter concentrations in the SCN with subsequent adjustments by the clock mechanism to alter the expressed rhythm of the clock. On a daily basis, this process of frequent clock adjustments to maintain synchrony with the exogenous light-dark cycle is known as photoentrainment.

Many studies to explore the circadian role of glutamate in photic resetting of the clock have centred on the ionotropic N-methyl-D-aspartate (NMDA) receptor.

Application of agonist NMDA directly to the SCN *in vivo*, at set circadian timings have been shown to induce clock-driven changes in behaviour consistent with those seen by acute light stimulation at similar times (Morin and Allen, 2006, Mintz et al., 1999).

In addition to ionotropic receptor signalling, glutamate also activates several classes of metabotropic receptor (mGluR). However, the role of mGluRs in driving clock adjustment and behaviour has not been fully resolved. Application of an mGluR agonist has been shown to potentiate clock delays following acute light exposure whilst the use of antagonists has resulted in potentiated clock advances and inhibition of delays (Haak et al., 2006, Gannon and Millan, 2011). Therefore it would appear this group of glutamate receptors play a temporal modulatory role in light-driven clock re-setting.

1.3.3 The photic phase response curve

Photic information reaches the central circadian pacemaker and adjustments are made by the clock to align the daily rhythm with the external environment. This area can be explored within the laboratory setting in 'perturbation experiments' where discrete pulses of light are applied for investigation into the light-induced effects on wheel-running behaviour of rodents (vanderLeest et al., 2009).

Typically a group of nocturnal rodents under constant environmental conditions demonstrating a free-running activity pattern in wheel-running are subjected to a discrete light stimulus of fixed duration (such as 15 minutes) at one specific circadian hour. This process is repeated in additional similar groups with pulses applied at each of the circadian hours thereby building a complete picture over all

24 circadian hours. The subsequent 10 days of wheel-running activity can then be examined to determine any change in activity start time following a pulse.

Generally, where pulses are applied during the subjective night (CT 12-0), there is a notable change in activity start time in the following cycle. Where applied during the subjective day portion of the cycle (CT 0-12, when light is not novel) there is little reaction. Any advance or delay in commencement of activity is referred to as a 'phase shift' and can be measured as deviance from the predicted start time from the free-running activity rhythm.

Application of light in the early portion of the subjective night results in the animal waking later, which can be visualised as a delay phase shift. When light is applied to the latter portion of the subjective night, the animal will wake earlier the following day and an advance phase shift will be observed. (Antle et al., 2009). The animal will maintain the predicted waking times with no phase shifts where pulses are applied during the subjective day. This expressed change in behaviour occurs as a result of the light-driven adjustment of the central clock, to the light information received (Dibner et al., 2010). Despite the alteration in activity commencement, these brief light stimuli do not cause a change in tau, τ or alter the length of time the animal is active (Dibner et al., 2010).

The resultant magnitude of the phase shift is dependent on the light applied in addition to the circadian timing of the light stimulus. The light intensity, spectral composition and duration are all factors in the degree of shift observed, whilst both the circadian timing of the stimulus and the photoperiod of the cycle will also affect phase shifting capacity (vanderLeest et al., 2009).

By exploring the behavioural response from light pulse application throughout a 24 hour period, a phase response curve (PRC) can be constructed. See Figure 1.6.

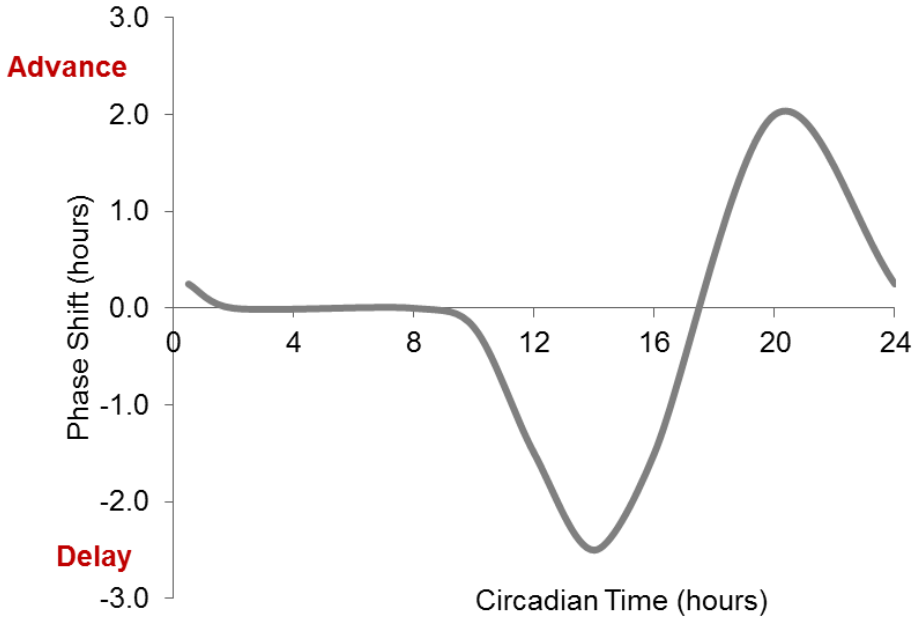

Figure 1.6: Representation of a Phase Response Curve (PRC) for a photic stimulus applied to a free-running mammalian system.

Demonstrated phase shifts in activity are measured and plotted as a function of circadian time.

Pulses applied during late subjective night: activity commenced early, measurements of phase shifts are given a positive value and described as advancements.

Pulses applied during early subjective night: activity postponed, measurements of phase shifts are given a negative value and described as delays. Pulses applied during subjective day: No measured change in activity start time.

The precise shape of the curve varies by species studied, with hamsters showing greater advances compared to delays, with the reverse being true for the mouse. This variance is a reflection of the free-running period, tau, of the animal (Pittendrigh and Daan, 1976b).

In hamsters tau is greater than 24 hours, thereby requiring daily advances of the clock to achieve a state of entrainment to the Earth's rotational day. Therefore additional light at the end of the subjective night results in large phase advances in an attempt to adjust the clock to this unpredicted light pulse. In the mouse, with tau less than 24 hours, daily delays in the clock facilitate successful entrainment to a 24 hour day therefore additional light at the beginning of the subjective night results in large phase delays to correct to this unexpected light stimulus.

However, regardless of species, the early subjective night is always the time of delay phase shifting, the latter portion of the subjective night, the time of advancement (Refinetti, 2006).

A similar PRC can also be observed following microinjection of NMDA directly to the rodent SCN at intervals across the circadian cycle. The photic-like phase shifts in behaviour follow the same pattern as light stimulation with delays observed following application during early subjective night and advances following late night treatment (Mintz et al., 1999).

1.3.4 Non-photic stimuli

The ability to alter the phase of the clock is not strictly limited to light. Non-photic stimuli, largely behavioural in nature, are able to influence the circadian clock. Examples include food availability, social interactions, induced locomotor activity and novel environments (Mistlberger and Skene, 2004, Mistlberger, 1994, Reebs and Mrosovsky, 1989, Mrosovsky, 1988).

A regular external stimulus (zeitgeber) other than light, when applied to a free-running system, may become an entraining cue, leading to regular daily activity onsets and offsets. This pattern of activity indicates a stable relationship between

the expressed rhythm being driven by the clock and the zeitgeber (Reebs and Mrosovsky, 1989).

Non-photic signalling to the SCN occurs largely from the IGL and is communicated via the GHT resulting in the release of GABA, NPY and in many rodent species, enkephalins to the SCN (Morin and Blanchard, 1995, Morin and Allen, 2006). An additional serotonergic projection from the Raphe nuclei provides further innervation from social/behavioural stimuli (Abrahamson and Moore, 2001). Along with non-photic communication, the IGL imparts photic information derived from the RHT projection, allowing interaction between both types of stimulus (Abrahamson and Moore, 2001, Morin and Blanchard, 1995).

Through in vivo and in vitro studies, the role of NPY has been investigated, where direct application of NPY to the SCN produced phase shifts similar to those produced by induced activity. The use of an NPY antagonist resulted in an attenuation of phase shifts, with no compensation by GABA (Lall and Biello, 2003). Despite the abundance of GABA in the SCN, NPY is considered to be one of the primary neurotransmitters in non-photic phase shifting.

1.3.5 The Non-photic phase response curve

An acute application of a non-photic stimulus is able to shift the phase of the clock in a predictable manner according to the circadian timing of the stimulus. When applied to a free-running system at different timings throughout the circadian cycle, a PRC may be constructed, in a similar manner to photic response. See Figure 1.7.

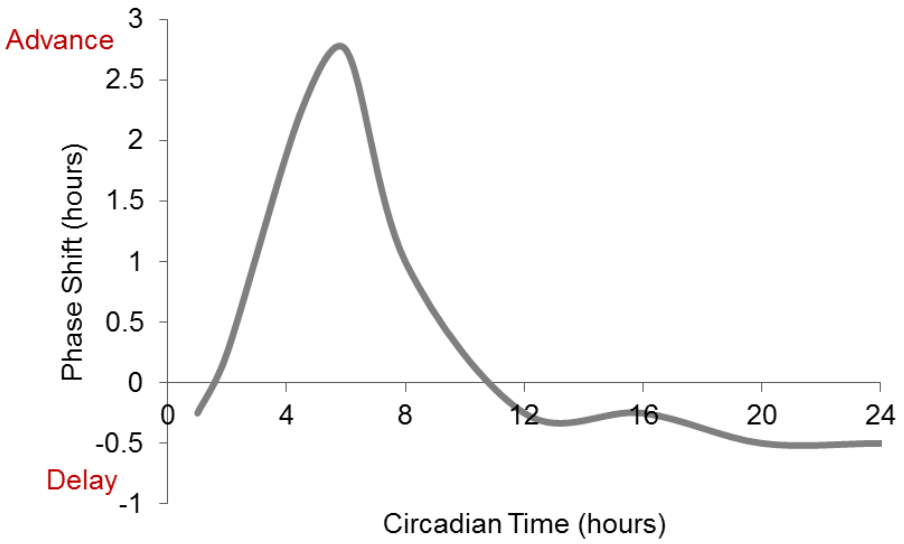

Figure 1.7: Representation of Phase Response Curve (PRC) for a non- photic stimulus applied to a free-running mammalian system.

Demonstrated phase shifts in activity are measured and plotted as a function of circadian time.

Stimulus applied during subjective day: activity commenced early, measurements of phase shifts are given a positive value and described as advancements.

Stimulus applied during subjective night: activity postponed, measurements of phase shifts are given a negative value and described as delays.

However, in contrast to the photic PRC, the non-photic PRC demonstrates maximal advance phase shifts in the middle of the subjective day rather than during the subjective night. In addition, with light being the most prominent of entraining agents, the response to weaker non-photic zeitgebers may produce less reliable results as the clock may not fully adjust to these signals (Reebs and Mrosovsky, 1989, Mrosovsky, 1988)

To ensure the observed behaviour is not a result of cognitive learning, all external signals other than the cue under investigation are avoided (Fuller et al., 2009).

This is achieved by having all environmental surroundings constant including lighting which is usually maintained as 24 hour darkness (DD) in these experiments, to fully eliminate any photic influence to the system under investigation.

In nature however, non-photic stimuli are often accompanied by photic cues, such as feeding or social relations at dawn/dusk rather than occurring in isolation. It is therefore crucial for the SCN to be able receive and resolve interacted signals from behaviour and light.

From laboratory experiments conducted into photic and non-photic signalling, induced activity has been shown to attenuate light effects on the clock whilst light pulses have been able to attenuate activity-related effects, clearly demonstrating a complex interaction between the two types of input to the clock (Lall and Biello, 2002). The neurotransmitter NPY has been shown to act in a modulatory role in these interactions, attenuating direct effects of light on the clock and in doing so, providing a method of control and regulation of circadian rhythms (Lall and Biello, 2002).

1.4 The Visual System

1.4.1 Retinal physiology

The mammalian retina is a sheet of tissue approximately 200μm thick which lines an extensive area of the eyeball (Masland, 2012). See Figure 1.8.

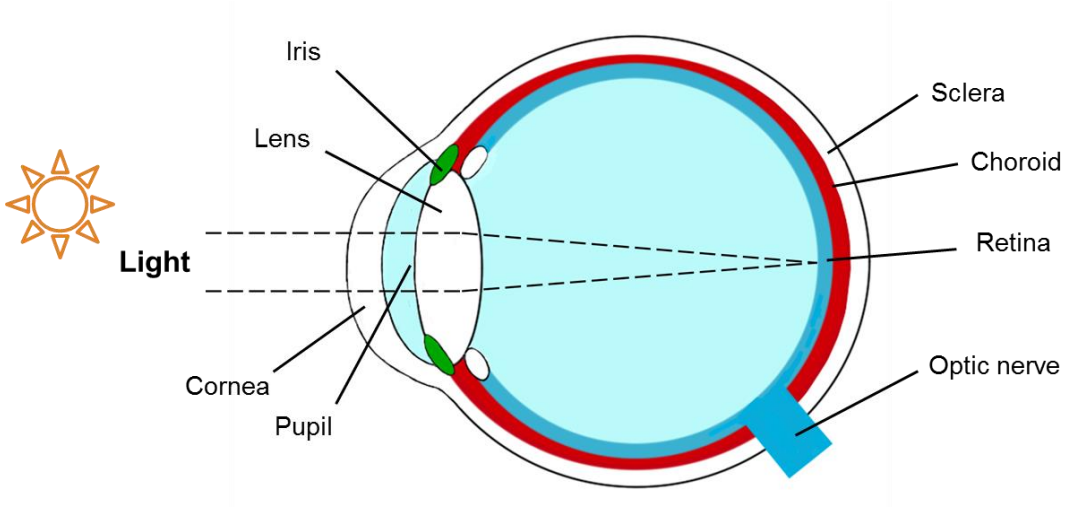

Figure 1.8 Schematic cross-section of the mammalian eye showing location of major tissues. Light enters the eye via the pupil, travels through the lens and is ultimately absorbed and decoded by the retina. Note the large area of the retina which lines the majority of the eye. [Adapted from Tortora et al., 2006].

The retina has a dual physiological role in producing both a high resolution pictorial map of the surroundings and conducting a separate non-image-forming (NIF) function of detecting ambient light intensity (irradiance) (Lucas and Foster, 1999). These functions are achieved by a combination of sensory neurons and intricate neuronal circuitry for the beginnings of image processing (Kolb, 2003). Ultimately all signals are communicated via the optic nerve for further processing and interpretation within specific regions of the brain.

The bodies of retinal neurons, including bipolar, amacrine, horizontal and ganglion cells, are arranged in layers according to function and interspersed with a network of synaptic connections (Masland, 2012, Kolb, 2003). See Figure 1.9.

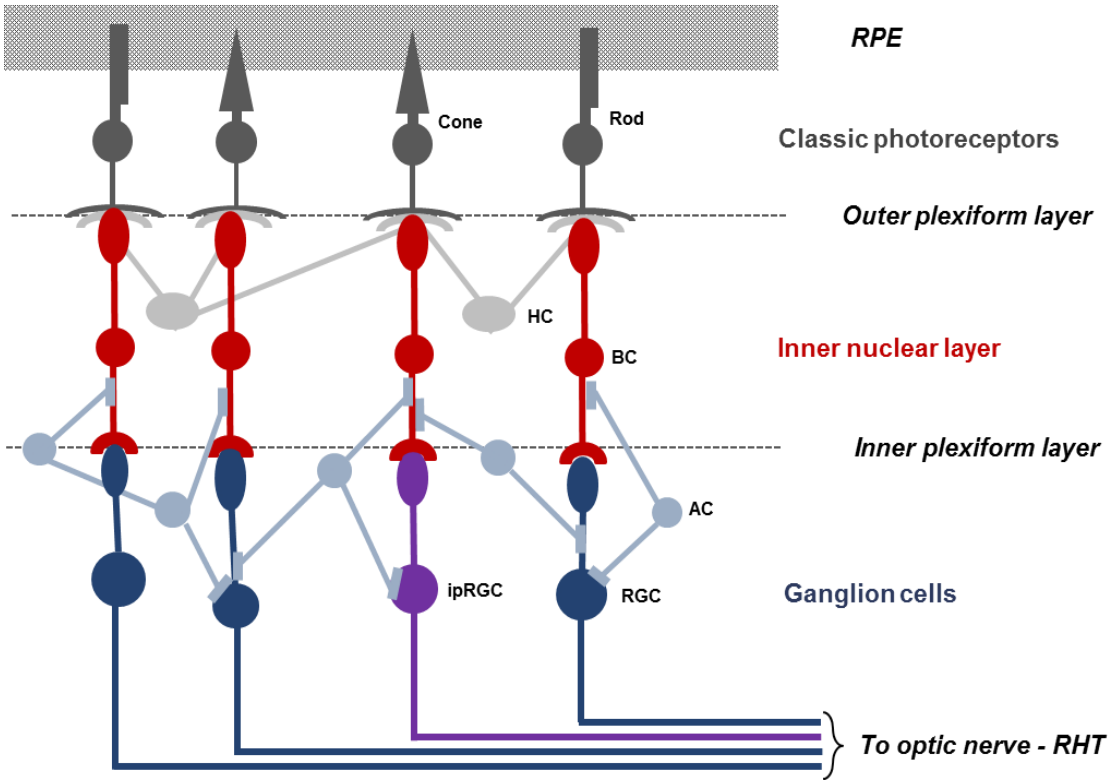

Figure 1.9 Diagram showing neuronal cells of the retina.

Classic photoreceptors, rods and cones, lie at the very back of the retina in contact with the retinal pigment epithelium (RPE). Following phototransduction, light information in communicated via bipolar cells (BC) to retinal ganglion cells (RGC). Additional interneural communication occurs via horizontal cells (HC) across the outer plexiform layer whilst amacrine cells form synaptic connections throughout the inner plexiform layer (AC). A small subset of RGCs is intrinsically photoreceptive (ipRGCs), the axons of which make up the retino-hypothalamic tract (RHT) of the optic nerve. [Adapted from 'How the Retina Works' (Kolb, 2003)].

Light enters the eye via the pupil, travelling through the lens to reach the retina where classic photoreceptors rods and cones are situated in contact with the retinal pigment epithelium. This locality ensures a supply of retinal (Vitamin A), essential for phototransduction (Kolb, 2003). Additionally, within the inner retina, intrinsically photoreceptive ganglion cells (ipRGCs) decode irradiance for NIF responses (Lucas et al., 2001, Lucas, 2013).

Communication from rods and cones to bipolar cells, and subsequently, ganglion cells, occurs largely by release or absence of the neurotransmitter glutamate (Kolb, 2003). Other accessory retinal cells, including horizontal and amacrine cells, use a variety of neuropeptides and nitric oxide.

During darkness photoreceptor membranes are depolarised with glutamate release and free-flowing Na^+ ions. On light activation they become hyperpolarised from closure of Na^+ channels, resulting in cessation of glutamate release. On reaching bipolar cells, the variation in receptors – some excitory, some inhibitory - produce ON and OFF pathways for accurate light signalling to ganglion cells (Masland, 2012, Kolb, 2003, Snellman et al., 2008).

1.4.2 Phototransduction: retinal decoding of light

When light reaches the back of the retina rod and cone 'classic' photoreceptors begin a series of cellular molecular processes known as the phototransduction cascade. This begins with the activation of retinal-bound chromophore proteins, opsins, which undergo a light-induced transformation in chemical structure. All rods contain an identical rhodopsin pigment whilst cones contain one of three types of photopsin, which vary in sensitivity to wavelength of light and form the basis of colour vision (Masland, 2012).

The light-evoked structural change, photoisomerisation, brings about a conformational change within the opsin protein, which in turn activates transducin proteins to bind guanosine triphosphate (GTP) in place of the original guanosine diphosphate (GDP). The presence of GTP bound transducin subsequently triggers the enzyme phosphodiesterase (PDE) to break down a small molecule, cyclic guanosine monophosphate (cGMP), thereby lowering the concentration of this molecule.

The level of cellular cGMP acts on specialised ion channels in the outer membrane with high levels required to open channels for influx of sodium and calcium ions. Therefore during light absorption, low levels of cGMP result in sodium channel closure and subsequent hyperpolarisation of the photoreceptor cell (Korenbrot, 2012, Blumer, 2004). Any change in the flow of ions through the photoreceptor membrane by alteration of cGMP levels produces an electrical signal and therefore a change in cellular excitability. This signal is conveyed through the many layers of the retina to the ipRGCs, the axons of which form the RHT (Guler et al., 2008).

To effectively turn off this light-induced phototransduction, such as under dark conditions, the transducin molecules hydrolyse the bound GTP molecules to GDP. In contrast to GTP, the GDP molecule has low affinity for PDE which results in deactivation of the enzyme, a consequent increase in cGMP levels which in turn leads to the opening of GMP-gated Na^+ ion channels and, subsequently, cellular depolarisation (Blumer, 2004).

Once more this change in membrane potential is transmitted through the retinal layers to the ipRGCs. See Figure 1.10.

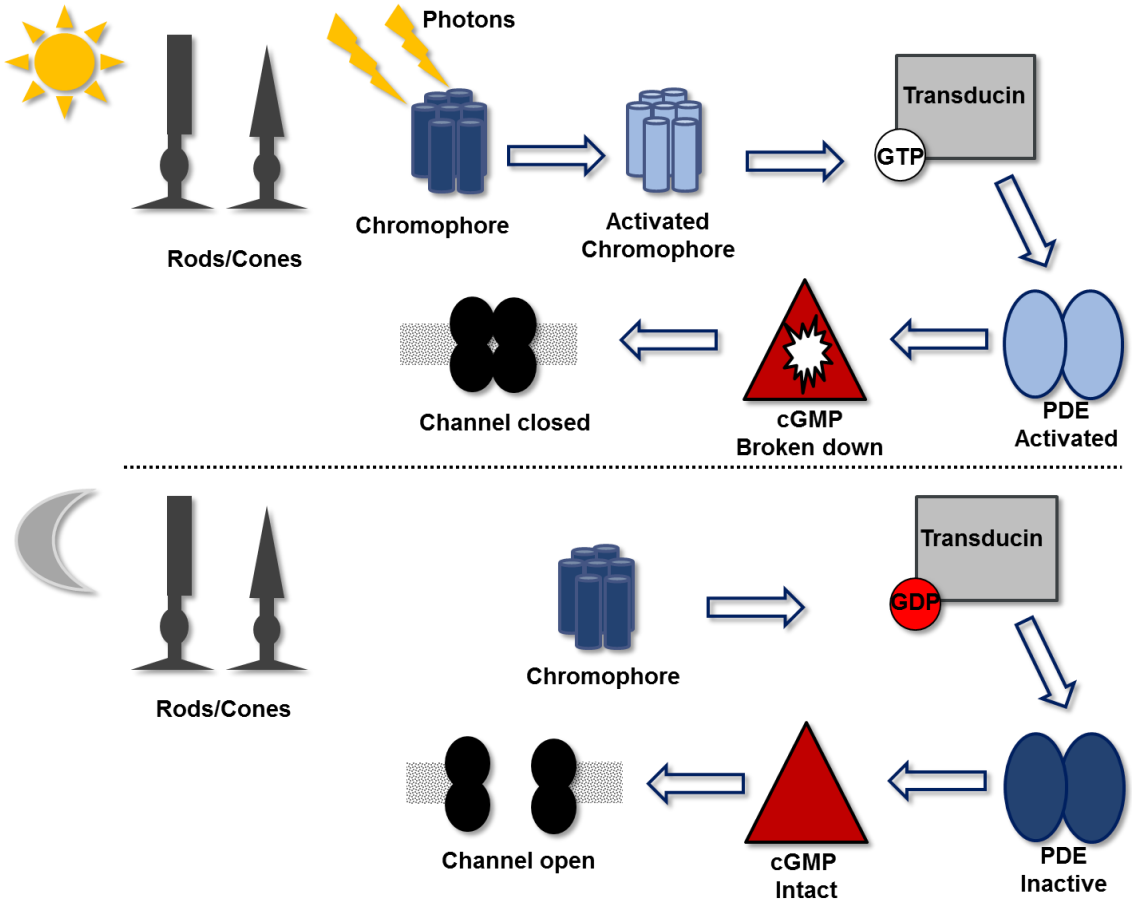

Figure 1.10: Graphic representation of the phototransduction cascade within the retina.

Top: Light detection by rods and/or cones results in photon absorption by chromophore protein beginning the cascade. The subsequent activation of transducin, results in binding of guanosine triphosphate (GTP), leading to phosphodiesterase (PDE) activation of cyclic guanosine monophosphate (cGMP) breakdown. The consequent low levels of cGMP prevent outer membrane GMP-gated Na^+ ion channels from opening and cellular hyperpolarisation results.

Bottom: Darkness prevents the rod/cone absorption of photons and therefore chromophore protein remains deactivated. Transducin binds guanosine diphosphate (GDP) under these conditions, which in turn maintains PDE in an inactive state and cGMP molecules intact. As the level of cGMP increases sufficient GMP-gated Na^+ ion channels open leading to cellular depolarisation.

The ipRGCs relay all photic information from the retina to the SCN, acting as conduits via the multisynaptic circuitry of the retinohypothalamic tract with additional monosynaptic projections extending to the intergeniculate leaflet (IGL) and olivary pretectal nucleus (OPN) (Guler et al., 2008, Berson, 2003, Hattar et al., 2006). Additionally, this small, specific population of retinal ganglion cells (RGCs) containing retinaldehyde-based photopigment melanopsin are intrinsically-photoreceptive and are able to directly detect and communicate environmental light via the RHT (Lucas et al., 2001, Ecker et al., 2010).

1.4.3 Non-image forming responses to light

The light-evoked innervation from the complimentary actions of all classes of photoreceptors, rods, cones and ipRGCs, drive NIF behavioural and physiological mechanisms including circadian photoentrainment, pupillary light reflex, masking and pineal melatonin suppression for sleep propensity (Guler et al., 2008, Lall et al., 2010, Peirson et al., 2009, Hattar et al., 2003).

The role of each photoreceptor class involved in NIF function has been studied by the use of transgenic KO murine models over a range of light intensities to fully establish limits of photosensitivity. Research has been shown that illumination far too dim to elicit one particular NIF response, such as pupillary constriction, may still contribute to entrainment (Butler and Silver, 2011).

Under dim light (scotopic levels), rods are considered to be solely accountable for retinal light detection and NIF response with high-sensitivity rhodopsin signalling through the rod-bipolar pathway. At these minimal intensities of light both cones and ipRGCs are far too insensitive to contribute (Altimus et al., 2010, Lall et al., 2010). As ambient light increases to photopic levels all classes of photoreceptor

become involved with outer retinal cone and rod signalling via the cone pathway and significant inner retinal ipRGC signalling (Lall et al., 2010).

At the highest light intensities the ipRGCs are the only photoreceptor class capable of driving a photic response as rods, and eventually cones, become fully saturated (Altimus et al., 2010).

Further studies into the role of melanopsin have revealed that in its absence, NIF function is reliant purely on rod-cone light detection at sub-saturating intensities which results in reduced pupillary light reflex (PLR) and entrainment capabilities. Moreover, ordinary RGCs can become intrinsically photoreceptive by viral transduction of the melanopsin photopigment (Xue et al., 2011, Guler et al., 2008). Conversely, removal of the melanopsin pigment from ipRGCs renders them no longer intrinsically photosensitive (Lucas et al., 2003, Hattar et al., 2003).

Although initially thought to be a homogenous class of cells, evidence from studies using reporter genes within mouse models has revealed several morphologically-distinct subtypes of melanopsin-containing ipRGC denoted as M1-4 subtypes (Baver et al., 2008, Ecker et al., 2010, Schmidt et al., 2011). In addition to differences in structure and form, the individual subtypes are diverse in their projections, with both NIF and visual regions of the brain targeted (Ecker et al., 2010).

The conventional ipRGCs, now known as M1 cells, are the most light-sensitive subtype of ipRGCs primarily involved in signally for NIF responses to light (Schmidt and Kofuji, 2009). These cells are the principal innovators of the SCN for photoentrainment via the RHT and, additionally, project to the shell of the olivary pretectal nucleus (OPN) to drive PLR (Ecker et al., 2010). Conversely, the M2

subtype exhibit much smaller responses to light; are at least one log unit less sensitive and have minimal projections to the SCN (Schmidt and Kofuji, 2009, Baver et al., 2008). Generally much less is known about the non-M1 subtypes of ipRGC, with M3 target regions still to be discovered. They are considered to have a similar role to M2 and M4 cells which innervate visual areas of the brain including the dorsal lateral geniculate nucleus and superior colliculus and are likely to play a role in pattern vision (Ecker et al., 2010, Schmidt et al., 2011).

Throughout the circadian cycle, photosensitivity and the associated retinal output has been studied and shown to be subject to variation. However, there is a need to ascertain whether this variation is due to clock gene expression or photoreceptor sensitivity changes. A study into the role of clock gene cryptochrome, a potential blue-light photopigment mediating photosensitivity, compared the effects of ablation of cryptochrome in isolation and also with additional photoreceptor loss. The conclusion from this research was that any sensitivity loss was due to clock malfunction thereby confirming that the circadian clock modulates the sensitivity of NIF photoreception (Owens et al., 2011).

1.4.4 Pupillary light reflex

The mammalian eye is able, in part, to control the amount of light entering the eye by adjustment of pupil size. The surrounding iris contains circular and radial muscle fibres which bring about a dilation or constriction of the pupil in response to environmental light, irradiance. This autonomic function is known as the pupillary light reflex (PLR).

Photic information is communicated from the retina to the SCN via glutamatergic neurons of the RHT. Furthermore, a branch of the RHT projects directly to the

olivary pretectal nucleus (OPN) area of the brain in order to mediate PLR through communication with the iris muscle fibres to constrict/dilate the pupils consensually (McNeill et al., 2011, Hattar et al., 2002). During high light intensities, parasympathetic innervation and contraction of circular muscle fibres (sphincter pupillae) results in pupillary constriction whereas during dim lighting conditions sympathetic innervation and contraction of radial muscle fibres (dilator pupillae) produces pupil dilation (Tortora et al., 2006).

The firing rate of OPN neurons is linearly proportional to the level of light falling on the retina, which in turn produces a proportionate response in the iris thereby regulating the level of light reaching the retina (Campbell and Lieberman, 1985).

PLR is a non-image-forming (NIF) response brought about by ipRGC signalling to the OPN. This action occurs independently of pictorial vision as demonstrated by research conducted on mice lacking this cell population through genetic ablation - These animals showed an attenuated NIF response of PLR, but remained capable of forming visual images (Guler et al., 2008). The detection of light by rods and cone phototransduction also contributes to the PLR. These classic photoreceptors are activated at lower levels of illumination than the melanopsin-expressing RGCs, thereby allowing functionality at all intensities of light encountered during the natural day-night cycle (Altimus et al., 2010).

Under very dim light, rods provide extremely sensitive irradiance detection with cones providing a limited contribution at higher intensities (Lall et al., 2010). However, for typical pupil constriction at all irradiances, the ipRGCs are required to relay rod-cone signalling to the OPN (Guler et al., 2008).

Temporal properties of ipRGCs also differ from rods and cones in that they have a slow onset with sustained depolarisation which may last up to 30 seconds after lights off, unlike rods and cones which show a rapid, short-lived response to light (Markwell et al., 2010). The distinct differences in temporal properties between melanopsin, rods and cones extends the dynamic range over which a retinal response may be elicited. Moreover, within the cones there are short and medium wavelength subtypes (and in some mammalian species, long) which extend the spectral range of sensitivity (Kolb, 2003).

1.4.5 The irradiance response curve

Measurement of pupil area as a function of irradiance provides a method of assessing the NIF response of PLR and the relative contribution and sensitivity of different classes of photoreceptor in detecting and signalling light information to the SCN and OPN. This technique therefore is extremely valuable in researching light-driven regulation of the circadian clock. See Figure 1.11.

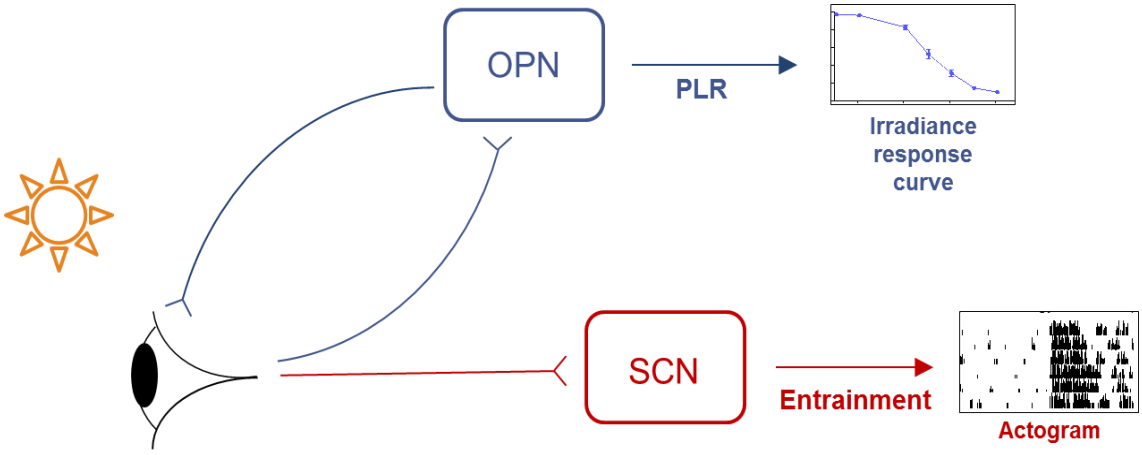

Figure 1.11: Retinal signalling pathways for NIF responses of PLR and photoentrainment

Schematic of retinal photoreception being transmitted to the olivary pretectal nucleus (OPN) for regulation of pupillary light reflex (PLR) whilst signalling light information to the suprachiasmatic nucleus (SCN) for photoentrainment.

Fully dark-adapted pupils are measured prior to light exposure to provide a base-line for normalisation of constricted pupil areas. As light is applied to one eye, the consensual constriction of the pupil of the other eye is recorded and measured over time to establish the maximum constriction achieved.

The intensity of light entering the eye is manipulated by the use of neutral density (ND) filters, thereby allowing a range of lighting conditions from very dim conditions indicative of highly-sensitive rod signalling, through to high daytime illumination signalled by the ipRGCs (Lall et al., 2010). Normalised pupil areas are plotted against irradiance to allow the construction of an irradiance response curve. See Figure 1.12: A.

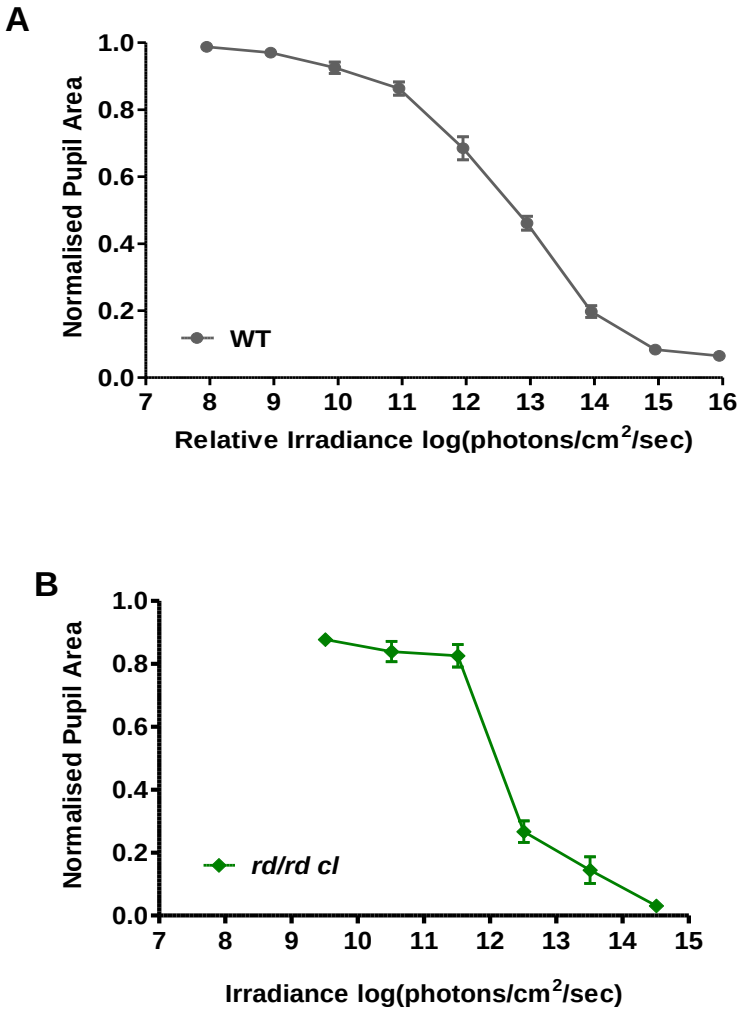

Figure 1.12: Example Irradiance Response Curves (IRC) for murine Pupillary Light Reflex (PLR) in WT and *rd/rd cl* transgenic mice.

Normalised pupil area calculated and plotted against the log value of irradiance in A, WT mice (Atkinson, 2014) and B, transgenic mice lacking functional rods and cones (*rd/rd cl*, Lall, 2007).

Note the dissimilarity of IRC shape between strains and the differences in normalised pupil area at sub-saturating irradiances.

Additionally, alteration of the spectral composition of the light source can also target a specific population of photoreceptors according to their peak sensitivity. For instance in the mouse: rod has a peak sensitivity of 498nm, s-cone 360nm, m-cone, 511nm, and melanopsin, a peak sensitivity of 480nm (Lall et al., 2010).

Transgenic knock-out (KO) mouse models for specific photoreceptors have demonstrated significant alterations in their IRCs according to the class of receptor ablated and properties of the light source. Research conducted on mice lacking only the melanopsin protein (*Opn*$^{-/-}$) demonstrated a shift in sensitivity compared to wild type mice of similar background strain. This difference is apparent at high levels of intensity where there is an attenuated response, highlighting the critical role of melanopsin for full pupillary constriction to saturating light (Lucas et al., 2003). However, at sub-saturating light intensities the combined normal action of rods and cones produced a pupillary response similar to that of wild type mice. Furthermore, mice lacking functional rods and cones with intact ipRGCs (*rd/rd cl*) demonstrate significant reduction in pupillary constriction over a range of irradiances, whilst still being able to achieve a full constriction at saturating light levels. See Figure 1.12: B. This study provides additional evidence that under sub-saturating light conditions, PLR is a function reliant on rod and cone action, with ablation resulting in attenuated response even in the presence of ipRGCs. However, when light reaches saturating levels, it is the action of melanopsin-containing ipRGCs which produce the PLR independent of rods and cones (Lall et al., 2010). Additionally, disabling of all three classes of photoreceptor - rods, cones and ipRGCs, essentially eliminates all PLR action (Hattar et al., 2003).

The importance of ipRGCs in PLR has been explored thoroughly, and has been shown to extend to maintenance of the pupil diameter in light conditions and also post-illumination recovery (Markwell et al., 2010).

1.4.6 Intrinsic pupillary light reflex

Some nocturnal and crepuscular mammals including mouse, rat, hamster, rabbit, cat and dog have been shown to exhibit an intrinsic PLR independent of neuronal innervation via the optic nerve. Research has demonstrated intact freshly isolated eyes from these species to be capable of a pupillary constriction when subjected to illumination for up to a minute after removal (Xue et al., 2011). Moreover, the pupillary response was found to have a linear relationship to light intensity with maximum sensitivity (λ_{max}) at 480nm, a wavelength characteristic of melanopsin photopigment. Further investigations with transgenic mice have confirmed the intrinsic response to be absent in melanopsin KO models (Xue et al., 2011, Semo et al., 2014).

Additional KO models for photopigment rhodopsin and clock gene cryptochrome found these models able to maintain an intrinsic PLR, ruling out rod or cryptochrome involvement, attributing this intrinsic property entirely to the melanopsin system (Xue et al., 2011). Recent studies to further characterise the intrinsic PLR have found the response to be sensitive to cholinergic neurotransmission blockade, and propose this to be a melanopsin-driven constriction of the iris by cholinergic-dependant relaxation of the dilator muscle (Semo et al., 2014).

To date, this autonomic response has not been found in any primate species, suggesting this property provides an advantage to nocturnal and crepuscular mammals active during dawn and dusk transitions. The ability of the iris to constrict with almost immediate effect would feasibly protect the eyes from sudden high levels of irradiance. Moreover, this constriction would enable greater

visual resolution by reducing bleaching of classic photoreceptors during pupillary adaptation to changing environmental illuminance.

1.4.7 Masking to light

In bright light nocturnal rodents exhibit an acute suppression of activity known as negative masking. In conjunction with circadian photoentrainment, this NIF retinal response, acting independently of the circadian pacemaker, serves to confine activity to hours of darkness (Mrosovsky et al., 2001). In circadian biology the examination of masking behaviour provides an additional marker of irradiance detection by the retina, with amount of activity cessation demonstrating sensitivity to the given light stimulus.

In order to establish the origin of the masking at the level of retina, several studies have examined this response using retinal transgenic mice with specific photoreceptor ablation. Research into classic photoreceptor contributions to masking concluded that negative masking is spared in the retinally degenerate mouse, *rd/rd , rd/rd cl*, with virtually complete ablation of rods and cones resulting in similar masking behaviour to wild-type controls (Mrosovsky et al., 1999, Thompson et al., 2008). In stark contrast, loss of melanopsin in mutant $Opn^{-/-}$ ($mop^{-/-}$) mice significantly impaired negative masking in both intensity and duration during prolonged light pulses (Mrosovsky and Hattar, 2003). Taken together, these studies indicate that negative masking is a melanopsin-dependant mechanism, acting independently of outer photoreception. Further research conducted on triple knock-out mice lacking all known photo detection systems, $Opn^{-/-}Gnat^{-/-}Cnga3^{-/-}$, found no evidence of masking with approximately equal

amounts of activity during light and dark phases of the cycle, suggesting all major contributors to masking have been accounted for (Hattar et al., 2003).

In opposition to negative masking dim light exposure has been shown to increase nocturnal rodent activity, in a response referred to as positive masking. This phenomenon is thought to occur as a result of increased visual guidance during movement enabling greater locomotor activity (Thompson et al., 2008).

1.5 The Molecular Clock

1.5.1 Clock genes

The molecular control of the biological clock is brought about by levels of translated clock gene products acting in an auto-regulatory manner. This is achieved through interacting negative and positive feedback loops inhibiting or promoting transcription respectively (Dunlap, 1999, vanderLeest et al., 2009, Colwell, 2011).

In mammals, one of the most studied molecular clock mechanisms is that of the mouse where the transcription/translation cycle of three Period genes (*mPer1, 2, 3*), with 'm' denoting murine genes, and two Cryptochrome genes (*mCry 1, 2*) are mediated by the transcription of *Clock* (Circadian Locomotor Output Cycle Kaput) and *Bmal1* (Brain and Muscle ARNT-Like 1)(Reppert and Weaver, 2001, Sukumaran et al., 2010).

This complex mechanism within circadian oscillators begins with the association of a CLOCK: BMAL1 complex activating *mPer, mCry, mRev-erbα* and *mRORA* gene transcription through binding to a promoter region 'Ebox' (CACGTG). The resulting accumulation of mPER and mCRY proteins within the cytoplasm form heterodimers which are able to translocate to the nucleus of the cell along with the generated mREV-ERBα and mRORA proteins. Once inside the nucleus, mCRY proteins act directly to inhibit the function of heterodimers CLOCK: BMAL1. Addition regulation of CLOCK: BMAL1occurs via mREV-ERBα and mRORA products within the nucleus which act in opposition to inhibit and up regulate transcription respectively. Conversely, the produced mPER2 proteins accrue within the nucleus where they directly contribute towards *Bmal1* gene

transcription in a positive feedback loop (Edery, 2000, Schwartz et al., 2011). The resultant increased level of BMAL1 proteins facilitates further CLOCK: BMAL1 dimerisation, which in turn inhibits the transcription of *Per* in a negative feedback loop. This reduction in mPER protein production results in lower availability of mPER: mCRY dimers which in turns results in less inhibition of CLOCK: BMAL1 - thereby restarting the transcription-translation cycle once again (Reppert and Weaver, 2001, Shearman et al., 2000). See Figure 1.13.

The role of casein kinase ε enzyme in the molecular mechanism of the clock is a complex one. Excess mPER proteins accumulating within the cytoplasm are phosphorylated marking them for degradation, which is thought to influence circadian timing. The destabilisation of mPER by this method prevents mPER accumulation other than when mCRY proteins are rising and also serves to modulate the formation of mPER: mCRY dimers which in turn regulates the inhibition of CLOCK: BMAL1 complex (Reppert and Weaver, 2001). Further, the phosphorylation of mPER1 protein by casein kinase ε is also thought to play a role in allowing this protein to enter the nucleus of the cell without CRY interaction (Reppert and Weaver, 2001).

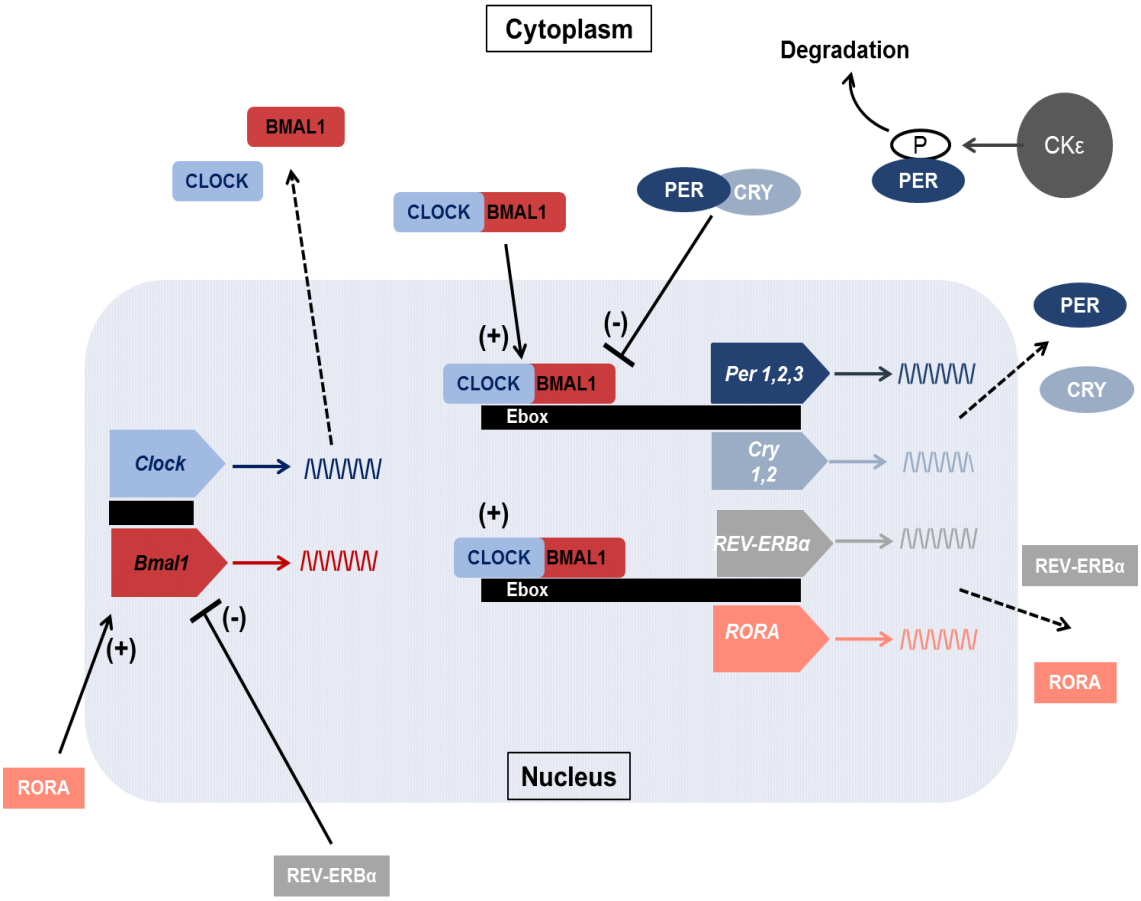

Figure 1.13: Simplified schematic of the mammalian molecular clock.

Transcription of *Clock* and *Bmal1* genes result in high availability of CLOCK and BMAL1 protein products within the cytosol. These heterodimerise, re-enter the nucleus, and up-regulate transcription of genes *mPer* , *mCry*, *mRev-erbα*, and *mRORA*. The produced mREV-ERBα proteins re-enter the nucleus to inhibit BMAL1 function whilst the generated mRORA up-regulate transcription of BMAL1. Cytosolic mPER proteins heterodimerise with mCRY which, on reaching the nucleus, down-regulate the CLOCK:BMAL1 complex acting on their own promoters. Excess PER proteins within the Cytosol are phosphorylated by CKε leading to degradation.

1.5.2 Photic re-setting of clock phase

As a result of neuronal innervation from photic and non-photic stimuli, adjustments occur at a molecular level within the SCN to bring about necessary changes in both clock period and phase (timing of peak/trough)of the cycle. These adjustments are the method by which the clock adjusts in order to synchronise with the detected environmental condition. When tau is perceived as being too long, the clock will adjust to bring about a decrease in cycle length, presenting as a phase advance. When the reverse condition occurs and tau is considered too short, the clock corrects by lengthening the cycle and a phase delay results (Schwartz et al., 2011). This phenomenon of phase shifting is achieved by the switching on and off of the clock genes within the SCN which in turn lead to behavioural changes and differences in the overt rhythm.

Light provides the principal cue for clock resetting which is primarily brought about through changes in expression of period genes within the molecular clock which, in turn, lead to phase resetting. Both *Per*1 and *Per*2 genes are up-regulated as an acute response to light, with *Per* 3, contrastingly, being unresponsive to photic stimuli (Reppert and Weaver, 2001). Light exposure at night is known to result in a rapid increase in *Per1* transcription in as little as 10 minutes. *Per*2 induction however is largely confined to early night light exposure, with little reaction seen during the late night, highlighting the role of this gene in delay phase-shifting (Reppert and Weaver, 2001).

The use of *Per* mutant mice has facilitated genes to be studied individually, with *Per*2 mutant mice exhibiting phase advances following late night light exposure but a lack of delay phase-shifting to light exposure early night (Albrecht et al., 2001, Spoelstra et al., 2004). Studies on *Per*1 mutant mice have shown ablation of this

gene attenuates advance phase-shifting whilst maintaining full capability to delay following light exposure at times when WT mice would demonstrate these responses (Albrecht et al., 2001, Spoelstra et al., 2004).

1.5.3 Peripheral clocks

Although mammalian circadian rhythms are controlled centrally by the SCN, tissues throughout the body have oscillators located within them for local control of daily rhythms and physiology. This hierarchal arrangement allows specific demands of organs and systems to be met fully whilst maintaining alignment with the external day. These local time-keepers are referred to as peripheral clocks, and are located in all major organ systems (Tahara et al., 2012, Hastings et al., 2014).

The multiple oscillators of the SCN generate a synchronised circadian output rhythm which is communicated through neural, behavioural and endocrine pathways to the peripheral oscillators (Shearman et al., 2000, Hastings et al., 2014). However, the control of peripheral rhythm synchronisation remains under the control of the central pace-maker. Cell culture experiments have demonstrated SCN neurons are able to express a self-sustained circadian rhythm for weeks *in vitro* whilst peripheral tissue cells lose this ability after just a few cell cycles, indicating SCN innervation is required to both generate and synchronise cell cycles (Richter et al., 2004). However, *in vivo* studies using a luciferase-based fusion protein have revealed peripheral tissues in mice can exhibit self-sustained oscillations for 20 cycles or more (Yoo et al., 2004). Further, SCN lesion studies in these mutant mice did not eliminate rhythms, merely bringing about phase desynchrony (Yoo et al., 2004). Together these findings suggest the role of the SCN

is that of an orchestrator of rhythms with peripheral clocks being self-sustaining oscillators under both local and central governance.

The autonomic nervous system enables regulation of circadian rhythms in peripheral tissues by receiving information directly from the hypothalamus and then imparting this onto nearly all peripheral organs and tissues including liver, kidney, pancreas, muscle etc. (Sukumaran et al., 2010). It is therefore not surprising that the neuronal activity of the autonomic nervous system changes according to the light/dark cycle.

An additional mechanism for peripheral tissue rhythm control occurs by the innervation of the pineal gland by the sympathetic nervous system and the subsequent release of the hormone melatonin. This hormone, known to play an important role in sleep-wake cycles, reaches a peak level during the night, with only very low levels during the day as production is suppressed by light. Melatonin receptors are expressed in cells of the SCN where a feedback mechanism exists to further covey day-length information. There are also melatonin receptors in many key peripheral tissues (Sukumaran et al., 2010)

1.5.4 Retinal clocks

The retina is a specific example of a peripheral clock with oscillators controlling local physiology including retinal sensitivity, rod disc shedding, electroretinogram waveform and gene expression (Guido et al., 2010). This regulation is vital for full retinal function, in particular in anticipation of light intensity changes occurring daily.

One defining factor that these retinal clocks are genuinely peripheral oscillators is that they are able to exhibit sustained gene rhythms out of phase to that of the

master pace-maker. However, this independence is limited as demonstrated by in vitro studies where rhythms dampen rapidly following isolation from the SCN innervation (Green and Besharse, 2004).

The period of the retinal clock has been shown to reflect the circadian period of the master pacemaker with cultured retinas from tau mutant hamsters exhibiting the same short period in melatonin expression rhythm as the locomotor activity rhythm under the direct control of the SCN (Green and Besharse, 2004).

Studies within different retinal cell types have shown clock gene expression of *Per1*, *Clock* and *Bmal1* mRNA within the inner retina of the mouse along with *Cry1* and *Cry2* in retinal ganglion cells, suggesting retinal oscillators may impact deeply on the circadian system as a whole through retinal clock/SCN clock 'cross-talk' (Green and Besharse, 2004, Guido et al., 2010).

1.6 Potassium Ion Channels

1.6.1 Potassium channels in neuronal excitability

In animal cells, ions cannot move freely across the cell membrane, requiring ion-specific pores and dedicated pathways in order to traverse the lipid bilayer. Potassium channels are transmembrane proteins structured to form a potassium ion (K^+) selective pore to facilitate the necessary passage of K^+ in and out of the cell under tight regulatory conditions. Physiologically, the potassium ion channels play a fundamental role in the maintenance of neuronal RMP. In addition to potassium, sodium and chloride ions also play a key role in membrane potential, with many channel types and subtypes reported (Goldstein et al., 2001).

There is selective permeability of K^+ across the cell membrane at RMP, producing a chemical gradient across the membrane with resultant movement of K^+ in an outward direction, down this gradient. In opposition, an electrical transmembrane gradient builds from the movement of charged ions generating a potential difference. Together, this is referred to as the electrochemical gradient of the ion, and is quantified by the Nernst equation. In mammalian cells, the voltage is typically around -60 to -90 mV, classed as negative by convention due to the increased negativity inside the cell relative to the outside. For the generation of action potentials, neuronal membranes must reach a minimum threshold of around -40mV in order to activate voltage-gated channels (Goldstein et al., 2001).

During neuronal action potential firing, the RMP increases to a level where voltage-gated sodium channels open, leading to rapid membrane depolarisation as sodium moves into the cell, known as the depolarising phase. At maximum depolarisation, sodium channels inactivate and voltage-gated potassium channels open to

facilitate the repolarising phase through potassium leaving the cell. The re-establishment of the RMP follows an afterhyperpolarisation (AHP) where potassium channels inactivate due to the membrane potential temporarily dropping to a lower value than the resting state (Bean, 2007). Once stabilised, the resting state is restored with both sodium and potassium channels closed, allowing further action potential firing to occur. See Figure 1.14.

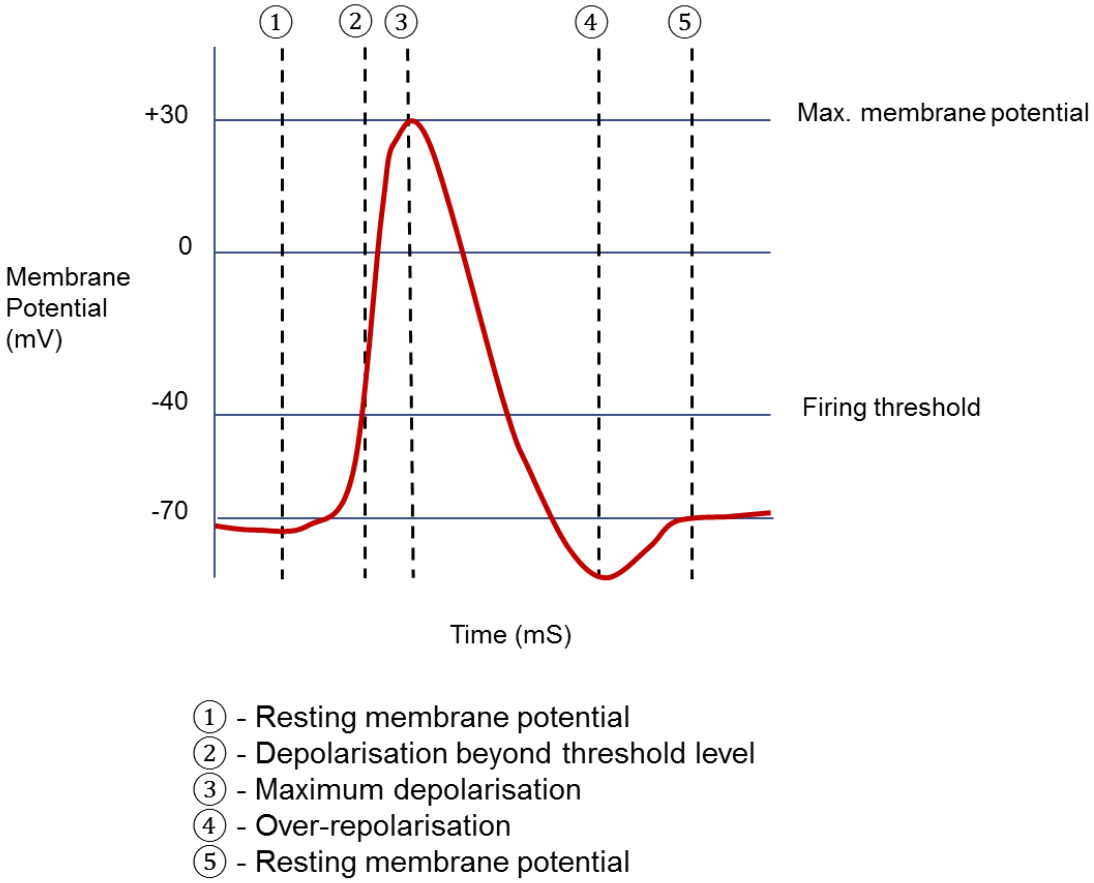

Figure 1.14: The actions of voltage-gated sodium (Na+) and potassium (K+) channels during action potential firing.

1- At resting membrane potential –Na+ and K+ channels remain closed 2- Depolarisation beyond threshold level - Na + channels open, K+ channels remain closed 3- Maximum depolarisation - Na+ channels close, K+ channels open 4- Afterhyperpolarisation - Na+ channels remain closed, K+ channels close 5- At resting membrane potential - Na+ and K+ channels remain closed, further action potentials may occur

The concentration of sodium and potassium ions in cytosol and extracellular fluid is restored through subsequent active transport mechanisms such as the sodium-potassium pump, utilising ATP to restore internal concentrations of low Na^+ and high K+ (Goldstein et al., 2001).The shape, rate and firing patterns of action potentials vary according to neuronal type and physiological role with many variations reported within the mammalian brain (Bean, 2007).

In mammals potassium channel proteins may contain 6, 4 or 2 transmembrane domains and combine as either tetramers or dimers to form a functional ion-selective pore. These structural differences are associated with the distinct properties of the channel such as being voltage-gated, ligand-gated or background 'leak' channels.

1.6.2 Two-pore domain background 'leak' potassium channels

Background 'leak' conductance is used to describe the current maintaining RMP whilst a cell is at rest. The existence of background leak currents was proposed by Hodgkin and Huxley in 1952, but it wasn't until 1995 that the first two-pore-domain potassium (K_{2P}) channel was fully characterised by cloning studies of the budding yeast *Saccharomyces cerevisiae*. (Goldstein et al., 2001). The discovered 'TOK-1' subunit, predicted to have two pore regions and eight transmembrane domains, was revealed in the sequence database leading to further investigations into the presence of K_{2P} background leak channels elsewhere. (Goldstein et al., 2001).

Further research has shown an individual subunit of a mammalian K_{2P} channel to consist of four transmembrane domains (known as M1-M4) along with the two pore loops (P1 and P2). See Figure 1.15. From these subunits, functional channels are formed by dimerisation - either *homo* or *hetero*, to give a single potassium-selective conductance pore (Czirjak and Enyedi, 2002, Aller et al., 2005). This configuration is unusual in comparison with other groups of potassium channels with single pore (P) loop subunits, combining as a tetramer to produce the functional pore (Bayliss and Barrett, 2008).

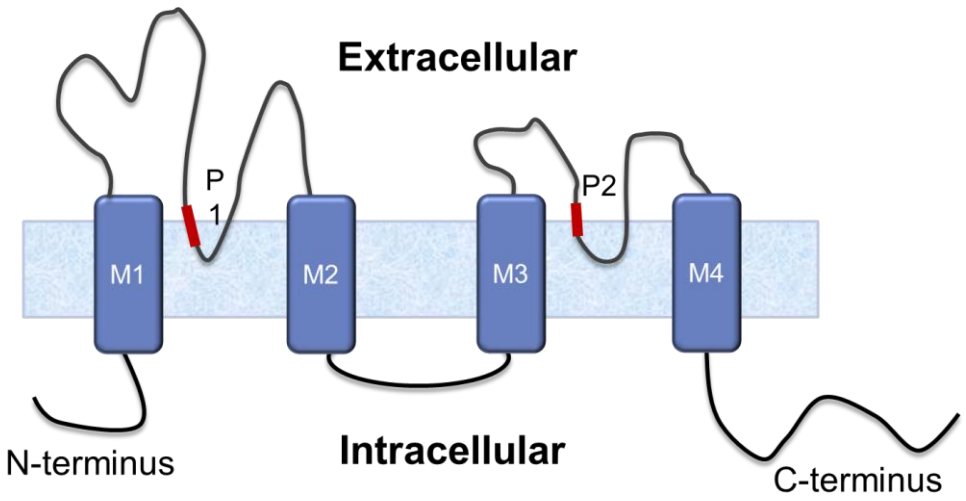

Figure 1.15: The generalised structure of a two-pore-domain potassium (K_{2P}) channel subunit.

Transmembrane domains are shown numbered M1-M4, with pore regions P1 and P2.

In contrast to voltage-gated K+ channels, all members of the K_{2P} family lack the voltage-sensing S4 transmembrane domain thereby having open probability which is largely voltage-independent. This property allows outward leak currents at resting potential conditions (Brown, 2000). However, the leak conductance is not simply seepage of ions, but a deliberate flux through selective pathways to allow control of cellular excitability by stabilisation of membrane potential (Goldstein et al., 2001).

The presence of K_{2P} channels is widespread in mammalian tissue from early development through to maturity with essential roles in regulating neuronal transmission and function (Aller and Wisden, 2008, Talley et al., 2001, Goldstein et al., 2005). The ability of K_{2P} channels to activate instantaneously over a wide voltage range facilitates the shaping of action potential duration, frequency and amplitude (Goldstein et al., 2001, Zanzouri et al., 2006).

Increased background leak currents result in stable, hyperpolarised cells below firing threshold through potassium leaving the cell - in some respects this action is similar to the repolarisation stage of action potential firing. Decreased leak current is associated with depolarisation and excitation of neurons, as prevention of potassium efflux leads to a build-up of potassium within the cell. Under usual physiological conditions, ionic gradient is maintained at a level of low intracellular sodium/high intracellular potassium through active transport via the sodium-potassium pump. However, when intracellular potassium concentration is very high and extracellular low, a larger outward current of potassium ions results to regulate excitability as the RMP is drawn closer to the threshold for action potential firing (Goldstein et al., 2001).

Similar to other ion channel currents, regulation of background leak conductance is achieved through expression levels and probability of pores being open. Far from being constitutively active, K_{2P} channels are dynamic modulators of membrane potential (Talley et al., 2003). Under physiological conditions of high intracellular/ low extra cellular potassium levels, K_{2P} channels show greater outward rather than inward current through movement of K^+ movement down the concentration gradient. The resultant negative charge within the cell eventually limits further K^+ flux, leading to a state of equilibrium where efflux equals influx (Goldstein et al., 2001). The functionality of K_{2P} channels is kept under strict regulation by a number of physiological mediators. These include pH, lipids, heat, mechanical stretch, nitric oxide and calcium levels and the actions of G-protein-coupled-receptors (Goldstein et al., 2005, Lotshaw, 2007). These properties alter the open probability of the channels and therefore affect processes as diverse as neuroprotection, depression, regulation of aldosterone production and pulmonary vasoconstriction (Mathie et al., 2010a).

Additionally, chemical stimuli such as general anaesthetic agents, cannabinoids, zinc, barium and ruthenium red have also been demonstrated to regulate K_{2P} channels (Mathie et al., 2010a, Linden et al., 2007, Lotshaw, 2007, Mathie and Veale, 2007).

1.6.3 The K_{2P} channel family

To date, there are 15 mammalian genes encoding K_{2P} channels, divided into seven subfamilies based on similarity of structure and/or function along with common evolutionary development. See Figure 1.16.

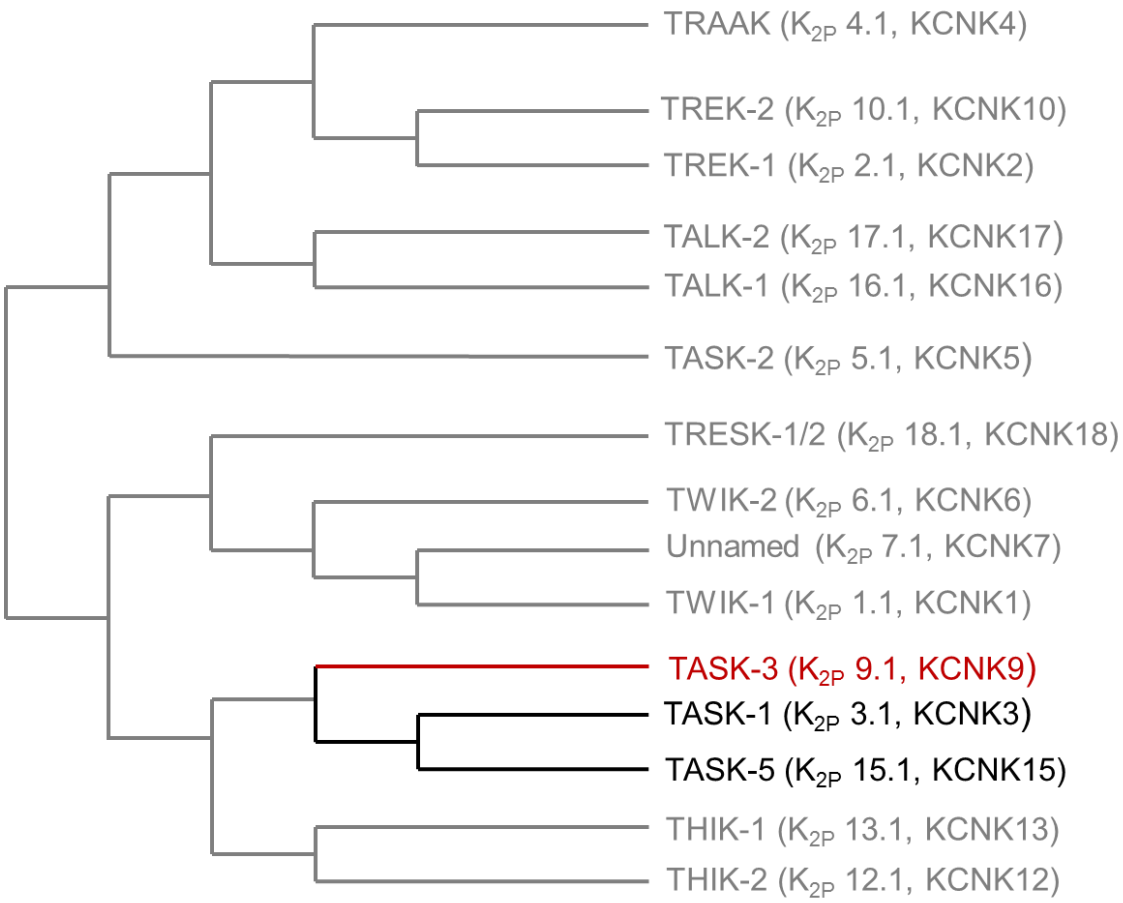

Figure 1.16: The evolutionary tree of the K_{2P} family

The 15 members of the K_{2P} family are shown with common nomenclature from phylogenetic analysis (adapted from Goldstein et al., 2005). Close members of the TASK subfamily are shown in black with TASK-3 highlighted in red.

Note: TASK-2 is not considered a 'true' member of the TASK family due to AA sequencing and physiological properties and is therefore shown in grey.

During the discovery of K_{2P} channels many different notations were used, but now they are commonly known as the TWIK (Tandem of pore domains in a weak inward rectifying K^+ channel) , TREK (TWIK-related K^+ channel), THIK (tandem-pore domain halothane inhibited K +channel) , TALK (TWIK-related alkaline pH activated K^+ channel) , TRESK (TWIK-related spinal cord K^+ channel), TRAAK (TWIK-related arachidonic acid-stimulated K^+ channel) and TASK (TWIK-related acid-sensitive K^+ channel) subfamilies (Enyedi and Czirjak, 2010).

K_{2P} family members have been shown to exhibit distinct differences in their inhibition, excitation and distribution in tissues, thought to directly relate to their specific physiological roles (Lotshaw, 2007). As yet, not all K_{2P} channels have functional roles assigned to them, but from those that have, there is much physiological diversity (Duprat et al., 2007).

In addition to differences in their roles and tissue distribution, subfamilies also show differences in their amino acid sequences. Some members of the same family share much homology, for example TASK-1 and TASK-3 sharing 54% identity in amino acid sequence, whilst TASK-3 and TASK-2 share only 30%, a similar amount to that with members of other subfamilies (Kim et al., 2000).

1.7 The TASK-3 Channel

1.7.1 The TASK family

The name 'TASK' is a widely-adopted acronym for TWIK-related Acid-Sensitive K^+ reflective of the high sensitivity of this K_{2P} subfamily to extracellular pH. Following much characterisation of channel properties through electrophysiological studies, the mammalian TASK family is currently limited to TASK-1, TASK-3 and TASK-5. Previous members, TASK-2 and TASK-4 are now considered to be a closer match to the TALK subfamily (Czirjak and Enyedi, 2002, Goldstein et al., 2005, Lotshaw, 2007). Despite an initial lack of consistency in naming K_{2P} channels in early investigations, the standardised formal nomenclature for TASK-1, 3 and 5 have now been defined as $K_{2P}3.1$, $K_{2P}9.1$ and $K_{2P}15.1$ respectively (Goldstein et al., 2005).

Functional channels comprise two subunits and may be formed from two TASK-3 subunits, a TASK-3 homomer, or alternatively with a TASK-1 subunit to form a TASK-1/TASK-3 heteromer (Czirjak and Enyedi, 2002, Goldstein et al., 2005, Lotshaw, 2007).

1.7.2 Structure and properties of TASK-3

Structurally the TASK-3 subunit has a short N-terminus, and long C-Terminus typical of K_{2P} channel proteins with a long extra-cellular pre-core region within the subunit known as the M1P1 loop (Kim et al., 2000). TASK family members contain a conserved histidine residue (His98) immediately after the first pore sequence for channel inhibition by extracellular acidification (Sabbadini and Yost, 2009). Mutation studies have confirmed that in TASK channels, the His-98 residue is also involved in channel regulation by zinc, in a mechanism referred to as the zinc block

(Clarke et al., 2008, Sabbadini and Yost, 2009). This unusual action, which differs between TASK-3 and TASK-1 according to extracellular pH, has been shown to directly regulate channel activity (Clarke et al., 2004, Clarke et al., 2008). The binding of zinc is most potent when residues from both subunits of a TASK-3 homomer form the binding site in conjunction with Glu 70 residues, with TASK-1/TASK-3 chimeras showing insensitivity to zinc ions (Clarke et al., 2008). Further, the Glu 70 residue within the M1P1 loop is thought to be responsible for the selective inhibition of TASK-3 channels by ruthenium red (Duprat et al., 2007).

Contrary to other TASK family member's voltage-independence, TASK-3 has been shown to exhibit voltage-dependent gating (Mathie et al., 2010a). However, under mammalian physiological states, this channel maintains an outwardly-rectifying steady-state current/voltage relationship with instantaneous activation (Lotshaw, 2007).

With the TASK-3 protein having the role of an ion channel, membrane surface expression is essential for functionality. The transport of the protein is reliant on an association with 14-3-3 protein in order to be released from the endoplasmic reticulum, following translation. Conversely, interaction of TASK-3 with COP1 leads to a decreased surface expression level and accumulation of this protein in the endoplasmic reticulum. The advancement/detainment provides an additional, specific mechanism for TASK-3 regulation (Mathie et al., 2010b).

1.7.3 Regulation of TASK-3 currents

K_{2P} channels are strictly regulated by a variety of physiological agents including G protein-coupled receptor (GPCR) pathways and protein kinases. The most commonly occurring G-protein mediated regulation appears to be $G\alpha_q$ inhibition of TASK and TREK subfamilies (Mathie, 2007). Inhibition of TASK conductance by a variety of $G\alpha_q$-coupled receptors has been reported including glutamate, serotonin and acetylcholine (Kettunen et al., 2003, Hopwood and Trapp, 2005, Mathie, 2007). The exact mechanism of TASK-3 inhibition by $G\alpha_q$ mediated pathways remains unclear but is thought to occur either through direct binding to the TASK-3 channel or indirectly through second messenger action of phospholipid PIP_2 from phospholipase C (PLC) activity (Mathie, 2007, Kettunen et al., 2003, Chen et al., 2006).

Further, sequence analysis of the TASK-3 protein has revealed several sites for protein kinase C (PKC) phosphorylation within the C terminus (Veale et al., 2007). PKC activity has been demonstrated to inhibit TASK-3 current in a calcium-dependant manner *in vitro* thereby revealing an alternative regulatory mechanism in addition to $G\alpha_q$ action (Veale et al., 2007, Chen et al., 2006).

1.7.4 Physiological roles of TASK-3

In contrast to early reports stating a general wide expression of TASK-3 channels in mammals, including kidney, liver, lung, colon, stomach etc., later studies have confirmed variation in this protein distribution by species, with TASK-3 being almost exclusively confined to the central nervous system in mice (Kim et al., 2000, Goldstein et al., 2005). During murine foetal development, TASK-3 is strongly expressed in the CNS from an early stage (Aller and Wisden, 2008). Furthermore,

postnatally, TASK-3 is one of the genes dominating development of the brain and spinal cord where it is thought to influence brain/nervous system development through control of membrane potential (Aller and Wisden, 2008).

Studies in cerebellar granule neurons (CGNs) have shown TASK-3 expression to increase during maturation following migration of to their adult position (Zanzouri et al., 2006). This governance in TASK-3 expression is considered to play a role in the transition of immature neurons to their mature state during development.

The presence on TASK-3 channels within the CNS is essentially to set neuronal RMP. Under physiological conditions the increased potassium permeability of the cell membrane results in a net outward flow of K^+. This in turn leads to hyperpolarisation of the neuron away from action potential firing threshold and subsequent reduced cellular excitability (Goldstein et al., 2001, Patel and Honore, 2001). In vitro studies in CGNs have demonstrated TASK-3 ablation results in RMP being on average 10 mV more depolarised than Wild Type controls (Brickley et al., 2007). In the absence of TASK-3, cells were incapable of supporting sustained high-frequency action potential firing and exhibited marked accommodation (Brickley et al., 2007). Further, this study reveals TASK-3 currents play a role in shaping action potentials in addition to firing regulation, with ablation of functional channels resulting in a reduction in AP amplitude with increased width. These properties were not observed following TASK-1 ablation (Brickley et al., 2007, Aller et al., 2005).

Reduced neuronal excitability from TASK-3 conductance also has a major effect on transmission of excitory neurotransmitter glutamate. Hyperpolarisation of RMP increases the voltage-dependant Mg^{2+} block on postsynaptic ionotropic NMDA

receptors, thereby attenuating NMDA-mediated transmission (McBain and Traynelis, 2006). Moreover, the metabotropic glutamate receptors (mGluR) acting as modulators of glutamate-induced responses have been shown to act through TASK-3 channels. Following glutamate release, the activation of G_q-coupled Group I mGluRs inhibit TASK-3 conductance which leads to potentiation of glutamate-mediated depolarisation and consequently, increased action potential firing (Chemin et al., 2003). The mechanism involved in the block of TASK-3 channels is thought to be through second messenger PIP_2 depletion within the PLC signalling pathway as TASK-3 has been demonstrated to be sensitive to levels of this phospholipid (Chemin et al., 2003).

Along with expression within the brain, K_{2P} channels have been identified within retinal glial cells, exhibiting a 'TASK-like' conductance during electrophysiological recordings. Despite low levels of TASK-3 mRNA detected within the rat glial cells the role of TASK currents, comprising TASK-1, TASK-2 and TASK-3, within these cells are considered to be diverse and significant. Suggested contributions include reduction of osmotic swelling and clearance of excess extracellular K^+ in addition to maintenance of RMP (Skatchkov et al., 2006).

Aside from influencing neural excitability through stabilisation of RMP, TASK-3 is also known to have a role in cell apoptosis. High expression of this channel leads to K^+ dependent apoptosis through excess efflux of K^+, resulting in low intracellular levels (Zanzouri et al., 2006). TASK-3 has been found to be over-expressed in several cancerous conditions including breast, lung, colon and metastatic prostate tumours (Zanzouri et al., 2006).

Much research into the distribution and functionality of mammalian TASK-3 channels has centred on the murine gene, located on chromosome 15 (Talley et al., 2001, Goldstein et al., 2005, Brickley et al., 2007, Aller et al., 2005). The production of a specific knock-out model for this gene has facilitated further examination and understanding of the role of this potassium background leak channel in isolation (Brickley et al., 2007, Mulkey et al., 2007, Sabbadini and Yost, 2009).

1.7.5 TASK-3 knock-out mouse models

To date, two TASK-3 KO murine models have successfully been produced through homologous recombination targeting either the first or second exon of chromosome 15 to eliminate channel structure and function (Brickley et al., 2007, Mulkey et al., 2007). The production of these global KO models has facilitated in vivo investigations into behavioural and pharmacological properties of this channel in isolation.

Due to the known presence of TASK-3 in the CNS, with high expression within the cerebellum and regions of the thalamus, research has largely been centred on balance and behaviour (Talley et al., 2001, Marinc et al., 2014, Linden et al., 2007, Gotter et al., 2011). Research has revealed the behavioural phenotype of the TASK-3 KO mouse to include impairment in working memory, cognitive ability and balance despite behaviour being generally unremarkable (Linden et al., 2007, Brickley et al., 2007, Gotter et al., 2011). Assessment of mood through tail suspension and forced swim tests also exposed a lack of immobility indicative of decreased despair in the absence of TASK-3 (Gotter et al., 2011).

Measurement of locomotor activity by infra-red beam break analysis has revealed TASK-3 KO mice to have significantly greater nocturnal activity than wild type

controls (Linden et al., 2007, Gotter et al., 2011). This increase in motion, along with reported fragmented sleep episodes, may be suggestive of TASK-3 currents contributing to circadian rhythm control (Linden et al., 2007, Pang et al., 2009). The behavioural differences seen in these studies are thought to be a consequence of altered membrane potential creating a change in neuronal excitability within the regions of the brain where TASK-3 is expressed (Sabbadini and Yost, 2009).

Pharmacologically, the TASK-3 KO mouse has been shown to have a reduced sensitivity to inhalational anaesthetics halothane and isofluorane at clinically relevant concentrations whilst the sensitivity to local anaesthetic agent lidocaine remains unaltered (Linden et al., 2007). These findings tie in with previous reports where activation of K_{2P} channels by volatile anaesthetics such as halothane lead to hyperpolarisation of relay neurons (Meuth et al., 2003). The shift in membrane potential out of functional range for action potential firing results in a block in transfer of sensory and motor activity which in turn leads to a state of analgesia, loss of awareness and suppressed motor activity (Meuth et al., 2003).

Additional research exploring potential targets for depression has demonstrated an absence of antidepressant effects from the drug fluoxetine in TASK-3 KO mice, indicative of TASK-3 channels being directly involved in this therapeutic pathway (Gotter et al., 2011).

1.7.6 The Role of TASK-3 in mammalian circadian rhythm regulation

TASK-3 K^+ channels are present in high concentration in several areas of the mammalian brain, particularly the cerebellar granule neurons, the SCN and raphe nuclei (Talley et al., 2001, Marinc et al., 2014). With the SCN being the confirmed site of the master pacemaker, it is plausible therefore that these channels may play

a crucial role in the regulation of neural excitability within the biological clock and in doing so, have major effects on circadian rhythm regulation.

Electrophysiology studies have demonstrated SCN neurons to exhibit robust rhythms in RMP in constant darkness. However, following application of tetraethyl ammonium (TEA), a block of traditional K^+ currents, a rhythm in K^+ current amplitude persists (Kuhlman and McMahon, 2006). As K_{2P} channels are insensitive to traditional K+ blockers including TEA it is likely that this current within the SCN is due to leak conductance via K_{2P} channels (Lotshaw, 2007). Additionally, TASK-3 is known to be expressed highly in this region, suggesting this channel may play an essential role in the regulation of SCN RMP and subsequently, neural excitability.

Additionally, a recent study has considered the role of background leak channels in regulating SCN neuronal activity through neuronal redox state. As transcription of clock genes is known to be sensitive to metabolic changes in reduction and oxidation, it follows that the circadian clock maybe subject to the redox state of neurons within the pacemaker. The findings from this investigation conducted in rodents, found a circadian pattern of daytime reduced state/depolarised RMP with a contrasting night time oxidised state/hyperpolarised RMP (Wang et al., 2012). These findings were further characterised through the use of a transgenic KO for clock gene *Bmal1*, demonstrating the role of this gene in circadian redox state oscillations. The use of specific potassium current blockers supports the background leak channels as a target for this regulation (Wang et al., 2012).

Studies isolating individual K_{2P} channel types have revealed TASK-1/TASK-3 channels provide the principal constituents of sleep-wake response through conductance (Meuth et al., 2003). During the sleep process, oscillatory activity is

of low frequency with rhythmic bursts of action potentials in thalamocortical relay neurons. In contrast, during wakefulness, the frequency is high with sequences of single action potentials (Meuth et al., 2003). During transition from sleep to wakefulness there is a characteristic change in frequency of oscillatory activity by electroencephalogram (EEG) accompanied by a depolarisation of membrane potential brought about by a decrease in leak conductance (Meuth et al., 2003). But where decreased leak currents exist, for instance in the TASK-3 KO mouse, it is likely that distinct differences in sleep-wake transitions will be observed due to lack of ability to decrease the already low background leak current. This hypothesis was explored using electroencephalogram (EEG) recordings from a TASK-3 KO mouse model. Here a disrupted, fragmented sleep behaviour with changes in REM sleep patterns was reported (Pang et al., 2009).

However, this movement from sleep to wakefulness (and vice versa) is brought about via SCN neural output rhythms which present as the overt circadian phenotype in locomotor activity studies. The timing of sleep and activity are driven by the circadian clock and reflect either entrainment to exogenous stimuli or, where conditions are held constant, are driven by endogenous clock signals. Therefore it is feasible TASK-3 channels may play a role in the process of sleep itself, but also the circadian behavioural output rhythm.

Additionally, several neurotransmitters, known to play a role in the regulation of sleep and arousal, have been shown to alter their release as a consequence of TASK-3 channel modulation (Gotter et al., 2011). It is clear, therefore, that the role of this channel in the regulation of sleep-wake rhythms is multifactorial.

The Present Study

This project examines the role of TASK-3 K_{2P} channels in the regulation of circadian rhythms through the use of a transgenic KO mouse model.

With a focus on light, this research investigates retinal decoding of irradiance and subsequent molecular changes within the SCN, through to the behavioural output rhythms representative of the overt circadian rhythm. Additionally, behaviour has been studied in the absence of light, DD, for examination of free-running circadian rhythms dictated purely by the biological clock. Together, these investigations explore the physiological consequence of global TASK-3 ablation in relation to photic and endogenous regulation of the biological clock.

Several *in vivo* studies have highlighted alterations in sleep cycles and nocturnal activity following TASK-3 loss, but have fallen short of elucidating the role of this channel in circadian photoentrainment (Linden et al., 2007, Pang et al., 2009, Gotter et al., 2011). Therefore the contribution of this channel in producing adaptive, predictive, robust daily rhythms, either aligned to environmental stimuli or intrinsically-generated, is yet to be uncovered. Further, *in vitro* studies have revealed the extent to which TASK- currents contribute to maintaining control of neuronal excitability and the impact on action potential firing properties in the absence of this channel (Aller et al., 2005, Brickley et al., 2007).

This work provides a further insight into the role of K_{2P} channels - highlighted as having therapeutic potential for pathologies as diverse as stroke, depression and migraine (Mathie and Veale, 2007, Lafreniere et al., 2010). TASK-3 specifically has been implicated in Birk Barel syndrome and the sleeping sickness associated with African trypanosome infections (Barel et al., 2008, Kristensson et al., 2010).

Through furthering our understanding of the role of this channel in physiology and behaviour it is hoped targeted therapies for these conditions may be developed with health, social and economic benefits.

2. TASK mRNA Expression in Wild Type Mice

2.1 Introduction

Potassium background leakage currents are known to exist across mammalian cell membranes when the cell is at rest. Under typical physiological conditions two members of the K_{2P} TASK subfamily of leak channels, TASK-1 and TASK-3, produce outwardly rectifying currents which influence neural excitability by the setting RMP (Goldstein et al., 2001, Patel and Honore, 2001, Lotshaw, 2007). In addition to forming homomers, TASK-1 and TASK-3 combine as heteromers in regions of co-localisation (Czirjak and Enyedi, 2002, Brickley et al., 2007)

In mice TASK-3 expression occurs almost exclusively within regions of the CNS where there is abundance within the cerebellum and a presence within many nuclei including the SCN (Talley et al., 2001, Lotshaw, 2007, Goldstein et al., 2005). Contrastingly, TASK-1 expression has a much wider distribution including high levels reported within heart, lungs, kidney and gastrointestinal tract in addition to specific regions of the CNS, but has low expression within the SCN (Talley et al., 2001, Aller et al., 2005, Lotshaw, 2007, Goldstein et al., 2005).

This work sets out to confirm the presence and relatively quantify *TASK* mRNA in tissues of interest by reverse-transcriptase real-time polymerase chain reaction (RT-PCR) in WT mice. The chosen tissues of SCN and retina are imperative to light-driven circadian rhythm regulation, with cerebellum and heart selected for TASK-3 detection sensitivity as these tissues are known to have high and low expression respectively (Talley et al., 2001, Kim et al., 2000). For TASK-1, the heart is reported to have very high expression with CNS expression generally low. Together, these expression assays will provide confirmation of variance between

TASK-3 and *TASK-1* gene expression within the circadian clock whilst determining presence of specific *TASK* transcripts within the retina. In the event of both *TASK* genes being present within a given tissue, it is plausible heteromers are performing a physiological role in WT mice which would fall on TASK-1 homomers to perform in the TASK-3 KO mouse model.

Additional investigations will establish whether *TASK-3* gene transcription within the SCN of WT mice exhibits a circadian pattern or is constitutively expressed over the 24 hour cycle. TASK-3 has been shown to be the most abundant K_{2P} channel within the master pacemaker in rodents and therefore the expression of this channel throughout the circadian cycle is of great relevance to the study (Goldstein et al., 2005, Talley et al., 2001, Marinc et al., 2014).

2.2 Experimental methods

2.2.1 Subjects

Wild Type (C57 BL/6J) mice were obtained from Charles River Laboratories (Kent). Mice 3-6 months of age were housed in polypropylene cages measuring approximately 34cm (l) x 16cm (W) x 13cm (h), either individually or in litter groups under 12:12 LD cycle (7am-7pm) for a minimum of 7 days prior to start of experiment. Food and water were available *ad libitum*.

All experimental procedures were performed with approval from the University of Kent Animal Welfare Ethics Review Board (AWERB) and in accordance with the Animals (Scientific Procedures) Act 1986.

2.2.2 Tissue retrieval

TASK gene expression: Mice were sacrificed by cervical dislocation at ZT 2-4 (where ZT12 corresponds to lights off). Eyes, brains and hearts were removed into chilled nuclease-free water, rinsed and dissected. Coronal brain slices revealed the SCN which was extracted by bespoke tissue punch and placed into RNAlater (Sigma, Gillingham, UK) along with isolated retinas, cerebellar tissue and heart tissue.

TASK-3 time course: Mice were sacrificed by cervical dislocation at selected time points of ZT 2, 6, 10, 16, 22. Brains were removed under room light for day sampling, or dim red light if during the night (ZT16, 22) and placed into chilled nuclease-free water with SCN extracted and placed into RNAlater as detailed above.

Samples were stored frozen at -80 C for subsequent preparation for measurement of TASK-1 and TASK-3 expression by real-time quantitative RT-PCR.

2.2.3 RNA isolation and cDNA synthesis

Total RNA was isolated from tissue extracts using TRI Reagent (Applied Biosystems, Warrington, UK). 400ng total RNA isolate was subjected to DNase treatment (Primerdesign, Southampton, UK) before being reverse transcribed by Nanoscript reverse transcription kit (Primerdesign, UK).

2.2.4 Gene expression analysis by Real-Time PCR

20 µL reactions were prepared in triplicate in a 96-well white plate (Alpha Laboratories, Hants, UK) comprising 10µL 2x SYBR Green Mix (Primer design, UK), 7µL nuclease-free water, 1µL sample cDNA and 1µL of each 0.5µM forward and reverse primers for gene of interest (Aller et al., 2005). See Table 2.1.

Gene ID	Primer sequence
TASK-1	F: 5'-CGGCTTCCGCAACGTCTAT-3' R: 5'-TTGTACCAGAGGCACGAGCA-3'
TASK-3	F: 5'-GACGTGCTGAGGAACACCTACTT-3' R: 5'-GTGTGCATTCCAGGAGGGA-3'
18S rRNA (Reference)	F: 5'CGCCGCTAGAGGTGAAATTC-3' R: 5'CGAACCTCCGACTTTCGTTCT-3'

Table 2.1: Primer sequences used for TASK gene expression by RT-PCR.

Reactions were run on a LightCycler 480 instrument (Roche Applied Sciences, Sussex, UK) with pre-incubation at 95°C for 5 minutes before 50 cycles of 95°C for 10s, 60°C for 30s, 72°C for 10s. Detection of fluorescence occurred at 80°C after each cycle.

Relative quantification of mRNA levels was determined using the $2^{-\Delta\Delta C_T}$ method where crossing point (C_T) of target gene in each sample is normalised to reference value (18S rRNA) to give a ΔC_T value (Livak and Schmittgen, 2001). For the time course comparison of ΔCT values between time-points relative to ZT2 (zero baseline value) provides the $\Delta\Delta C_T$ value. See appendix I. Statistical significance was determined using GraphPad Prism 5 software (San Diego, CA) by one-way analysis of variance (ANOVA) with Tukey's multiple comparison post hoc test. All data presented as mean ± SEM (standard error of mean) and statistical significance defined as being $P < 0.05$.

2.3 Results

2.3.1 TASK gene expression in WT mice

Quantification of *TASK-3* mRNA by RT-PCR within SCN, retina and cerebellum of WT mice relative to heart demonstrated a higher expression within the CNS compared to heart. The highest level of expression occurred in the cerebellum ($\Delta C_T = 2.705 \pm 0.549$), with strong expression in the SCN ($\Delta C_T = 1.201 \pm 0.498$) and a weaker expression within the retina ($\Delta C_T = 0.327 \pm 0.455$, n = 5). See Figure 2.1: A. In contrast, *TASK-1* mRNA expression within the same samples showed lower levels of expression in each of these tissues relative to heart with cerebellum closest in expression ($\Delta C_T = -2.301 \pm 0.476$) followed by retina ($\Delta C_T = -3.889 \pm 0.267$) and very low expression detected in the SCN ($\Delta C_T = -4.293 \pm 0.423$, n = 5). See Figure 2.1: B.

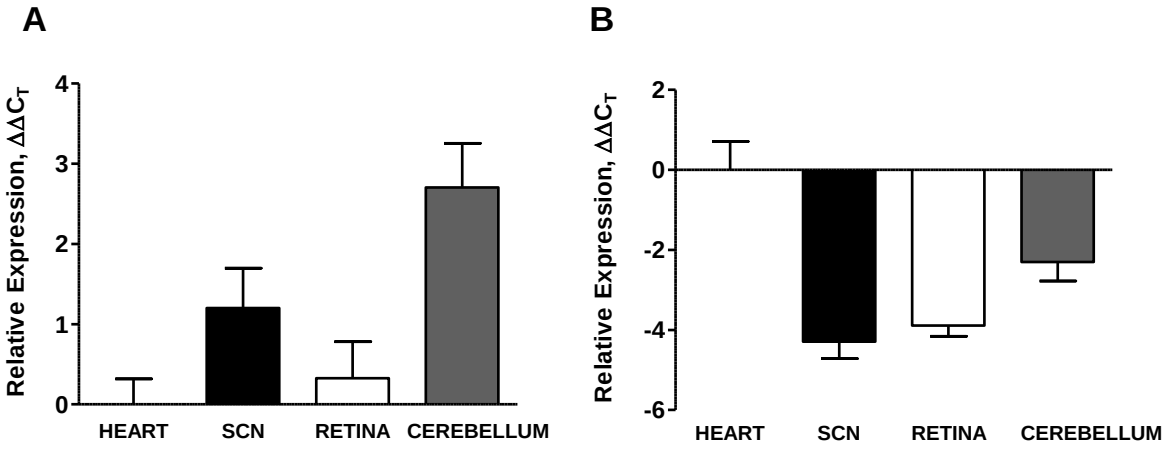

Figure 2.1: TASK mRNA expression in WT mice.

(A) Real-time PCR analysis of WT mouse *TASK-3* mRNA expression in the SCN, retina and cerebellum relative to heart, where expression is typically low (n=5).

(B) Real-time PCR analysis of WT mouse *TASK-1* mRNA expression in the SCN, retina and cerebellum relative to heart, where expression is typically high (n=5).

2.3.2 TASK-3 mRNA time course in WT mice

SCN sampling at specific time points over 24 hours with relative quantification by RT-PCR demonstrated a circadian variation in *TASK-3* mRNA expression within WT mice. Relative to early morning (ZT2) expression, a nadir was observed at midday, ZT6 ($\Delta\Delta C_T$ = -2.590 ± 0.184) before a return to similar levels of expression late morning ZT10 ($\Delta\Delta C_T$ = 0.911 ± 0.238), early night ZT16 ($\Delta\Delta C_T$ = 1.463 ± 0.154) and late night ZT22 ($\Delta\Delta C_T$ = 1.261 ± 0.522). ZT6 expression was significantly lower than all other time points (one-way ANOVA: $P < 0.01$, n=5). See Figure 2.2.

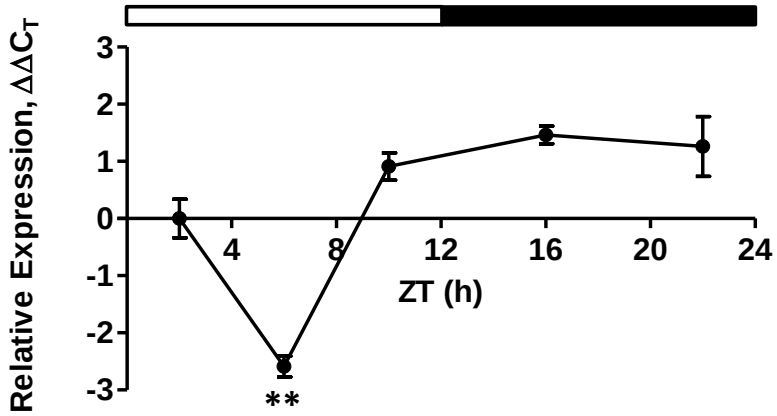

Figure 2.2: Time course of *TASK-3* mRNA expression within the WT mouse SCN.

***TASK-3* mRNA expression in the WT mouse SCN over 24 hours relative to early morning (ZT2) expression. Expression shows midday (ZT6) nadir, significantly lower than all other time points, one-way ANOVA $P < 0.01$. White and black bar represents hours of light and darkness respectively (n=5).**

2.4 Discussion

These findings support published research on the distribution of TASK-1 and TASK-3 channels within the rodent CNS and periphery whilst revealing the presence of *TASK-3* mRNA within the murine retina (Talley et al., 2001, Goldstein et al., 2005, Marinc et al., 2014, Kim et al., 2000).

The high levels of *TASK-3* mRNA expressed within the SCN with very low levels of TASK-1 are indicative of the prominence of this potassium leak channel in regulating the excitability of the circadian master clock. The circadian variation in TASK-3 expression observed under photoentrainment suggests a phasic role for this channel in governing RMP. With TASK-3 outwardly rectifying potassium current, and subsequently hyperpolarising RMP, a reduction in this conductance would lead to depolarisation and increased cell excitability (Brickley et al., 2007, Goldstein et al., 2005). Therefore this finding raises the question whether a midday nadir in TASK-3 expression is essential for maintaining increased daytime action potential firing within the SCN.

The next chapter considers the role of TASK-3 in light and clock-driven behaviour.

3 Examining Locomotor Activity in TASK-3 KO mice

3.1 Introduction

Mammals housed under a stable LD cycle adopt robust rhythms in activity and rest. The expressed behaviour arises through light-driven synchronisation of the clock to the light signal. In the absence of all time cues, including both light and non-light stimuli, daily cycles of activity and rest are driven endogenously by the circadian clock and the circadian rhythm is described as free-running.

In the laboratory environmental light can be manipulated to fully examine the effects of light on behavioural activity whilst all other environmental conditions are kept constant. This allows photoentrainment to be studied in relative isolation.

The experiments in this chapter will examine locomotor activity rhythms in TASK-3 KO and WT mice under a stable light-dark cycle and in constant darkness. With TASK-3 being highly expressed in the WT mouse SCN it is feasible to hypothesise the change in neuronal excitability within the biological clock will lead to disturbances in circadian rhythms (Talley et al., 2001).

The use of a stable 12:12h LD cycle will assess the impact of TASK-3 loss on light-driven behaviour and determine whether TASK-3 channels are essential for photoentrainment. Previous research under this lighting regime has shown the absence of TASK-3 to result in nocturnal hyperactivity, examined by the breaking of photo-beams (Linden et al., 2007, Gotter et al., 2011). Here locomotor activity will be examined in detail by wheel-running with measurement of intensity and phase angle of entrainment along with assessment of rhythm robustness and distribution of activity.

Following investigations under a stable LD cycle, a similar set of experiments will be conducted in the absence of light to fully explore the endogenous, free-running activity rhythm following TASK-3 ablation. Comparison of WT and TASK-3 KO activity intensity, endogenous period (tau) and rhythm robustness will demonstrate the contribution of TASK-3 K_{2P} channels in initiating and maintaining endogenous circadian rhythms.

The final investigations in this chapter explore re-setting of the clock by acute light stimuli. A light pulse delivered early in the subjective night when light is novel is known to induce a delay shift in clock phase in WT mice, clearly identifiable by a change in timing of activity onset (Pittendrigh and Daan, 1976b, Antle et al., 2009). These experiments use different light intensities to examine both clock resetting capability and sensitivity of TASK-3 KO mice relative to WT.

3.2 Experimental methods

3.2.1 Subjects

Male WT (C57 BL/6J) mice were obtained from Charles River Laboratories (Kent), with transgenic TASK-3 KO (TKO) mice bred and maintained as homozygotes under license. For genotyping see Appendix II. Mice were housed individually in polypropylene cages measuring approximately 34cm (l) x 16cm (W) x 13cm (h) fitted with a running wheel. Wheel revolutions were recorded in 1-minute bins using Chronobiology Kit (Stanford Software Systems, Santa Cruz, CA, USA) to produce actograms with percentile distribution. Food and water were available *ad libitum.* All mice were aged 2-4 months at start of each protocol detailed below.

All experimental procedures were performed with approval from the University of Kent Ethical Review Committee and in accordance with the Animals (Scientific Procedures) Act 1986.

3.2.2 Behavioural activity recording under 12:12 LD cycle

Experiments were conducted under controlled LD conditions to investigate light-driven locomotor activity by wheel running. Illumination within animal room provided by 2 fittings with paired T5 (152cm) fluorescent tubes producing light levels of approximately 350 lux/relative irradiance 3.0 x 10^{14} photons/cm^2/s at cage level. See Appendix III. Light intensity was measured by lux meter (R S Components, Corby, UK) and optical power meter (Thorlabs, Ely, UK). Lighting was controlled by timer to allow 12:12 programming of LD cycle with lights on between 7am and 7pm. All subjects were maintained under a standard 12:12h light-dark (LD) cycle for a minimum of 7 days prior to beginning of experiment.

Measurements for analysis were as follows:

(i) Daily locomotor activity: Means calculated from measurement of total daily revolutions for 10 days.

(ii) Percentage of activity in dark and light portions of 12:12 LD cycle: Percentage of total daily activity conducted during the light phase calculated from total daily revolutions completed within light and dark portions of the LD cycle for 10 days.

(iii) Phase angle of entrainment: Activity onsets measured for 14 days by eye-fit from timing of lights off on single-plotted actograms, with distance of onset from position of lights off converted into minutes. See Appendix IV.

(iv) Chi square periodogram amplitude: Mean Chi square periodogram amplitude calculated for 10 days using Chronobiology Kit auto-correlated data. See Appendix V.

(v) 24hr locomotor activity profile: 24-hour profile constructed from mean revolutions collected in 10-minute bins for 10 days.

Statistical significance was determined using GraphPad Prism 5 software (San Diego, CA) by student's *t* tests. All data presented as mean ± SEM (standard error of mean) and statistical significance defined as being $P < 0.05$.

3.2.3 Behavioural activity recording under DD cycle

To investigate behaviour in the absence of light, the animal room was maintained in constant darkness, DD, with health checks and feeding carried out under dim red light. All subjects were given a minimum of 7 days in DD for free-running behaviour to be established prior to beginning of experiment.

Measurements for analysis were as follows:

(i) Daily locomotor activity: Means calculated from measurement of total daily revolutions for 10 days.

(ii) Tau: Free-running period, tau, determined by linear regression lines placed by eye through daily activity onsets for 10 days.

(iii) Chi square amplitude: Mean Chi square periodogram amplitude calculated for 10 days using Chronobiology Kit auto-correlated data.

(iv) 24hr activity profile: 24-hour profile constructed from mean revolutions collected in 10-minute bins for 10 days.

Statistical significance was determined using GraphPad Prism 5 software (San Diego, CA) by student's t tests and One-way ANOVA with Tukey's multiple comparison post hoc test. All data presented as mean ± SEM (standard error of mean) and statistical significance defined as being $P < 0.05$.

3.2.4 Phase re-setting of the clock by acute light stimuli

(i) Aschoff type I protocol: Wheel running activity recorded and analysed for 7 days in DD to provide accurate individual circadian timings during established free-running.

On day 8, WT and TKO experimental groups were placed individually in a light-tight box at calculated CT14 (2 hours after activity onset from actogram) whilst remaining in home cage. A single 10 minute light pulse generated from 96 x white LEDs generating approximately 1000lux/6.7 x 10^{14} photons/cm^2/s relative irradiance was delivered before replacing mice into animal room under DD conditions for a further 14 days wheel running data collection. See Appendix III.

WT and TKO control group treated as per experimental group but with LEDs switched off throughout the pulse.

(ii) Aschoff type II protocol: Wheel running locomotor activity recorded for 7 days under a 12:12 hour LD for a stable synchronised rhythm with illumination provided by LED lighting generating approximately 2500lux/relative irradiance 1.83×10^{15} photons/cm^2/s at cage level. See Appendix III. On day 8 WT and TKO mice received a 20 minute light pulse at ZT14 from LEDs before being placed into DD for 14 days, followed by 14 days in 12:12 hour LD for re-entrainment. This protocol was repeated with reduced light intensities by neutral density filter at approximately 250 lux/relative irradiance 1.83×10^{14} photons/cm^2/s, and 25 lux/relative irradiance 1.83×10^{13} photons/cm^2/s. A final 'non-light' control pulse was conducted with LEDs switched off during the pulse.

Phase shifts for Aschoff type I protocol determined by linear regression lines fitted by eye through activity onsets on actograms before and after light/non-light pulse. For Aschoff type II protocol phase shifts determined by linear regression lines fitted through timing of lights off and activity onsets on actograms after light/non-light pulse. See Appendix IV.

For both protocols the first three days following pulse were disregarded as transients, with extrapolation of regression lines allowing distance between lines to be measured on day of pulse. Statistical significance was determined using GraphPad Prism 5 software (San Diego, CA) by student's *t* tests, one-way analysis of variance (ANOVA) with Tukey's multiple comparison post hoc test and two-way ANOVA. All data presented as mean ± SEM (standard error of mean) and statistical significance defined as being $P < 0.05$.

3.3 Results

3.3.1 Altered locomotor activity in TASK-3 KO mice under 12:12 LD cycle

When housed under a stable 12:12h LD cycle TKO mice exhibited marked differences in wheel-running behaviour compared to WT controls with a significantly lower number of revolutions being completed daily (WT = 7902 revolutions ± 1026, TKO = 1066 revolutions ± 454, student's *t* test: $P < 0.0001$) and an increased daytime activity, expressed as a percentage of total daily activity (WT = 5.33% ±1.23, TKO = 17.60% ± 2.83, student's *t* test: $P = 0.0006$, n=12). See Figures 3.1: A-C, The phase angle of entrainment was similar in WT and TKO mice with no significant difference in timing of activity onset relative to lights off (WT = -9.64 minutes ± 1.59, TKO = -3.61 minutes ± 4.11, student's *t* test: $P > 0.05$). However Chi-square analysis of locomotor activity, a marker of rhythm robustness by stationarity, revealed a significant reduction in rhythm amplitude in TKO mice relative to WT = 5917 ± 126.5, TKO = 3243 ± 469.3 (student's *t* test: $P < 0.0001$, n=12). See Figures 3.1: D, E.

A profile of locomotor activity over the 12:12h LD cycle highlights rhythm alteration and reduction in intensity in the absence of TASK-3 KO compared to the intact WT mouse (n=12). See Figure 3.2.

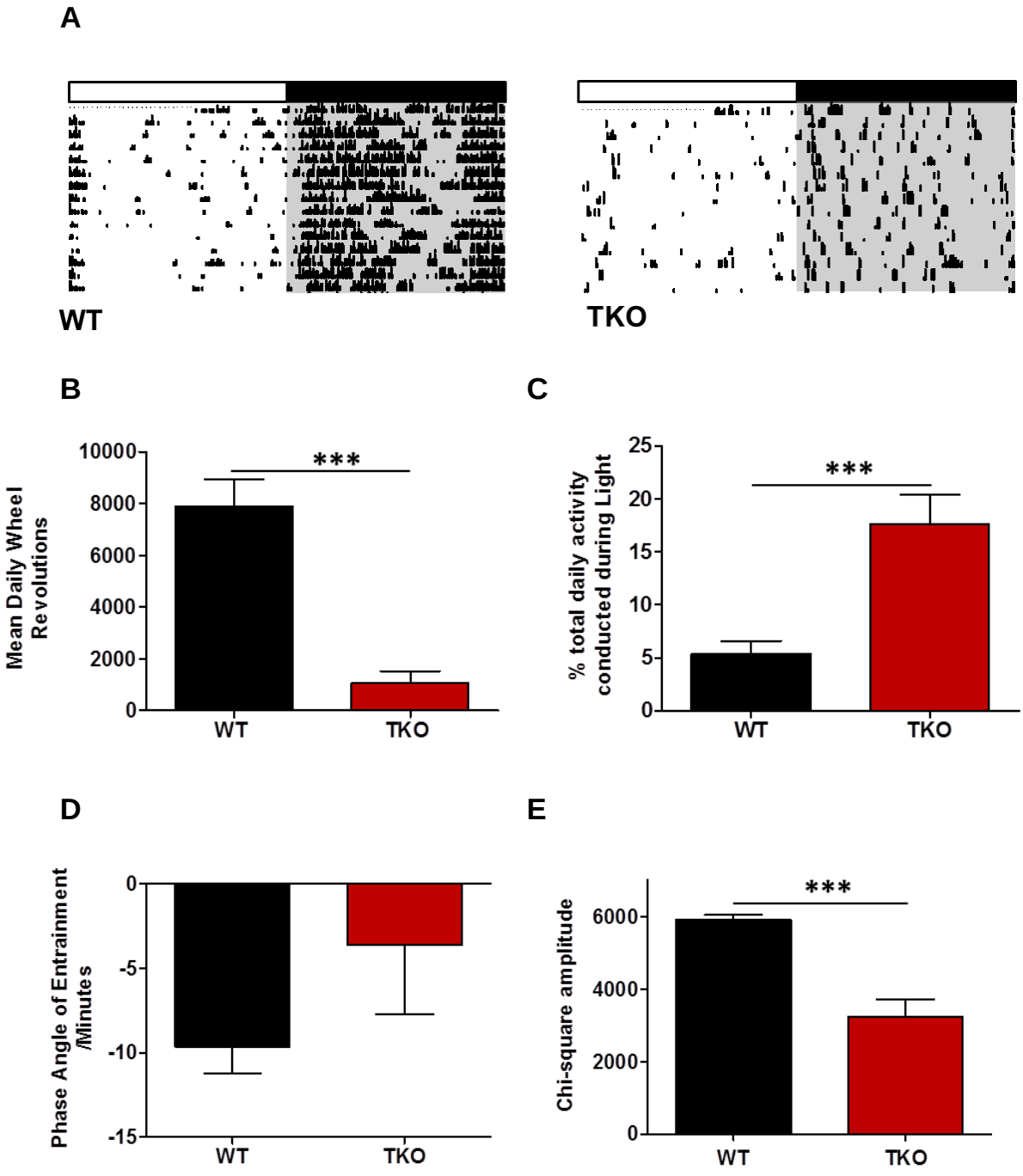

Figure 3.1: Locomotor activity under 12:12 LD cycle

(A) Representative actograms of WT and TKO mice demonstrate differences in intensity of wheel running activity under photoentrainment. Data presented as percentile distribution over 14 days, with horizontal bar signifying hours of light (white) and darkness (black).

(B) Mean wheel revolutions completed daily are significantly lower in TKO mice compared to WT, student's t test: $P < 0.0001$ (n=12), with (C) an exaggerated percentage of total activity completed within the light portion of the 24 hour cycle, student's t test: $P = 0.0006$ (n=12).

(D) Onset of activity relative to light cycle demonstrates there is no significant difference in phase angle of entrainment between TKO and WT mice, student's t test: $P > 0.05$ (n=12), whilst (E) analysis of daily locomotor activity by chi-square analysis reveals a significant reduction in TKO amplitude, student's t test: $P < 0.0001$ (n=12).

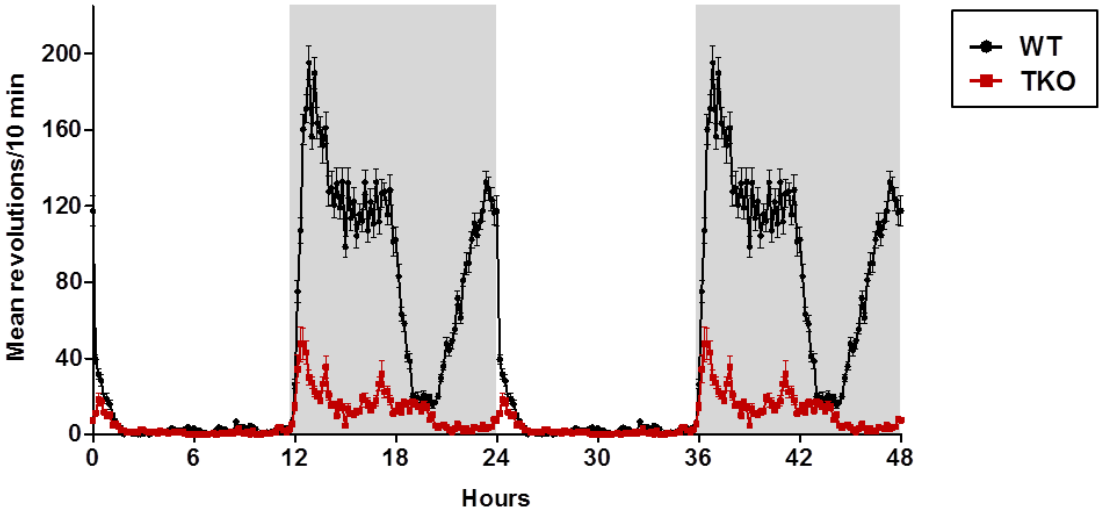

Figure 3.2: Locomotor activity profile over the 12:12h LD cycle

Wheel-running activity double-plotted over 24hours for TKO (red) and WT (black) mice under a stable LD cycle highlights distribution of activity relative to LD cycle. Data points represent mean values collected in 10 minute time bins (n=12).

3.3.2 Loss of TASK-3 impacts activity intensity and rhythm in constant darkness

In the absence of light TKO mice displayed an attenuated locomotor activity pattern relative to WT controls, producing significantly less wheel revolutions per day (WT = 5549 revolutions ± 1057, TKO = 474 revolutions ± 115, student's *t* test: $P < 0.0001$, n=12). Furthermore, TKO mice exhibited differences in their behavioural rhythms with a significantly lengthened free-running period, tau (WT = 23.89 hours ± 0.02, TKO = 23.96 hours ± 0.01, student's *t* test: $P = 0.006$) and diminished Chi-square amplitude (WT = 5026 ± 292.9, TKO = 1679 ± 175.3, student's *t* test: $P < 0.0001$, n=12). Comparison of Chi-square amplitude under 12:12h LD and DD conditions reveals a significant reduction in TKO amplitude when free-running compared to values under entrainment (One-way AVOVA with Tukey's post hoc test, $P < 0.01$). Contrastingly, there is no significant different in WT Chi square amplitude under LD and DD conditions (One-way AVOVA with Tukey's post hoc test, $P > 0.05$). See Figures 3.3: A-E.

A profile of locomotor activity over the circadian cycle in DD demonstrates the extent of reduction in activity in the absence of TASK-3. On resizing axes, the TKO rhythm is revealed. See Figure 3.4.

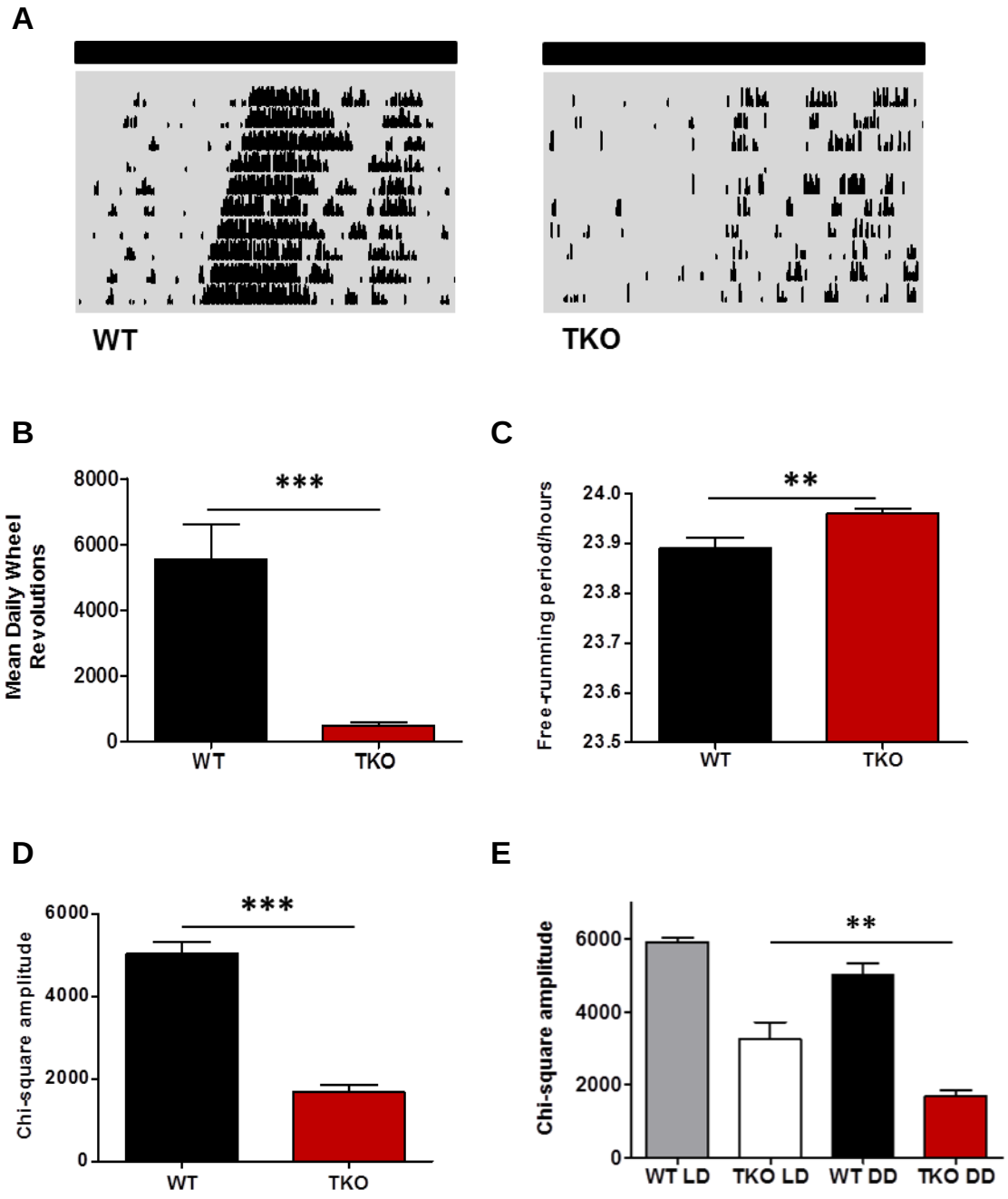

Figure 3.3: Locomotor activity in constant darkness, DD

(A) Representative actograms of WT and TKO mice showing differences in wheel running activity in the absence of light. Data presented as percentile distribution over 10 days, with horizontal black bar signifying continuous darkness.

(B) Mean wheel revolutions completed in 24 hours cycles of darkness are significantly lower in TKO mice compared to WT, student's t test: $P < 0.0001$ (n=12), with (C), a significantly lengthened free-running period, student's t test: $P < 0.01$ (n=12).

(D) Analysis of endogenous locomotor activity rhythms by reveals significant reduction chi-square amplitude in TKO mice relative to WT, student's t test: $P < 0.0001$ (n=12). (E) Comparison of WT and TKO chi square amplitude under 12:12h LD and DD reveals a significant drop in TKO endogenous rhythm amplitude compared to light-driven entrainment, one-way ANOVA with Tukey's post hoc test, $P < 0.01$, which is not seen in WT mice, $P > 0.05$.

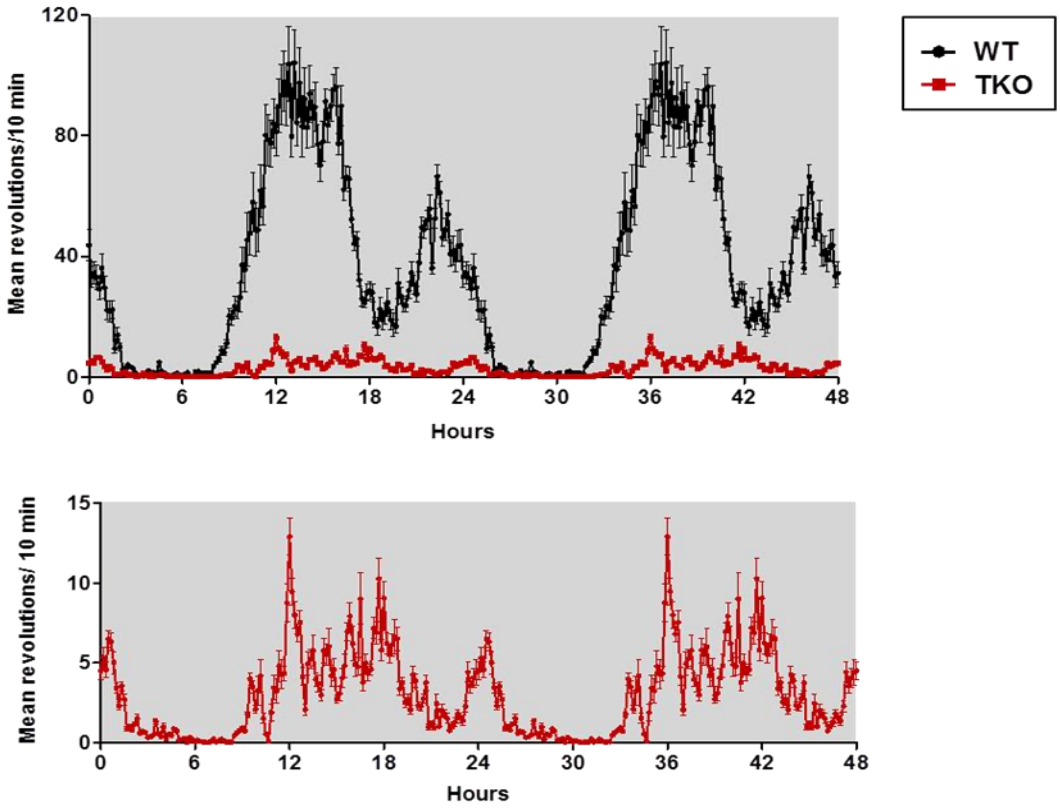

Figure 3.4: Locomotor activity profile over the circadian cycle under DD

Wheel-running activity double-plotted over 24hours for free-running TKO (red) and WT (black) mice in DD highlights inter-strain differences in activity intensity, and WT distribution of activity. TKO activity is only apparent when plotted on re-sized Y- axis. Data points represent mean values collected in 10 minute time bins (n=12).

3.3.3 TASK-3 ablation diminishes phase shifts to highest intensity light

The application of an acute saturating light pulse 2 hours after activity onset in free-running WT and TKO mice (Aschoff type I paradigm) produced a significantly greater phase shift in experimental groups compared to non-light controls. Following correction for non-light controls by deduction of non-light phase shift values (WT = 8.93 minutes ± 2.01, TKO = 14.88 minutes ± 4.65), WT and TKO mice exhibited light-induced phase shifts which were not significantly different (WT = 48.81 minutes ± 3.38, TKO = 30.36 minutes ± 7.59, Student's t test $P = 0.0506$, n = 6/group). See Figures 3.5: A-C.

Acute light pulses applied 2 hours after lights off in WT and TKO mice synchronised to the LD cycle (Aschoff type II paradigm) resulted in intensity-dependant delay phase shifts in experimental groups, with smaller shifts observed in non-light controls.

Following correction for non-light controls by deduction of non-light phase shift values (WT = 49.52 minutes ± 4.47, TKO = 47.14 minutes ± 5.37), WT mice exhibited significantly greater shifts in activity onset to saturating and low intensity light compared to TKO (2,500 Lux: WT = 72.19 minutes ± 3.33, TKO = 46.36 minutes ± 4.69, Student's *t* test $P = 0.0003$; 25 lux WT = 37.91 minutes ± 3.57, TKO minutes = 6.00 ± 5.83 Student's *t* test $P = 0.0002$). In contrast sub-saturating light resulted in shifts which were not significantly between WT and TKO mice (WT = 48.19 minutes ± 4.08, TKO = 37.86 minutes ± 5.63 Student's *t* test $P > 0.05$) n=8-12/group). Taken together, these results show significant variation by light intensity and within strains (Two-way ANOVA: Strain of mouse $P < 0.0001$, Light intensity $P < 0.0001$. See Figures 3.6: A-C.

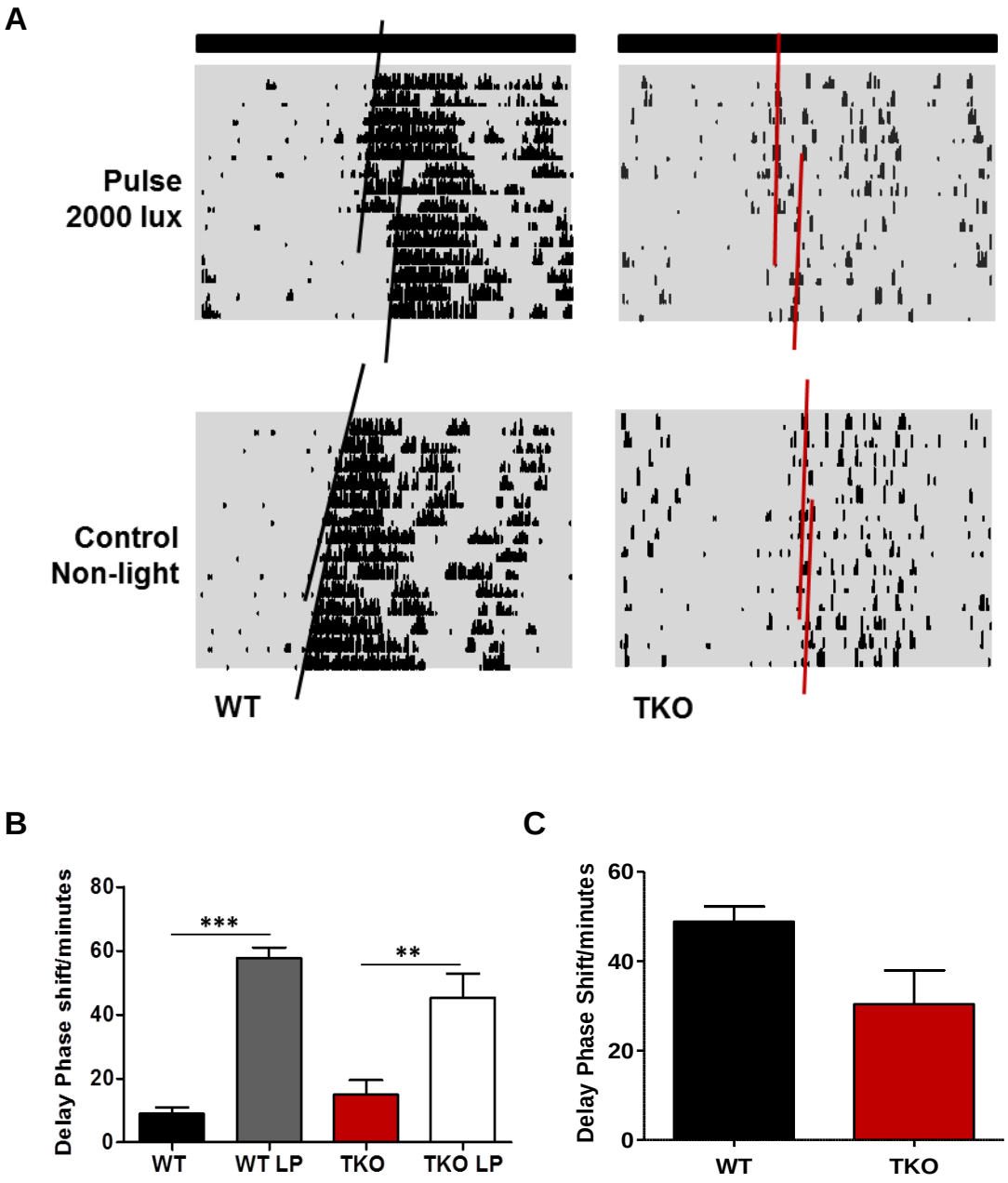

Figure 3.5: Phase shifts to saturating light by Aschoff type I paradigm.

(A)Representative actograms for WT and TKO mice demonstrating delay phase shifts in activity onset following an acute light pulse or non-light control pulse at CT14. Vertical black and red lines represent linear regression lines fitted by eye through WT and TKO activity onsets respectively, pre and post pulse.

(C) WT and TKO phase shifts to an acute saturating light pulse at CT14 by Aschoff type I paradigm are significantly greater than their respective non-light controls, One-way ANOVA with Tukey's post hoc test, $P < 0.01$ (n=6). (C) Data normalised to non-light control values reveals WT and TKO phase shifts are not significantly different, student's t test: $P > 0.05$.

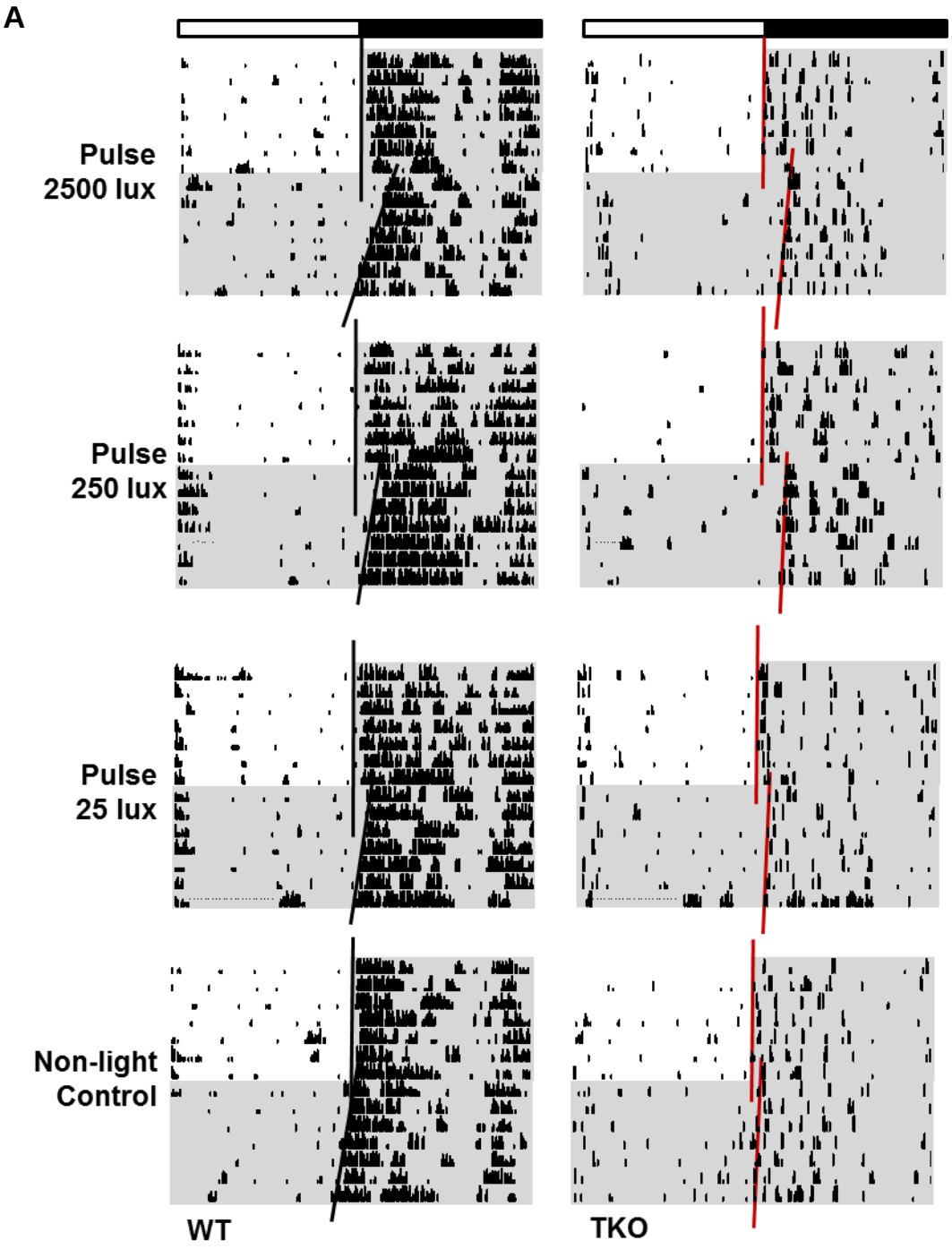
A
Pulse
2500 lux
Pulse
250 lux
Pulse
25 lux
Non-light
Control
WT
TKO

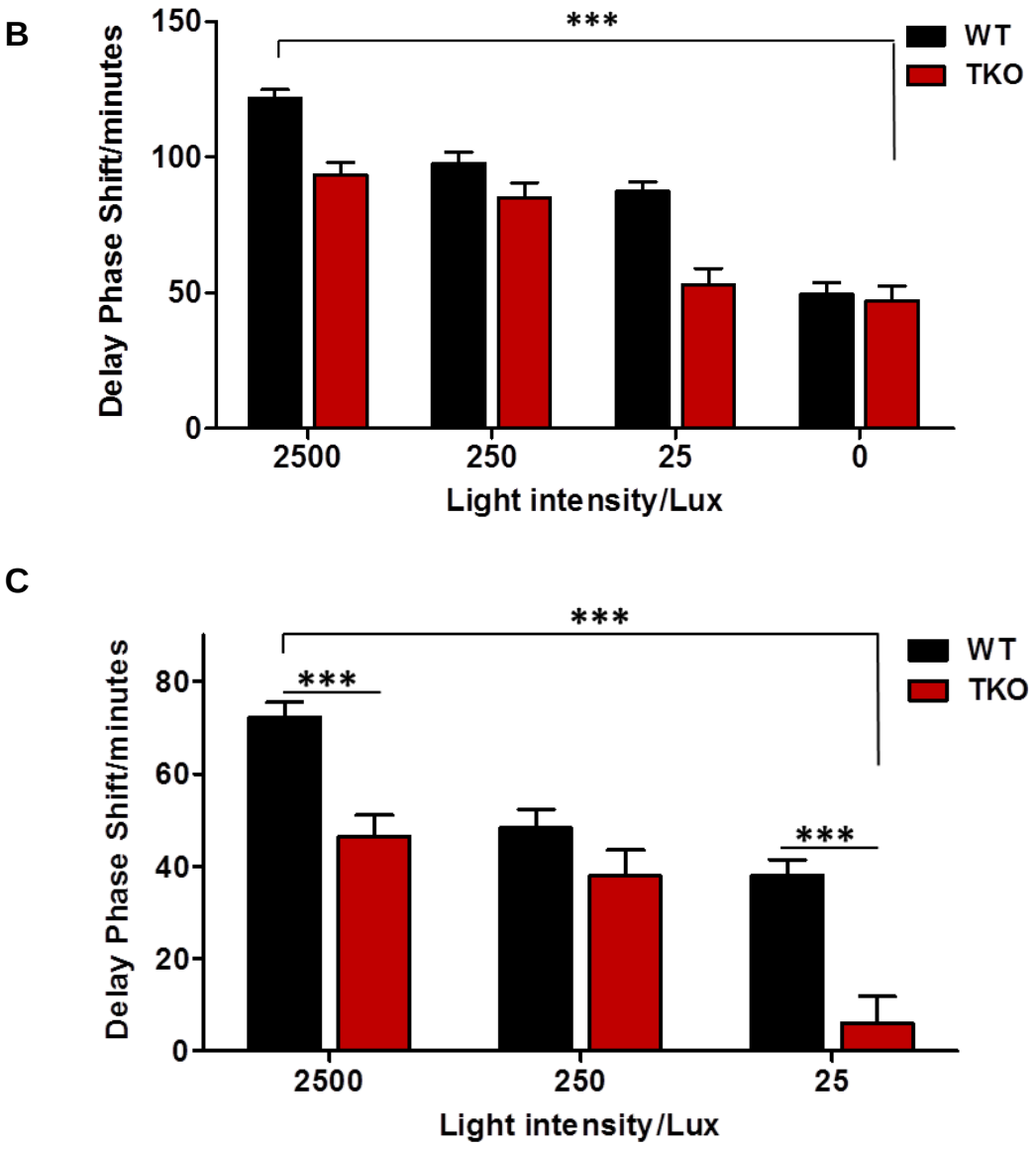

Figure 3.6: Phase shifts to saturating and non-saturating light by Aschoff type II paradigm.

(A)Representative actograms for WT and TKO mice demonstrating delay phase shifts in activity onset following an acute light pulse of 2,500, 250, 25 lux or non-light control pulse at ZT14. Vertical black and red lines represent linear regression lines fitted by eye through WT and TKO activity onsets respectively, pre and post pulse.

(B) Measured phase shifts in WT and TKO mice to acute light pulses at ZT14 by Aschoff type II paradigm show significant difference by strain and intensity, two-way ANOVA: $P < 0.0001$ (n=8-12). (C) Normalising data to non-light control values does not change the significant difference by strain and intensity, two-way ANOVA: $P < 0.0001$. Note WT mice exhibit a dose response to light intensity whilst TKO mice responses saturate at lower intensity light, Student's t test: 2,500 and 25 Lux, $P < 0.001$; 250 Lux, $P > 0.05$.

3.4 Discussion

This chapter has revealed significant alteration in TASK-3 KO locomotor activity under standard 12:12h LD cycles and in constant darkness. Surprisingly, under stable photoentrainment, TKO mice exhibited significantly reduced wheel-running, which was totally unexpected as this finding is in stark contrast to previously published data with significantly increased activity following global TASK-3 loss (Linden et al., 2007, Gotter et al., 2011). This outcome may be a consequence of differences in methodology, with previous research measuring activity by breaking of photo-beams as opposed to wheel-running. These two approaches are dissimilar in that beam-breaking will measure general movements within the cage including feeding and exploration, whereas wheel-running is a voluntary activity.

In addition to low intensity activity, TKO mice demonstrated exaggerated daytime activity which, again, differed to previous findings of increased nocturnal activity (Linden et al., 2007). Yet the loss of TASK-3 did not prevent synchronisation to the LD cycle as demonstrated by a similar phase angle of entrainment to WT mice. On closer inspection of activity distribution over the 24-hour cycle these results are suggestive of accurate detection of lights going off at dusk, but a lack of inhibition of activity at dawn.

Further examination of light-driven activity under by Chi-square analysis highlighted significantly reduced rhythm amplitude in TKO mice relative to WT. With Chi-square periodogram quantifying any extent of non-stationarity within a rhythmic process, this analysis suggests TASK-3 loss impacts the stationarity of the rhythm. However, the Chi-square periodogram evaluates robustness through variance in daily means and variance in daily variances (Refinetti, 2006).

Therefore any noise within the daily rhythm (variation in daily mean, amplitude or period) will decrease the maximal value. With TASK-3 mice having significantly reduced activity intensity, small daily variations in mean and amplitude are more pronounced than in WT mice where intensity is far greater. However, this statistic has been demonstrated to be dependent on the parameters of period, amplitude and waveform of the rhythm rather than mean levels per se, providing mean levels are stable over time (Refinetti, 2004). Therefore the results from this analysis suggest the absence of TASK-3 results in deterioration of rhythm robustness.

Studies of the endogenous rhythm under constant darkness revealed TASK-3 KO activity intensity to be lowered further in the absence of light suggesting light may act as a driver of activity in these transgenic mice. Interestingly the TKO free-running rhythm, tau, is lengthened compared to WT, indicating an alteration in the speed of the clock. Examination of TKO activity rhythm in DD by Chi-square analysis displays significantly lower amplitude to that under entrainment, whilst in WT mice the results are similar. It would seem, therefore, that TASK-3 loss has a greater impact on the stationarity and robustness of endogenous circadian rhythms compared to light-driven rhythms.

After exploring light-driven and endogenous locomotor activity, it is of interest to study the method by which light resets the biological clock. It is well established in mammalian circadian biology that the application of light at a time when light is novel leads to shifts in clock phase observed through changes in activity onset over the following days (Antle et al., 2009). Here, initial investigations in free-running WT and TKO mice in constant darkness (Aschoff type I paradigm) resulted in similar phase shifts following an acute light pulse delivered at ZT14. This data, therefore, suggests loss of TASK-3 does not impact clock resetting to light.

However, this paradigm relies on exact timings of light pulse delivery according to individual free-running rhythms, which can be challenging in TKO mice.

To overcome this difficulty an Aschoff type II paradigm was applied where all mice are housed under a stable LD cycle prior to the application of a light pulse 2 hours after lights off. Further, the use of differing light intensities under this paradigm allowed the sensitivity of clock re-setting to be explored. The size of observed phase shifts were intensity-dependant in both experimental groups, however, TKO mice appeared to have exhibit a decrease in sensitivity by a log unit of light when compared to WT shifts. At the brightest and dimmest light intensity, TKO phase shifts were significantly smaller than WT, with only sub-saturating light resulting in similar phase shifts between strains. These results suggest WT mice follow a dose response pattern whilst TKO mice saturate sooner, typically at sub-saturating light intensities. These observed differences in clock resetting may occur as a result of attenuated light detection and communication in the absence of TASK-3 or may relate to the clock mechanism itself and the lengthened daily period, requiring little adjustment to maintain synchrony with a 24-hour cycle.

The next chapter will further examine the impact of global ablation of TASK-3 with challenges to explore robustness, adjustment and adaptation of rhythms for clock synchrony during changes in environmental light.

4 Adapting to Changing Light

4.1 Introduction

The previous chapter highlighted key differences in circadian phenotype of TASK-3 KO mice compared to WT controls, with both light-driven and endogenous activity rhythms affected by TASK-3 ablation. The attenuated phase shifts to saturating and low intensity light suggests TASK-3 currents are essential for adaptation to environmental light cues at differing intensities. Additionally the lack of rhythm robustness in DD compared to LD, quantified by chi square analysis, demonstrates the role TASK-3 channels play in maintaining endogenous rhythms. This chapter explores the mechanism of clock resetting and photoentrainment further through a number of light challenges with a view to exposing the limitations of clock adjustment in the absence of TASK-3, thereby highlighting the role of this channel in photic regulation of the clock.

To assess the ability of the circadian system to entrain under diminishing lighting conditions locomotor activity will be studied under decreasing room illumination. This experiment will highlight any differences in sensitivity to light and its effects on driving locomotor activity rhythms. At a level where day and night transitions are no longer detected, mice are expected to go into a free-running rhythm as the environment is perceived as being in constant darkness.

The adjustment of the biological clock is initially examined by advancing and delaying a standard 12:12h LD cycle by 6 hours and monitoring WT and TKO rate of re-entrainment. This paradigm will assess the ability of the clock to adjust to a large difference in the timing of environmental light, representative of humans undertaking trans-meridian flights. Under these conditions, full re-entrainment

takes several days as the change in dawn and dusk signals are processed by the SCN and adjustments made in output rhythms to drive clocks in peripheral tissues (Davidson et al., 2009, Albrecht, 2012). Through monitoring the onsets and offsets of activity in TKO mice relative to WT, the rate of adjustment by re-entrainment can be assessed.

Following the rate of re-entrainment investigations, WT and TKO mice will be further assessed for clock adjustment by a seasonal adjustment paradigm. Here mice will be subjected to a 2-hour increase in photoperiod each week culminating in constant light conditions. This protocol will challenge the clock to confine activity to fewer and fewer hours of darkness thus reducing the duration of active period. The pliancy of the clock to effectively compress and decompress activity according to photoperiod is vital for seasonal adjustment with long summer, and short winter, days (Pittendrigh and Daan, 1976d). This paradigm will also highlight the ability of the TKO clock to track changes in the timings of dawn and dusk and adapt behaviour accordingly. These properties will be assessed through recording of locomotor activity throughout this process with measurement of phase angle of entrainment and duration of active period, commonly denoted as alpha (α).

The final stage of this experiment will provide information on period lengthening in the TKO mouse. This NIF response is known to occur in WT mice housed under constant light, LL, and provides further confirmation of effective irradiance detection and modification of clock gene expression leading to behaviour changes (Pittendrigh and Daan, 1976c, Spoelstra and Daan, 2008).

4.2 Experimental methods

4.2.1 Subjects

Male WT (C57 BL/6J) mice were obtained from Charles River Laboratories (Kent), with transgenic TASK-3 KO (TKO) mice bred and maintained as homozygotes under license. For genotyping see Appendix II. Mice were housed individually in polypropylene cages measuring approximately 34cm (l) x 16cm (W) x 13cm (h) fitted with a running wheel. Wheel revolutions were recorded in 1-minute bins using Chronobiology Kit (Stanford Software Systems, USA). Food and water were available *ad libitum*. All mice were age-matched and between 2 to 8 months.

All experimental procedures were performed with approval from the University of Kent Ethical Review Committee and in accordance with the Animals (Scientific Procedures) Act 1986.

4.2.2 Behavioural activity recording during decreasing irradiance

Experiment conducted under 12:12h LD conditions to investigate light-driven locomotor activity by wheel running under decreasing irradiance. Maximum illumination within animal room was provided by 2 fittings with paired T5 (152cm) fluorescent tubes producing approximately 350 lux/relative irradiance 3.0×10^{14} photons/cm^2/s at cage level. See Appendix III. Initial reduction in illumination was achieved by through the removal of one light fitting and thereafter by photographic stops via neutral density filter (Lee filters, Andover, UK). Light intensity was measured by lux meter (R S Components, Corby, UK) and optical power meter (Thorlabs, UK). Lighting was controlled by timer to allow 12:12 programming of LD cycle with lights on between 7am and 7pm. All subjects

were maintained under maximum light for a minimum of 7 days prior to the beginning of the experiment. The reductions in light intensity occurred as follows:

Week 1-2: Full intensity light from 2 fittings

Week 3: Light from 1 fitting only

Week 3 to 16: Light from 1 fitting progressively reduced by 1 photographic stop every 2 weeks

Week 17 to 18: Return to full intensity light from 2 fittings

Locomotor activity was recorded throughout the experiment with baseline activity intensity and phase angle of entrainment calculated from 14 days activity under full illumination (350 lux/relative irradiance 3.0 x 10^{14} photons/cm^2/s). See Appendices III and IV.

For each light intensity: mean daily revolutions were recorded for day 3-5 with days 1 and 2 disregarded. Activity intensity was normalised by dividing current daily revolutions by baseline recording under full illumination. Phase angle of entrainment was calculated for day 3-5 with days 1 and 2 disregarded.

Statistical significance determined using GraphPad Prism 5 software (San Diego, CA) by one-way analysis of variance (ANOVA). All data presented as mean ± SEM (standard error of mean) and statistical significance defined as being $P < 0.05$.

4.2.3 Behavioural activity recording during 6-hour changes in LD cycle

TKO and WT mice were maintained under standard 12:12h LD conditions with lights on 7am-7pm for 7 days prior to beginning of experiment. Room illumination was provided by 2 fittings with paired T5 (152cm) fluorescent tubes producing relative irradiance of 350 lux/3.0 x 10^{14} at cage level. See Appendix III. At the start

of the protocol, TKO and WT mice were maintained for 13 days under 12:12 h LD cycle for collection of stable entrainment data. On the following day the LD cycle timer was advanced 6 hours at ZT10. All animals were maintained under this new LD cycle for 27 days for full re-entrainment to the new cycle, after which the light cycle was delayed by 6 hours at ZT10, and data collected for an additional 14 days Phase angle of entrainment was measured during week 1 to establish mean timing of onset for individual mice.

Following the advance in LD cycle, shifts in activity onset for 21 days were measured from phase angle of entrainment measured during week 1. During week 5 phase angle of entrainment was measured from activity offset to establish mean timing of offset for individual mice. Following the 6-hour delay in LD cycle shifts in activity offset for 14 days were measured from phase angle of entrainment measured during week 5. Activity offsets were used to measure rate of re-entrainment to a delayed LD cycle to eliminate effects of negative masking.

Re-entrainment or individual mice was considered complete when total shift in activity onset (for advancing) or activity offset (for delaying) reached 6 hours ± 0.5.

Statistical significance determined using GraphPad Prism 5 software (San Diego, CA) by student's *t* tests. All data presented as mean ± SEM (standard error of mean) and statistical significance defined as being $P < 0.05$.

4.2.4 Behavioural activity during increasing photoperiod

TKO and WT mice were maintained under standard 12:12h LD conditions with lights on 7am-7pm for 7 days prior to beginning of experiment. Room illumination was provided by 2 fittings with paired T5 (152cm) fluorescent tubes producing relative irradiance of 350 lux/3.0 x 10^{14} at cage level. See Appendix III.

At the start of the protocol, TKO and WT mice were maintained for 13 days under 12:12 h LD cycle for collection of stable entrainment data. On day 14 the photoperiod was increased by 1 hour at dawn and dusk thereby providing 14:10h LD cycle which was maintained for 7 days. A 2-hour increase in light hours was performed weekly to provide 7 day periods of 16:8h, 18:6h, 20:4h, 22:2h LD cycles, with a final 2 week period in constant light, LL. Phase angle of entrainment measured over the first 13 days under 12:12h LD and then from day 3-5 following change in photoperiod with days 1 and 2 disregarded. Total active period, α, was also measured daily for the first 13 days under 12:12h LD and then from day 3-5 following change in photoperiod with days 1 and 2 disregarded. See chapter 1: 1.1.3.

Statistical significance determined using GraphPad Prism 5 software (San Diego, CA) by student's *t* tests and one-way analysis of variance (ANOVA). All data presented as mean ± SEM (standard error of mean) and statistical significance defined as being $P < 0.05$.

4.2.5 Behavioural activity under constant light, LL

TKO and WT mice were maintained under standard 12:12h LD conditions with lights on 7am-7pm for 13 days prior to beginning of experiment. Room illumination was provided by LED lighting generating approximately 2500lux/relative irradiance 1.83×10^{15} photons/cm^2/s at cage level. See Appendix III. On day 14 lights did not turn off at ZT 12, remaining on for a further 2 weeks.

Free-running period, tau, was determined by linear regression lines placed by eye through daily activity onsets from day 19 to 28. The gradient of the line was measured and converted to hours of variance. See Appendix IV.

Statistical significance determined using GraphPad Prism 5 software (San Diego, CA) by student's *t* tests. All data presented as mean ± SEM (standard error of mean) and statistical significance defined as being $P < 0.05$.

4.3 Results

4.3.1 A decline in TASK-3 KO locomotor activity during decreasing irradiance

The weekly reduction in light intensity under a standard 12:12h LD cycle produced markedly different effects in both activity intensity and photoentrainment in WT and TKO mice. Comparison of normalised mean daily wheel revolutions under each intensity within strain revealed a significant reduction in TKO activity under conditions of decreased lighting, not apparent in the WT mice (One-way ANOVA WT: $P > 0.05$, TKO: $P = 0.0088$, n=5). See Figure 4.1: A, B.

Measurement of phase angle of entrainment by activity onset was only possible in 3 out of 5 TKO mice for the first half of the experiment due to extremely low wheel running activity. Under the light intensities measured TKO mice showed no evidence of free-running. In contrast, WT activity onsets remained clearly identifiable and consistent throughout the experiment, maintaining entrainment to <1 lux/1.34 x 10^{13} photons/cm^2/sec, after which they exhibited a free-running rhythm of varying period length (n=5). See Figure 4.1: A, C, D.

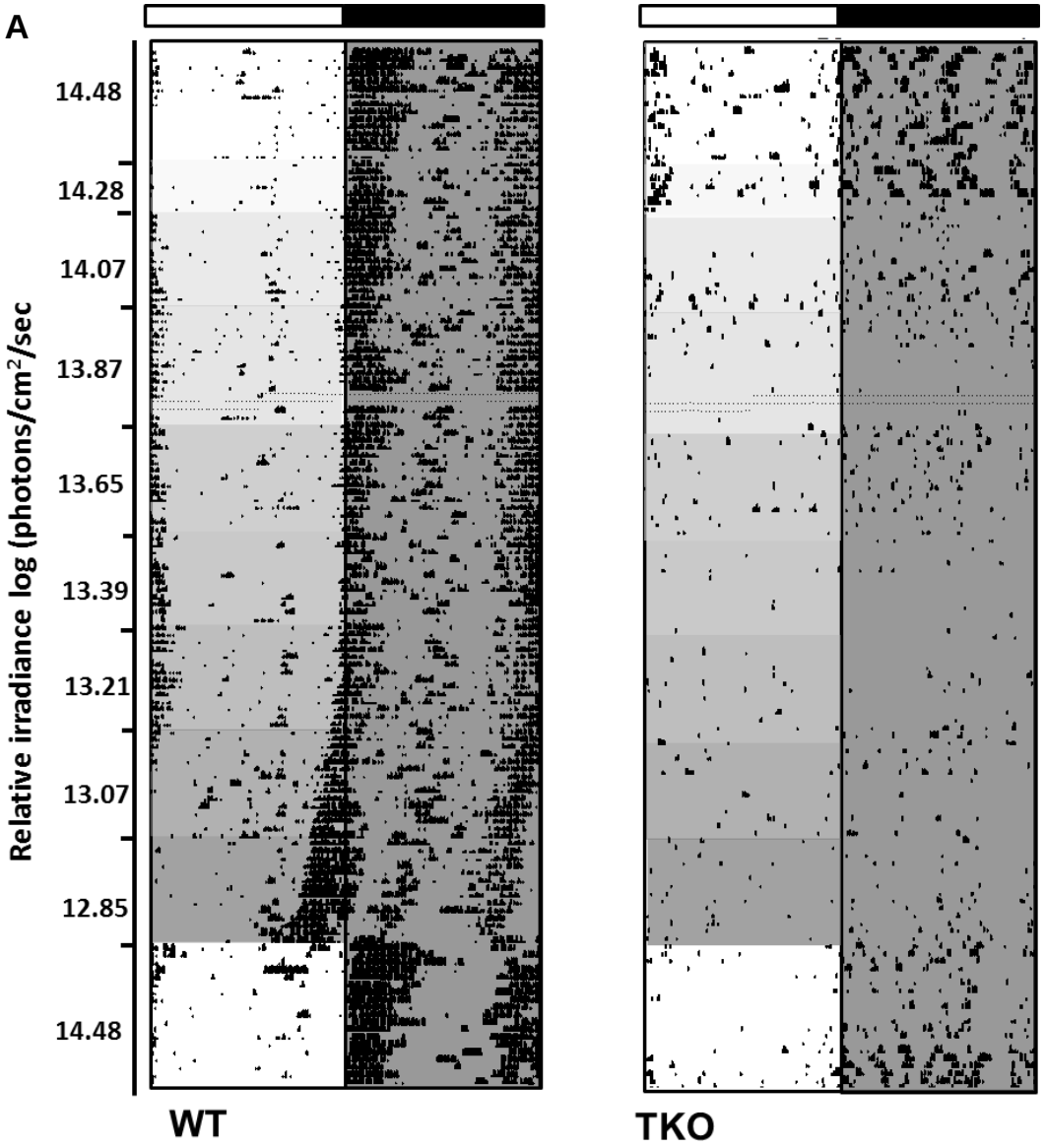
A
14.48
14.28
14.07
13.87
13.65
13.39
13.21
13.07
12.85
14.48
Relative irradiance log (photons/cm2/sec
WT
TKO

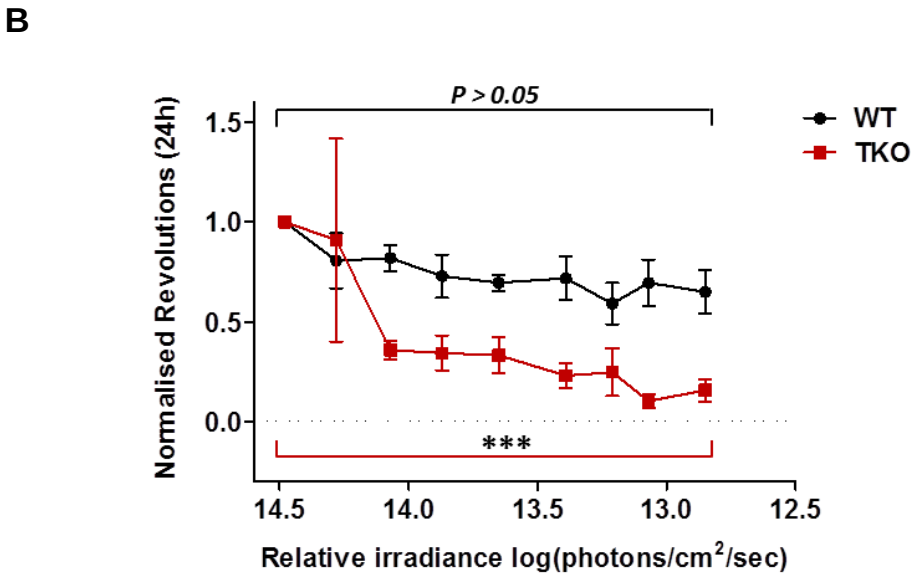
B
P > 0.05
WT
TKO
Normalised Revolutions (24h)
1.5
1.0
0.5
0.0
***
14.5
14.0
13.5
13.0
12.5
Relative irradiance log(photons/cm2/sec)

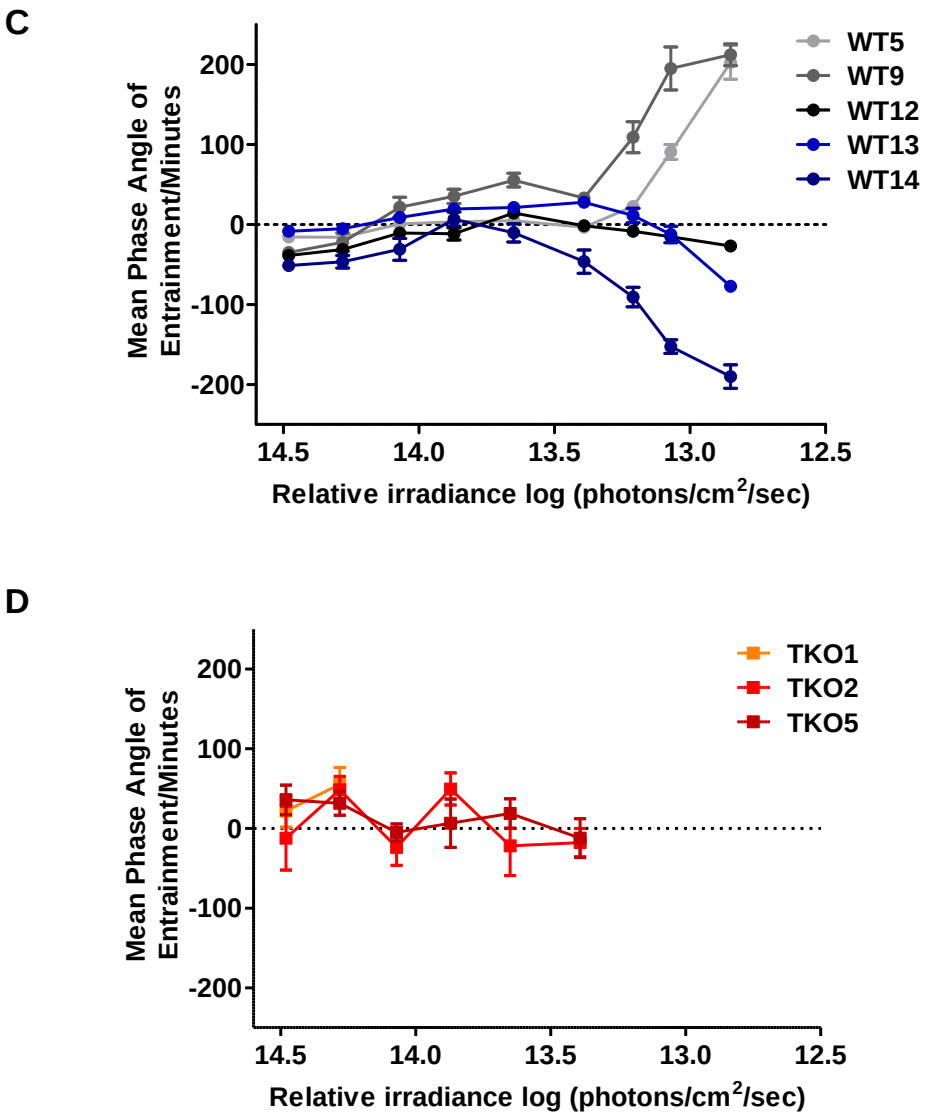

Figure 4.1: Locomotor activity in WT and TKO mice during decreasing irradiance.

(A) Representative actograms of WT and TKO mice wheel-running activity throughout conditions of decreasing irradiance. Note how TKO activity decreases to almost undetectable levels as light decreases, in contrast to WT which maintains entrainment until relative irradiance of approximately 1.34 x 10^{13} photons/cm^2/sec is reached, after which goes into a free-run.

(B) Normalised wheel revolutions completed in 24 hours are significantly reduced under decreasing irradiance in TKO mice but show no significant difference in WT, One-way ANOVA WT: $P > 0.05$, TKO: $P < 0.001$ (n=5).

(C) Phase angle of entrainment by activity onset reveals demonstrates WT mice going into a free-run at relative irradiance of 1.34 x 10^{13} photons/cm^2/sec, whilst in (D) TKO mice phase angle of entrainment was only measurable for the first half of the experiment in 3 mice, and not at all in the remaining 2 mice, due to low intensity of activity. There were no signs of free-running rhythm in the TKO mice.

4.3.2 Altered rates of re-entrainment in the absence of TASK-3

A jetlag paradigm with 6-hour changes in the timing of the 12:12h LD cycle was used to compare rates of re-entrainment in TKO and WT mice. Following the 6-hour advance, TKO mice took significantly longer to fully re-entrain to the new LD cycle timing than WT (WT: 8.88 days ± 0.40, TKO: 14.14 days ± 1.64, student's *t* test $P = 0.0055$). Moreover, measurement of rate of re-entrainment by phase shift in daily onset of activity revealed significant attenuation in in the TKO mice from day 2 to 9 by student's *t* test ($P < 0.01$), day 11 ($P < 0.01$), day 12 ($P < 0.05$) and day 21 *(*$P < 0.001$, n=7-8). See Figure 4-2: A-C.

Following a 6-hour delay to the LD cycle, the rate of re-entrainment by could not be reliably measured in the TKO mice, therefore a comparison could not be made with WT mice. The low levels of TKO mouse activity, in conjunction with fragmented bouts of dawn activity, prevented accurate tracking of phase shifts in activity offset during this period of adjustment.

A

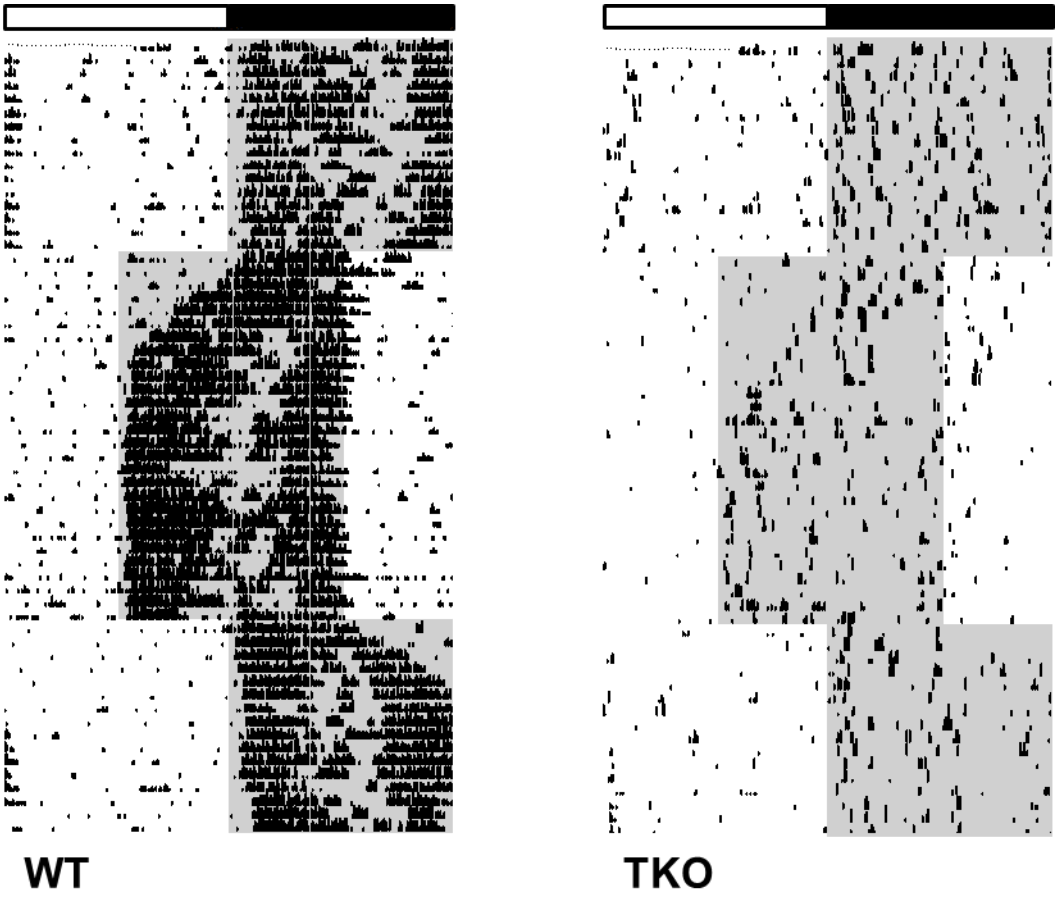
WT
TKO

B

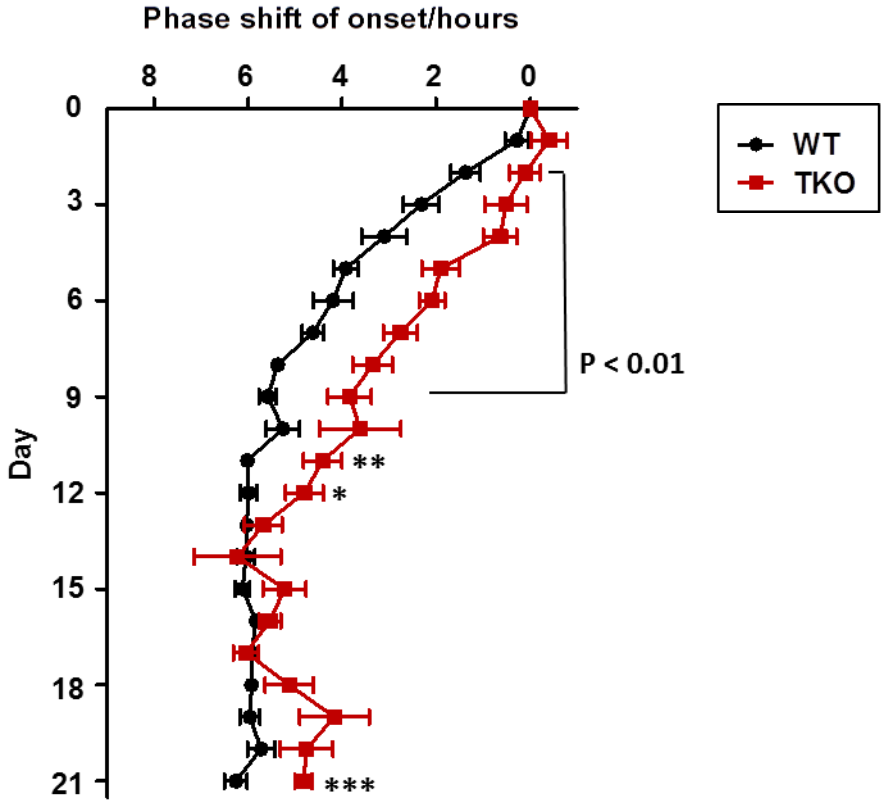
Phase shift of onset/hours
8
6
4
2
0
0
3
6
9
12
15
18
21
Day
WT
TKO
P < 0.01
**
*
***

[121]

C

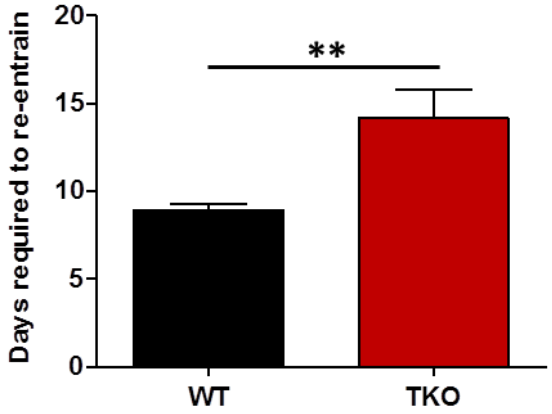

Figure 4.2: Rates of re-entrainment following a 6 hour advance in 12:12h LD cycle timing.

(A) Representative actograms of WT and TKO mice wheel-running activity during 6-hour advance and delay in timing of 12:12h LD cycle demonstrating changes in activity.

(B) Significantly attenuated daily phase shifts in TKO activity onset occurred on days 2-9, Student's t test: $P < 0.01$; day 11, $P < 0.01$; day 12, $P < 0.05$ and day 21, $P < 0.001$ of re-entrainment (n=7-8). (C) Total number of days required to re-entrain to a 6 hour advance is significantly increased in TKO mice relative to WT, Student's t test: $P > 0.01$ (n=7-8)

4.3.3 Loss of TASK-3 impacts adjustment to increasing photoperiod

A paradigm incorporating weekly increases in photoperiod allows two important aspects of compression to be investigated: the ability to track changes in timing of dawn and dusk, and the ability to confine and compress activity into decreasing hours of darkness.

The measurement of phase angle of entrainment by activity onset revealed an exaggerated response in TKO mice to the delaying of lights going off. Despite being similar at the beginning of the experiment, under 12:12h LD, increasing photoperiod led to TKO mice anticipating dusk with positive phases angles of entrainment which were significantly different to WT at 10, 6 and 4 hours of darkness analysed by student's t test (12:12h LD WT: -18.61 minutes ± 1.67, TKO:

-11.92 minutes ± 6.27, $P > 0.05$; 14:10h LD WT: -8.14 minutes ± 1.72, TKO: 7.46 minutes ± 6.36, $P = 0.0134$; 16:8h LD WT: -1.71 minutes ± 1.76, TKO: 12.50 minutes ± 11.82, $P > 0.05$; 18:6h LD WT: -7.50 minutes ± 3.66, TKO: 24.00 minutes ± 12.66, $P = 0.0136$; 20:4h LD WT: -11.14 minutes ± 3.29, TKO: 18.86 minutes ± 10.93, $P = 0.0070$, n= 6-8). During the final stage of increased photoperiod, 22:2h LD, data was not analysed for phase angle of entrainment as both strains had gone into a free-run and therefore no longer synchronised to the LD cycle. See Figure 4.3: A, B.

The analysis of active phase, α, during this paradigm showed TKO mice to be active for significantly longer than WT throughout the experiment analysed by student's *t* test (*12:12h LD* WT: 11.00 hours ± 0.12, TKO: 11.52 hours ± 0.24, $P = 0.0377$; *14:10h LD* WT: 9.64 hours ± 0.09, TKO: 11.37 hours ± 0.28, $P < 0.0001$; *16:8h LD* WT: 8.92 hours ± 0.18, TKO: 10.82 hours ± 0.44, $P < 0.0001$; *18:6h LD* WT: 7.60 hours ± 0.13, TKO: 9.98 hours ± 0.77, $P < 0.0001$; *20:4h LD* WT: 7.12 hours ± 0.26, TKO: 10.72 hours ± 0.68, $P < 0.0001$, n= 6-8). Under changing light conditions both WT and TKO mice demonstrated significant variance in values as a consequence of changing photoperiod (One –way ANOVA WT: $P < 0.0001$, TKO: $P = 0.0002$). However, on closer examination, α continually decreases in WT mice in contrast to a more generalised variability in the TKO mice. To further quantify the overall compression achieved through this paradigm, activity under standard 12:12h LD cycles at the beginning of the experiment was analysed with 20:4h LD cycle activity which demonstrated a significant reduction in WT active phase which was not seen in TKO mice (student's t test: WT: $P < 0.0001$, TKO: $P > 0.05$). See Figure 4.3: C-E.

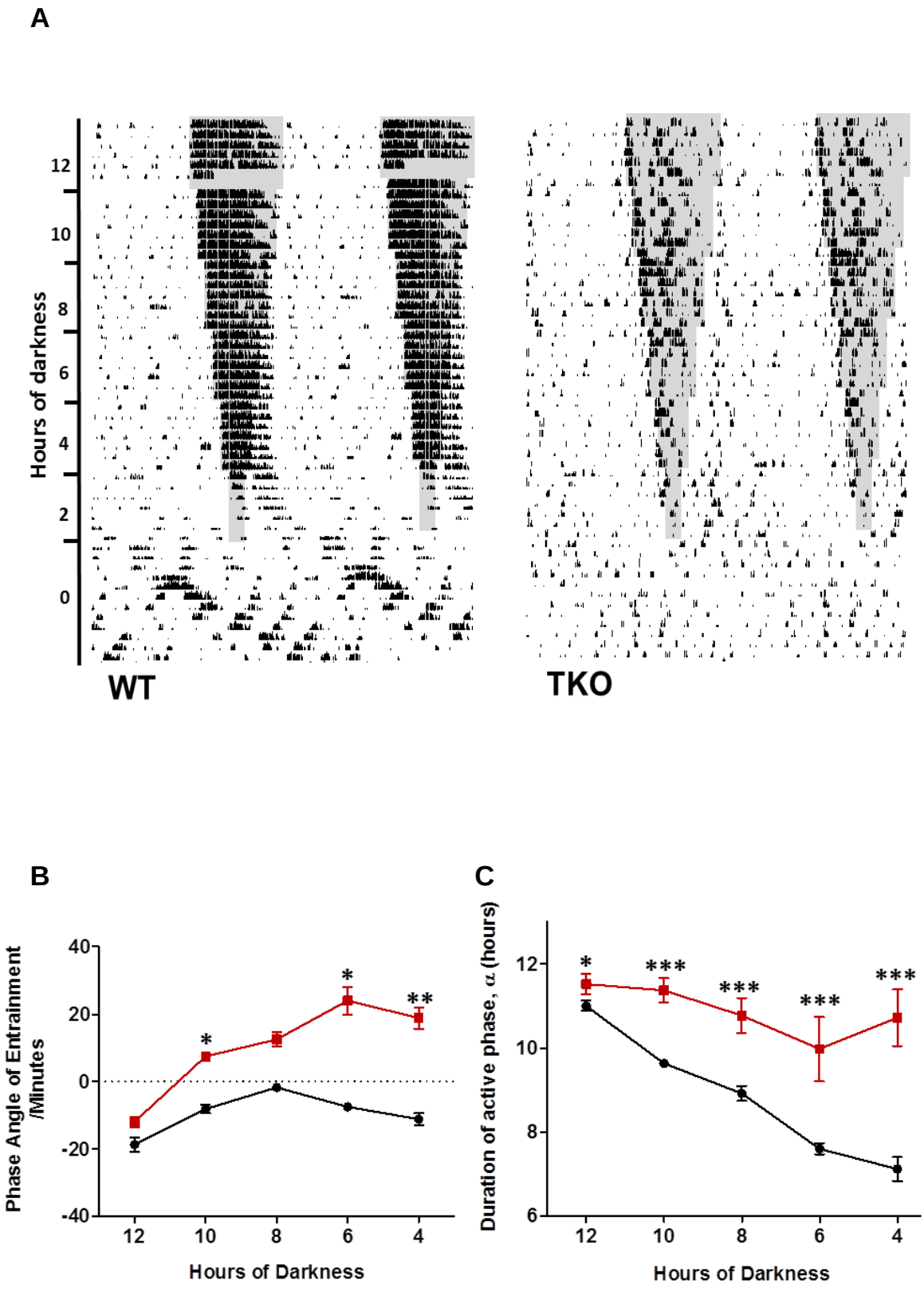
A
Hours of darkness
12
10
8
6
4
2
0
WT
TKO
B
Phase Angle of Entrainment /Minutes
40
20
0
-20
-40
12
10
8
6
4
Hours of Darkness
*
*
**
C
Duration of active phase, α (hours)
12
10
8
6
*
***
***
***
***
Hours of Darkness

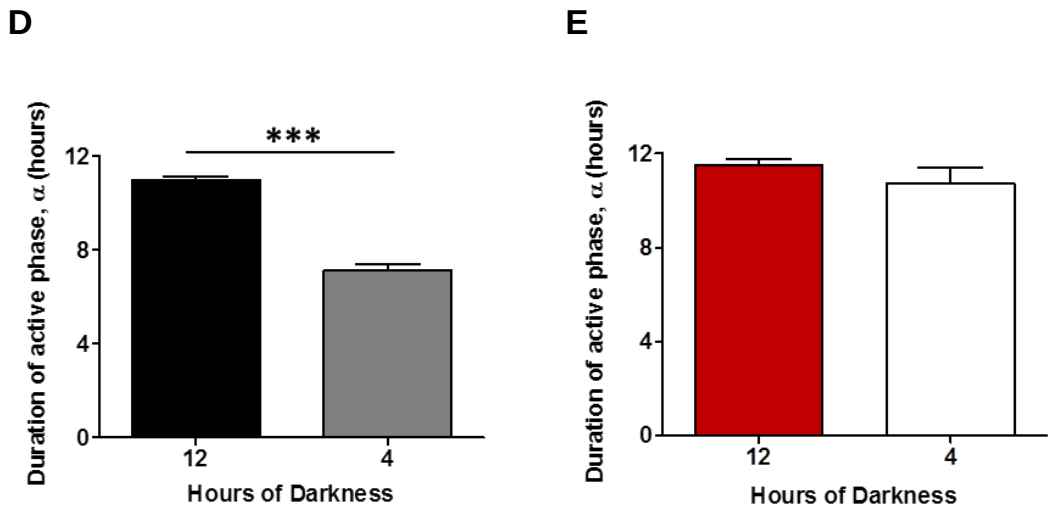

Figure 4.3: Compression of locomotor activity during increasing photoperiod.

(A) Representative double-plotted actograms of WT and TKO mice wheel-running activity throughout the compression paradigm concluding with free-running activity under a 22:2h LD cycle and later, constant light, LL.

(B) Analysis of activity onset demonstrates TKO mice exhibit an exaggerated response to changing light conditions compared to WT. Increasingly positive phase angles of entrainment were significantly different between strains at 10 hours, Student's t test: $P < 0.05$; 6 hours, $P < 0.05$ and 4 hours of darkness, $P < 0.01$ (n=6-8).

(C) Length of active phase, α, is significantly longer in TKO mice relative to WT under all LD cycles examined. During decreasing hours of darkness both TKO and WT mice exhibit significant variation in α, Student's t test: $P < 0.001$, with generalised fluctuations in TKO mice compared to a consistent decrease in WT (n=6-8).

(D) Analysis of 12:12h LD activity versus 20:4h LD reveals significant shortening of α in WT mice, Student's t test: $P < 0.0001$, whilst in (E) there is no significant change in TKO α, Student's t test: $P > 0.05$.

4.3.4 Lengthening of tau under constant light

TKO and WT mice placed under conditions of constant light, LL exhibited significant lengthening of free-running period, tau (WT: 25.32 hours ± 0.06, TKO: 25.28 hours ± 0.05) compared to constant darkness, DD (WT = 23.89 hours ± 0.02, TKO = 23.96 hours ± 0.01, Student's *t* test, $P < 0.0001$, n=6-9). Values of LL tau were not significantly different between strains (student's *t* test, $P > 0.05$). See Figure 4.4.

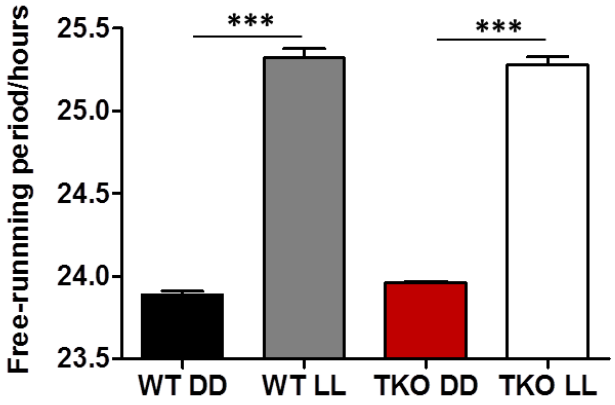

Figure 4.4: Free-running period in constant darkness and constant light.

Under constant light, LL, both TKO and WT free-running period is significantly lengthened compared to constant dark conditions, DD, Student's t test: $P < 0.0001$. There is no significant difference in length of LL free-running period between strains, Student's t test: $P > 0.05$ (n=6-9).

4.4 Discussion

These experiments demonstrate TASK-3 is fundamental for effective adaptation to changes in light intensity, timing of dawn and dusk, and duration of photoperiod.

A weekly reduction in light intensity in photographic stops under a stable 12:12h LD cycles resulted in attenuation of TKO wheel-running activity to such a degree that phase angle of entrainment was only measurable in 3 out of 5 mice, and only for the first half of the experiment. This differed greatly from the WT mice where stable entrainment was maintained to very low levels of light, after which free-running rhythms were observed. These findings suggest that in the absence of TASK-3, light is required to drive locomotor activity and as the intensity decreases, the intensity drops too. At the end of the experiment where the brightest illumination was restored the actograms show there was a clear recovery of TKO wheel-running. It is unlikely the attenuated activity is due to diminished sensitivity to light from TASK-3 loss as an inabaility to detect light would lead to mice going into an earlier free-running rhythm which was not seen in the transgenic mice.

The re-entrainment paradigm, with a 6-hour advance to the timing of the LD cycle, investigated adjustment to large changes in light-dark timing in TKO mice, typical of human trans-meridian flight. Here the loss of TASK-3 significantly impacted the rate of re-entrainment to an advanced LD cycle. The findings from this experiment may relate to the endogenous period of the TKO mice being very close to 24 hours in length and therefore requiring minimal adjustment each day to maintain entrainment to standard 12:12h LD cycles. However, despite being significantly

lengthened, the increase in TKO Tau is very small and therefore these results are more likely to represent an alteration in the clock adjustment and plasticity.

The importance of TASK-3 in clock plasticity was further demonstrated during the compression paradigm with increasing photoperiod and decreasing hours of darkness. Under these conditions WT mice were able to adapt phase angles of entrainment to each new LD cycle, whereas TKO mice began activity increasingly earlier, suggesting an inability to adjust behaviour to the LD cycle. Moreover, the measurement of active period, alpha, highlighted significant differences in WT and TKO response to changing photoperiod. Where WT mice exhibited progressively shorter active periods as a function of hours of darkness, TKO mice showed general variation in alpha, with no significant reduction under 20:4h LD cycles relative to the start of the experiment under 12:12h LD

This paradigm, representative of seasonal change, demonstrates how WT mice are able to compress nocturnal activity during long summer days in accordance with early studies (Pittendrigh and Daan, 1976d). The TASK-3 KO mice, however are not able to maintain the same level and confinement of activity to an increased photoperiod, demonstrating TASK-3 currents are vital for fine-tuning entrainment to meet the demands of changes in the natural environmental across the seasons.

The final stages of the compression paradigm with a 22:2h LD cycle forced both WT and TKO mice into a free-running rhythm with a lengthened tau. This photoperiod was too extreme for even WT mice to adapt to and therefore the endogenous rhythm was adopted. Under 22:2h LD and constant light, LL, at the end of the compression paradigm both strains exhibited the characteristic lengthening of tau to over 24-hours in length (Pittendrigh and Daan, 1976c,

Pittendrigh and Daan, 1976d). This NIF response to light was also studied in a separate experiment where mice were housed under12:12h LD before switching to LL to confirm this finding was not purely an artefact from the compression paradigm, but a genuine response to the light.

This series of behavioural experiments demonstrate the importance of TASK-3 for effective adaptation to changing light conditions. The properties of maintaining entrainment, re-entrainment and activity compression are all compromised in the absence of this channel, and what becomes clear is that light is the all-important driver of locomotor activity. What is not defined, however, is whether the observed differences are due to alteration in retinal decoding and/or the clock, these elements will be considered separately in the following chapters.

5 Negative masking in TASK-3 KO mice

5.1 Introduction

Experiments conducted under challenging LD conditions in the previous chapter have demonstrated TASK-3 KO mice exhibit significantly altered responses compared to WT in re-entrainment and activity compression for seasonal adjustment. This chapter continues to explore the consequence of TASK-3 ablation on light-driven responses by investigating the phenomenon of negative masking.

Negative masking is the acute inhibition of activity by bright light observed in WT nocturnal rodents. In conjunction with photoentrainment, this response serves to confine activity to hours of darkness (Mrosovsky, 1999). In contrast to clock-driven entrainment, masking is a NIF retinal response. Following the detection of *TASK-3* mRNA within the WT retina, described in chapter 2, this chapter will begin to unravel the role of TASK-3 at the level of the retina and the impact of this on light-driven behaviour.

Initial experiments are designed around the application of an acute light pulse delivered in the early part of the night. Pulses of 1 hour will examine whether inhibition of activity occurs in TKO and WT mice, whilst longer duration pulses of 3 hours will investigate whether inhibition can be sustained. The final masking experiment uses an ultradian LD cycle which will investigate masking responses across the whole circadian cycle (Mrosovsky and Hattar, 2003).

5.2 Experimental Methods

5.2.1 Subjects

Male WT (C57 BL/6J) mice were obtained from Charles River Laboratories (Kent), with transgenic TASK-3 KO (TKO) mice bred and maintained as homozygotes under license. For genotyping see Appendix II. Mice were housed individually in polypropylene cages measuring approximately 34cm (l) x 16cm (W) x 13cm (h) fitted with a running wheel. Wheel revolutions were recorded in 1-minute bins using Chronobiology Kit (Stanford Software Systems, USA). Food and water were available *ad libitum*. All mice were age-matched and between 2 to 8 months.

All experimental procedures were performed with approval from the University of Kent Ethical Review Committee and in accordance with the Animals (Scientific Procedures) Act 1986.

Mice were maintained under standard 12:12h LD conditions with lights on 7am-7pm for a minimum of 2 weeks prior to beginning of each experiment. Room illumination provided by LED lighting generating approximately 2500lux/relative irradiance 1.83×10^{15} photons/cm^2/s at cage level. See Appendix III.

5.2.2 Application of acute light pulses

Wheel-running activity during an acute light pulse was compared to a baseline value measured the night before under darkness according to 12:12 LD cycle.

Day1: standard 12:12h LD cycle for baseline activity recording

Day2: 12:12h LD conditions with LED light pulse starting at ZT14

Day 3: standard 12:12h LD cycle for recovery

This 3-day protocol was conducted for 3 rounds with LEDs on for 1 hour (ZT14-15) followed by 3 rounds with LEDs on for 3 hours (ZT14-17).

For each round, total wheel revolutions completed within the targeted time frame (for 1 hour pulse, ZT14-15; for 3 hour pulse, ZT14-17) on night of baseline recording were compared to total revolutions completed during respective light pulse the following night. Additionally, 3-hour light pulses and baseline recordings were analysed in 10-minute time bins to assess maintenance of light inhibition. Statistical significance determined using GraphPad Prism 5 software (San Diego, CA) by student's *t* tests. All data presented as mean ± SEM (standard error of mean) and statistical significance defined as being $P < 0.05$.

5.2.3 Ultradian LD cycles

TKO and WT mice were placed under a 3.5:3.5h ultradian cycle for 7 days for examination of masking responses across the circadian cycle. Under this paradigm dawn and dusk will fall at each circadian time point (ZT hours) over the course of the week. A 7-hour profile was constructed from mean revolutions collected in 10-minute bins for 7 days.

Statistical significance determined using GraphPad Prism 5 software (San Diego, CA) by student's *t* tests. All data presented as mean ± SEM (standard error of mean) and statistical significance defined as being $P < 0.05$.

5.3 Results

5.3.1 TASK-3 functionality is not required for acute masking responses

The application of a 1-hour light pulse at ZT14-15 inhibited wheel-running activity in both TKO and WT mice. Total wheel revolutions were significantly reduced during light pulse compared to baseline recording analysed by student's *t* test (WT: baseline 1346 revolutions ± 187.3, pulse 24 revolutions ± 6.24, $P < 0.0001$, TKO: baseline 298 revolutions ± 97.64, pulse 13 revolutions ± 3.72, $P = 0.0048$, n=10-12). See Figure 5.1: A-C.

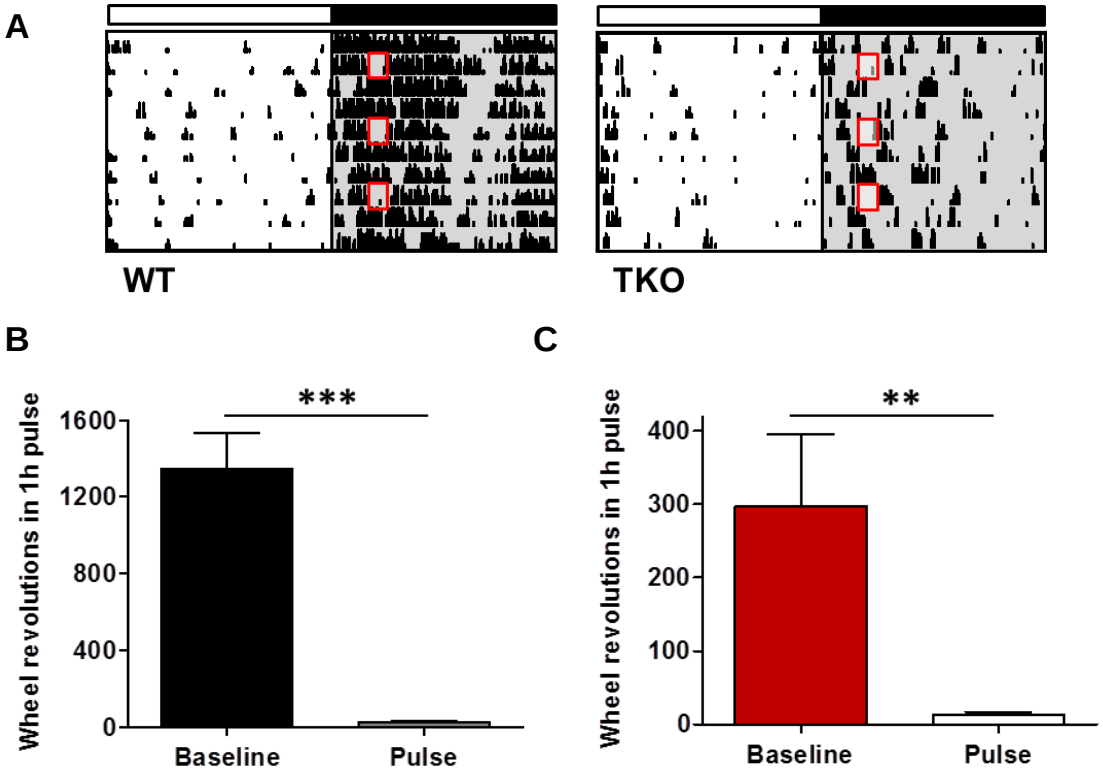

Figure 5.1: Acute inhibition of activity during a 1-hour light pulse.

(A)) Representative actograms of WT and TKO mice wheel-running activity under 12:12h LD with inhibition of activity during 1-hour light pulses applied every third cycle at ZT14-15 (red boxes).

(B) Mean revolutions completed by WT mice during 1-hour light pulse were significantly lower than baseline recording taken the previous night at a similar time, student's *t* test, $P < 0.0001$ (n=10). (C) Despite lower intensity activity, TKO mice also completed significantly less revolutions during the light pulse than baseline recording from the previous night, student's *t* test, $P < 0.01$(n=12).

5.3.2 Sustained masking in TASK-3 KO mice

The use of an extended light pulse of 3 hours duration (ZT14-17) inhibited wheel-running activity in both TKO and WT mice in a similar fashion to the 1-hour pulse described previously. Total wheel revolutions were significantly less during light pulse compared to baseline recording analysed by student's *t* test (WT: baseline 1991 revolutions ± 294.5, pulse 137 revolutions ± 42.05, $P < 0.0001$; TKO: baseline 534 revolutions ± 151.4, pulse 48 revolutions ± 11.82, $P = 0.0048$, n=10-12). See Figure 5.2: A-C Analysis of light pulse activity compared to baseline in 10-minute time bins reveals light inhibition during pulse was maintained by both WT and TKO mice for the full 3 hours. See Figure 5.2: D, E .

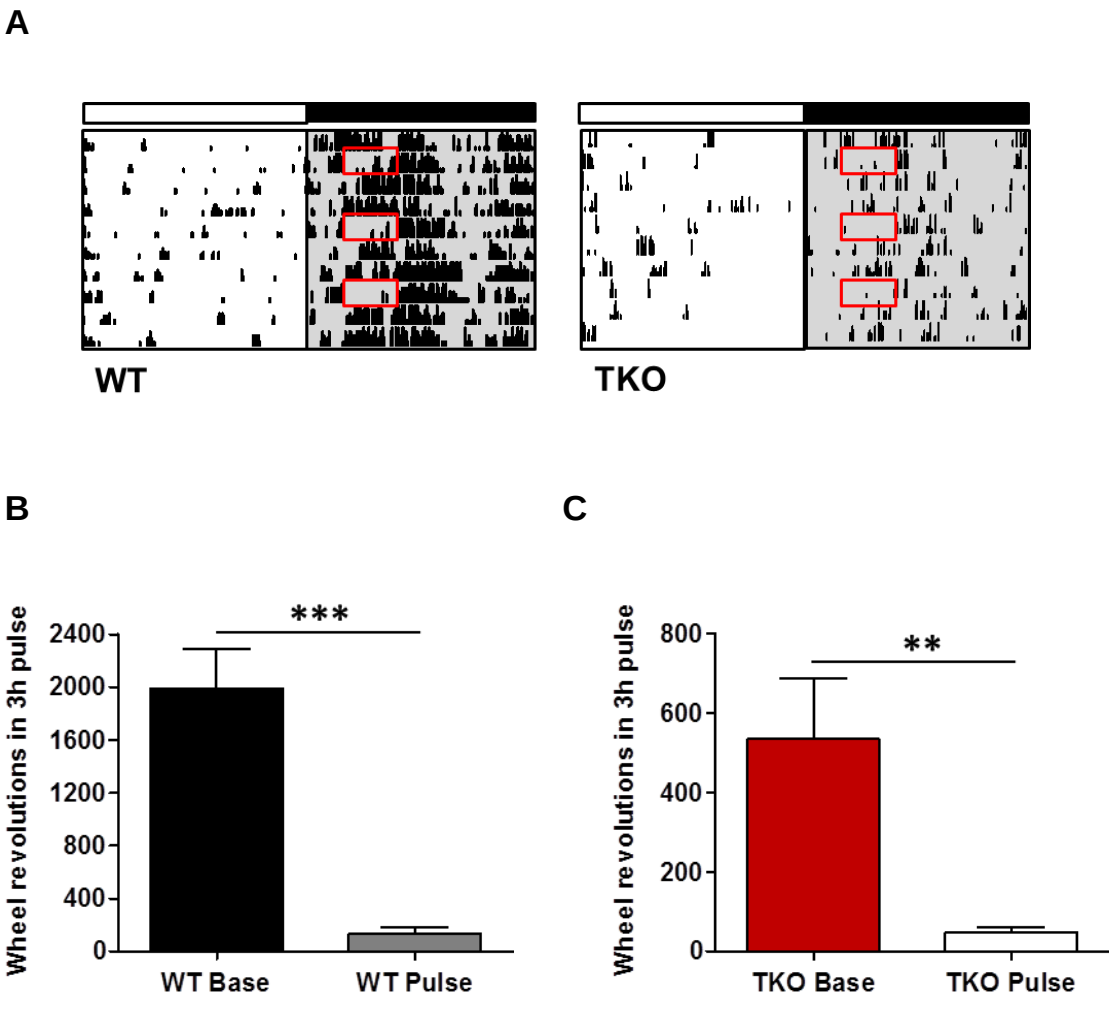

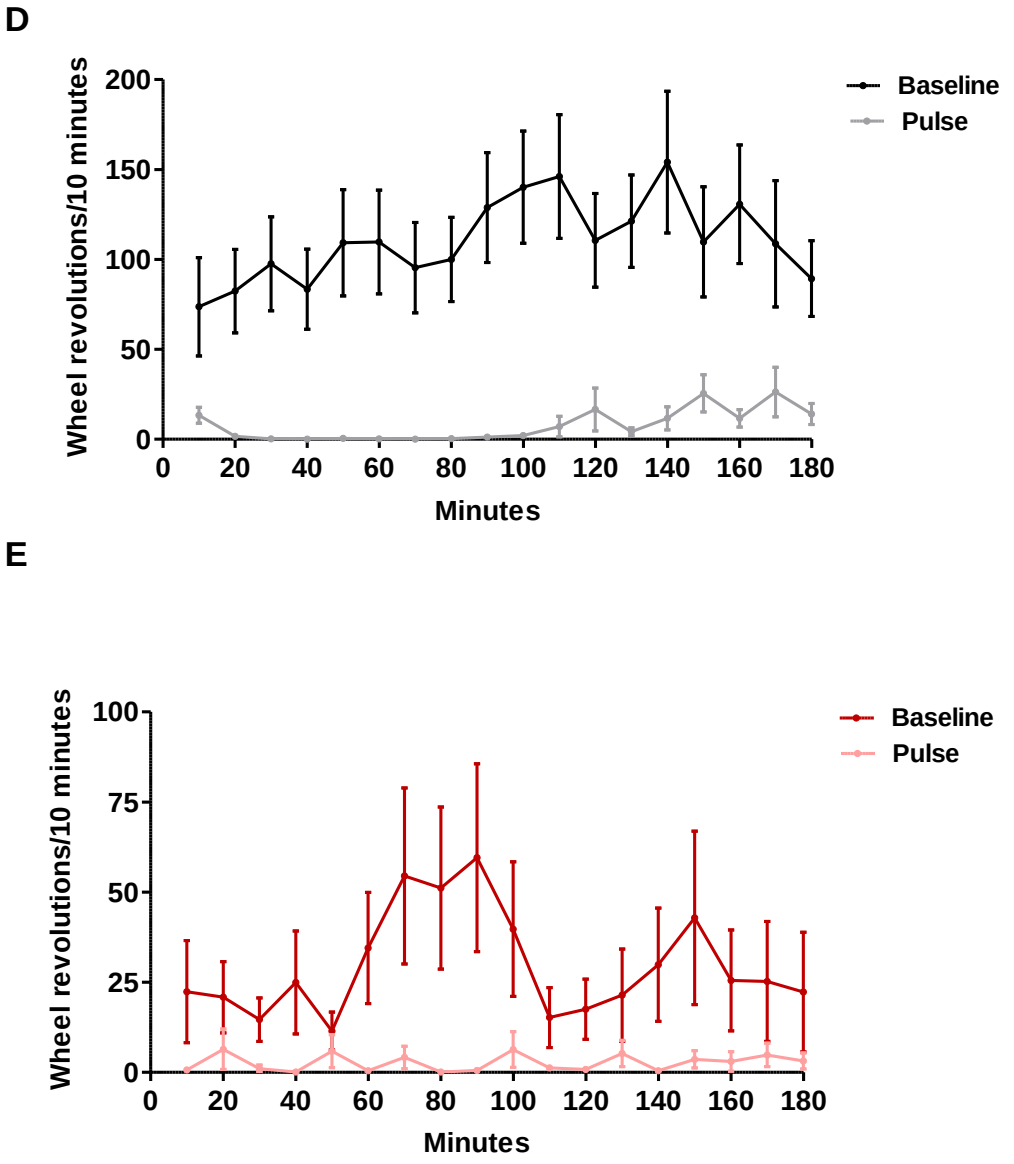

Figure 5.2: Acute inhibition of activity during a 3-hour light pulse.

(A)) Representative actograms of WT and TKO mice wheel-running activity under 12:12h LD demonstrating inhibition of activity during 3-hour light pulses applied every third cycle at ZT14-17 (red boxes).

(B) Mean revolutions completed by WT mice during 1-hour light pulse were significantly lower than baseline recording taken the previous night at a similar time, student's *t* test, *P* < 0.0001 (n=10). (C) Likewise, TKO mice completed significantly less revolutions during the light pulse than during darkness at this time on the previous night, student's *t* test, *P* = 0.0048 (n=12).

(D) Mean revolutions conducted by WT mice during 3-hour light pulse compared to baseline from previous night. Data presented in 10-minute time bins, with (E) mean revolutions conducted by TKO mice.

5.3.3 Ultradian LD cycles reveal masking across the circadian cycle

TKO and WT mice housed under an ultradian 3.5:35h LD cycle were largely able to confine locomotor activity to the dark portions of the cycle, demonstrating clear inhibition of activity during the light phase. Quantification of mean revolutions by light conditions revealed significantly reduced running in the light portion of the cycle in both TKO and WT mice (WT: Light mean = 285 revolutions ± 77.43 Dark mean = 1349 revolutions ± 327.5, student's *t* test, $P = 0.0054$; TKO: Dark mean = 540 revolutions ± 168.4, Light mean 157 revolutions ± 49.47, student's t test $P = 0.0402$; n=10-12). See Figure 5.3: A-D.

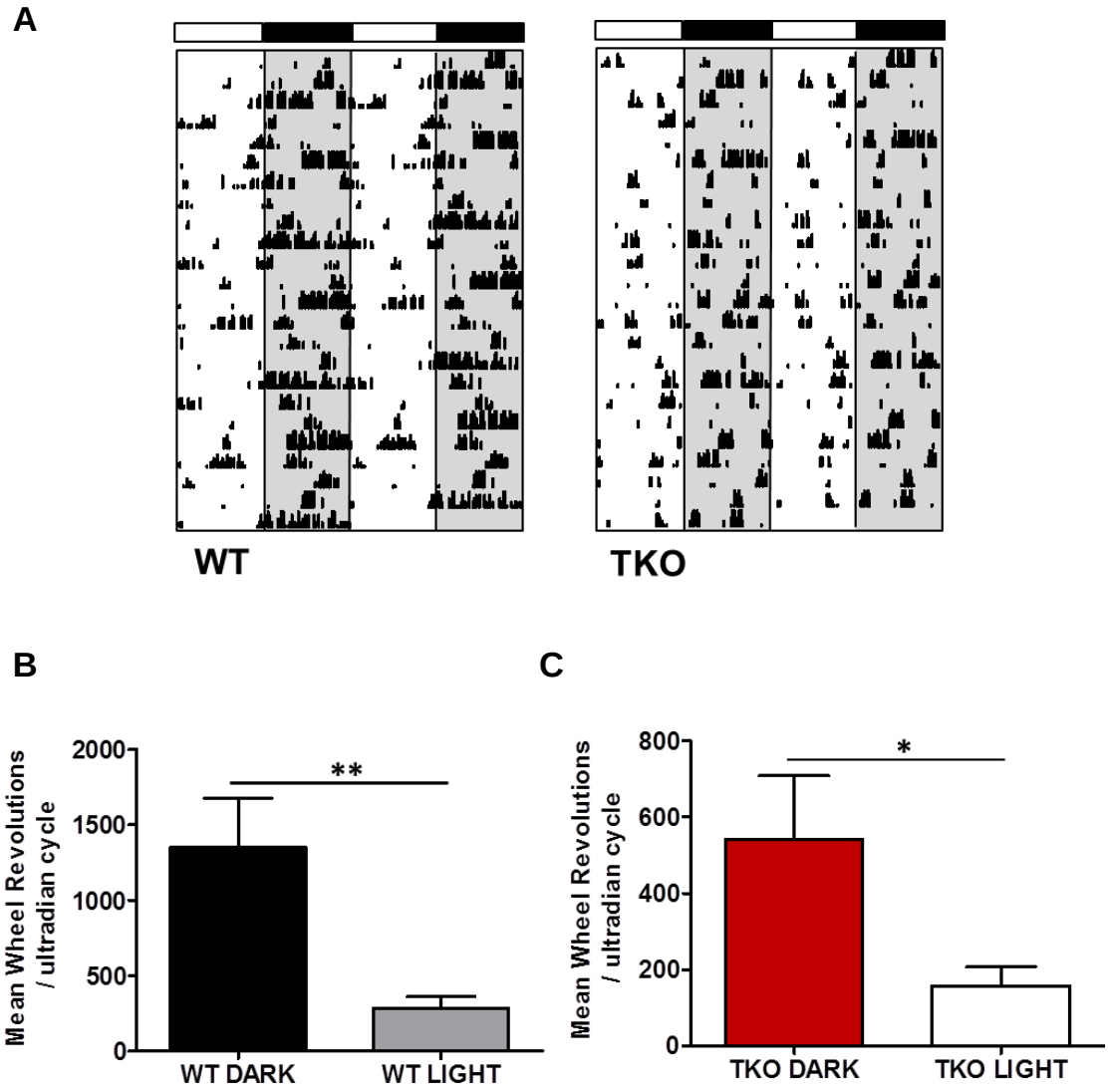

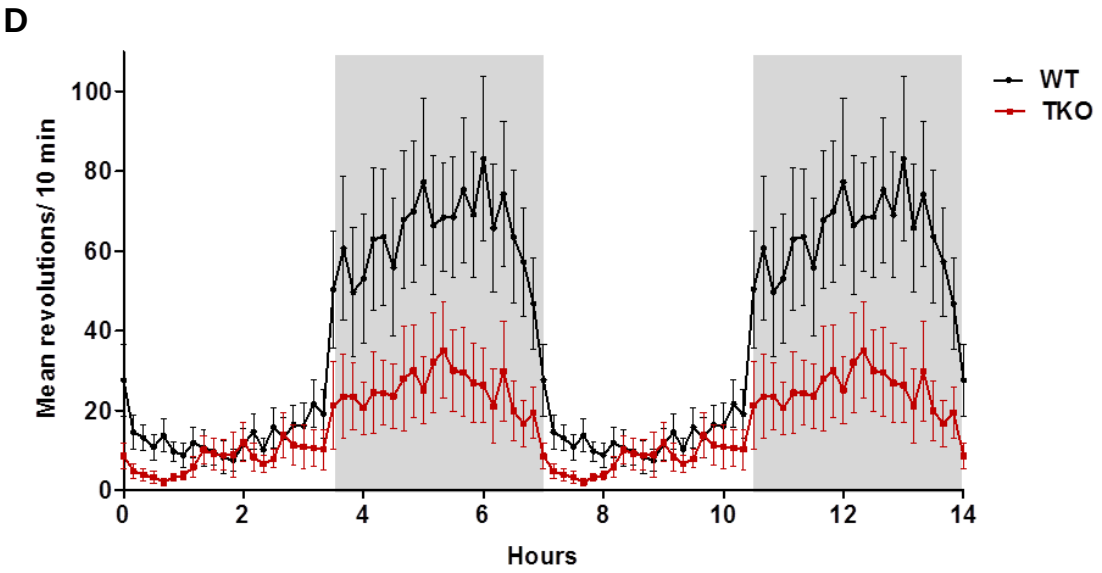

Figure 5.3: Locomotor activity cycles under 3.5:3.5h LD ultradian cycles.

(A) Representative double-plotted actograms of WT and TKO mice wheel-running activity under an ultradian 3.5:3.5h LD cycle.

(B) Mean revolutions completed by WT mice show significantly less activity during the light portion of the ultradian cycle, student's *t* test, $P < 0.01$(n=10). (C) Likewise, TKO mice completed significantly less revolutions during the light demonstrating negative masking persists in the absence of TASK-3, student's *t* test, $P < 0.05$ (n=12).

(D) Wheel-running activity double-plotted over 7 hours in TKO (red) and WT (black) mice highlights inhibition of activity during light portions of the cycle with majority of activity confined to darkness. Data points represent mean values collected in 10 minute time bins.

5.4 Discussion

These investigations demonstrate TASK-3 channel functionality is not essential for the NIF response of negative masking. The application of acute pulses during the early night resulted in negative masking, observed as significant inhibition of wheel running, in both WT and TKO activity. During longer duration pulses of 3 hours activity remained supressed, indicative of a functional melanopsin response. Previous research has shown genetic ablation of melanopsin prevents sustained masking during 3 hours of light with full recovery of activity after just 100 minutes (Mrosovsky and Hattar, 2003).

When placed under ultradian LD cycles with a period of just 7 hours, both strains of mice conducted significantly more of their activity during the dark portions of the cycle. The profile analysis clearly demonstrates activity suppression beginning at dawn and ending at dusk in both strains of mice thereby displaying effective tracking of photoperiod. This response is indicative of masking rather than photoentrainment as rodents find it difficult to entrain to cycles of this shortened period in multiples of 7 hours (Mrosovsky and Hattar, 2003).

In contrast to the alteration in light-driven behaviour described in chapter 4, these negative masking experiments demonstrate this retinal response is unaffected by TASK-3 loss. The role of TASK-3 in retinal decoding of light will be further examined by pupillometry in chapter 6.

6 Retinal decoding in the absence of TASK-3

6.1 Introduction

The biological clock receives light information exclusively via the retina and is therefore subject to regulation by the pupillary light reflex (Foster, 1998). As light is the most prominent of stimuli influencing circadian timing, the detection and communication of environmental irradiance is of upmost importance in synchronising many aspects of gross physiology (Lall et al., 2010).

On receiving light, retinal photoreceptors decode irradiance and communicate photic information to the brain for visual processing but also to the SCN and OPN for NIF responses via the hypothalamic tract. This NIF signalling is essential for circadian entrainment and pupillary light reflex (PLR). See Figure 1.11.

The process of PLR is known to be reliant on the ipRGC population, as ablation of this photopigment results in attenuation of this response (Lucas et al., 2003). However, the additional actions of the classic photoreceptors, rods and cones, are required for sensitivity across the full range of irradiances encountered during daylight hours (Hattar et al., 2003, Lall et al., 2010).

The ipRGCs are the least sensitive of all photoreceptor classes, requiring sustained high intensity illumination for activation (Hattar et al., 2003, Lucas et al., 2003, Lucas et al., 2012). In addition to their role in detection of light, they also act as conduits for the communication of light information from classic photoreceptor decoding by rods and cones (Guler et al., 2008). In contrast, cones are able to activate over a range of intensities including detection of acute changes - however they too have limited sensitivity in low level light. Thus under dim light, the highly sensitive rods provide the greatest contribution in encoding environmental light.

Through the combined actions of all three major classes of photoreceptor detection of irradiance, and consequent pupillary constriction, is commensurable to the intensity of light entering the eye.

This chapter will build on findings from chapters 2 and 5 with the detection of *TASK-3* mRNA within the WT retina and the persistence of the retinal NIF response of negative masking in the absence of TASK-3. Here, pupillometry investigations will establish the impact of TASK-3 ablation on PLR as a method of assessing irradiance detection by the retina. The absence of TASK-3 current has been shown to depolarise RMP and alter firing rates in a number of excitory cells (Brickley et al., 2007, Meuth et al., 2003). The exact location of TASK-3 in the retina is yet to be confirmed and therefore the impact on cells and decoding of light is currently unknown. As ipRGCs depolarise in response to light in a manner consistent with most CNS neurons they may exhibit increased excitability from TASK-3 loss as RMP is likely to be closer to firing threshold (Lucas, 2013). Conversely rods and cones hyperpolarise on receiving light and therefore in the absence of TASK-3 this signal may be attenuated as greater drive will be required to obtain hyperpolarisation from a depolarised resting state (Masland, 2012, Kolb, 2003). In addition to photoreceptor cells, the absence of TASK-3 may influence other excitable cells including bipolar, horizontal and amacrine cells. With much shared circuitry and multi synaptic transmission between rods and cones pinpointing exact pathways influenced by TASK-3 channels may present a challenge. This will addressed by exploiting differences in sensitivity.

Utilising published data on photoreceptor sensitivity according to wavelength, polychromatic and monochromatic light will selected to maximally activate specific classes of photoreceptor, thereby highlighting any differences in sensitivity

in TKO mice compared to WT (Partridge and De Grip, 1991, Lall et al., 2010, Lucas et al., 2012). See Figure 6.1.

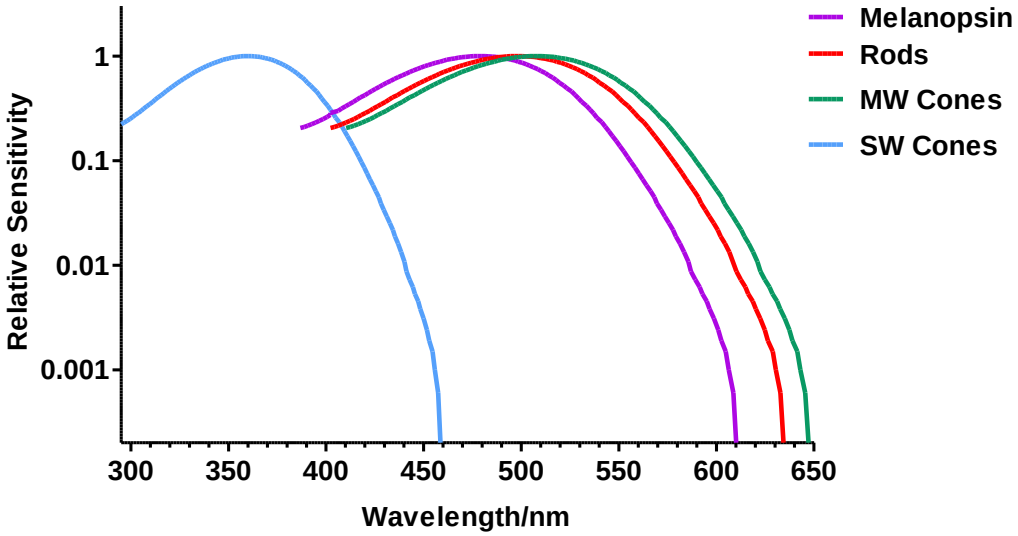

Figure 6.1: Model spectra demonstrating photoreceptor sensitivity according to wavelength.

Model spectra demonstrating relative sensitivity of each major photoreceptor class according to wavelength of visible light with melanopsin shown in purple, rods in red, mid-wavelength cones in green and short-wavelength cones in blue.

[Adapted from (Partridge and De Grip, 1991)].

Finally, intrinsic pupillometry (iPLR) investigations will be conducted to specifically draw out any differences within the melanopsin-driven pathway from TASK-3 loss. This response has been demonstrated in a number of nocturnal rodents and crepuscular species, and has been found to be entirely melanopsin-dependant (Xue et al., 2011). Through the use of an isolated eye preparation, PLR can be examined in the absence of all neuronal circuitry to the brain, relying purely on signalling between the iris and retina. Therefore this novel method provides an additional indictor of ipRGC functionality in the TASK-3 KO mouse retina.

6.2 Experimental methods

6.2.1 Subjects

WT (C57 BL/6J) mice were obtained from Charles River Laboratories (Kent), with transgenic TKO mice bred and maintained as homozygotes under license. For genotyping see Appendix II. Male and female mice were housed in polypropylene cages measuring approximately 34cm (l) x 16cm (W) x 13cm (h) in litter groups under 12:12LD cycle. Food and water were available *ad libitum*. All mice were age-matched and between 2 to 8 months of age at time of procedure.

All experimental procedures were performed with approval from the University of Kent Ethical Review Committee and in accordance with the Animals (Scientific Procedures) Act 1986.

6.2.2 Pupillometry in WT and TKO intact visual system

Mice were dark-adapted for a minimum of 1 hour prior to procedure.

Under infra-red illumination, individual mice were removed from home cage at ZT 4-8 and held in position by hand against the integrating sphere such as to allow irradiant light (OptoSource High Intensity Arc, Cairn Research, Faversham) to enter the right eye whilst images of consensual response in left eye were captured by CCD camera (Best Scientific, Swindon). Shutter was programmed to capture fully-dilated pupil images through to maximum constriction, at a rate of 3.75 frames per second. See Figure 6.2: A, B.

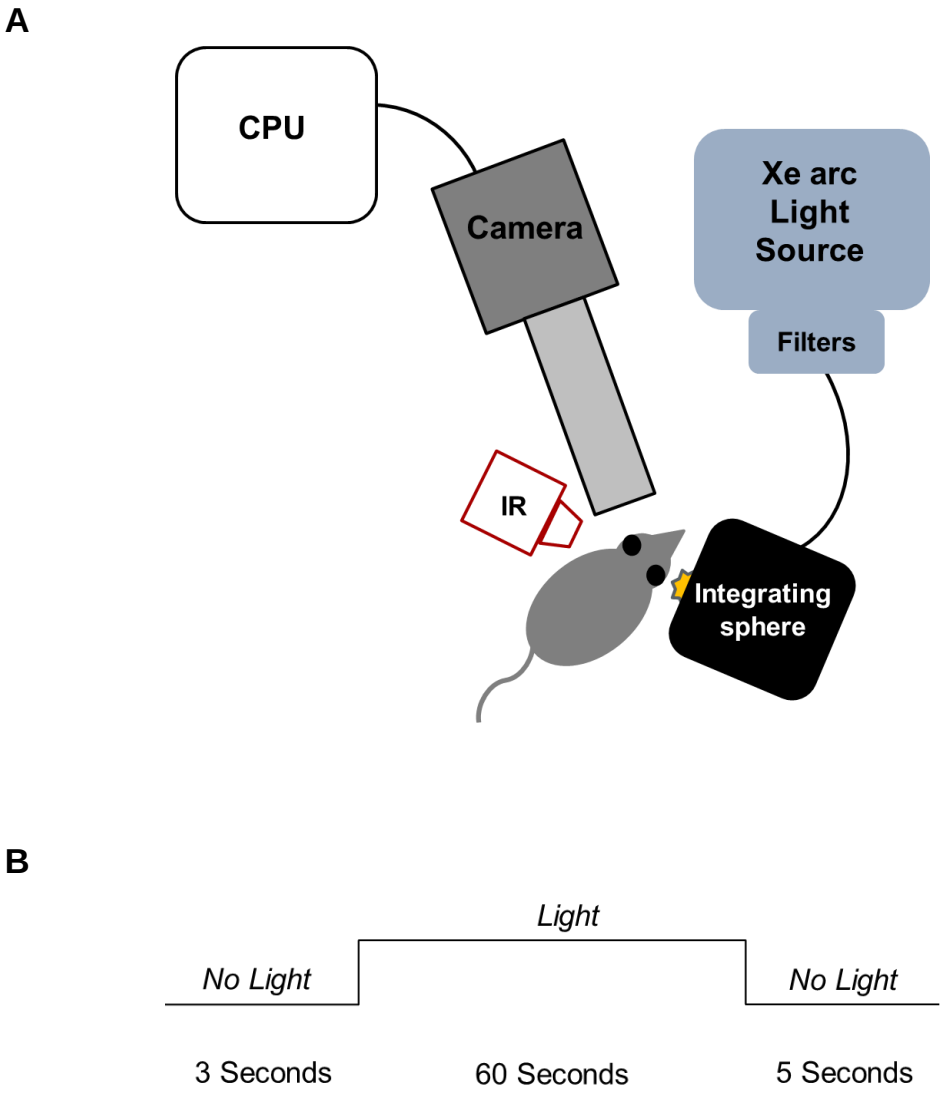

Figure 6.2: Arrangement of apparatus and timings for PLR of the intact visual system.

(A) Dark-adapted mice held by hand against integrating sphere to allow irradiant Xenon arc light to enter right eye whilst consensual pupillary response captured by camera under infra-red (IR) illumination and recorded by CPU. Intensity and wavelength of light manipulated by neutral density and bandpass filters.

(B) Shutter programme outlining timings of light exposure.

Specific light intensities produced through the use of neutral density (ND) filters with wavelength selection by bandpass filters ± 2nm (Thorlabs, UK). See Figure 6.3.

Light intensity measured by Optical power meter (Thorlabs, UK) and converted to irradiance (photon flux). See Appendix III.

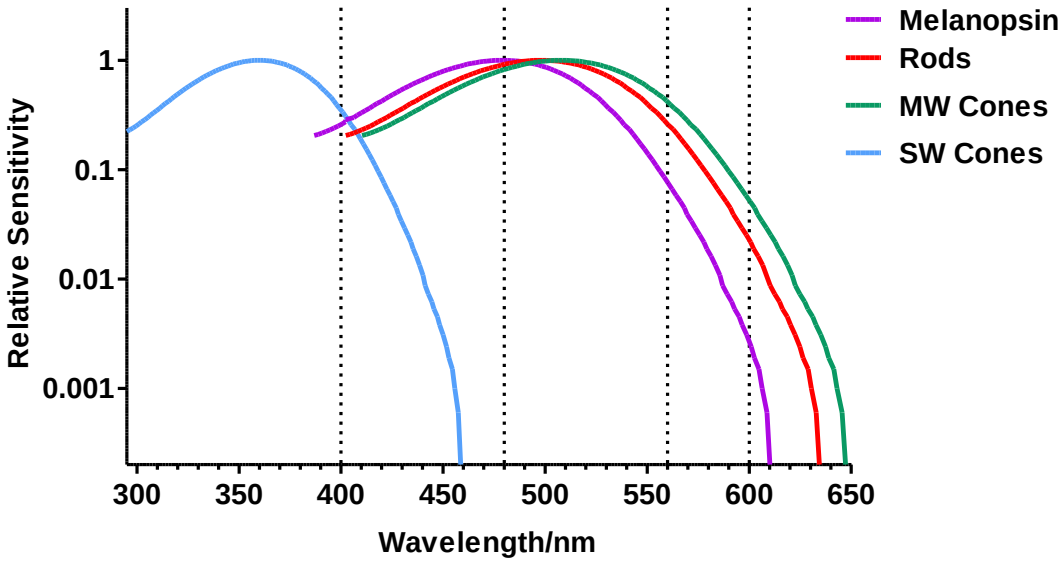

Figure 6.3: Model spectra demonstrating photoreceptor sensitivity at selected wavelengths.

Model spectra demonstrating relative sensitivity of each major photoreceptor class according to wavelength of visible light with melanopsin shown in purple, rods in red, mid-wavelength cones in green and short-wavelength cones in blue

[Adapted from (Partridge and De Grip, 1991)].

6.2.3 Pupillometry using isolated eye preparation

Mice were dark-adapted for a minimum of 1 hour prior to procedure. Under infra-red illumination, individual mice were sacrificed by cervical dislocation at ZT 4-8. Both eyes were removed immediately and submerged in neurobasal media (Thermo Fisher Scientific, Loughborough, UK) within separate bespoke holders at approximately 30°C. One eye placed in position for application of direct polychromatic (white) light from Xenon arc source whilst second eye temporarily covered to protect from light. Images captured by camera (Cairn, UK) with shutter programmed to capture fully-dilated pupil images through to maximum constriction, at a rate of 3.75 frames per second. The process was then repeated with second eye. See Figure 6.4: A, B.

A range of light intensities were produced through the use of neutral density (ND) filters (Thorlabs, UK) with optical power measured by meter (Thorlabs, UK) and converted to irradiance (photon flux) as described above.

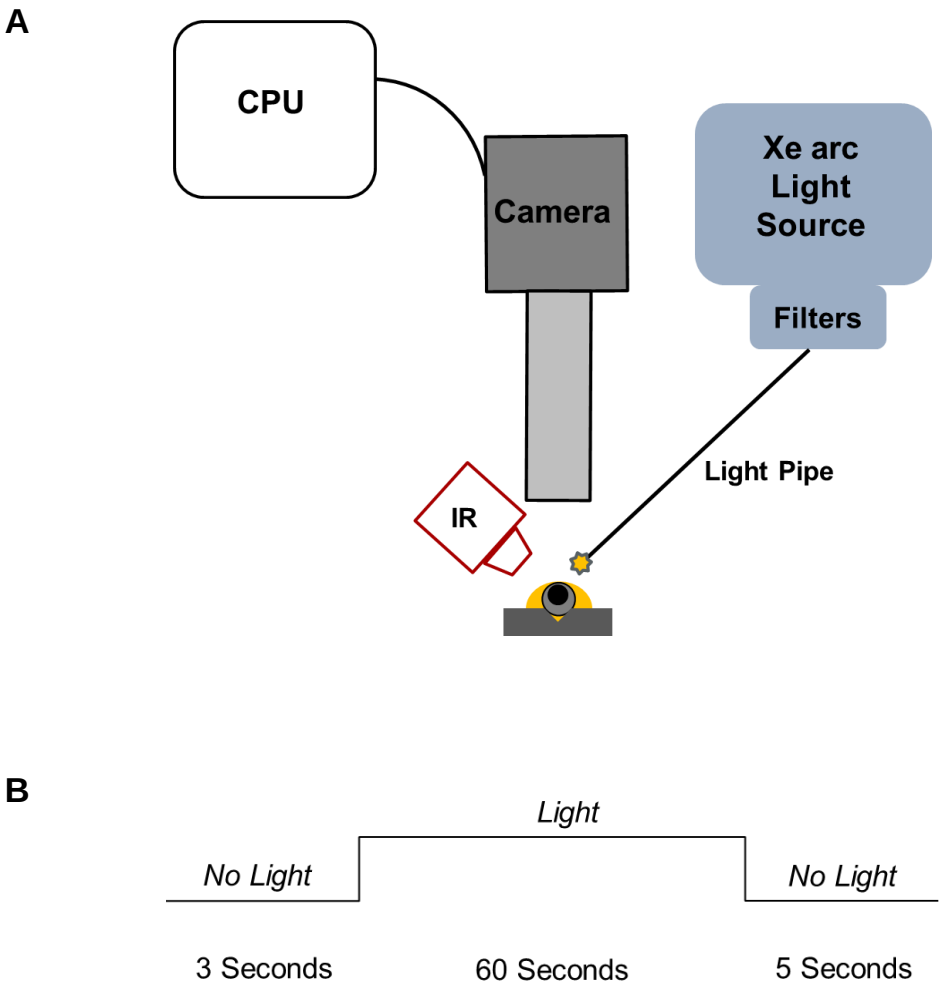

Figure 6.4: Arrangement of apparatus and timings for intrinsic PLR.

(A) Isolated eye from dark-adapted mouse placed into bespoke holder with neurobasal media (shown in yellow). Direct light applied by Xenon arc light for capture of intrinsic pupillary response by camera under infra-red (IR) illumination and recorded by CPU. Light intensity manipulated by neutral density filters.

(B) Shutter programme outlining timings of light exposure

6.2.4 Analysis of images

Pupil images were analysed for dark-adapted fully-dilated pupil size and maximal constriction to light using *Imagej* software (NIH, USA). See Figure 6.5.

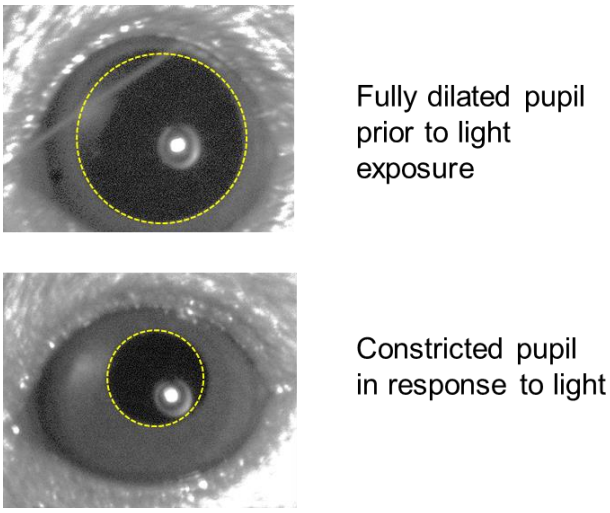

Figure 6.5: Use of *Imagej* software for measurement of pupillary constriction.
Fully dilated and constricted pupils are fitted with circumference marker (shown in yellow) to determine pupil area in pixels. Normalised pupil area is calculated for individual mice to eliminate physiological differences.

Normalised pupil area of maximal response was calculated according to the formula:

$$\textit{Normalised pupil area} = \frac{\textit{minimum pupil size during light exposure}}{\textit{maximum dark-adapted pupil area}}$$

Maximum rate of pupillary constriction was analysed by measurement of normalised pupil area for every WT and TKO image during first 5 seconds of highest intensity light and plotted as a function of time.

Statistical significance was determined using GraphPad Prism 5 software (San Diego, CA) by student's *t* tests and non-linear regression of curve (log [irradiance] Vs normalised response) for irradiance response curves. Rate of pupillary constriction was analysed by non-linear regression of curve (exponential decay). Data presented as mean ± SEM (standard error of mean) with statistical significance defined as being $P < 0.05$.

6.3 Results

6.3.1 Pupillary constriction to 400nm is unchanged by TASK-3 loss

The use of 400nm light for the initial PLR investigation targeted the sub-class of short-wavelength (SW) cones, known to exhibit maximum sensitivity (λ_{max}) at 360nm, whilst remaining in the visible range (Hattar et al., 2003, Lucas et al., 2012). At this wavelength there were no significant differences in TKO and WT PLR from 10^8 to 10^{15} photons/cm^2/s light intensities. Additionally, both strains were able to achieve similar maximal constriction to highest irradiance (10^{15} photons/cm^2/s, normalised pupil area: WT 0.089 ± 0.005, TKO 0.095 ± 0.009, Student's t test: $P > 0.05$ (n=4-6). See Figure 6.6: A-C.

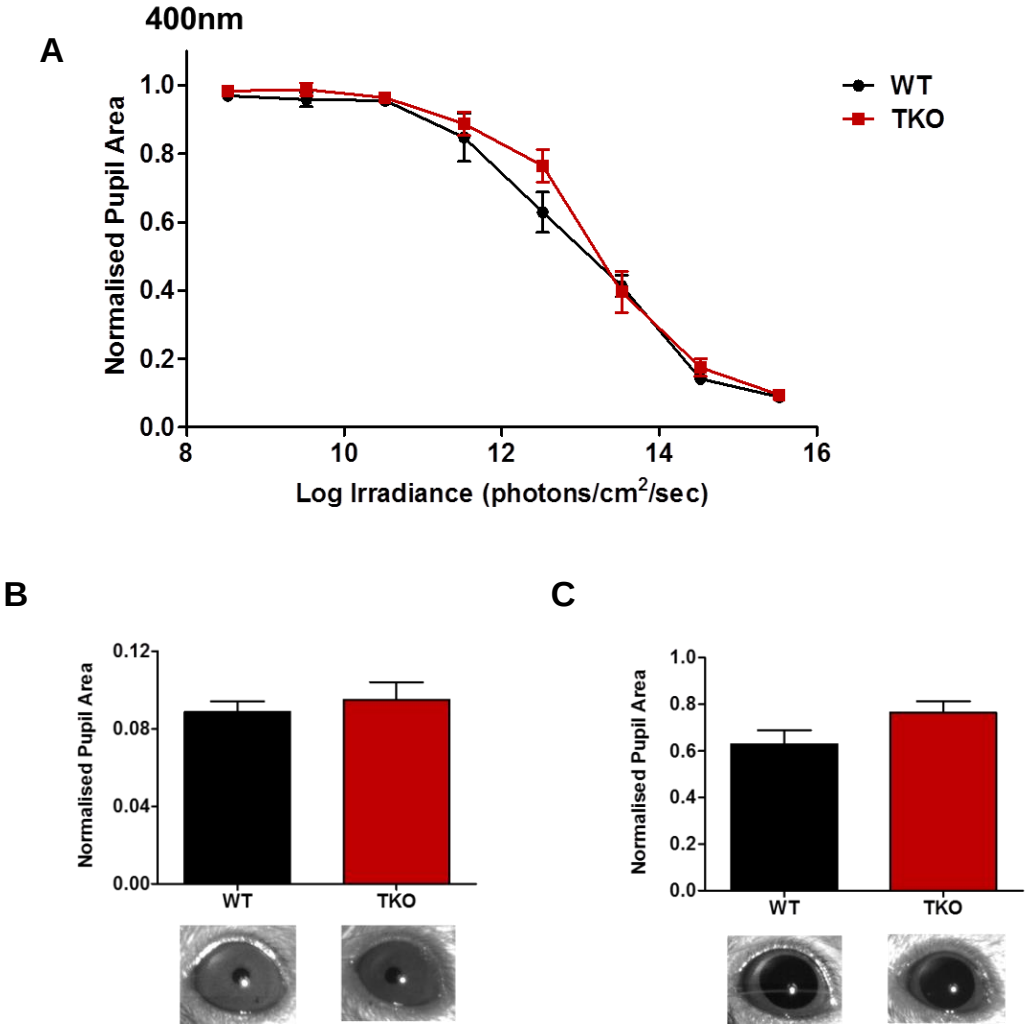

Figure 6.6: Irradiance response curves (IRCs) for WT and TKO mice to 400nm monochromatic light.

(A) WT and TKO IRCs to 400nm light demonstrating no significant difference in normalised pupil area across all intensities examined, 10^{8} to 10^{15} photons/cm^2/s, Student's t test: $P > 0.05$ with (B) showing similar WT and TKO mean normalised pupil area at highest irradiance 10^{15} photons/cm^2/s, and (C) at 10^{12} photons/cm^2/s; with representative pupil images (n=4-6).

6.3.2 TASK-3 KO mice show altered irradiance response curves to monochromatic light of 480-600nm wavelength

At 480nm all three major classes of photoreceptor are fully activated, with melanopsin photopigment at its most sensitive (λ_{max}). Whilst the ipRGCs play a major role in decoding high intensity light along with MW cones, at low levels of irradiance rods are activated and decode light of this wavelength (Hattar et al., 2003, Lucas et al., 2012). Here, measurements of normalised pupil area to irradiance of 10^7 to 10^{14} photons/cm^2/s demonstrated significant attenuation in TKO PLR relative to WT at 10^{11} to 10^{13} photons/cm^2/s by Student's t test (10^{11} photons/cm^2/s WT 0.525 ± 0.042, TKO 0.760 ± 0.027, P = 0.0002; 10^{12} photons/cm^2/s: WT 0.257 ± 0.012, TKO 0.417 ± 0.030, P = 0.0009; 10^{13} photons/cm^2/s: WT 0.141 ± 0.008, TKO 0.210 ± 0.025 P = 0.0168). However there was no significant difference in TKO and WT constriction observed to highest intensity light (10^{14} photons/cm^2/sec, normalised pupil area: WT 0.085 ± 0.008, TKO 0.107 ± 0.008, P > 0.05, n=5-10). See Figure 6.7: A-C.

To draw out the contribution of classic photoreceptors from ipRGCs, a longer wavelength of 560nm was selected. See Figure 6.3. At this wavelength melanopsin activation is greatly reduced whilst MW cone, and to lesser extent rod, sensitivity remains (Hattar et al., 2003, Lucas et al., 2012). Maximal constriction to irradiance of 10^6 to 10^{14} photons/cm^2/s revealed significantly diminished PLR from 10^{10} to 10^{12} photons/cm^2/s in the TKO mice compared to WT by Student's t test (10^{10} photons/cm^2/s: WT 0.854 ± 0.033, TKO 0.954 ± 0.007, P = 0.0153; 10^{11} photons/cm^2/s: WT 0.704 ± 0.051, TKO 0.911 ± 0.018, P = 0.0023; 10^{12} photons/cm^2/s: WT 0.556 ± 0.029, TKO 0.726 ± 0.048, P = 0.0073). Once more there was no significant change in PLR to highest irradiance from TASK-3 loss

(10^{14} photons/cm^2/s: WT 0.203 ± 0.014, TKO 0.217 ± 0.016, $P > 0.05$, n=4-10). See Figure 6.8: A-C.

The final monochromatic wavelength selected at 600nm is considered to be beyond melanopsin sensitivity, with MW cones and rods exhibiting a low sensitivity (Hattar et al., 2003, Lucas et al., 2012). Pupillometry to this wavelength from 10^8 to 10^{14} photons/cm^2/s showed a significant reduction in TKO constriction relative to WT at the highest intensity light only (10^{14} photons/cm^2/s, WT 0.404 ± 0.056, TKO 0.627 ± 0.050, Student's t test: $P = 0.0118$, n=3-5). See Figure 6.9: A-C.

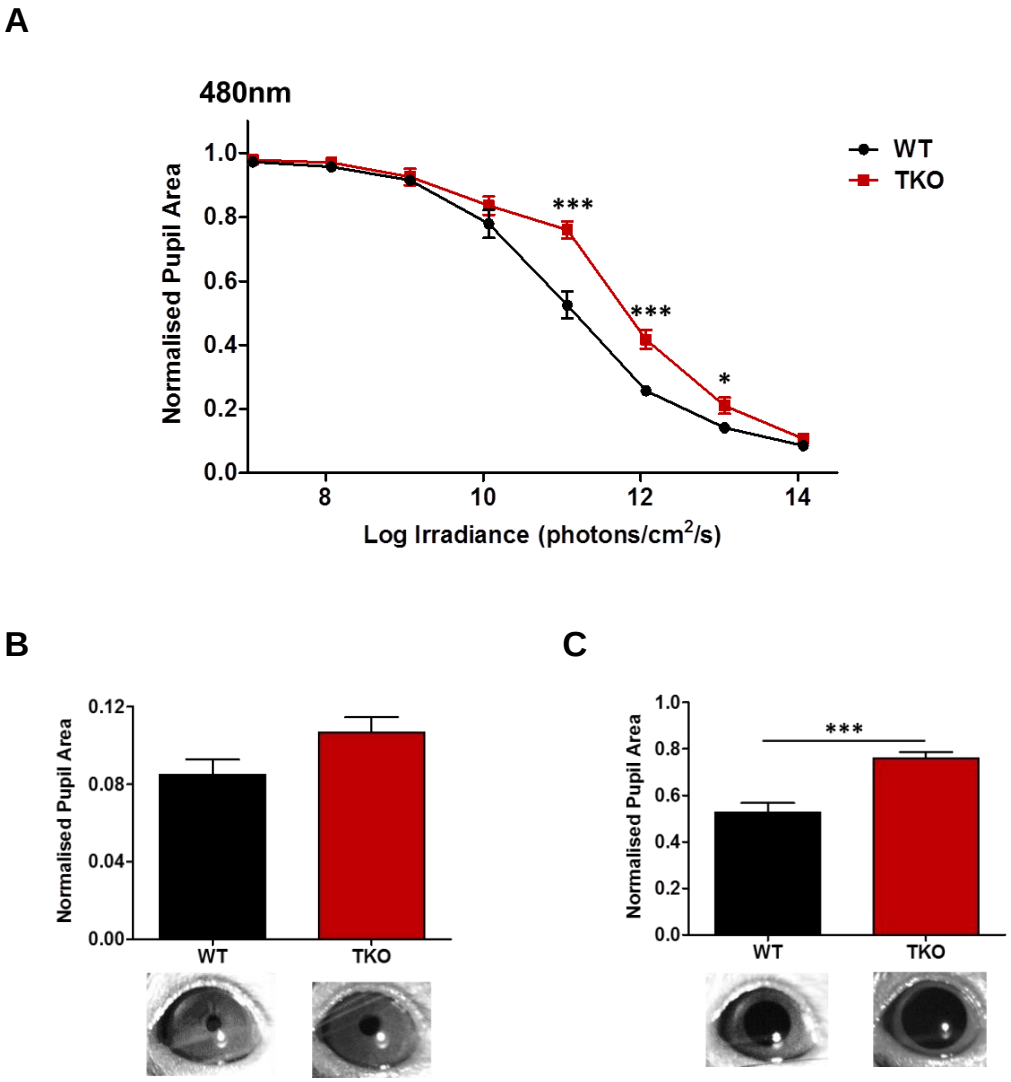

Figure 6.7: Irradiance response curves (IRCs) for WT and TKO mice to 480nm monochromatic light.

(A) WT and TKO IRCs to 480nm light (10^7 to 10^{14} photons/cm^2/s) demonstrating significant attenuation in TKO PLR at 10^{11} to 10^{13} photons/cm^2/s, Student's t test: $P < 0.05$ with (B) illustrating similar WT and TKO pupillary constriction to highest irradiance, 10^{14} photons/cm^2/s , Student's t test: $P > 0.05$, and (C) highlighting significant reduction in TKO constriction at 10^{11} photons/cm^2/s, Student's t test: $P < 0.001$, with representative pupil images (n=5-10).

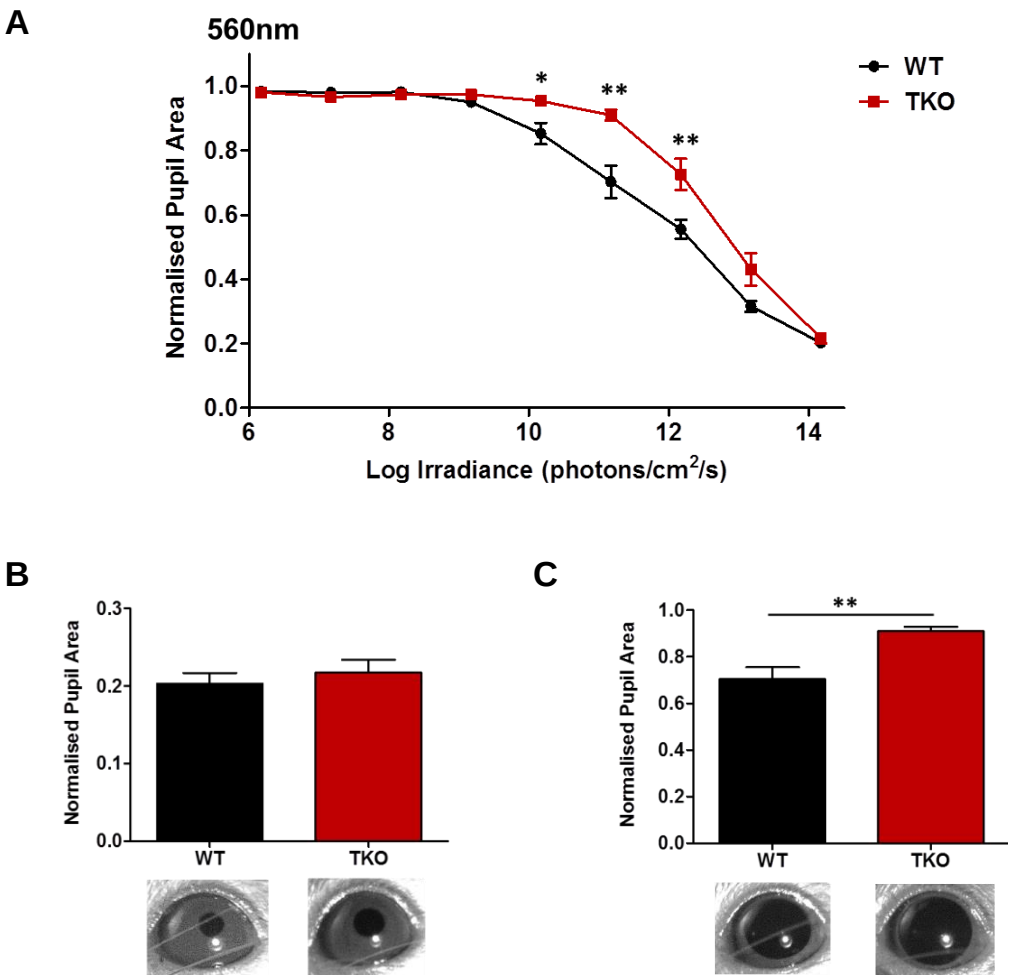

Figure 6.8: Irradiance response curves (IRCs) for WT and TKO mice to 560nm monochromatic light.

(A) WT and TKO IRCs to 560nm light (10^6 to 10^{14} photons/cm^2/s) demonstrating significant attenuation in TKO PLR at 10^{10} to 10^{12} photons/cm^2/s, Student's t test: $P < 0.05$ with (B) showing no significant difference in PLR to highest irradiance, 10^{14} photons/cm^2/s, from TASK-3 loss, Student's t test: $P > 0.05$, and (C) highlighting significantly diminished PLR in TKO mice compared to WT at 10^{11} photons/cm^2/s, Student's t test: $P < 0.01$, with representative pupil images (n= 4-10).

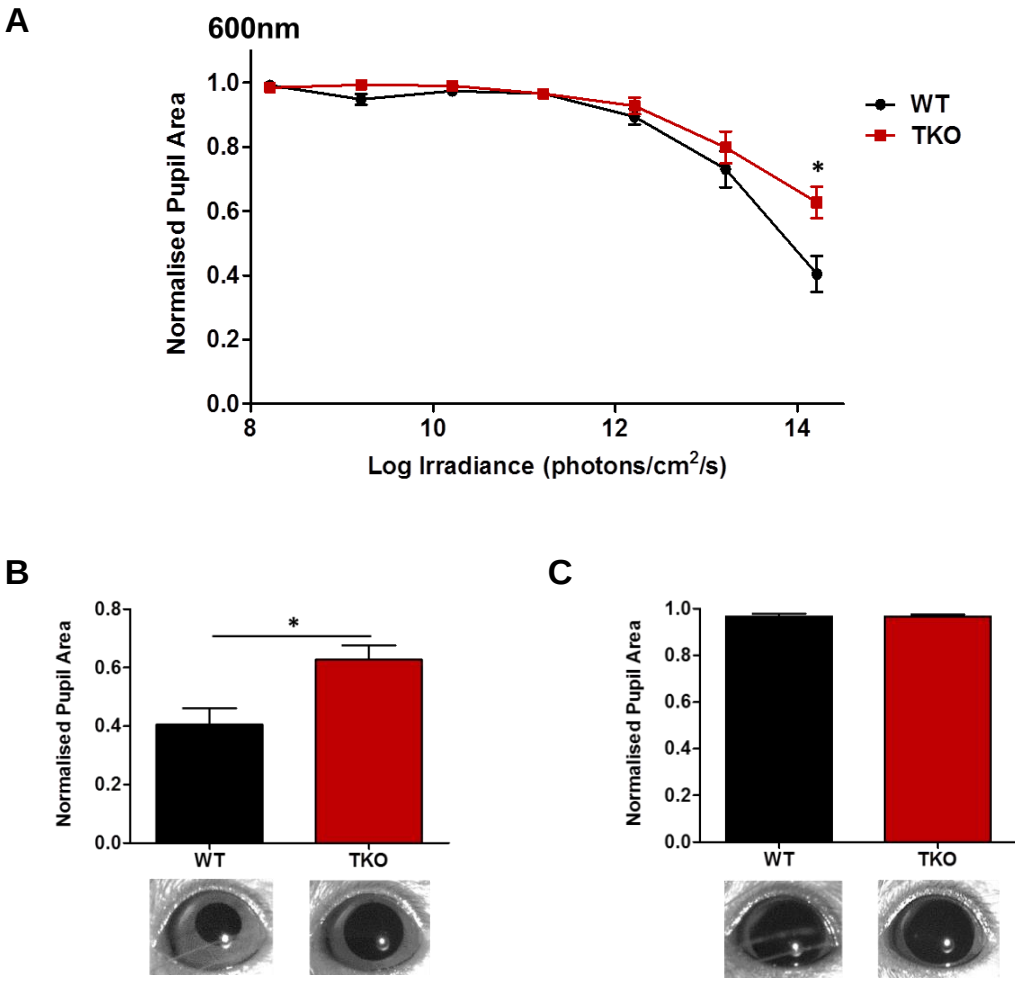

Figure 6.9: Irradiance response curves (IRCs) for WT and TKO mice to 600nm monochromatic light.

(A) WT and TKO IRCs to 600nm light (10^6 to 10^{14} photons/cm^2/s) revealing significant attenuation in TKO PLR at 10^{14} photons/cm^2/s only, Student's t test: $P < 0.05$ with (B) highlighting this difference in WT and TKO normalised pupil area at 10^{14} photons/cm^2/s and (C) demonstrating similar WT and TKO constriction at 10^{11} photons/cm^2/s, Student's t test: $P > 0.05$, with representative pupil images (n= 3-5).

6.3.3 Persistence of pupillary light reflex to polychromatic light in the absence of TASK-3

Following pupillometry conducted with monochromatic light of specific wavelength, broad spectrum white light was used to examine WT and TKO PLR to a range of intensities of environmental light. Measurements of normalised pupil area to irradiances of 10^8 to 10^{16} photons/cm^2/s demonstrated significant attenuation in TKO PLR relative to WT at sub-saturating light of 10^{12} photons/cm^2/s only by Student's t test (WT 0.685 ± 0.034, TKO 0.837 ± 0.050, P = 0.020). However there was no significant difference in TKO and WT constriction observed to highest intensity light (10^{16} photons/cm^2/s, normalised pupil area: WT 0.065 ± 0.004, TKO 0.0.063 ± 0.009, $P > 0.05$, n=7-13). See Figure 6.5: A-C. Interestingly, there was no significant difference in WT and TKO PLR at irradiances equivalent to room lighting conditions used for behavioural experiments in chapters 3-5. See Figure 6.10: A-C.

In order to eliminate any possible contribution of SW cones to PLR, white light minus UV wavelengths of less than 400nm was used across a range of intensities. Under this light regime measurements of normalised pupil area showed no significant difference between WT and TKO mice to irradiances of 10^{10} to 10^{16} photons/cm^2/s. However the maximum pupillary constriction to highest intensity light was slightly reduced compared to full spectrum white light (WT 0.088 ± 0.007, TKO 0.069 ± 0.006, Student's t test: $P > 0.05$, n=5-9). See Figure 6.11: A-C.

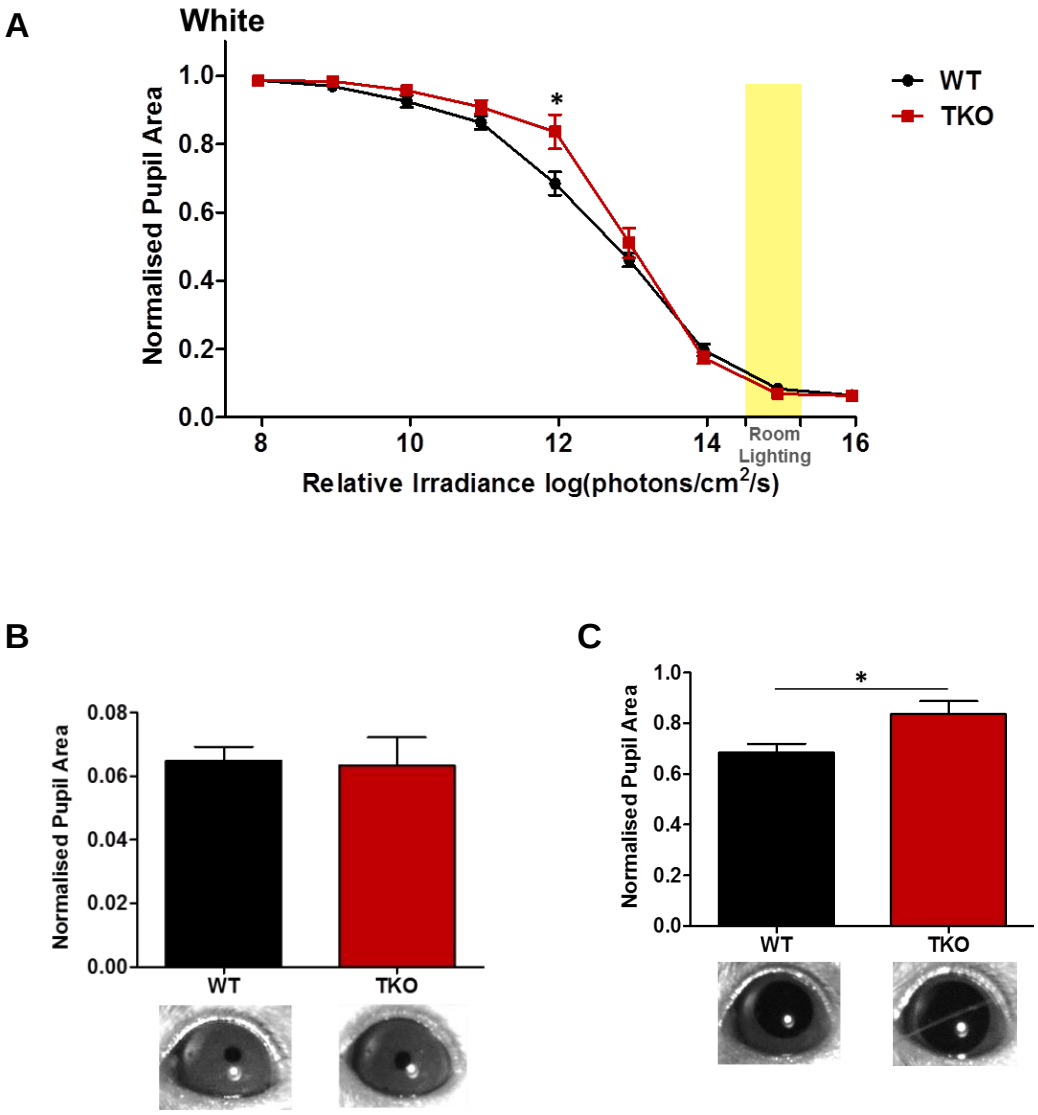

Figure 6.10: Irradiance response curves (IRCs) for WT and TKO mice to broad spectrum white light

(A) WT and TKO IRCs to broad spectrum white light (10^8 to 10^{16} photons/cm^2/s) demonstrating significant attenuation in TKO PLR at 10^{12} photons/cm^2/s only, Student's t test: $P < 0.05$ with (B) illustrating similar WT and TKO maximal pupillary constriction to highest irradiance, 10^{16} photons/cm^2/s, Student's t test: $P > 0.05$, and (C) highlighting significant reduction in TKO constriction at 10^{12} photons/cm^2/s, Student's t test: $P < 0.05$, with representative pupil images. Note how WT and TKO constrictions saturate at 10^{15} photons/cm^2/s, with no further decrease in normalised pupil area achieved at higher - irradiance of 10^{16} photons/cm^2/s (n=7-13).

Yellow bar denotes relative irradiance of room illumination during behavioural experiments.

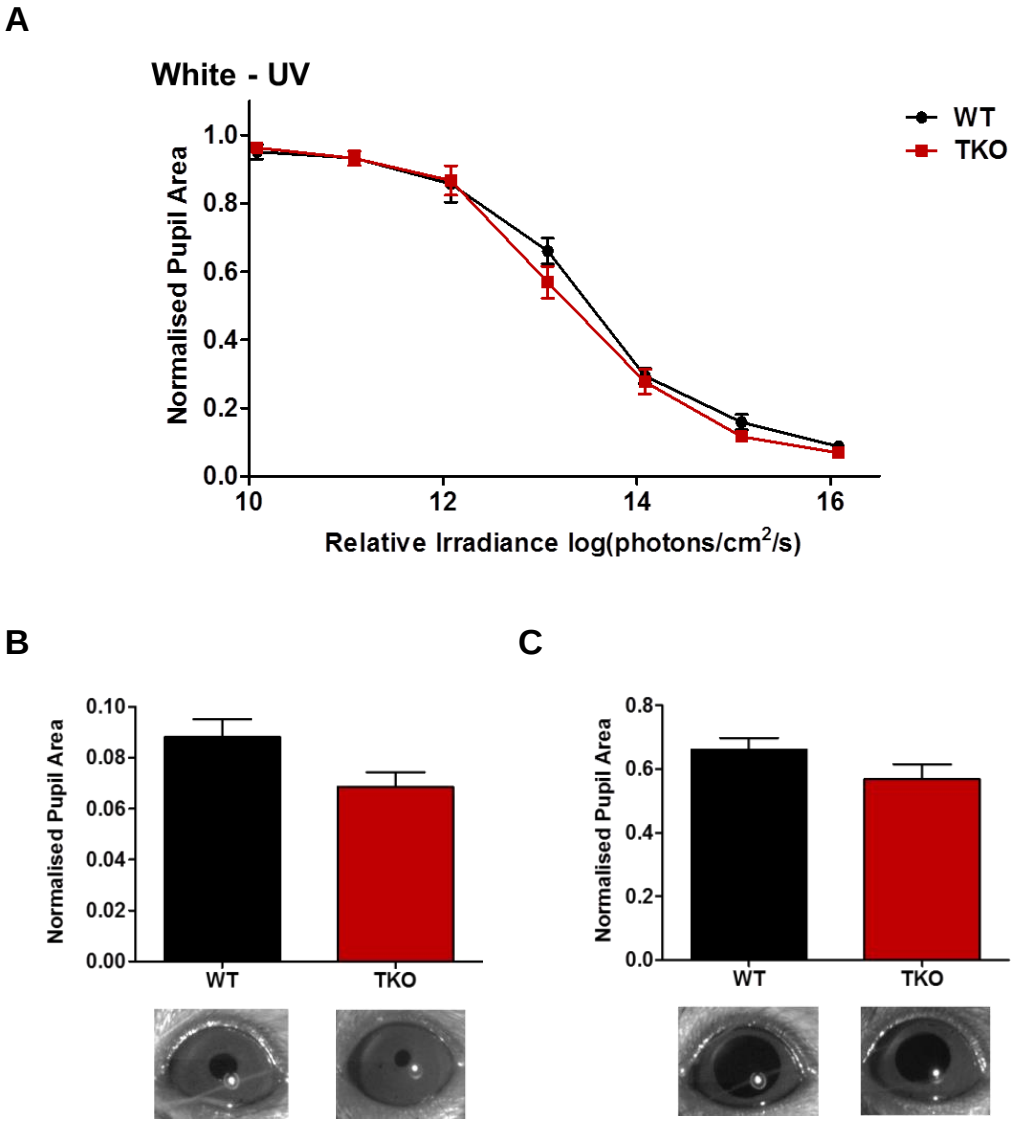

Figure 6.11: Irradiance response curves (IRCs) for WT and TKO mice to broad spectrum white light with white light minus UV wavelengths less than 400nm.

(A) WT and TKO IRCs to white light minus UV wavelengths less than 400nm demonstrating no significant difference in normalised pupil area across all intensities examined (10^{10} to 10^{16} photons/cm^2/s, Student's t test: $P > 0.05$) with (B) highlighting similar pupillary constriction between WT and TKO strains at highest irradiance 10^{16} photons/cm^2/s, and (C) at 10^{13} photons/cm^2/s, with representative pupil images (n=5-9).

6.3.4 TASK-3 loss impacts rate of pupillary constriction at specific wavelengths

Despite WT and TKO mice exhibiting similar PLR to the highest intensity light (10^{14} photons/cm^2/s) at 400, 480 and 560nm, the rate of pupillary constriction over the initial five seconds of light exposure varied significantly between strains, according to wavelength. At 400nm WT pupils constrict significantly faster than TKO (non-linear regression, $P = 0.0034$), whereas at 480nm the TKO rate of constriction is faster (non-linear regression, $P < 0.0001$). Analysis of response to 560nm wavelength showed no significant difference in the rate of constriction between strains (non-linear regression, $P > 0.05$). See Figure 6.12: A-F.

When pupillary response rates to 400-560nm light were analysed within strain according to wavelength, WT mice show a significant decrease in rate as wavelength increases (non-linear regression, $P < 0.0001$). A similar analysis in TASK-3 KO mice reveals a significant difference according to wavelength (non-linear regression, $P < 0.0001$), but with the fastest response occurring at 480nm. See Figure 6.13: A-D.

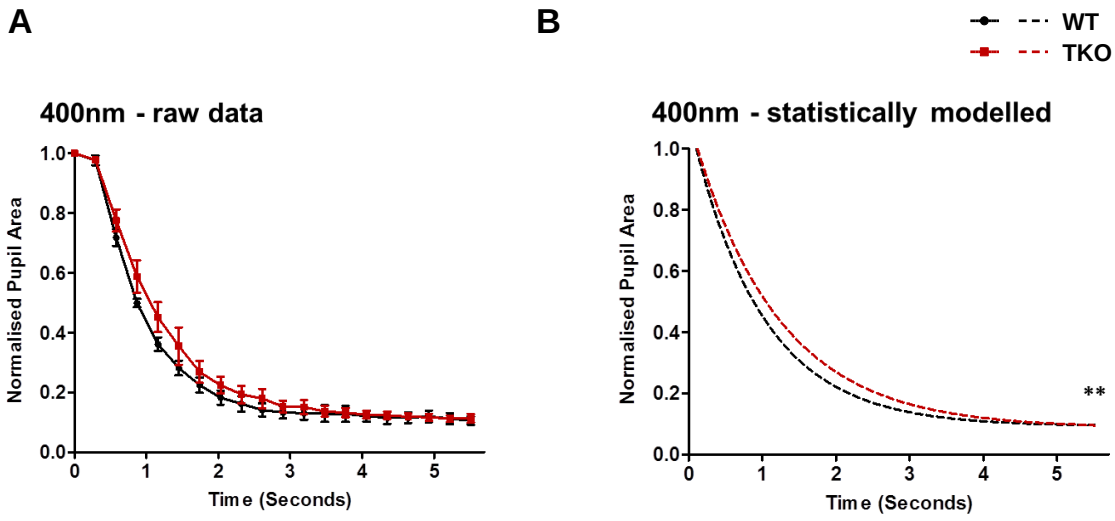

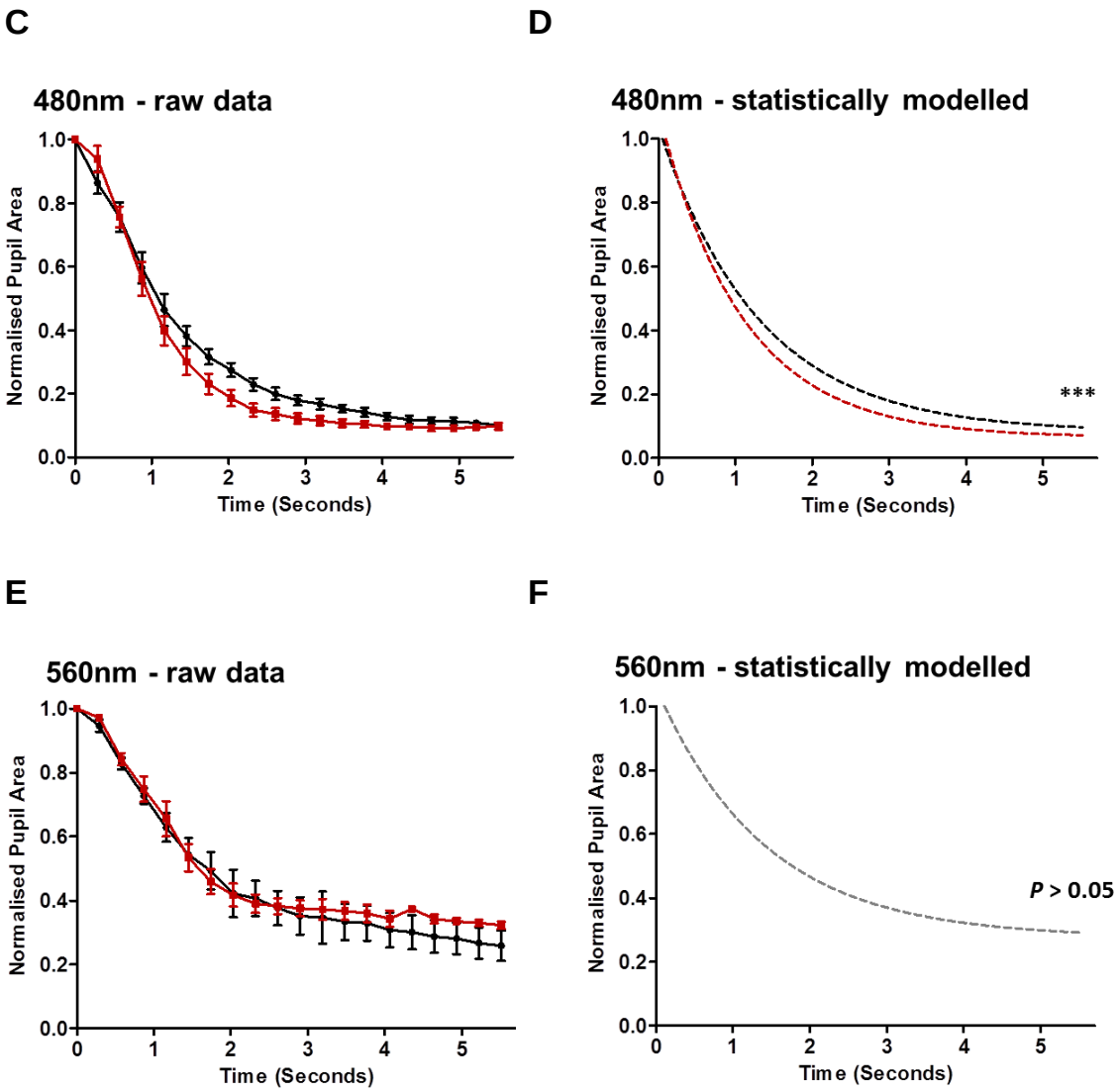

Figure 6.12: Rates of WT and TKO pupillary constriction to saturating light of 400, 480 and 560nm wavelengths.

(A) Rates of constriction in WT and TKO mice over initial 5 seconds of exposure to saturating 400nm light showing a slower pupillary response in the absence of TASK-3 with (B) showing significant difference in curves fitted by linear regression analysis, $P < 0.01$.

(C) Rates of constriction in WT and TKO mice over initial 5 seconds of exposure to saturating 480nm light showing a faster pupillary response following TASK-3 loss with (D) showing significant difference in curves fitted by linear regression analysis, $P < 0.0001$.

(E) Rates of constriction in WT and TKO mice over initial 5 seconds of exposure to saturating 560nm light with (F) showing no significant difference in rate, one curve serves both data sets fitted by linear regression analysis, $P > 0.05$.

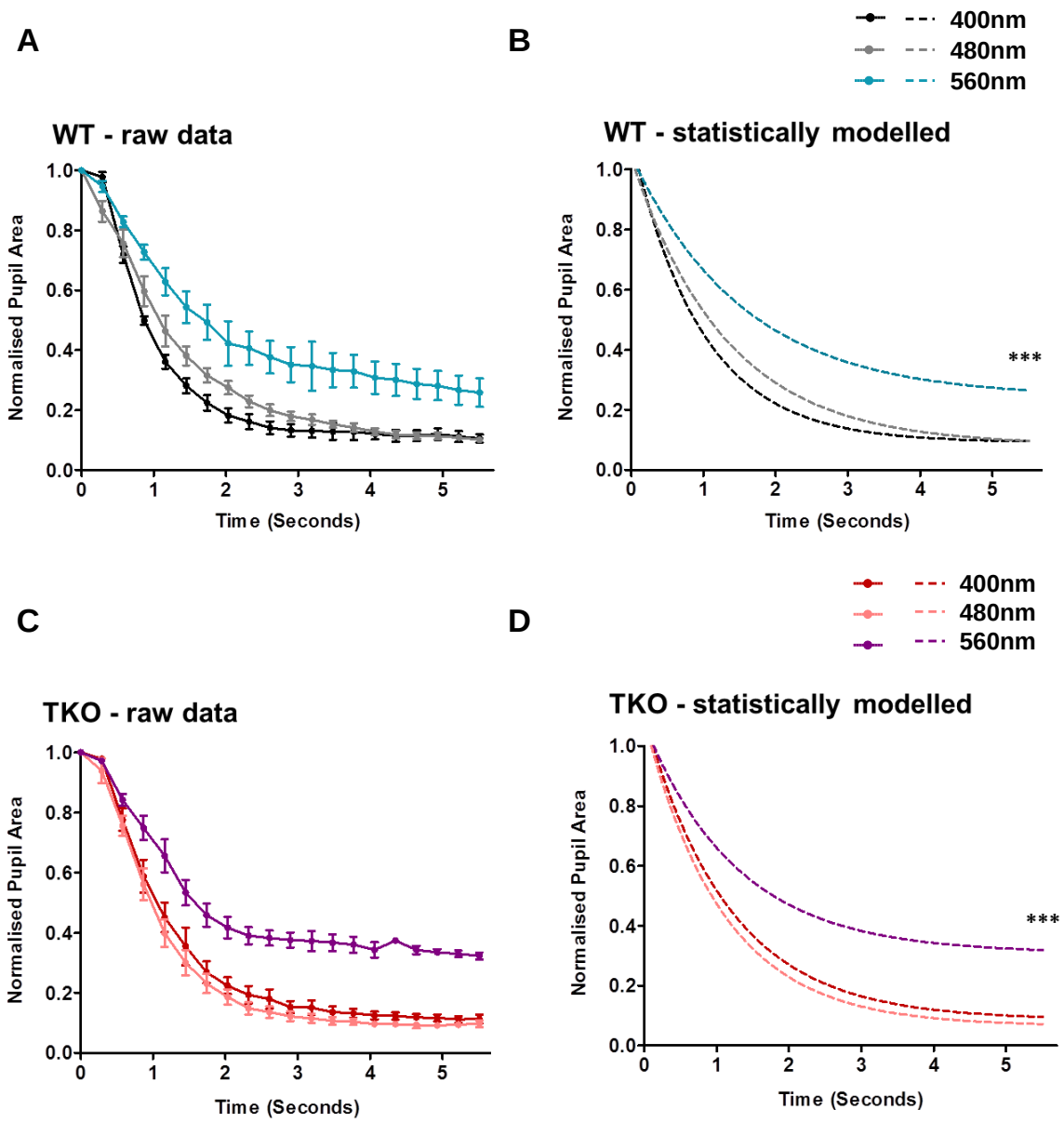

Figure 6.13: Comparing rates of pupillary constriction within WT and TKO strains to saturating light of 400, 480 and 560nm wavelengths.

(A) Comparison of WT rates of constriction to saturating light of 480, 400 and 560nm wavelength demonstrating how response rate decreases with increasing wavelength with (B) showing significant difference in curves fitted by linear regression analysis, $P < 0.0001$.

(C) Comparison of TKO rates of constriction to saturating light of 480, 400 and 560nm wavelength demonstrates how response rate varies according to wavelength with fastest constriction at 480nm with (D) showing significant difference in curves fitted by linear regression analysis, $P < 0.0001$.

6.3.5 Removal of UV component of polychromatic light does not affect rate of pupillary constriction in TASK-3 KO mice

Pupillometry to broad spectrum white light demonstrated an equal maximal constriction to the highest intensity light (10^{16} photons/cm^2/s) in WT and TASK-3 KO strains. However, the rate of pupillary constriction over the initial 5 seconds of light exposure is significantly attenuated in the absence of TASK-3 (non-linear regression, $P < 0.0001$). See Figure 6.14: A-D.

Removal of UV light by cutting off wavelengths of less than 400nm significantly slowed the WT pupillary response (non-linear regression, $P < 0.0001$) but had no effect on the TASK-3 KO mice (non-linear regression, $P > 0.05$). Therefore, in the absence of UV light, TASK-3 KO mice have a faster pupillary constriction than WT (non-linear regression, $P < 0.0001$). See Figure 6.15: A-D.

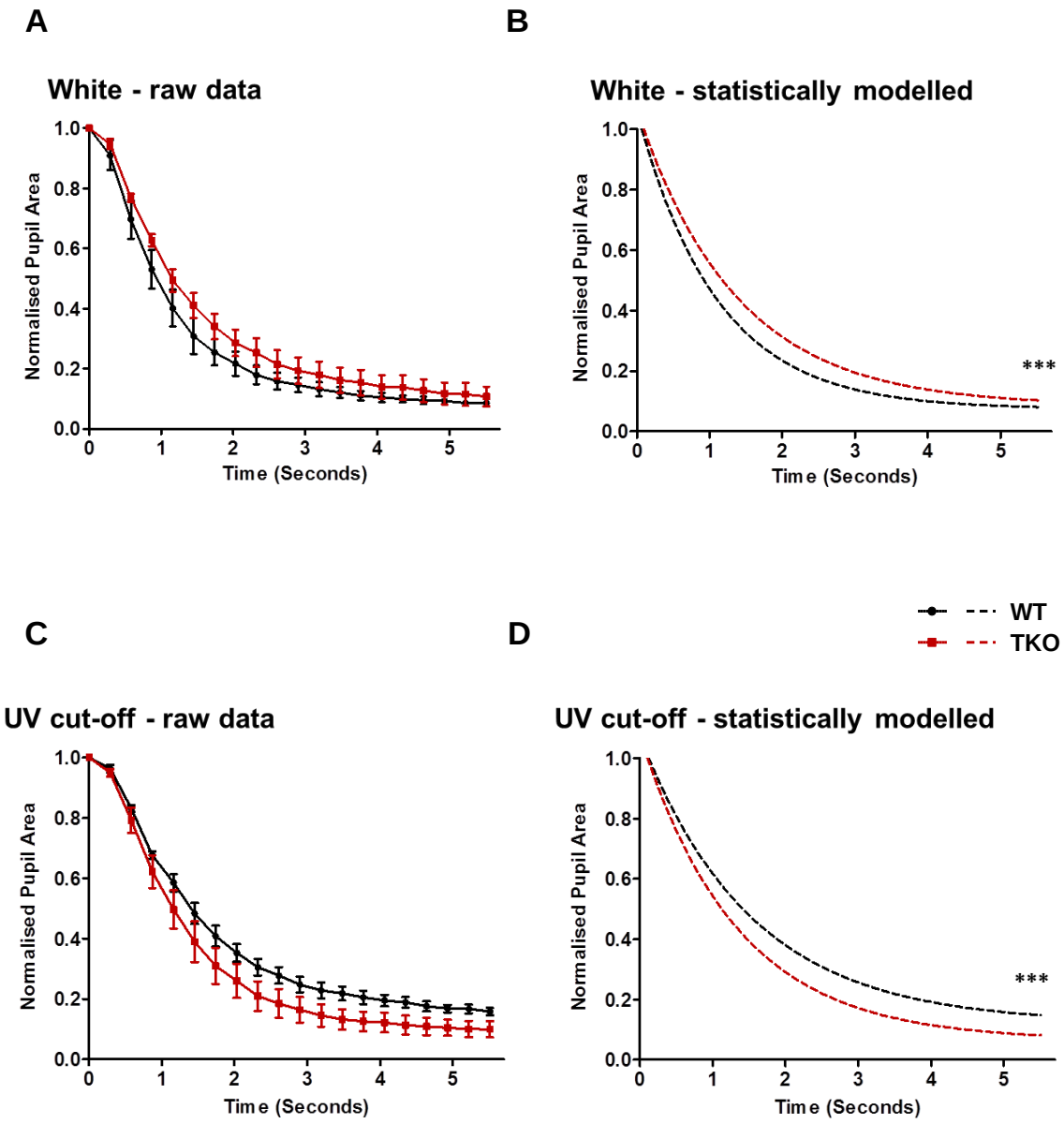

Figure 6.14: Rates of pupillary constriction in WT and TKO mice to saturating polychromatic light with, and without, UV of less than 400nm wavelength.

(A) Rates of constriction in WT and TKO mice over initial 5 seconds of exposure to saturating broad spectrum white light showing a slower pupillary response in TASK-3 KO mice relative to WT with (B) showing significant difference in curves fitted by linear regression analysis, $P < 0.0001$.

(C) Rates of constriction in WT and TKO mice over initial 5 seconds of exposure to saturating white light following elimination of UV (< 400nm wavelength)showing a faster pupillary response in the TASK-3 KO mice with (D) showing significant difference in curves fitted by linear regression analysis, $P < 0.0001$.

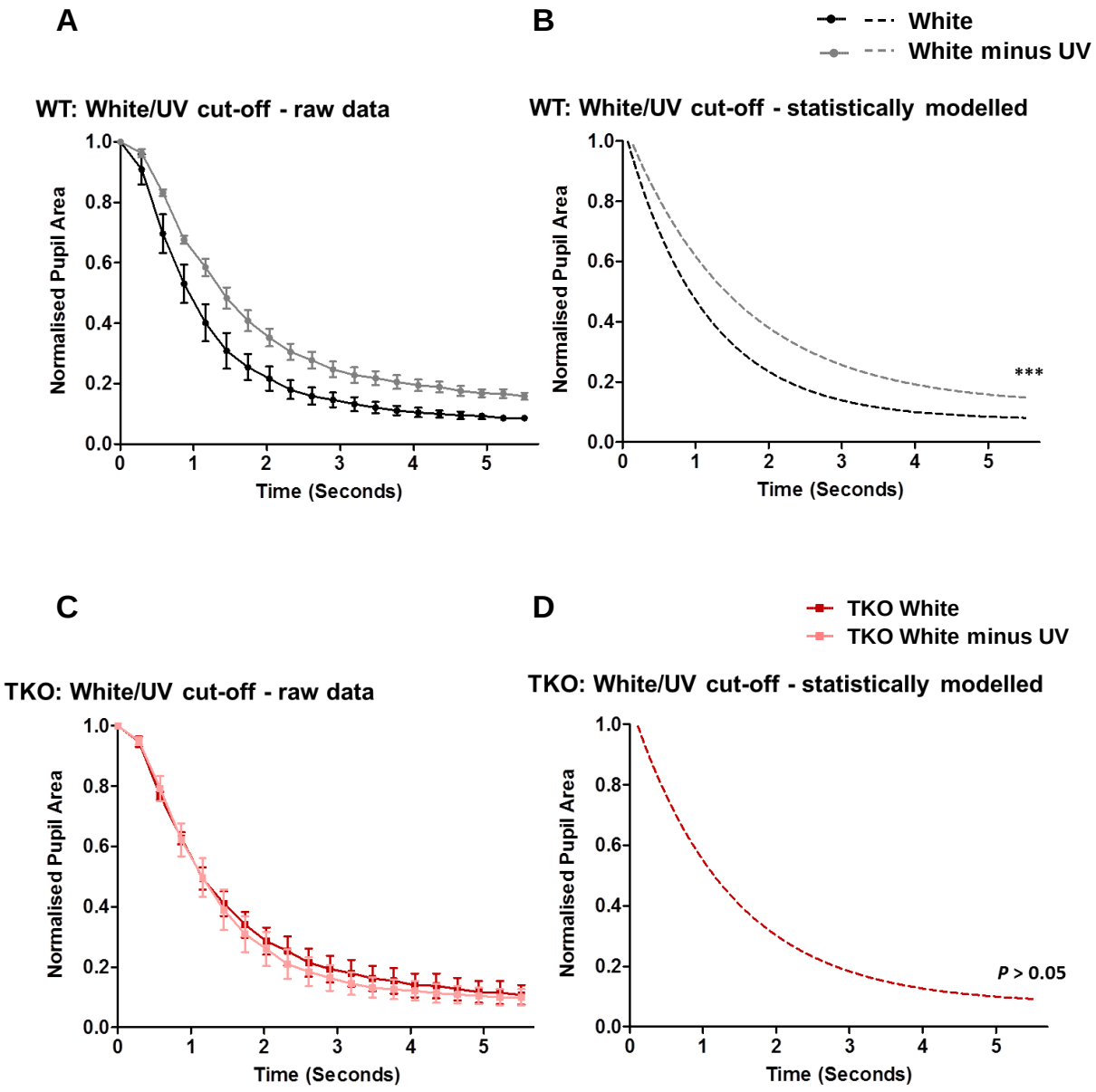

Figure 6.15: Comparing rates of pupillary constriction within WT and TKO strains to saturating polychromatic light with, and without, UV of less than 400nm wavelength.

(A) Comparison of WT rates of constriction to saturating broad spectrum white light and white light with wavelengths less than 400nm removed highlights the attenuation in rate of pupillary response in the absence of UV light, with (B) showing significant difference in curves fitted by linear regression analysis, $P < 0.0001$.

(C) Comparison of TKO rates of constriction to saturating broad spectrum white light and white light with wavelengths less than 400nm removed reveals no change in rate of response from elimination of UV light, with (D) showing no significant difference in rates, one curve serves both data sets fitted by linear regression analysis, $P > 0.05$.

6.3.6 Intrinsic PLR in WT and TKO mice

Pupillometry using the isolated eye preparation to radiant light of 10^{13} to 10^{16} photons/cm^2/s reveals a significant attenuation in TKO intrinsic pupillary constriction to sub-saturating light at 10^{13} and 10^{14} photons/cm^2/s in comparison to WT responses by Student's t test (normalised pupil area 10^{13} photons/cm^2/s: WT 0.853 ± 0.019, TKO 0.965 ± 0.011, P = 0.0002; 10^{14} photons/cm^2/s: WT 0.703 ± 0.046, TKO 0.872 ± 0.022, P = 0.0035, n=4-8). Maximum intrinsic PLR to highest intensity light was not significantly different between WT and TKO mice (normalised pupil area 10^{16} photons/cm^2/s: WT 0.402 ± 0.039, TKO 0.513 ± 0.051, P > 0.05). See Figure 6.16: A-C.

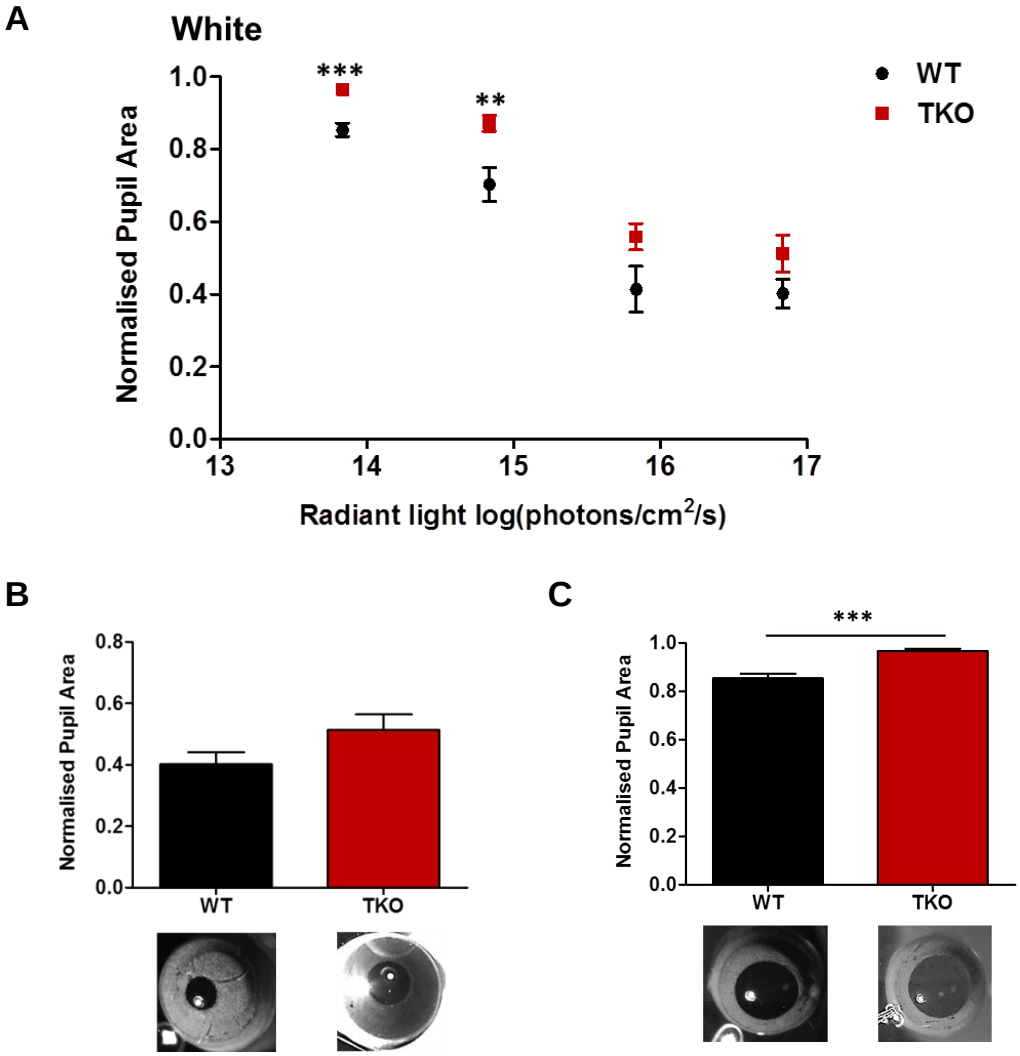

Figure 6.16: Intrinsic PLR in WT and TKO mice to broad spectrum white light.

(A) WT and TKO intrinsic IRCs to broad spectrum white light (10^{13} to 10^{16} photons/cm^2/s) demonstrating significant attenuation in TKO PLR at sub saturating light at 10^{13} and 10^{14} photons/cm^2/s, Student's t test: $P < 0.05$, with (B) illustrating similar WT and TKO maximal pupillary constriction to highest irradiance, 10^{16} photons/cm^2/s, Student's t test: $P > 0.05$, and (C) highlighting significant reduction in TKO constriction at 10^{13} photons/cm^2/s, Student's t test: $P < 0.05$, with representative pupil images (n=4-8).

6.4 Discussion

These data highlight the impact of TASK-3 loss on PLR with significant alteration in sensitivity and rate of constriction to selected monochromatic and polychromatic stimuli.

Detailed research has demonstrated each major class of photoreceptor; rods, cones and melanopsin-containing RGCs; to have a specific range of sensitivity according to wavelength, see Figure 6.1(Lall et al., 2010, Lucas et al., 2012). Considering the monochromatic IRCs at 480 and 560nm wavelength, the attenuated PLR to sub-saturating intensities of light in the TASK-3 KO mice suggest the loss of this channel has an impact on cone-driven responses. At the highest light intensity WT and TKO mice exhibit an equal constriction indicative of a functional melanopsin system which has been confirmed by PLR to be essential for maximal constriction to saturating light (Lucas et al., 2003). Moreover, the equal maximal response demonstrates a physiological capability to fully constrict in the absence of TASK-3. However as irradiance decreases to approximately 10^{10} to10^{12} photons/cm^2/s the TKO IRC demonstrates a lack of sensitivity by approximately one log unit. This range of light intensity is known to activate cones with the overall melanopsin contribution decreasing as light intensity reduces (Lall et al., 2010, Lucas et al., 2012). The highly-sensitive rods would be unlikely major contributors at this range of intensity due to bleaching; making cones a prospective candidate for the observed differences (Altimus et al., 2010). Furthermore the significant differences occur over a limited range of intensity and wavelength rather than a generalised attenuation. Therefore the nature of this shift in sensitivity is indicative of being associated with an alteration within a specific class or classes of photoreceptor.

The IRC to 600nm light supports the notion of TASK-3 loss having an effect on the cone-driven pathway with TKO constriction to the highest intensity light being attenuated relative to WT. This longer wavelength is considered to be almost beyond the range for melanopsin activation whilst MW cones retain some sensitivity, albeit reduced (Lucas et al., 2012). All irradiances below maximum intensity resulted in little response from either strain of mice highlighting the limits of PLR to longer wavelength light. At the opposite end of the visual spectrum the 400nm IRC showed similar responses in WT and TKO mice across all intensities examined. Here there is an additional contribution from SW cones which acts in conjunction with melanopsin, MW cones and rods to decode shorter wavelength light including UV (Nikonov et al., 2006). It would seem therefore, at this wavelength, the combined action of all these classes of photoreceptor compensate for any diminution in pupillary response brought about by the loss of TASK-3. This hypothesis was further strengthened by investigations using polychromatic light with wavelengths less than 400nm removed where once again there was no significant difference in irradiance response curves between strains.

Pupillometry conducted to polychromatic light demonstrates retinal decoding of broad spectrum white light is largely unaffected by TASK-3 ablation. The attenuation observed at sub-saturating intensity of 10^{12} photons/cm^2/s was far below that of room irradiance under which behavioural experiments were conducted. This persistence in PLR in the absence of TASK-3 suggests behavioural differences observed in light-driven activity rhythms in chapter 3 and later, rates of re-entrainment and compression in chapter 4; are not a consequence of diminished retinal decoding of room irradiance.

Measurement of rate of pupillary constriction to the highest intensity light provides a further insight into the impact of TASK-3 loss on retinal decoding with outcome varying according to wavelength. Despite reaching a similar maximal constriction, at 400nm the initial rate of constriction was significantly slower in the TASK-3 KO mice compared to WT. However, at 480nm the reverse is true with WT mice being significantly slower, whilst at 560nm the rates were similar between strains. Considering response latency as an indicator of photoreceptor contribution, these findings suggest that at 400nm, TKO mice are slower than WT due to a reduction in the SW cone-mediated contribution to the response. This reduction would lead to a largely melanopsin-mediated constriction at this wavelength, which is known to be delayed by approximately 300ms relative to classic photoreceptors (Lucas et al., 2001, Lucas, 2013). The faster constriction at 480nm in the TASK-3 KO mice is indicative of a fully functional melanopsin system as demonstrated by the similar maximal constriction to high intensity light. All differences in sensitivity between WT and TKO mice on the IRC at this wavelength occurred at lower, sub-saturating intensities. The similar rate at 560nm is feasibly due to an overall decrease in photoreceptor sensitivity at this longer wavelength generally delaying rates of constriction, and once again any differences between strains on the IRC occurred at lower levels of light.

To further draw out the effects of TASK-3 loss on PLR, rates of pupillary constriction to broad spectrum white light were compared with and without the use of a UV cut-off filter. In WT mice, elimination of wavelengths less than 400nm resulted in a significant slowing of rate of constriction at maximum intensity light which was absent in the TASK-3 KO mice, who exhibited a similar constriction rate throughout. The removal of wavelengths under 400nm essentially removes any

contribution from SW cones therefore the differences observed in WT mice as a result of this change in spectrum can be attributed to this sub-class of cones. The fact that TKO mice did not exhibit any change in rate of pupillary constriction would therefore indicate that this pathway is influenced by TASK-3 channel function.

The examination of intrinsic PLR is useful in that this response has been found to be entirely melanopsin-driven and therefore the similar responses between strains observed at saturating light levels demonstrates functionality of the melanopsin system without TASK-3 (Xue et al., 2011, Semo et al., 2014). However, the significant differences seen at sub-saturating levels indicate reduced sensitivity in the TASK-3 KO mice compared to WT which is puzzling. Loss of TASK-3 may attenuate a mechanism specific to this response which reduces sensitivity, or alternatively there is a cone-mediated element to this response at lower levels of irradiance which is compromised in the absence of TASK-3.

From all these data, the big question is why does TASK-3 loss appear to affect cone-mediated PLR and not attenuate rod or melanopsin pathways? Chapter 2 reveals the presence of TASK-3 within the WT retina, but the exact location remains unknown. TASK-3 may act within the cones and prevent effective decoding of light or have an effect on cone-specific bipolar cells thereby attenuating the signalling pathway. Research has shown TASK-3 ablation to depolarise cells of the CNS by approximately 10mV – this change in RMP may negatively impact cones and prevent adequate hyperpolarisation on receiving light (Brickley et al., 2007). The post-firing repolarisation should also be considered as a lack of TASK-3 has been shown to attenuate this process thereby preventing sustained high-frequency firing (Brickley et al., 2007). Conversely melanopsin-

containing RGCs depolarise with light and therefore loss of TASK-3 may increase excitability of these cells, although the potential repolarisation issue would remain. The association of TASK-3 and the cone system could be further investigated through cross-breeding with a transgenic LW cone KI mouse (Lall et al., 2010).

Alternatively loss of TASK-3 channels may impact the availability of cone opsin as TASK channels have been reported within Muller cells of the retina. Muller cells are thought to assist in the recycling of opsin as a supplementary system to the retinal pigment epithelium, and therefore loss of this channel may lead to premature bleaching of this photoreceptor class (Skatchkov et al., 2006).

This chapter has considered the role of TASK-3 at the level of the retina and the implications on behaviour, the next chapter will explore the role of TASK-3 at a molecular level within the SCN.

7 The role of TASK-3 at the level of the SCN

7.1 Introduction

Within the SCN clock genes form the essential molecular basis of clock timing with circadian patterns in transcription driving complex interacting transcription-translation feedback loops to produce peak and nadir protein levels as a function of time of day (Reppert and Weaver, 2001, Shearman et al., 2000). See Chapter 1: 5.1. Core components of the mammalian molecular clock including *Clock*, *Bmal1*, *Per* and *Cry* genes drive and regulate rhythms of the master circadian pacemaker for endogenous rhythmicity and maintenance of entrainment (Reppert and Weaver, 2001, Sukumaran et al., 2010).

In chapter 2 the *TASK-3* gene was demonstrated to be highly expressed within the SCN consistent with published research highlighting TASK-3 as the most abundant K_{2P} channel within this region (Talley et al., 2001, Goldstein et al., 2005, Marinc et al., 2014). This chapter investigates whether the absence of TASK-3 influences the expression of core clock genes within the SCN under stable entrainment.

Given the significant differences in light-driven and endogenous behaviour in chapters 3 and 4, with attenuated clock plasticity and a lack of rhythm robustness, it is reasonable to propose alteration at a molecular level within the clock mechanism. In view of this, four core clock genes were selected for investigation: *Clock and Bmal1* for their central role in circadian rhythm maintenance; *Per2* and *Cry1*, to study light-responsive genes and their role in photoentrainment.

7.2 Experimental methods

7.2.1 Subjects

Wild Type (C57 BL/6J) mice were obtained from Charles River Laboratories (Kent), with transgenic TKO mice bred and maintained as homozygotes. For genotyping see Appendix II. Male and female mice 2-6 months of age were housed in polypropylene cages measuring approximately 34cm (l) x 16cm (W) x 13cm (h), either individually or in litter groups under 12:12 LD cycle (7am-7pm) for a minimum of 7 days prior to start of experiment. Food and water were available *ad libitum*.

All experimental procedures were performed with approval from the University of Kent Animal Welfare Ethics Review Board (AWERB) and in accordance with the Animals (Scientific Procedures) Act 1986.

7.2.2 Tissue retrieval

Mice were sacrificed by cervical dislocation at selected time points of ZT 2, 6, 10, 16, 22 (where ZT12 corresponds to lights off). Brains were removed under room light for day sampling, or dim red light if during the night (ZT16, 22) and placed into chilled nuclease-free water. Coronal brain slices revealed the SCN which was extracted by bespoke tissue punch and placed into RNAlater (Sigma, UK).

Samples were stored frozen at -80 C for subsequent preparation for measurement of *Clock*, *Bmal1*, *CKε*, *Per2* and *Cry1* gene expression by real-time quantitative RT-PCR.

7.2.3 RNA isolation and cDNA synthesis

Total RNA was isolated from tissue extracts using TRI Reagent (Applied Biosystems, UK). 400ng total RNA isolate was subjected to DNase treatment (Primerdesign, Southampton, UK) before being reverse transcribed by Nanoscript reverse transcription kit (Primerdesign, UK).

7.2.4 Gene expression analysis by Real-Time PCR

20 µL reactions were prepared in triplicate in a 96-well white plate (Alpha Laboratories, UK) comprising 10µL 2x SYBR Green Mix (Primerdesign, UK), 7µL nuclease-free water, 1µL sample cDNA and 1µL of each 0.5µM forward and reverse primers for gene of interest (Wisor et al., 2008). See Table 7.1.

Gene ID	Primer sequence
CLOCK	F: 5'CCACATGCCTCCCACTTTTC-3' R: 5'TGCGGATGAGGCTGGACTA-3'
BMAL1	F: 5'GAACAGCTATCTTCCTCGGACACT-3' R: 5'GGAAGTCCAGTCTTGGCATCA-3'
PER2	F: 5'GTCCACCTCCCTGCAGACAA-3' R: 5'TCATTAGCCTTCACCTGCTTCAC-3'
CRY1	F: 5'TGGCCAAATGGGCAGAAG-3' R: 5'CCCTCCTGACGAAGCTGAGT-3'
18S rRNA (Reference)	F: 5'CGCCGCTAGAGGTGAAATTC-3' R: 5'CGAACCTCCGACTTTCGTTCT-3'

Table 7.1: Primer sequences used for clock gene expression by RT-PCR.

Reactions were run on a LightCycler 480 instrument (Roche Applied Sciences, Sussex, UK) with pre-incubation at 95°C for 5 minutes before 50 cycles of 95°C for 10s, 60°C for 30s, 72°C for 10s. Detection of fluorescence occurred at 80°C after each cycle.

Relative quantification of mRNA levels were determined using the $2^{-\Delta\Delta C_T}$ method where crossing point (C_T) of target gene in each sample is normalised to reference value (18S rRNA) to give a ΔC_T value (Livak and Schmittgen, 2001). Comparison of ΔCT values between time-points relative to WT ZT2 (zero baseline value) provides the $\Delta\Delta C_T$ value. See Appendix I. Statistical significance was determined using GraphPad Prism 5 software (San Diego, CA) by student's *t* tests and one-way analysis of variance (ANOVA) with Tukey's multiple comparison post hoc test. All data presented as mean ± SEM (standard error of mean) and statistical significance defined as being $P < 0.05$.

7.3 Results

7.3.1 TASK-3 loss alters daily rhythms in CLOCK and BMAL1 mRNA expression

Sampling of WT and TKO SCN at specific time points within the 12:12h LD cycle and relative quantification by RT-PCR revealed distinct differences in *Clock* and *Bmal1* mRNA daily rhythms. With all values relative to WT ZT2, *Clock* mRNA expression in the TKO mice demonstrated significantly lower values at midday, ZT6 ($\Delta\Delta C_T$ = -0.680 ± 0.171) and early night, ZT16 ($\Delta\Delta C_T$ = -0.681 ± 0.177) compared to early morning, ZT2 ($\Delta\Delta C_T$ = 0.713 ± 0.290) (one-way ANOVA: P = 0.0042, Tukey's post hoc test $P < 0.05$, n=3). In contrast, *Clock* mRNA in WT mice remained consistent throughout the cycle with no significant variation between timings (one-way ANOVA: $P > 0.05$, Tukey's post hoc test $P > 0.05$). Comparison of *Clock* expression at ZT16 shows a significant reduction in TKO mRNA compared to WT (student's *t* test: $P = 0.010$). See Figure 7.1: A, C.

WT mice also exhibited unchanging levels of *Bmal1* mRNA across the cycle, with no significant variation in expression (one-way ANOVA: $P > 0.05$, Tukey's post hoc test $P > 0.05$). In TKO mice there was a significant variation over 24 hours although this did not reach significance between time points (one-way ANOVA: $P = 0.031$, Tukey's post hoc test $P > 0.05$). Comparison of *Bmal1* mRNA expression between WT and TKO strains at each time point shows no significant difference (student's *t* test: $P > 0.05$, n=3). See Figure 7.1: B, C.

A

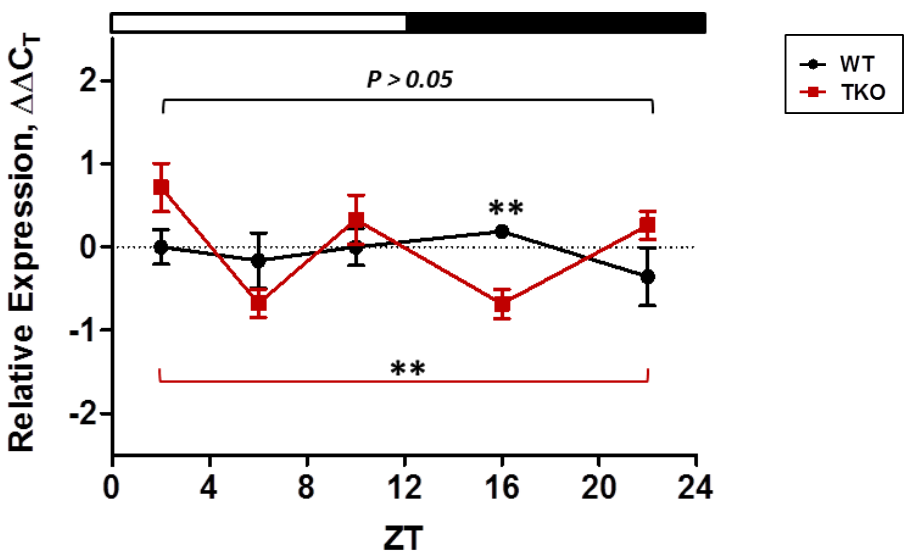
Relative Expression, ΔΔC_T
P > 0.05
**
**
WT
TKO
2
1
0
-1
-2
0
4
8
12
16
20
24
ZT

B

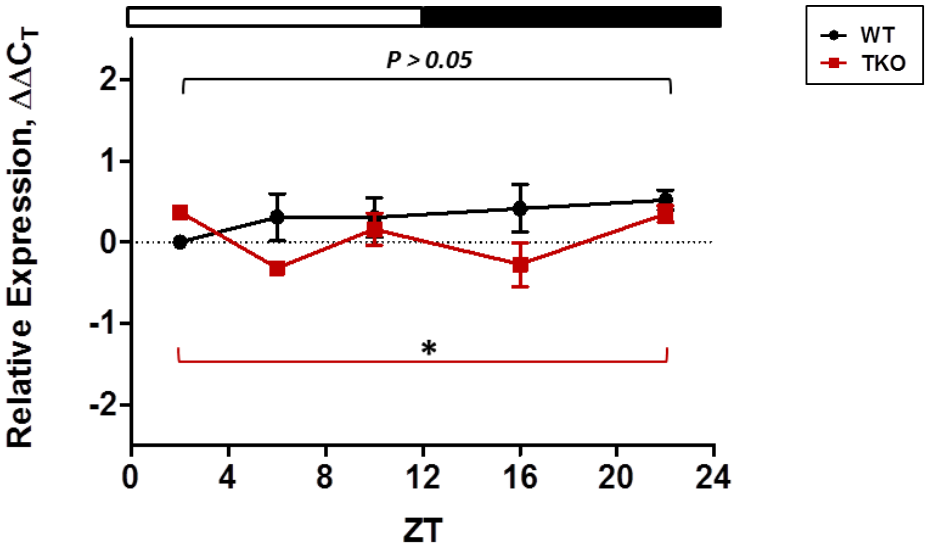
Relative Expression, ΔΔC_T
P > 0.05
*
WT
TKO
2
1
0
-1
-2
0
4
8
12
16
20
24
ZT

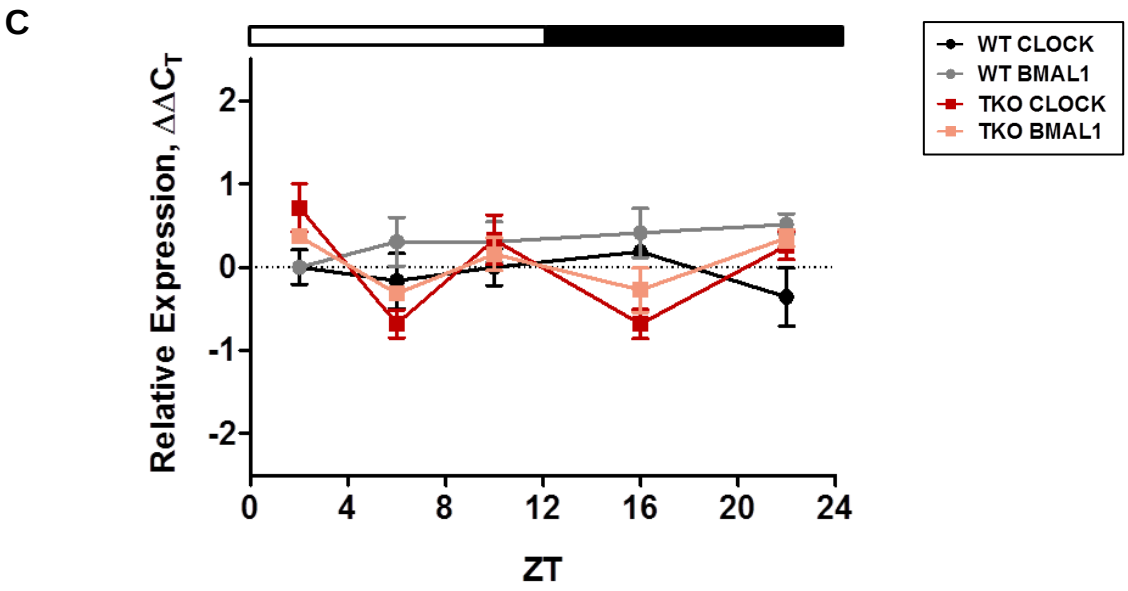

Figure 7.1: Time courses in *Clock* and *Bmal1* mRNA expression in the SCN of WT and TKO mice.

(A) Relative expression of *Clock* mRNA in the SCN of WT and TKO mice over 24 hours shows TKO mice exhibit significant variation over the cycle, One-way ANOVA: $P < 0.01$, with lower expression at midday (ZT6) and early night (ZT16) compared to other time points, Tukey's post hoc test, $P < 0.05$. In contrast, WT mice exhibit no significant variation throughout the circadian cycle, One-way ANOVA with Tukey's post hoc test: $P > 0.05$. Comparison of *Clock* mRNA levels at ZT16 reveals a significant reduction in TKO expression of this gene, student's *t* test, $P < 0.01$ (n=3).

(B) Relative expression of *Bmal1* mRNA in the SCN of WT and TKO mice over 24 hours shows TKO mice also exhibit significant variation in this gene over the circadian cycle, One-way ANOVA: $P < 0.05$; however differences between time points do not reach significance, $P > 0.05$. Once more, WT *Clock* expression remains consistent, One-way ANOVA with Tukey's post hoc test: $P > 0.05$ (n=3).

(C) Plotting *Clock* and *BmaL1* expression over the circadian cycle highlights patterns in expression in WT and TASK-3 KO mice. Whilst WT mice exhibit consistent levels during the day and night in both genes, TKO mice exhibit variation over the cycle with lower expression in both genes at the same time points - midday and early night, although not all reach statistical significance.

White and black bar represents hours of light and darkness respectively.

7.3.2 TASK-3 KO mice exhibit a circadian rhythm in PER2 mRNA expression but not CRY1

Relative quantification of *Per2* and *Cry1* mRNA expression within the SCN of WT and TKO mice by RT-PCR shows persistence of rhythms in the absence of TASK-3. With all values relative to WT ZT2, *Per2* mRNA demonstrates a significant variation in daily expression in WT and TKO mice (One-way ANOVA: WT $P = 0.002$, TKO $P = 0.044$). Peak expression exhibited by WT mice in the later part of the day, ZT10 ($\Delta\Delta C_T = 1.029 \pm 0.162$) is significantly higher than baseline value at ZT2, and expression at midday, ZT6 ($\Delta\Delta C_T = 0.059 \pm 0.089$) and early night, ZT16 ($\Delta\Delta C_T = 0.004 \pm 0.160$) (Tukey's post hoc test, $P < 0.05$) but does not reach significance in TKO mice (Tukey's post hoc test, $P > 0.05$). Comparison of *Per2* mRNA expression between WT and TKO strains at each time point shows no significant difference (student's *t* test: $P > 0.05$, n=3). See Figure 7.2: A, C.

In WT mice *Cry1* mRNA expression shows a similar pattern in expression to *Per2* with significant daily variation (One-way ANOVA: WT $P = 0.014$) with a peak level during the late day, ZT10 ($\Delta\Delta C_T = 1.259 \pm 0.203$), significantly higher than baseline value at ZT2 and expression at midday, ZT6 ($\Delta\Delta C_T = 0.082 \pm 0.169$) and late night, ZT22 ($\Delta\Delta C_T = 0.216 \pm 0.299$) (Tukey's post hoc test, $P < 0.05$). However, this rhythm is lost in TASK-3 KO mice with no significant variance over the circadian cycle (One-way ANOVA with Tukey's post hoc test, $P > 0.05$). Comparison of *Cry1* mRNA expression between WT and TKO strains at each time point shows no significant difference (student's *t* test: $P > 0.05$, n=3). See Figure 7.2: B, C.

A

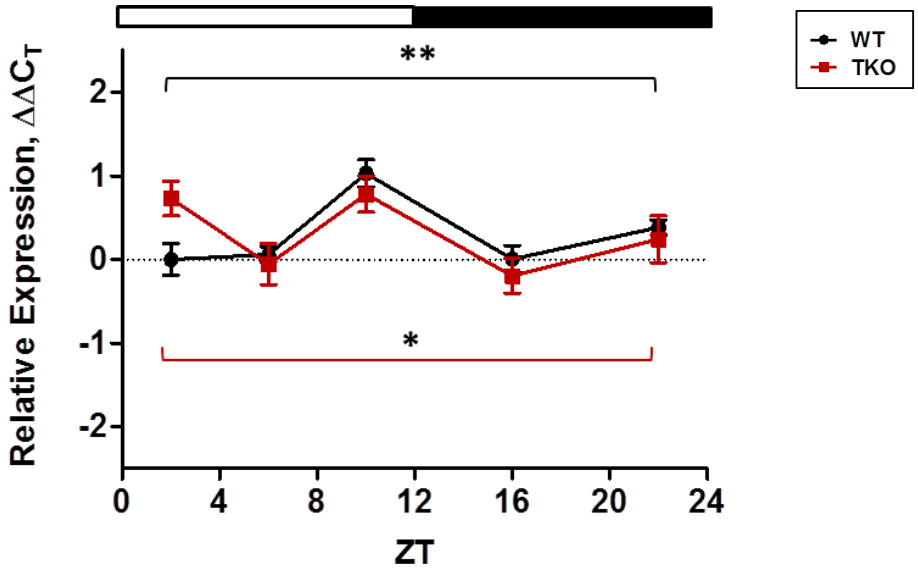
WT
TKO
**
*
Relative Expression, ΔΔC$_T$
2
1
0
-1
-2
0
4
8
12
16
20
24
ZT

B

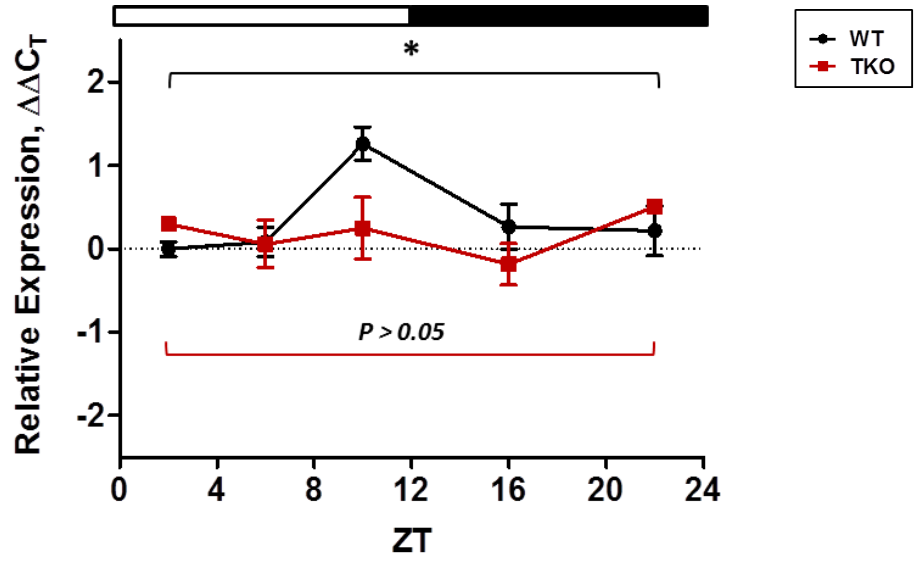
WT
TKO
*
P > 0.05
Relative Expression, ΔΔC$_T$
2
1
0
-1
-2
0
4
8
12
16
20
24
ZT

C

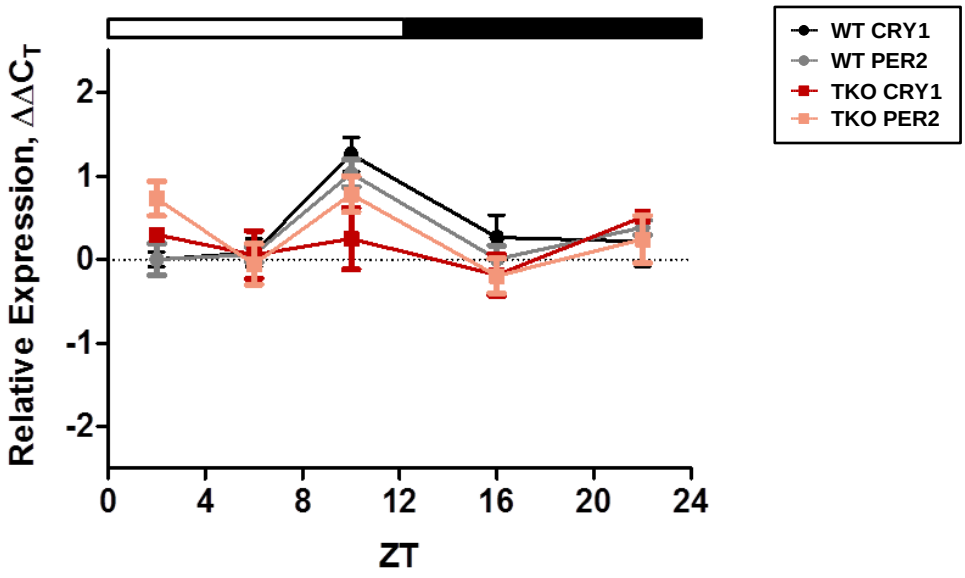

Figure 7.2: Time courses in *Per2* and *Cry1* mRNA expression in the SCN of WT and TKO mice.

(A) Relative expression of Per2 mRNA in the SCN of WT and TKO mice over 24 hours shows WT and TKO mice exhibit significant variation over the cycle, One-way ANOVA: WT $P < 0.01$, TKO $P < 0.05$. Both strains reach peak levels of expression at midday (ZT6) compared to other time points, which is significant in the WT mice only, Tukey's post hoc test, $P < 0.05$ (n=3).

(B) Relative expression of *Cry1* mRNA in the SCN of WT and TKO mice over 24 hours shows a loss of rhythm in the TKO mice with no significant variance, One-way ANOVA, $P > 0.05$. In contrast, WT mice have a significant rhythm, One-way ANOVA, $P < 0.05$, with a significant rise in expression at ZT10, Tukey's post hoc test, $P < 0.05$ (n=3).

(C) Plotting *Per2* and *Cry1* expression over the circadian cycle highlights the similarity in WT rhythms, with both having significant ZT10 peak expression. In TKO mice the *Per2* rhythm is more varied and Cry1 expression remains low throughout the cycle with no significant variation in mRNA levels.

White and black bar represents hours of light and darkness respectively.

7.4 Discussion

These findings demonstrate TASK-3 KO mice have altered gene expression within the master circadian pacemaker, the SCN. Under an entrained paradigm, each of the clock genes investigated, *Clock*, *Bmal1*, *Per2* and *Cry1*, show key differences in mRNA quantity and/or rhythm across the circadian cycle.

Clock and *Bmal1* expression were of interest to this study as transcription of these genes is central to the molecular clockwork. Following translation CLOCK/BMAL1 heterodimer formation drives the transcription of *Per* and *Cry* genes, the products of which associate and in turn initiate a negative feedback loop to inhibit *Clock* and *Bmal1* transcription. These interacting positive and negative feedback loops comprise the core timekeeping mechanism of the molecular clock (Reppert and Weaver, 2001, Shearman et al., 2000, Richter et al., 2004)

Initial studies in *Clock* and *Bmal1* transcription revealed generalised significant variance throughout the LD cycle in TASK-3 KO mice in contrast to the almost constant expression observed in WT. The constitutive expression of *Clock* under entrainment is well established although the *Bmal1* rhythm observed in WT mice lacked amplitude in comparison to published data (Shearman et al., 2000, Maywood et al., 2003, Ko and Takahashi, 2006). Interestingly there have been conflicting reports with BMAL1 exhibiting constitutive expression (Richter et al., 2004, von Gall et al., 2003). What this study highlights is the instability in *Bmal1* mRNA rhythm in the TASK-3 KO mice compared to the stable WT expression throughout the 24-hour cycle.

The instability in core clock genes in the absence of TASK-3 suggests changes in expression of several other genes as translated CLOCK and BMAL1 proteins form

an essential positive arm of the molecular clock mechanism, driving transcription of several genes including *Period* (*Per 1, 2, 3*) and *Cryptochrome* genes (*Cry1, 2*) with encoded proteins acting in feedback loops to terminate the cycle (Reppert and Weaver, 2001, Shearman et al., 2000, Maywood et al., 2007). Hence the effects of CLOCK and BMAL1 disturbance are likely to be multifaceted. This is supported in research in *Clock* mutant mice where disruption of the *Clock* gene resulted in significant decreases in *Per* rhythm amplitude in both homozygous and heterozygous models (Vitaterna et al., 2006).

Studies into *Per2* and *Cry1* gene expression permitted a fuller representation of the impact of TASK-3 ablation on the SCN. Exploration of *Per2* mRNA showed expression was largely unaffected by TASK-3 loss in both relative quantity and amplitude. However the increased variation between time points throughout the cycle resulted in the peak expression during the late day, ZT10, not reaching significance. In WT mice the rise in mRNA levels was significant at ZT10 with little change in expression at all other time points which ties in with published research (Maywood et al., 2003, Maywood et al., 2007). These results demonstrate TASK-3 loss does not significantly alter impact the *Per2* mRNA rhythm, but results in increased variability in *Per2* expression across all other time points. This instability may be a direct result of altered *Clock* and *Bmal1* gene expression discussed previously, or vice versa as PER2 is known to regulate *Bmal1* transcription (Schwartz et al., 2011).

In contrast to *Per2* findings, *Cry1* mRNA expression was heavily affected by TASK-3 loss, with no peak in *Cry1* levels at ZT10, and low amplitude variation across the cycle as a whole which did not reach significance. In WT mice there was a clear peak in *Cry1* expression at ZT10 as expected from previous work, with little

variation between all other time points (Ko and Takahashi, 2006). Again, the alteration in *Cry1* gene expression may be a stand-alone result or a consequence of altered *Clock* and *Bmal1* expression. Further, CRY1 has been shown to regulate PER2 expression, suggesting alteration from TASK-3 loss in *Cry1* mRNA may be a contributing factor in the instability of the observed TASK-3 KO *Per2* rhythm (Maywood et al., 2007, Vitaterna et al., 1999).

The disturbances in *Clock, Bmal1, Per2* and *Cry1* mRNA expression highlighted in these experiments may be responsible for the significant findings in behavioural studies conducted in chapters 3 and 4. The alterations at the level of the TASK-3 KO SCN with variation in usually consistent *Clock* and *Bmal1* expression along with a loss of daytime peak in Cry1 expression feasibly supports the lack of endogenous rhythm robustness observed in DD. Moreover the diminished capacity to adjust and re-entrain the clock to changes in the LD cycle in TASK-3 KO mice may arise from diminished amplitude and instability in light-induced genes such as *Cry1* and *Per2.* Many of the effects observed in the absence of TASK-3 are more subtle than those reported for clock gene mutants, with preservation of phase shifting capacity and rhythmic free-running in DD, but in this K_{2P} KO model the clock genes are still present, just with altered expression (Yan et al., 2003, van der Horst et al., 1999, Vitaterna et al., 2006).

8 General Conclusions

8.1 TASK-3 as a regulator of circadian entrainment

Circadian entrainment is the process by which internal timing is aligned to the external environment for maintaining optimal conditions for physiology and behaviour. In mammals, circadian entrainment is accomplished by the SCN making the properties of this structure of great interest to circadian biologists in furthering knowledge and understanding of endogenous time-keeping.

The communication to and from the SCN are reliant on electrical state of excitable cells, brought about by changes in membrane potential which is stabilised by a family of K_{2P} background leakage channels which are active at rest. Within the SCN the most abundant K_{2P} channel is TASK-3 and therefore this channel was the central focus of this work to establish the role in entrainment of the clock (Talley et al., 2001, Marinc et al., 2014). The expression of *TASK-3* mRNA within the WT SCN is demonstrated in Chapter 2, Figure 2.1.

Examination of behaviour under a stable 12:12h LD cycle in Chapter 3, Figure 3.1 demonstrates TASK-3 loss does not prevent synchronisation as both WT and TASK-3 KO strains exhibit a similar phase angle of entrainment. Nevertheless, the series of experiments in Chapter 4 reveals differences in rate of re-entrainment to an advanced light cycle and diminished capacity to adjust to lengthening photoperiods. These altered behavioural outputs are indicative of a lack of clock plasticity for adjustment in clock phase and an inability to regulate and confine activity to hours of darkness. Further, the cessation of activity observed during

decreasing irradiance suggests light is required to drive locomotor activity in the absence of TASK-3.

Locomotor activity investigations in constant darkness also show TASK-3 to be essential for rigorous endogenous time-keeping as channel loss results in significant reduction in behavioural output rhythm robustness, quantified by analysis of rhythm stationarity, see Figure 3.3 and appendix V. This finding in the absence of light suggests TASK-3 loss has an impact at the level of the SCN as there are no input timing cues to drive the endogenous rhythm. The lack of hyperpolarisation in SCN neurons from the elimination of TASK-3 conductance may therefore be having an effect within the core clock mechanism by diminishing interneural communication or alternatively TASK-3 has a role in coherence of output rhythms and therefore loss of this channel reduces rigor.

In addition to *TASK-3* mRNA presence within the SCN, Chapter 2 also reveals a presence within the retina which has previously been shown for this sub-family of K_{2P} channels although not confirmed specifically for TASK-3 (Skatchkov et al., 2006). With light being the most prominent cue for circadian entrainment, establishing the role of TASK-3 within the retina is of great importance as changes in retinal decoding of light are likely to have effects on the clock and essentially, behaviour.

Taking these findings together, TASK-3 conductance is likely to have a multifaceted role in circadian entrainment through regulation of neural excitability. Research on cerebellar granule neurons has shown TASK-3-driven hyperpolarisation of RMP to be essential for controlled, sustained firing rhythms (Brickley et al., 2007). Ablation of TASK-3 increases excitability of neurons as closer to firing threshold,

but firing cannot be sustained over time due to the influence on voltage-gated sodium channels, attenuating the required repolarisation (Brickley et al., 2007). Applying this theory to the SCN it is likely TASK-3 loss is reducing the hyperpolarisation of RMP and therefore impacting the communication between neurons. This change in electrical properties may influence gene expression rhythms within the molecular clock thereby affecting clock phase and re-setting. Further, the output signalling may be disrupted from a lack of regulation within the SCN which will impact output rhythms to the periphery leading to changes in physiological and behavioural patterns.

The light input to the clock should also be considered as removal of TASK-3 currents in the retina may affect communication of light to the clock from alteration within photoreceptor cells, in retinal signalling pathways with bipolar, amacrine and horizontal cells and the association with ipRGCs making up the afferent RHT pathway to directly deliver photic information to the clock. See Figure 8.1.

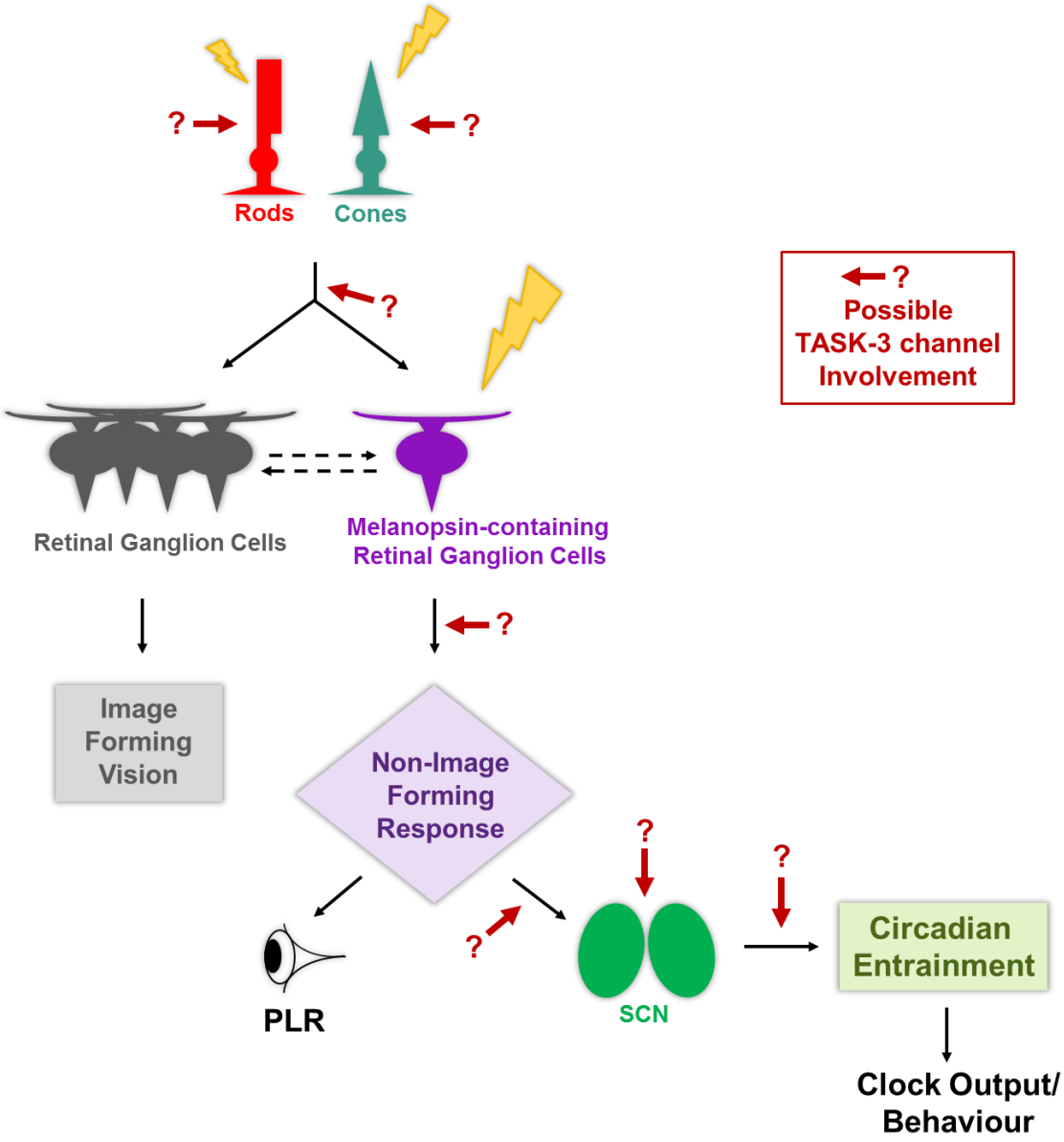

Figure 8.1: Schematic diagram with proposed areas of TASK-3 contribution to circadian entrainment.

Findings from this project suggest TASK-3 currents may play a role in several key areas of entrainment including photoreceptor decoding of light and signalling pathways, afferent communication to the SCN, within the core clock mechanism and clock output rhythms.

Proposed locations for TASK-3 contribution shown as red arrows with question marks.

8.2 Rhythmic TASK-3 expression in the SCN is likely to contribute to patterns in neuronal excitation and behaviour

K_{2P} channels selectively transport potassium ions across membranes of excitable cells at rest, and in doing so, influence RMP and excitability. As TASK-3 is the most abundant K_{2P} channel in the rodent SCN, this project proposes this channel regulates the electrical activity of SCN neurons and, ultimately, the biological clock (Talley et al., 2001, Marinc et al., 2014). At physiological pH, TASK-3 channels facilitate the outward movement of potassium ions which hyperpolarises RMP away from the action potential firing threshold, acting essentially as a 'brake' on neuronal firing (Goldstein et al., 2005, Goldstein et al., 2001). With this in mind it is feasible to propose removal of TASK-3 conductance to reduce hyperpolarisation leading to increased neuronal excitability and firing.

Examination of *TASK-3* mRNA expression in the SCN of WT mice entrained to a stable 12:12h LD cycle reveals a variation across the circadian cycle with a significant midday nadir; see Chapter 2, Figure 2.2. Therefore this daily reduction in TASK-3 current in the SCN at midday is likely to produce a depolarising drive for increased neuronal excitability as RMP moves closer to firing threshold.

Electrophysiological studies in nocturnal rodents have demonstrated electrical activity within individual SCN neurons forms a vital part of the clockwork mechanism (Brown and Piggins, 2007). Excitable cells of the SCN are known to exhibit a circadian rhythm with increased action potential firing during the middle portion of the day (Brown and Piggins, 2009). Moreover, this increase in neuronal excitability during the day has been shown to coincide with a more depolarised RMP attributable to a decrease in potassium conductance which is active during the night (Meredith et al., 2006, Belle et al., 2009).

Circadian patterns in membrane potential have previously been proposed to regulate neuronal firing rate in the SCN in a number of studies (Kuhlman and McMahon, 2004, Pennartz et al., 2002). Therefore the data from this study showing a reduction in TASK-3 conductance at midday in WT mice correlates to the known output rhythms of the SCN and is indicative of TASK-3 regulating neuronal firing rhythms by influencing RMP. See Figure 8.2.

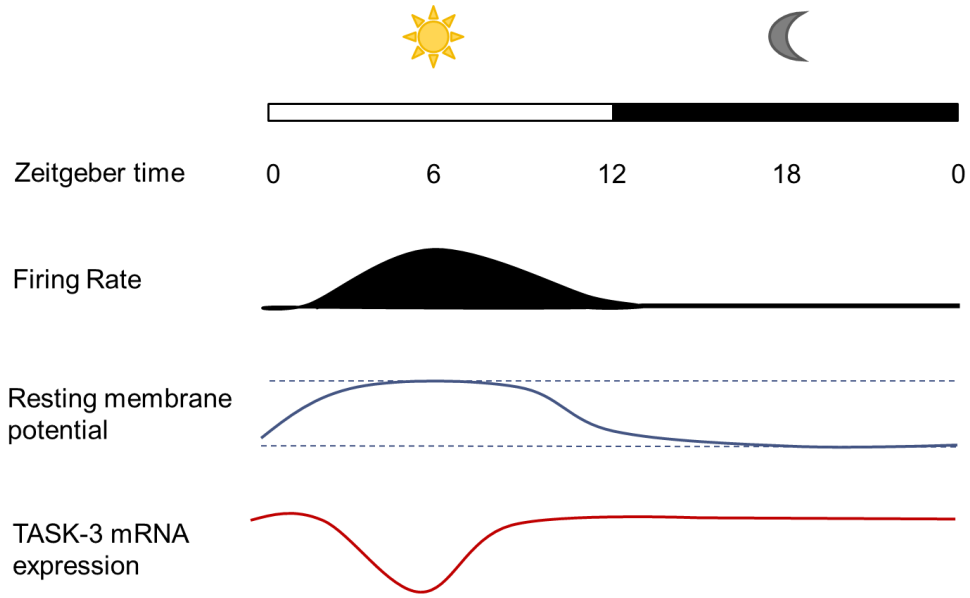

Figure 8.2: Schematic day-night variation in WT SCN neuronal properties.

Under conditions of entrainment to a 12:12h LD cycle the midday (ZT6) decrease in *TASK-3* mRNA expression within the WT SCN feasibly leads to depolarisation of resting membrane potential and, subsequently, increased neuronal firing rate.

In the absence of TASK-3 current altogether, such as in TASK-3 KO mice, a more generalised depolarisation of SCN neurons throughout the circadian cycle can be hypothesised, mirroring a persistent day-like state. From this a loss of circadian firing rhythm and night-time silencing of neurons can be predicted which would likely impact clock-driven rhythms in gene expression which drives behaviour and clock resetting. The molecular studies on core clock genes within the SCN in chapter 7 supports this theory with *Cry1* mRNA expression in TASK-3 KO mice having no significant rise in expression at ZT10 as expected from WT expression; see Figure 7.2. Here it is possible the continual day-like state following TASK-3 loss has diminished the rhythm in mRNA expression of this core clock gene.

The behavioural studies conducted in chapter 3 also correlate well with the proposed day-like state in TASK-3 KO mice. Under stable entrainment to a 12:12h LD cycle TASK-3 mice exhibit very low activity intensity and published research has shown increased excitability is associated with a reduction in behavioural output (van Oosterhout et al., 2012).

8.3 Adaptation to changing light requires TASK-3 functionality

The process of clock resetting to light can be divided has two distinct divisions: the acute phase shift in response to light exposure at night and the longer-term adjustment and adaptation required for maintenance of circadian entrainment under changing LD conditions. In TASK-3 KO mice both types of resetting showed varying degrees of alteration compared to WT.

Acute resetting of the clock by an Aschoff type I phase shifting paradigm demonstrated similar responses in WT and TASK-3 KO mice, suggesting this response occur independently of TASK-3 currents. However, this protocol relied heavily on accurate timing of light pulse application two hours into the subjective night. Analysis of behaviour for this timing was challenging in TASK-3 KO mice given their low intensity activity. To overcome inaccuracies in timing of light, an Aschoff type II paradigm was adopted where all mice were entrained to a stable 12:12h LD cycle and received light two hours into the hours of darkness. This protocol using the maximal intensity light resulted in significant attenuation of TASK-3 KO delay phase shifts and prompted further investigation at different light intensities to draw out any differences between strains. The responses in both WT and TASK-3 KO mice were dose-dependent, but in the later, there was decreased sensitivity with saturation occurring to less than maximum intensity light. The decreased TASK-3 KO sensitivity may relate to the day-like electrical properties of the clock described earlier in this chapter; see 8.2. Considering the classic phase response curve for WT mice in association with electrical output rhythms, WT mice are unresponsive to light pulses delivered during the subjective day, a time when RMP is less hyperpolarised and SCN neurons are firing most frequently; see Figure 1.6. If these properties are applied to the TASK-3 KO SCN in a persistent

day-like state, RMP is likely to remain less hyperpolarised and SCN neurons continue to fire during the night. These actions may dampen the sensitivity of the clock to reset to light, hence the reduced phase shifting responses observed in this transgenic strain of mice.

Furthermore expression of *Per2* mRNA within the SCN, which is associated with acute light-induced delays, was not significantly altered in TASK-3 KO mice, suggesting the alteration is likely to be associated with photic signalling- either to the SCN or in output signalling pathways.

The loss of TASK-3 is likely to affect the transmission of glutamate, the principal neurotransmitter of the RHT (Morin and Allen, 2006, Reghunandanan and Reghunandanan, 2006). Under normal (WT) conditions hyperpolarisation of RMP results in a voltage-dependant Mg^{2+} block on NMDA receptors for modulation of transmission (McBain and Traynelis, 2006). In the absence of TASK-3, the membrane potential is predicted to be less hyperpolarised, thereby moving it closer to firing threshold, leading to easier removal of this block and increased excitability through glutamate signalling. Conversely, the modulatory mGluR response inhibiting TASK-3 conductance for potentiation of glutamate-mediated depolarisation and increased action potential firing will be eliminated in TASK-3 KO mice, attenuating the overall glutamate response (Chemin et al., 2003). Therefore the predicted outcome for glutamate-mediated light responses in TASK-3 KO mice would be a largely NMDA-dependant response with no contribution from mGluR inhibition of TASK-3. However, these hypothesised mechanisms require experimental investigation to dissect out the exact role of TASK-3 in glutamate-mediated transmission in photic phase shifting.

Clock resetting for circadian entrainment following an advance in LD cycle timing and seasonal adjustment also showed significant alteration from TASK-3 loss with decelerated rates of re-entrainment to a 6-hour advance in LD cycle and an inability to compress and confine activity to decreasing hours of darkness during increased photoperiod.

These challenges require longer-term adaptation brought about and regulated by a combination of changes in electrical properties of clock neurons and molecular components to induce the required change in behaviour. Although the exact mechanisms driving photoentrainment are still to be deciphered, at the level of the clock the process begins with synaptic activity via the RHT inducing changes in membrane potential which activates second messenger proteins. These intracellular components communicate to the molecular clockwork inducing changes in clock gene transcription and translation with interacting feedback loops (Colwell, 2011). The produced proteins subsequently act on membrane properties to communicate change by alteration in electrical activity thereby driving clock output rhythms (Colwell, 2011, Kuhlman and McMahon, 2006). Clearly regulation of membrane potential is imperative in this complex process at the onset and conclusion.

The elimination of TASK-3 channels effectively removes the largest K_{2P} conductance within the biological clock with likely consequence of depolarised resting membrane potential, altered firing rates and attenuation in post-firing repolarisation (Talley et al., 2001, Lesage and Lazdunski, 2000, Brickley et al., 2007). Therefore in TASK-3 KO mice the RMP of afferent and efferent SCN pathways are likely to be closer to firing threshold and therefore feasibly more

sensitive to innervation, leading to increased sensitivity. However, it is unlikely a small increase in action potential firing would induce the necessary change to bring about clock resetting to a large shift in LD cycle timing of several hours, therefore the lack of ability to sustain firing in the absence of TASK-3 is likely to diminish responses and may account for the slower/attenuated adjustment observed in TASK-3 KO behavioural data in Chapter 4.

The reported loss of sustained firing in TASK-3 KO neurons is very likely to affect day-night transitions as these have been shown to be driven by distinct changes in neuronal firing rates (Houben et al., 2009). Research on WT mice by electrophysiological recording *in vivo* has shown precise changes in electrical discharge rate correlate with onsets and offsets of behaviour (Houben et al., 2009). This linking of behavioural and electrical properties in mice suggests the altered day-night transitions observed in TASK-3 KO mice during lengthening of photoperiod is feasibly a result of a lack of regulation in neuronal firing rates which failed to produce distinct reductions or increases to drive activity onsets and offsets. This would not be surprising given the proposed attenuation in sustained firing and a continual day-like state in electrical properties.

Elimination of TASK-3 may also impact intercellular communication within neurons of the SCN through altered electrical properties and excitability. Research in rodent SCN slices demonstrates large shifts in behaviour are brought about by a rapid shift in phase of a small population of SCN neurons which become highly synchronised to the new cycle timings to communicate and drive change in remaining cells (Rohling et al., 2011). In jetlag scenarios a rapid shift is seen within the ventral SCN with a much more gradual shift in dorsal areas (Meijer et

al., 2010). Molecular studies have shown this synchrony among SCN cells for re-entrainment to be VIP-dependant (An et al., 2013).

In contrast to shifted environmental cycles requiring intercellular communication for synchrony, seasonal adjustment is reported to be reliant on network organisation brought about by the phase relation between the dorsal and ventral zones of the SCN (Meijer et al., 2010). In the absence of TASK-3 there is significant alteration in both re-entrainment to shifted cycles and adaptation to changing photoperiods, suggestive of attenuation in both cell-to-cell and network communication. This supports findings by Brown and Piggins where photoperiodic response was shown to be encoded at the network level within the ventral SCN and at the level of individual cells within the dorsal SCN (Brown and Piggins, 2009).

These experiments highlight several contenders for the observed attenuation in clock resetting to light in TASK-3 KO mice including glutamate signalling, altered SCN firing rhythms and communication within the clock at the network and individual cellular level. At similar intensity light retinal decoding from pupillometry investigations was fully functional, indicating this attenuation is not occurring at the level of the retina; see Figure 6.10. With the high level of TASK-3 expression within the mouse SCN and the role of regulating RMP, it is feasible many, if not all of these pathways are subject to TASK-3 conductance.

8.4 Melanopsin-driven responses persist in the absence of TASK-3

The photopigment melanopsin has been shown to be essential in a number of retinal and circadian responses to light including full pupillary constriction to saturating light, period lengthening in conditions of constant light, negative masking and intrinsic PLR (Lucas et al., 2003, Ruby et al., 2002, Mrosovsky and Hattar, 2003, Hattar et al., 2003, Xue et al., 2011, Hatori et al., 2008). Because TASK-3 mRNA was detected within the WT retina it is important to this project to determine the role of this channel in melanopsin-mediated NIF responses to light; see Figure 2.1. Behavioural and pupillometry investigations in chapters 5 and 6 respectively reveals each of these responses appears to have been preserved in the TASK-3 KO mice, suggesting melanopsin-driven responses occur independently of this K_{2P} channel.

Several experiments within this study have considered the role of TASK-3 in melanopsin-dependant responses, yet there have been no significant alterations attributable to this photopigment. Pupillometry investigations to highest intensity polychromatic light and monochromatic light of 400nm, 480nm, and 560nm wavelength were not significantly different to WT; with the only attenuation observed to full intensity light occurring at 600nm light, a wavelength considered being beyond melanopsin sensitivity (Lucas et al., 2012). This is in stark contrast to PLR in melanopsin KO mice where maximal pupillary constriction was severely attenuated at saturating white light and monochromatic light of 480nm wavelength (Lucas et al., 2003).

In order to further rule out melanopsin involvement in TASK-3 KO attenuated pupillary responses, an isolated eye preparation was used to investigate intrinsic

PLR (iPLR). The ability of the mouse iris to constrict to light without projection from the brain is considered to be entirely melanopsin- dependant (Xue et al., 2011). This technique demonstrated iPLR responses in both WT and TASK-3 KO mice indicative of melanopsin functionality in the absence of TASK-3; see Figure 6.16. However, rather surprisingly, the iPLR irradiance response curve demonstrates a trend of TASK-3 loss reducing the pupillary constriction, which is significant at sub-saturating light intensities. This finding suggests although TASK-3 mice are physiologically able to exhibit iPLR, TASK-3 plays a role in this mechanism which is compensated for at saturating intensities but is observed when light decreases to sub-saturating levels.

One suggestion would be the involvement of other classes of photoreceptor in driving iPLR in addition to melanopsin. If iPLR is compared to classical PLR occurring within the intact visual system, the most likely candidate for the observed attenuation would be cones. Not only would this theory support the proposed cone-driven attenuation in cone-driven PLR, this class of photoreceptor plays a major role in decoding light of this intensity (Hattar et al., 2003, Lall et al., 2010). Moreover, the role of rhodopsin in iPLR has been ruled out through the use of rhodopsin KO (*Rho*$^{-/-}$) mice which exhibited a similar iPLR to WT (Xue et al., 2011).

The persistence of melanopsin-driven responses in the absence of TASK-3 currents was also established in behavioural studies with both WT and TASK-3 KO mice having comparable lengthened free-running periods in constant light. Furthermore, negative masking experiments demonstrated similar patterns in activity in TASK-3 KO and WT mice with sustained inhibition to 3 hour pulses, and activity largely confined to hours of darkness. Mice lacking a functional

melanopsin system are not able to sustained inhibition to light for this duration, with full intensity activity commencing after approximately 100 minutes despite the presence of bright light (Mrosovsky and Hattar, 2003).

Phase shifting capacity is also thought to be melanopsin-dependant, with loss of this opsin resulting in shifts of smaller magnitude (Panda et al., 2002, Ruby et al., 2002). In this project Aschoff type I phase shifting to maximum intensity light showed no significant difference between WT and TASK-3 KO mice, indicative once more of melanopsin functionality. However, additional studies by Aschoff type II paradigm with saturating and sub- saturating light revealed a reduction in magnitude of phase shifts in the TASK-3 KO mice relative to WT; see Figure 3.6. However, unlike findings by Panda et al., phase shifts were indicative of decreased sensitivity and premature saturation in TASK-3 KO mice rather than indiscriminate attenuation and are therefore not conclusive proof of deficiency in melanopsin response.

With TASK-3 having the role of stabilising RMP for regulation of neuronal excitability and facilitating repolarisation, it is surprising the melanopsin pathway should be spared following ablation of TASK-3. Although ipRGCs operate near firing threshold so that even small depolarisations can increase firing rate including membrane depolarisation from TASK-3 loss, previous research has shown marked accommodation in AP firing at threshold (Do et al., 2009, Brickley et al., 2007). One possible explanation is because ipRGCs integrate light throughout the course of the day they have comparatively slow response kinetics providing longer duration responses. This would allow for slower repolarisation rather than requiring fast-paced sustained firing which would be likely to require functional TASK-3 conductance (Do et al., 2009).

Additionally, the intrinsic photosensitivity of the melanopsin-containing RGCs does not rely on signalling to bipolar, amacrine and horizontal cells for eliciting a response. This lack of synaptic transmission may result in TASK-3 having less of an influence on this retinal pathway compared to outer retinal decoding and communication. Although this would not account for the significant attenuation in TASK-3 KO iPLR to sub-saturating light as this mechanism is thought to be driven directly by the iris sphincter muscle rather than from the retina (Xue et al., 2011).

8.5 The impact of TASK-3 loss on PLR is indicative of alteration in the cone-signalling pathway

While the melanopsin system appears intact following in TASK-3 KO mice, the significant diminution in PLR to sub-saturating light of several different wavelengths, suggests alteration in the cone-signalling pathway from the loss of this channel.

Pupillometry to 480nm monochromatic light, a wavelength where melanopsin, MW cones and rods are all highly sensitive, revealed a significant shift in TASK-3 KO sensitivity to sub-saturating light compared to WT at levels of irradiance beyond the limits of rod capability (Lall et al., 2010, Lucas et al., 2012). A similar shift in sensitivity was also observed at 560nm, where melanopsin sensitivity is reduced whilst cones remain highly sensitive and therefore have increased contribution to retinal decoding at this wavelength; see Figure 6.3. With similar maximal responses to saturating light demonstrating melanopsin functionality, the MW cone-signalling pathway becomes a likely candidate for the observed alterations in PLR to sub-saturating light (Lall et al., 2010, Lucas et al., 2003). This notion is further supported by the PLR at 600nm, where TASK-3 KO mice exhibit a reduced PLR to saturating light compared to WT. This wavelength was selected for being beyond the scope of melanopsin sensitivity but where a degree of MW cone sensitivity persists (Lucas et al., 2012).

The similar IRC to 400nm light in WT and TASK-3 KO mice suggests the SW cones are not affected in the same way, although all major classes of photoreceptor are highly sensitive at 400nm making it difficult to draw out contributions or attenuation in individual classes. There is also the possibility of compensation

occurring both at this wavelength and in polychromatic pupillometry studies where attenuation was observed at only a single specific sub-saturating intensity.

Additionally, the variation in speed of pupillary constriction between WT and TASK-3 KO strains suggests alteration in class(es) of photoreceptor producing the constriction as melanopsin responses are known to be subject to considerable latency compared to cone-driven responses (Berson et al., 2002, Lucas et al., 2001) The ON-OFF responses of cones are able to elicit fast, transient photic signals to changing conditions whereas melanopsin-mediated phototransduction integrates light information over time for full adaptation of the pupil to irradiance but is considered sluggish in comparison, being around 100 times slower than cones (Brown and Lucas, 2009, Drouyer et al., 2007).

These differences were particularly apparent in the polychromatic experiments where elimination of the UV component (and therefore essentially the contribution of SW cones) did not alter the rate of constriction to saturating light in the absence of TASK-3, but significantly attenuated the WT rate. This finding suggests the constriction in the TASK-3 KO mice occurred independently of SW cones and therefore principally melanopsin-driven whereas WT mice have a faster rate of constriction in the presence of UV as this response is driven by the combined contributions of SW cones and melanopsin. Once the UV is removed, WT PLR is significantly slower, relying on chiefly on melanopsin.

The behavioural experiments within this study also support an alteration in the cone-driven pathway rather than inner retinal photoreception as circadian entrainment, negative masking and phase shifting to acute light pulses are not

reliant on cone function, and are shown here to persist without TASK-3 conductance (Mrosovsky et al., 2001, Lall et al., 2010).

Contrary to ipRGCs, classic photoreceptors are depolarised at rest and become hyperpolarised on receiving light (Lucas, 2013, Korenbrot, 2012). This mechanism is a likely source of alteration in retinal decoding in the absence of TASK-3 as depolarisation of RMP from the loss of this K_{2P} channel would act in opposition to the required hyperpolarisation for effective signalling. Further, rod and cone signalling pathways are reliant on signal propagation through multiple layers of the retina comprising many types of accessory cell such as bipolar, amacrine and horizontal cells before transmission to ipRGCs. This arrangement with multi-synaptic communication requires strict regulation of membrane potential which may be compromised in the absence of the TASK-3 background leak conductance.

In cones, specifically, there are several classes of bipolar cell, some of which may be susceptible to effects from the loss of TASK-3. The major subtypes are divided into ON-cone and OFF-cone pathways according to how they convey presence or absence of light. This dual cone activity is achieved by signal switching in the ON-cone pathway as follows: On receiving light the cone hyperpolarises, stopping glutamate release to the ON-cone bipolar cell which then becomes depolarised and releases glutamate to trigger RGCs. Conversely when light goes off the cone depolarises and releases glutamate which binds to mGluR6 receptors on the ON-cone bipolar cell leading to hyperpolarisation and inhibition of the ON-cone pathway (Snellman et al., 2008, Yang et al., 2011). The OFF-cone pathway works in opposition, by having AMPA and Kainate glutamate receptors which during darkness bind to the released glutamate from cones, depolarise and release

glutamate to RGCs to signal the OFF response (Yang et al., 2011, Snellman et al., 2008).

As discussed previously, in TASK-3 KO mice it is likely the RMP of cells which usually express this channel will be less hyperpolarised than WT. Therefore in the presence of light both the ON-cone and OFF-cone pathways may modulate glutamate release leading to altered signalling to ipRGCs and ultimately, PLR. Further, in the absence of light ON-cone pathways utilise the novel group III mGluR6 to inhibit glutamate signalling whereas OFF-cone pathways have AMPA and Kainate receptors. It is feasible TASK-3 plays a role in this pathway as previous research has shown mGluRs to act through TASK-3 albeit group I mGluRs (Chemin et al., 2003). Loss of mGlu signalling would likely prevent hyperpolarisation and inhibition of the ON-cone signalling pathway. It is also interesting to note RGCs express NMDA, AMPA and Kainate glutamate receptors rather than mGluR6, which may account for the preservation of direct ipRGC responses in the absence of TASK-3 (Yang et al., 2011).

Phototransduction by rods and cones results in destruction of the opsin pigment which requires regeneration before the receptor can signal again (Wang and Kefalov, 2011). In Rods, where signalling is restricted to low level light, the demand for rhodopsin pigment is less than cones and responses are slower with a long refractory period (Wang and Kefalov, 2011, Tachibanaki et al., 2007, Kawamura and Tachibanaki, 2008). Conversely cones signal bright light and therefore require a fast turnaround time in pigment renewal in order to recover rapidly and prevent bleaching. This larger requirement for photopigment may be a further area of alteration in TASK-3 KO mice as loss of TASK-3 attenuates

repolarisation of excitable membranes and is known to negatively influence voltage-dependant channels, thereby exacerbating the effect (Brickley et al., 2007).

In view of this high demand for cone opsin, many species including mouse and humans have a retina visual cycle as an additional source of regenerated cone opsin to the pigment epithelium (Wang and Kefalov, 2011). This process is conducted by the Muller cells and is thought to extend the dynamic range of cones into bright light whilst also facilitating rapid dark adaptation after exposure (Wang and Kefalov, 2011, Skatchkov et al., 2006). TASK channels have been detected within the Muller cells where they are thought to assist in maintaining a hyperpolarised RMP, therefore the loss of TASK-3 is likely to have a substantial effect on these cells and their actions (Skatchkov et al., 2006). Attenuation in this recycling process may account for the shift in sensitivity observed in PLR in the TASK-3 KO mice at sub-saturating light intensities. At saturating intensities the melanopsin system is the principal driver of the PLR which operates independently of this cycle and therefore no attenuation is observed to the brightest light (Lall et al., 2010, Lucas, 2013). Despite contributions form cones being signalled along the ON-cone pathway to both M1 and M2 types of ipRGCs to drive PLR, it has been demonstrated that the M1 cells primarily rely on melanopsin-driven phototransduction (Schmidt and Kofuji, 2010). Therefore under high intensity light any deficit in cone-driven PLR responses are likely to be compensated by the melanopsin system, with attenuation only observed at intensities where reduced melanopsin sensitivity and contribution prevents this compensation.

8.6 Stability in molecular clockwork is TASK-3-dependant

Global ablation of TASK-3 results in disruption in the mRNA expression of core clock genes as reported in chapter 7, Figures 7.1, 7.2. Of particular note was the alteration in *Clock* expression which although constitutively expressed in WT, demonstrated significant variation in TASK-3 KO mice. Complete loss of the *Clock* gene is associated with reductions in *Per* and *Cry* rhythm amplitude along with lengthened tau and eventual arrhythmia in DD (Reppert and Weaver, 2001). Although conducted under entrainment, this research is consistent with previous findings as instability in *Clock* gene expression in the TASK-3 KO SCN was accompanied by diminished amplitude in *Cry1* rhythm with little increase in expression late in the day. Further, behavioural studies in DD revealed a distinct lack of rhythm robustness in TASK-3 KO mice relative to WT with significantly longer tau.

The loss of amplitude in *Cry1* expression from TASK-3 ablation may, in part, also account for the lack of rhythm robustness in free-running conditions as *Cry* is known to be essential for maintenance of endogenous time-keeping (van der Horst et al., 1999). Even under stable entrainment to 12:12h LD cycles, the loss of this daytime peak in core clock gene expression feasibly impacts the molecular clockwork comprising interacting transcriptional-translational feedback loops and is likely to be associated with the decreased rhythm amplitude, see Figure 3.1.

Further investigations measuring additional clock genes including *Per1* and *Cry2* would provide a more complete picture of the TASK-3 KO molecular clock, along with associated genes such as *Casein kinase δ* and *ε.*

Additionally, the expression of *Per* and *Cry* genes after a change in LD cycle timing would provide useful additional information on the impact of TASK-3 loss on re-entrainment of the clock at a molecular level.

8.7 TASK-3 as a future therapeutic target

Selective targeting of K_{2P} channels has been proposed as being of therapeutic use for a number of CNS conditions including stroke, depression and epilepsy (Mathie and Veale, 2007). TASK-3 specifically has also been identified as having oncogenic potential through altered apoptosis and tumorigenesis (Patel and Lazdunski, 2004). There is also a familial condition associated with the TASK-3 gene known as Birk Barel mental retardation dysmorphism syndrome arising from maternal inheritance of a missense mutation (Barel et al., 2008).

The findings from this project suggest TASK-3 channels play a key role in photic regulation of the circadian clock. Therefore pharmacological manipulation of TASK-3 channels may have therapeutic potential for the future by altering the rate of clock synchrony to light. This modulation may be of benefit in hastening synchronisation to new LD cycles following trans-meridian flight, thereby reducing the duration of jetlag. Moreover, alteration of TASK-3 conductance may be effective in relieving symptoms of seasonal affective disorder where diminishing hours of daylight lead to symptoms of depression (Miller, 2005). Despite previous studies showing ablation of TASK-3 mirroring antidepressant action, the results of this work suggest there would be a prolonged period of adaptation to changing hours of light (Gotter et al., 2011). Therefore it seems the exact role of TASK-3 in the diverse range of depressive disorders is yet to be fully established and is likely to depend on aetiology.

9 Future Work

The regulation of circadian rhythms is an important area of research in order to optimise alignment of physiology to the planetary day-night cycle. In humans clock desynchrony is linked to a number of health conditions from temporary jetlag to longer-term malady such as seasonal affective disorder, both of which are known to negatively impact sleep patterns, mood and appetite (Lall et al., 2012, Sack, 2009). Each of these conditions affect sleep patterns, mood and appetite; impacting quality of life. Circadian rhythm alignment is also associated with pathologies at a cellular level such as the increased incidence of breast cancer in women partaking in shift-work (Boivin and Boudreau, 2014).

This work has revealed TASK-3 to be a key player in circadian rhythm regulation and adjustment which may offer a future therapeutic target for clock-related disorders.

This project opens up many avenues for additional research to further elucidate the role of TASK-3 in circadian entrainment. These include building on previous findings to provide greater mechanistic knowledge and also the investigation of electrical properties as yet unexplored.

Each of the main techniques detailed in this thesis has room for expansion to deliver a new level of understanding. For example, the molecular studies could also include protein studies by western blot or immunohistochemistry to compliment the quantified mRNA expression. This addition would allow post-transcriptional modification and timing for translation to be taken into account when investigating circadian variation of specific genes. Further, both mRNA and protein expression could be quantified throughout re-entrainment processes

during changing light intensity or timings to demonstrate changes at the molecular level driving the behavioural outputs observed in locomotor activity. Additionally, cross-breeding of TASK-3 KO with a reporter gene transgenic strain such as PER2::LUC would be useful in this line of research (Yoo et al., 2004). Not only would this method highlight changes in protein expression during entrainment, but would also offer higher resolution of selected protein levels within the distinct core and shell regions of the clock.

The behavioural studies in this project revealed surprisingly low locomotor activity intensity compared to previous studies (Linden et al., 2007, Gotter et al., 2011). Although wheel-running is a renowned tool for measuring circadian entrainment, this series of experiments would benefit from additional studies using infra-red motion detection to determine any difference between patterns of voluntary activity and general movement throughout the cage.

In this work the absence of TASK-3 at the level of the retina has revealed significant differences in photic sensitivity indicative of a cone-driven response. There are many ways to examine contributions from specific photoreceptor classes in isolation including cross-breeding with retinal KO lines such as melanopsin KO mice (*Opn4*$^{-/-}$) eliminate inner retinal photoreception or rodless-coneless mice (*rd/rd cl*) to remove outer, classical photoreception (Hattar et al., 2003, Lucas et al., 2003, Mrosovsky and Hattar, 2003). These methods would be useful in this study to differentiate between cone and melanopsin-driven responses in the TASK-3 KO retina. However, cross-breeding with red-cone KI mice and examining pupillary responses to long-wavelength light beyond the normal range of mouse photoreception allows cone-driven contributions to be explored without

compensation of damage from photoreceptor loss (Guler et al., 2008, Lucas et al., 2012).

Alternatively specific pharmacological blockers can be used to remove specific classes - of particular interest are the recently discovered small-molecule antagonists of melanopsin-mediated phototransduction (Jones et al., 2013). These could be applied to TASK-3 KO mice prior to pupillometry in the intact visual system or prior to removal for isolated eye preparation thereby providing a method of assessing PLR and iPLR in the absence of melanopsin and TASK-3.

With TASK-3 having the role of a background leakage channel and stabilising resting membrane potential to influence neuronal excitability, a priority area for future work has to be the exploration of electrical activity of SCN neurons by electrophysiology. There are two ways which seem particularly suitable for this extension of the study – coronal brain slice preparation containing the whole SCN for patch-clamping of individual SCN neurons and *in vivo* electrophysiology (Brown et al., 2006, Karmazinova and Lacinova, 2010, Houben et al., 2009). Both of these techniques would allow the true impact of TASK-3 loss on electrical properties of SCN neurons to be ascertained, the later method having the additional advantage of offering concurrent behavioural study.

Finally, all the experiments in this thesis have been conducted on transgenic mice with global TASK-3 ablation. Despite Brickley et al., confirming other closely related channels are not altered in their expression by this process of transgenic process, it is impossible to fully rule out compensation for this loss (Brickley et al., 2007). The use of a selective TASK-3 antagonist would address this issue as application in WT mice would effectively remove TASK-3 function without

interference of other mechanisms (Coburn et al., 2011). Although this approach would not be feasible for long-term behavioural studies, this pharmacological intervention could be used for acute retinal studies such as PLR and perbutations for phase shifting experiments to study the involvement of TASK-3 in clock re-setting to light. Alternatively TASK-3 could be knocked down longer-term in WT mice through the use of siRNA technology (Agrawal et al., 2003). This approach would also eliminate compensation for gene loss during development, and would provide a very interesting comparison to the transgenic TASK-3 KO mice.

References

ABRAHAMSON, E. E. & MOORE, R. Y. 2001. Suprachiasmatic nucleus in the mouse: retinal innervation, intrinsic organization and efferent projections. *Brain Res,* 916**,** 172-91.

ACHER, F. C. 2006. Metabotropic Glutamate Receptors. *Tocris Bioscience Review Series,* 26**,** 1-12.

AGRAWAL, N., DASARADHI, P. V., MOHMMED, A., MALHOTRA, P., BHATNAGAR, R. K. & MUKHERJEE, S. K. 2003. RNA interference: biology, mechanism, and applications. *Microbiol Mol Biol Rev,* 67**,** 657-85.

ALBRECHT, U. 2012. Timing to perfection: the biology of central and peripheral circadian clocks. *Neuron,* 74**,** 246-60.

ALBRECHT, U., ZHENG, B., LARKIN, D., SUN, Z. S. & LEE, C. C. 2001. MPer1 and mper2 are essential for normal resetting of the circadian clock. *J Biol Rhythms,* 16**,** 100-4.

ALLER, M. I., VEALE, E. L., LINDEN, A. M., SANDU, C., SCHWANINGER, M., EVANS, L. J., KORPI, E. R., MATHIE, A., WISDEN, W. & BRICKLEY, S. G. 2005. Modifying the subunit composition of TASK channels alters the modulation of a leak conductance in cerebellar granule neurons. *J Neurosci,* 25**,** 11455-67.

ALLER, M. I. & WISDEN, W. 2008. Changes in expression of some two-pore domain potassium channel genes (KCNK) in selected brain regions of developing mice. *Neuroscience,* 151**,** 1154-72.

ALTIMUS, C. M., GULER, A. D., ALAM, N. M., ARMAN, A. C., PRUSKY, G. T., SAMPATH, A. P. & HATTAR, S. 2010. Rod photoreceptors drive circadian photoentrainment across a wide range of light intensities. *Nat Neurosci,* 13**,** 1107-12.

AN, S., HARANG, R., MEEKER, K., GRANADOS-FUENTES, D., TSAI, C. A., MAZUSKI, C., KIM, J., DOYLE, F. J., 3RD, PETZOLD, L. R. & HERZOG, E. D. 2013. A neuropeptide speeds circadian entrainment by reducing intercellular synchrony. *Proc Natl Acad Sci U S A,* 110**,** E4355-61.

ANTLE, M. C., SMITH, V. M., STERNICZUK, R., YAMAKAWA, G. R. & RAKAI, B. D. 2009. Physiological responses of the circadian clock to acute light exposure at night. *Rev Endocr Metab Disord,* 10**,** 279-91.

BAREL, O., SHALEV, S. A., OFIR, R., COHEN, A., ZLOTOGORA, J., SHORER, Z., MAZOR, G., FINER, G., KHATEEB, S., ZILBERBERG, N. & BIRK, O. S. 2008. Maternally inherited Birk Barel mental retardation dysmorphism syndrome caused by a mutation in the genomically imprinted potassium channel KCNK9. *Am J Hum Genet,* 83**,** 193-9.

BAVER, S. B., PICKARD, G. E. & SOLLARS, P. J. 2008. Two types of melanopsin retinal ganglion cell differentially innervate the hypothalamic suprachiasmatic nucleus and the olivary pretectal nucleus. *Eur J Neurosci,* 27**,** 1763-70.

BAYLISS, D. A. & BARRETT, P. Q. 2008. Emerging roles for two-pore-domain potassium channels and their potential therapeutic impact. *Trends Pharmacol Sci,* 29**,** 566-75.

BEAN, B. P. 2007. The action potential in mammalian central neurons. *Nat Rev Neurosci,* 8**,** 451-65.

BELLE, M. D., DIEKMAN, C. O., FORGER, D. B. & PIGGINS, H. D. 2009. Daily electrical silencing in the mammalian circadian clock. *Science,* 326**,** 281-4.

BERNARD, S., GONZE, D., CAJAVEC, B., HERZEL, H. & KRAMER, A. 2007. Synchronization-induced rhythmicity of circadian oscillators in the suprachiasmatic nucleus. *PLoS Comput Biol,* 3**,** e68.

BERSON, D. M. 2003. Strange vision: ganglion cells as circadian photoreceptors. *Trends Neurosci,* 26**,** 314-20.

BERSON, D. M., DUNN, F. A. & TAKAO, M. 2002. Phototransduction by retinal ganglion cells that set the circadian clock. *Science,* 295**,** 1070-3.

BLUMER, K. J. 2004. Vision: the need for speed. *Nature,* 427**,** 20-1.

BOIVIN, D. B. & BOUDREAU, P. 2014. Impacts of shift work on sleep and circadian rhythms. *Pathol Biol (Paris)*.

BRICKLEY, S. G., ALLER, M. I., SANDU, C., VEALE, E. L., ALDER, F. G., SAMBI, H., MATHIE, A. & WISDEN, W. 2007. TASK-3 two-pore domain potassium channels enable sustained high-frequency firing in cerebellar granule neurons. *J Neurosci,* 27**,** 9329-40.

BROWN, D. A. 2000. Neurobiology: the acid test for resting potassium channels. *Curr Biol,* 10**,** R456-9.

BROWN, T. M., BANKS, J. R. & PIGGINS, H. D. 2006. A novel suction electrode recording technique for monitoring circadian rhythms in single and multiunit discharge from brain slices. *J Neurosci Methods,* 156**,** 173-81.

BROWN, T. M. & LUCAS, R. J. 2009. Melanopsin phototransduction: great excitement over a poor catch. *Curr Biol,* 19**,** R256-7.

BROWN, T. M. & PIGGINS, H. D. 2007. Electrophysiology of the suprachiasmatic circadian clock. *Prog Neurobiol,* 82**,** 229-55.

BROWN, T. M. & PIGGINS, H. D. 2009. Spatiotemporal heterogeneity in the electrical activity of suprachiasmatic nuclei neurons and their response to photoperiod. *J Biol Rhythms,* 24**,** 44-54.

BUTLER, M. P. & SILVER, R. 2011. Divergent photic thresholds in the non-image-forming visual system: entrainment, masking and pupillary light reflex. *Proc Biol Sci,* 278**,** 745-50.

CAMERON, M. A., BARNARD, A. R. & LUCAS, R. J. 2008. The electroretinogram as a method for studying circadian rhythms in the mammalian retina. *J Genet,* 87**,** 459-66.

CAMPBELL, G. & LIEBERMAN, A. R. 1985. The olivary pretectal nucleus: experimental anatomical studies in the rat. *Philos Trans R Soc Lond B Biol Sci,* 310**,** 573-609.

CAMPBELL, S. S. & MURPHY, P. J. 1998. Extraocular circadian phototransduction in humans. *Science,* 279**,** 396-9.

CHEMIN, J., GIRARD, C., DUPRAT, F., LESAGE, F., ROMEY, G. & LAZDUNSKI, M. 2003. Mechanisms underlying excitatory effects of group I metabotropic glutamate receptors via inhibition of 2P domain K+ channels. *EMBO J,* 22**,** 5403-11.

CHEN, X., TALLEY, E. M., PATEL, N., GOMIS, A., MCINTIRE, W. E., DONG, B., VIANA, F., GARRISON, J. C. & BAYLISS, D. A. 2006. Inhibition of a background potassium channel by Gq protein alpha-subunits. *Proc Natl Acad Sci U S A,* 103**,** 3422-7.

CLARKE, C. E., VEALE, E. L., GREEN, P. J., MEADOWS, H. J. & MATHIE, A. 2004. Selective block of the human 2-P domain potassium channel, TASK-3, and the native leak potassium current, IKSO, by zinc. *J Physiol,* 560**,** 51-62.

CLARKE, C. E., VEALE, E. L., WYSE, K., VANDENBERG, J. I. & MATHIE, A. 2008. The M1P1 loop of TASK3 K2P channels apposes the selectivity filter and influences channel function. *J Biol Chem,* 283**,** 16985-92.

COBURN, C. A., LUO, Y., CUI, M., WANG, J., SOLL, R., DONG, J., HU, B., LYON, M. A., SANTARELLI, V. P., KRAUS, R. L., GREGAN, Y., WANG, Y., FOX, S. V., BINNS, J., DORAN, S. M., REISS, D. R., TANNENBAUM, P. L., GOTTER, A. L., MEINKE, P. T. & RENGER, J. J. 2011. Discovery of a Pharmacologically Active Antagonist of the Two-Pore-Domain Potassium Channel K(2P) 9.1 (TASK-3). *ChemMedChem*.

COLWELL, C. S. 2011. Linking neural activity and molecular oscillations in the SCN. *Nat Rev Neurosci,* 12**,** 553-69.

CUTLER, D. J., HARAURA, M., REED, H. E., SHEN, S., SHEWARD, W. J., MORRISON, C. F., MARSTON, H. M., HARMAR, A. J. & PIGGINS, H. D. 2003. The mouse VPAC2 receptor confers suprachiasmatic nuclei cellular rhythmicity and responsiveness to vasoactive intestinal polypeptide in vitro. *Eur J Neurosci,* 17**,** 197-204.

CZIRJAK, G. & ENYEDI, P. 2002. Formation of functional heterodimers between the TASK-1 and TASK-3 two-pore domain potassium channel subunits. *J Biol Chem,* 277**,** 5426-32.

DAAN, S. 2000. The Colin S. Pittendrigh Lecture. Colin Pittendrigh, Jurgen Aschoff, and the natural entrainment of circadian systems. *J Biol Rhythms,* 15**,** 195-207.

DAVIDSON, A. J., CASTANON-CERVANTES, O., LEISE, T. L., MOLYNEUX, P. C. & HARRINGTON, M. E. 2009. Visualizing jet lag in the mouse suprachiasmatic nucleus and peripheral circadian timing system. *Eur J Neurosci,* 29**,** 171-80.

DIBNER, C., SCHIBLER, U. & ALBRECHT, U. 2010. The Mammalian Circadian Timing System: Organization and Coordination of Central and Peripheral Clocks. *Annual Review of Physiology,* 72**,** 517-49.

DO, M. T., KANG, S. H., XUE, T., ZHONG, H., LIAO, H. W., BERGLES, D. E. & YAU, K. W. 2009. Photon capture and signalling by melanopsin retinal ganglion cells. *Nature,* 457**,** 281-7.

DROUYER, E., RIEUX, C., HUT, R. A. & COOPER, H. M. 2007. Responses of suprachiasmatic nucleus neurons to light and dark adaptation: relative contributions of melanopsin and rod-cone inputs. *J Neurosci,* 27**,** 9623-31.

DUNLAP, J. C. 1999. Molecular bases for circadian clocks. *Cell,* 96**,** 271-90.

DUPRAT, F., LAURITZEN, I., PATEL, A. & HONORE, E. 2007. The TASK background K2P channels: chemo- and nutrient sensors. *Trends Neurosci,* 30**,** 573-80.

ECKER, J. L., DUMITRESCU, O. N., WONG, K. Y., ALAM, N. M., CHEN, S. K., LEGATES, T., RENNA, J. M., PRUSKY, G. T., BERSON, D. M. & HATTAR, S. 2010. Melanopsin-expressing retinal ganglion-cell photoreceptors: cellular diversity and role in pattern vision. *Neuron,* 67**,** 49-60.

EDERY, I. 2000. Circadian rhythms in a nutshell. *Physiol Genomics,* 3**,** 59-74.

ENYEDI, P. & CZIRJAK, G. 2010. Molecular background of leak K+ currents: two-pore domain potassium channels. *Physiol Rev,* 90**,** 559-605.

FOSTER, R. G. 1998. Shedding light on the biological clock. *Neuron,* 20**,** 829-32.

FULLER, P. M., LU, J. & SAPER, C. B. 2009. Standards of evidence in chronobiology: A response. *J Circadian Rhythms,* 7**,** 9.

GANNON, R. L. & MILLAN, M. J. 2011. Positive and negative modulation of circadian activity rhythms by mGluR5 and mGluR2/3 metabotropic glutamate receptors. *Neuropharmacology,* 60**,** 209-15.

GOLDSTEIN, S. A., BAYLISS, D. A., KIM, D., LESAGE, F., PLANT, L. D. & RAJAN, S. 2005. International Union of Pharmacology. LV. Nomenclature and molecular relationships of two-P potassium channels. *Pharmacol Rev,* 57**,** 527-40.

GOLDSTEIN, S. A., BOCKENHAUER, D., O'KELLY, I. & ZILBERBERG, N. 2001. Potassium leak channels and the KCNK family of two-P-domain subunits. *Nat Rev Neurosci,* 2**,** 175-84.

GOTTER, A. L., SANTARELLI, V. P., DORAN, S. M., TANNENBAUM, P. L., KRAUS, R. L., ROSAHL, T. W., MEZIANE, H., MONTIAL, M., REISS, D. R., WESSNER, K., MCCAMPBELL, A., STEVENS, J., BRUNNER, J. I., FOX, S. V., UEBELE, V. N., BAYLISS, D. A., WINROW, C. J. & RENGER, J. J. 2011. TASK-3 as a potential antidepressant target. *Brain Res,* 1416**,** 69-79.

GREEN, C. B. & BESHARSE, J. C. 2004. Retinal circadian clocks and control of retinal physiology. *J Biol Rhythms,* 19**,** 91-102.

GREEN, D. J. & GILLETTE, R. 1982. Circadian rhythm of firing rate recorded from single cells in the rat suprachiasmatic brain slice. *Brain Res,* 245**,** 198-200.

GUIDO, M. E., GARBARINO-PICO, E., CONTIN, M. A., VALDEZ, D. J., NIETO, P. S., VERRA, D. M., ACOSTA-RODRIGUEZ, V. A., DE ZAVALIA, N. & ROSENSTEIN, R. E. 2010. Inner retinal circadian clocks and non-visual photoreceptors: novel players in the circadian system. *Prog Neurobiol,* 92**,** 484-504.

GULER, A. D., ECKER, J. L., LALL, G. S., HAQ, S., ALTIMUS, C. M., LIAO, H. W., BARNARD, A. R., CAHILL, H., BADEA, T. C., ZHAO, H., HANKINS, M. W., BERSON, D. M., LUCAS, R. J., YAU, K. W. & HATTAR, S. 2008. Melanopsin cells are the principal conduits for rod-cone input to non-image-forming vision. *Nature,* 453**,** 102-5.

HAAK, L. L., ALBERS, H. E. & MINTZ, E. M. 2006. Modulation of photic response by the metabotropic glutamate receptor agonist t-ACPD. *Brain Res Bull,* 71**,** 97-100.

HANNIBAL, J. 2002. Neurotransmitters of the retino-hypothalamic tract. *Cell Tissue Res,* 309**,** 73-88.

HARRINGTON, M. E., HOQUE, S., HALL, A., GOLOMBEK, D. & BIELLO, S. 1999. Pituitary adenylate cyclase activating peptide phase shifts circadian rhythms in a manner similar to light. *J Neurosci,* 19**,** 6637-42.

HASTINGS, M. H., BRANCACCIO, M. & MAYWOOD, E. S. 2014. Circadian pacemaking in cells and circuits of the suprachiasmatic nucleus. *J Neuroendocrinol,* 26**,** 2-10.

HATORI, M., LE, H., VOLLMERS, C., KEDING, S. R., TANAKA, N., BUCH, T., WAISMAN, A., SCHMEDT, C., JEGLA, T. & PANDA, S. 2008. Inducible ablation of melanopsin-expressing retinal ganglion cells reveals their central role in non-image forming visual responses. *PLoS One,* 3**,** e2451.

HATTAR, S., KUMAR, M., PARK, A., TONG, P., TUNG, J., YAU, K. W. & BERSON, D. M. 2006. Central projections of melanopsin-expressing retinal ganglion cells in the mouse. *J Comp Neurol,* 497**,** 326-49.

HATTAR, S., LIAO, H. W., TAKAO, M., BERSON, D. M. & YAU, K. W. 2002. Melanopsin-containing retinal ganglion cells: architecture, projections, and intrinsic photosensitivity. *Science,* 295**,** 1065-70.

HATTAR, S., LUCAS, R. J., MROSOVSKY, N., THOMPSON, S., DOUGLAS, R. H., HANKINS, M. W., LEM, J., BIEL, M., HOFMANN, F., FOSTER, R. G. & YAU, K. W. 2003. Melanopsin and rod-

cone photoreceptive systems account for all major accessory visual functions in mice. *Nature,* 424**,** 76-81.

HERZOG, E. D. 2007. Neurons and networks in daily rhythms. *Nat Rev Neurosci,* 8**,** 790-802.

HOPWOOD, S. E. & TRAPP, S. 2005. TASK-like K+ channels mediate effects of 5-HT and extracellular pH in rat dorsal vagal neurones in vitro. *J Physiol,* 568**,** 145-54.

HOUBEN, T., DEBOER, T., VAN OOSTERHOUT, F. & MEIJER, J. H. 2009. Correlation with behavioral activity and rest implies circadian regulation by SCN neuronal activity levels. *J Biol Rhythms,* 24**,** 477-87.

INOUYE, S. T. & KAWAMURA, H. 1979. Persistence of circadian rhythmicity in a mammalian hypothalamic "island" containing the suprachiasmatic nucleus. *Proc Natl Acad Sci U S A,* 76**,** 5962-6.

JONES, K. A., HATORI, M., MURE, L. S., BRAMLEY, J. R., ARTYMYSHYN, R., HONG, S. P., MARZABADI, M., ZHONG, H., SPROUSE, J., ZHU, Q., HARTWICK, A. T., SOLLARS, P. J., PICKARD, G. E. & PANDA, S. 2013. Small-molecule antagonists of melanopsin-mediated phototransduction. *Nat Chem Biol,* 9**,** 630-5.

KALSBEEK, A., FLIERS, E., HOFMAN, M. A., SWAAB, D. F. & BUIJS, R. M. 2010. Vasopressin and the output of the hypothalamic biological clock. *J Neuroendocrinol,* 22**,** 362-72.

KARMAZINOVA, M. & LACINOVA, L. 2010. Measurement of cellular excitability by whole cell patch clamp technique. *Physiol Res,* 59 Suppl 1**,** S1-7.

KAWAMURA, S. & TACHIBANAKI, S. 2008. Rod and cone photoreceptors: molecular basis of the difference in their physiology. *Comp Biochem Physiol A Mol Integr Physiol,* 150**,** 369-77.

KETTUNEN, P., HESS, D. & EL MANIRA, A. 2003. mGluR1, but not mGluR5, mediates depolarization of spinal cord neurons by blocking a leak current. *J Neurophysiol,* 90**,** 2341-8.

KIM, Y., BANG, H. & KIM, D. 2000. TASK-3, a new member of the tandem pore K(+) channel family. *J Biol Chem,* 275**,** 9340-7.

KO, C. H. & TAKAHASHI, J. S. 2006. Molecular components of the mammalian circadian clock. *Hum Mol Genet,* 15 Spec No 2**,** R271-7.

KOLB, H. 2003. How the Retina Works. *American Scientist,* 91**,** 28-35.

KORENBROT, J. I. 2012. Speed, sensitivity, and stability of the light response in rod and cone photoreceptors: Facts and models. *Prog Retin Eye Res,* 31**,** 442-66.

KRIEGSFELD, L. J. & SILVER, R. 2006. The regulation of neuroendocrine function: Timing is everything. *Horm Behav,* 49**,** 557-74.

KRISTENSSON, K., NYGARD, M., BERTINI, G. & BENTIVOGLIO, M. 2010. African trypanosome infections of the nervous system: parasite entry and effects on sleep and synaptic functions. *Prog Neurobiol,* 91**,** 152-71.

KUHLMAN, S. J. & MCMAHON, D. G. 2004. Rhythmic regulation of membrane potential and potassium current persists in SCN neurons in the absence of environmental input. *Eur J Neurosci,* 20**,** 1113-7.

KUHLMAN, S. J. & MCMAHON, D. G. 2006. Encoding the ins and outs of circadian pacemaking. *J Biol Rhythms,* 21**,** 470-81.

LAFRENIERE, R. G., CADER, M. Z., POULIN, J. F., ANDRES-ENGUIX, I., SIMONEAU, M., GUPTA, N., BOISVERT, K., LAFRENIERE, F., MCLAUGHLAN, S., DUBE, M. P., MARCINKIEWICZ, M. M., RAMAGOPALAN, S., ANSORGE, O., BRAIS, B., SEQUEIROS, J., PEREIRA-MONTEIRO, J. M.,

GRIFFITHS, L. R., TUCKER, S. J., EBERS, G. & ROULEAU, G. A. 2010. A dominant-negative mutation in the TRESK potassium channel is linked to familial migraine with aura. *Nat Med,* 16**,** 1157-60.

LALL, G. S., ATKINSON, L. A., CORLETT, S. A., BROADBRIDGE, P. J. & BONSALL, D. R. 2012. Circadian entrainment and its role in depression: a mechanistic review. *J Neural Transm,* 119**,** 1085-96.

LALL, G. S. & BIELLO, S. M. 2002. Attenuation of phase shifts to light by activity or neuropeptide Y: a time course study. *Brain Res,* 957**,** 109-16.

LALL, G. S. & BIELLO, S. M. 2003. Neuropeptide Y, GABA and circadian phase shifts to photic stimuli. *Neuroscience,* 120**,** 915-21.

LALL, G. S., REVELL, V. L., MOMIJI, H., AL ENEZI, J., ALTIMUS, C. M., GULER, A. D., AGUILAR, C., CAMERON, M. A., ALLENDER, S., HANKINS, M. W. & LUCAS, R. J. 2010. Distinct contributions of rod, cone, and melanopsin photoreceptors to encoding irradiance. *Neuron,* 66**,** 417-28.

LESAGE, F. & LAZDUNSKI, M. 2000. Molecular and functional properties of two-pore-domain potassium channels. *Am J Physiol Renal Physiol,* 279**,** F793-801.

LINDEN, A. M., SANDU, C., ALLER, M. I., VEKOVISCHEVA, O. Y., ROSENBERG, P. H., WISDEN, W. & KORPI, E. R. 2007. TASK-3 knockout mice exhibit exaggerated nocturnal activity, impairments in cognitive functions, and reduced sensitivity to inhalation anesthetics. *J Pharmacol Exp Ther,* 323**,** 924-34.

LIU, C., WEAVER, D. R., STROGATZ, S. H. & REPPERT, S. M. 1997. Cellular construction of a circadian clock: period determination in the suprachiasmatic nuclei. *Cell,* 91**,** 855-60.

LIVAK, K. J. & SCHMITTGEN, T. D. 2001. Analysis of relative gene expression data using real-time quantitative PCR and the 2(-Delta Delta C(T)) Method. *Methods,* 25**,** 402-8.

LOTSHAW, D. P. 2007. Biophysical, pharmacological, and functional characteristics of cloned and native mammalian two-pore domain K+ channels. *Cell Biochem Biophys,* 47**,** 209-56.

LUCAS, R. J. 2013. Mammalian inner retinal photoreception. *Curr Biol,* 23**,** R125-33.

LUCAS, R. J., DOUGLAS, R. H. & FOSTER, R. G. 2001. Characterization of an ocular photopigment capable of driving pupillary constriction in mice. *Nat Neurosci,* 4**,** 621-6.

LUCAS, R. J. & FOSTER, R. G. 1999. Neither functional rod photoreceptors nor rod or cone outer segments are required for the photic inhibition of pineal melatonin. *Endocrinology,* 140**,** 1520-4.

LUCAS, R. J., HATTAR, S., TAKAO, M., BERSON, D. M., FOSTER, R. G. & YAU, K. W. 2003. Diminished pupillary light reflex at high irradiances in melanopsin-knockout mice. *Science,* 299**,** 245-7.

LUCAS, R. J., LALL, G. S., ALLEN, A. E. & BROWN, T. M. 2012. How rod, cone, and melanopsin photoreceptors come together to enlighten the mammalian circadian clock. *Prog Brain Res,* 199**,** 1-18.

MARINC, C., DERST, C., PRUSS, H. & VEH, R. W. 2014. Immunocytochemical localization of TASK-3 protein (K2P9.1) in the rat brain. *Cell Mol Neurobiol,* 34**,** 61-70.

MARKWELL, E. L., FEIGL, B. & ZELE, A. J. 2010. Intrinsically photosensitive melanopsin retinal ganglion cell contributions to the pupillary light reflex and circadian rhythm. *Clin Exp Optom,* 93**,** 137-49.

MASLAND, R. H. 2012. The neuronal organization of the retina. *Neuron,* 76**,** 266-80.

MATHIE, A. 2007. Neuronal two-pore-domain potassium channels and their regulation by G protein-coupled receptors. *J Physiol,* 578**,** 377-85.

MATHIE, A., AL-MOUBARAK, E. & VEALE, E. L. 2010a. Gating of two pore domain potassium channels. *J Physiol,* 588**,** 3149-56.

MATHIE, A., REES, K. A., EL HACHMANE, M. F. & VEALE, E. L. 2010b. Trafficking of neuronal two pore domain potassium channels. *Curr Neuropharmacol,* 8**,** 276-86.

MATHIE, A. & VEALE, E. L. 2007. Therapeutic potential of neuronal two-pore domain potassium-channel modulators. *Curr Opin Investig Drugs,* 8**,** 555-62.

MAYWOOD, E. S., O'BRIEN, J. A. & HASTINGS, M. H. 2003. Expression of mCLOCK and other circadian clock-relevant proteins in the mouse suprachiasmatic nuclei. *J Neuroendocrinol,* 15**,** 329-34.

MAYWOOD, E. S., O'NEILL, J. S., REDDY, A. B., CHESHAM, J. E., PROSSER, H. M., KYRIACOU, C. P., GODINHO, S. I., NOLAN, P. M. & HASTINGS, M. H. 2007. Genetic and molecular analysis of the central and peripheral circadian clockwork of mice. *Cold Spring Harb Symp Quant Biol,* 72**,** 85-94.

MCBAIN, C. J. & TRAYNELIS, S. F. 2006. Malevolent lurkers no more: NMDA receptors come of age. *J Physiol,* 575**,** 317-8.

MCNEILL, D. S., SHEELY, C. J., ECKER, J. L., BADEA, T. C., MORHARDT, D., GUIDO, W. & HATTAR, S. 2011. Development of melanopsin-based irradiance detecting circuitry. *Neural Dev,* 6**,** 8.

MEIJER, J. H., MICHEL, S., VANDERLEEST, H. T. & ROHLING, J. H. 2010. Daily and seasonal adaptation of the circadian clock requires plasticity of the SCN neuronal network. *Eur J Neurosci,* 32**,** 2143-51.

MEREDITH, A. L., WILER, S. W., MILLER, B. H., TAKAHASHI, J. S., FODOR, A. A., RUBY, N. F. & ALDRICH, R. W. 2006. BK calcium-activated potassium channels regulate circadian behavioral rhythms and pacemaker output. *Nat Neurosci,* 9**,** 1041-9.

MEUTH, S. G., BUDDE, T., KANYSHKOVA, T., BROICHER, T., MUNSCH, T. & PAPE, H. C. 2003. Contribution of TWIK-related acid-sensitive K+ channel 1 (TASK1) and TASK3 channels to the control of activity modes in thalamocortical neurons. *J Neurosci,* 23**,** 6460-9.

MICHEL, S., ITRI, J., HAN, J. H., GNIOTCZYNSKI, K. & COLWELL, C. S. 2006. Regulation of glutamatergic signalling by PACAP in the mammalian suprachiasmatic nucleus. *BMC Neurosci,* 7**,** 15.

MICHEL, S., MAREK, R., VANDERLEEST, H. T., VANSTEENSEL, M. J., SCHWARTZ, W. J., COLWELL, C. S. & MEIJER, J. H. 2013. Mechanism of bilateral communication in the suprachiasmatic nucleus. *Eur J Neurosci,* 37**,** 964-71.

MILLER, A. L. 2005. Epidemiology, etiology, and natural treatment of seasonal affective disorder. *Altern Med Rev,* 10**,** 5-13.

MINTZ, E. M., MARVEL, C. L., GILLESPIE, C. F., PRICE, K. M. & ALBERS, H. E. 1999. Activation of NMDA receptors in the suprachiasmatic nucleus produces light-like phase shifts of the circadian clock in vivo. *J Neurosci,* 19**,** 5124-30.

MISTLBERGER, R. E. 1994. Circadian food-anticipatory activity: formal models and physiological mechanisms. *Neurosci Biobehav Rev,* 18**,** 171-95.

MISTLBERGER, R. E. & SKENE, D. J. 2004. Social influences on mammalian circadian rhythms: animal and human studies. *Biol Rev Camb Philos Soc,* 79**,** 533-56.

MOHAWK, J. A. & TAKAHASHI, J. S. 2011. Cell autonomy and synchrony of suprachiasmatic nucleus circadian oscillators. *Trends Neurosci,* 34**,** 349-58.

MORIN, L. P. 2007. SCN organization reconsidered. *J Biol Rhythms,* 22**,** 3-13.

MORIN, L. P. & ALLEN, C. N. 2006. The circadian visual system, 2005. *Brain Res Rev,* 51**,** 1-60.

MORIN, L. P. & BLANCHARD, J. 1995. Organization of the hamster intergeniculate leaflet: NPY and ENK projections to the suprachiasmatic nucleus, intergeniculate leaflet and posterior limitans nucleus. *Vis Neurosci,* 12**,** 57-67.

MORIN, L. P., SHIVERS, K. Y., BLANCHARD, J. H. & MUSCAT, L. 2006. Complex organization of mouse and rat suprachiasmatic nucleus. *Neuroscience,* 137**,** 1285-97.

MROSOVSKY, N. 1988. Phase response curves for social entrainment. *J Comp Physiol A,* 162**,** 35-46.

MROSOVSKY, N. 1999. Masking: history, definitions, and measurement. *Chronobiol Int,* 16**,** 415-29.

MROSOVSKY, N., FOSTER, R. G. & SALMON, P. A. 1999. Thresholds for masking responses to light in three strains of retinally degenerate mice. *J Comp Physiol A,* 184**,** 423-8.

MROSOVSKY, N. & HATTAR, S. 2003. Impaired masking responses to light in melanopsin-knockout mice. *Chronobiol Int,* 20**,** 989-99.

MROSOVSKY, N., LUCAS, R. J. & FOSTER, R. G. 2001. Persistence of masking responses to light in mice lacking rods and cones. *J Biol Rhythms,* 16**,** 585-8.

MULKEY, D. K., TALLEY, E. M., STORNETTA, R. L., SIEGEL, A. R., WEST, G. H., CHEN, X., SEN, N., MISTRY, A. M., GUYENET, P. G. & BAYLISS, D. A. 2007. TASK channels determine pH sensitivity in select respiratory neurons but do not contribute to central respiratory chemosensitivity. *J Neurosci,* 27**,** 14049-58.

NIKONOV, S. S., KHOLODENKO, R., LEM, J. & PUGH, E. N., JR. 2006. Physiological features of the S- and M-cone photoreceptors of wild-type mice from single-cell recordings. *J Gen Physiol,* 127**,** 359-74.

OWENS, L., BUHR, E., TU, D. C., LAMPRECHT, T. L., LEE, J. & VAN GELDER, R. N. 2011. Effect of circadian clock gene mutations on non-visual photoreception in the mouse. *Invest Ophthalmol Vis Sci*.

PANDA, S., SATO, T. K., CASTRUCCI, A. M., ROLLAG, M. D., DEGRIP, W. J., HOGENESCH, J. B., PROVENCIO, I. & KAY, S. A. 2002. Melanopsin (Opn4) requirement for normal light-induced circadian phase shifting. *Science,* 298**,** 2213-6.

PANG, D. S., ROBLEDO, C. J., CARR, D. R., GENT, T. C., VYSSOTSKI, A. L., CALEY, A., ZECHARIA, A. Y., WISDEN, W., BRICKLEY, S. G. & FRANKS, N. P. 2009. An unexpected role for TASK-3 potassium channels in network oscillations with implications for sleep mechanisms and anesthetic action. *Proc Natl Acad Sci U S A,* 106**,** 17546-51.

PARTRIDGE, J. C. & DE GRIP, W. J. 1991. A new template for rhodopsin (vitamin A1 based) visual pigments. *Vision Res,* 31**,** 619-30.

PATEL, A. J. & HONORE, E. 2001. Properties and modulation of mammalian 2P domain K+ channels. *Trends Neurosci,* 24**,** 339-46.

PATEL, A. J. & LAZDUNSKI, M. 2004. The 2P-domain K+ channels: role in apoptosis and tumorigenesis. *Pflugers Arch,* 448**,** 261-73.

PEIRSON, S. N., HALFORD, S. & FOSTER, R. G. 2009. The evolution of irradiance detection: melanopsin and the non-visual opsins. *Philos Trans R Soc Lond B Biol Sci,* 364**,** 2849-65.

PENNARTZ, C. M., DE JEU, M. T., BOS, N. P., SCHAAP, J. & GEURTSEN, A. M. 2002. Diurnal modulation of pacemaker potentials and calcium current in the mammalian circadian clock. *Nature,* 416**,** 286-90.

PITTENDRIGH, C. & DAAN, S. 1976a. A Functional Analysis of Circadian Pacemakers in Nocturnal Rodents - I. The Stability and Lability of Spontaneous Frequency. *Journal of Comparative Physiology,* 106**,** 223-252.

PITTENDRIGH, C. & DAAN, S. 1976b. A Functional Analysis of Circadian Pacemakers in Nocturnal Rodents - II. The Variability of Phase Response Curves. *Journal of Comparative Physiology,* 106**,** 253-266.

PITTENDRIGH, C. & DAAN, S. 1976c. A Functional Analysis of Circadian Pacemakers in Nocturnal Rodents - III. Heavy Water and Constant Light: Homeostasis of Frequency? *Journal of Comparative Physiology,* 106**,** 267-290.

PITTENDRIGH, C. & DAAN, S. 1976d. A Functional Analysis of Circadian Pacemakers in Nocturnal Rodents - V. Pacemaker Structure: A Clock for All Seasons. *Journal of Comparative Physiology,* 106**,** 333-355.

RALPH, M. & LEHMAN, M. 1991. Transplantation: a new tool in the analysis of the mammalian hypothalamic circadian pacemaker. *TINS,* 14**,** 362-366.

REEBS, S. G. & MROSOVSKY, N. 1989. Effects of induced wheel running on the circadian activity rhythms of Syrian hamsters: entrainment and phase response curve. *J Biol Rhythms,* 4**,** 39-48.

REFINETTI, R. 2004. Non-stationary time series and the robustness of circadian rhythms. *J Theor Biol,* 227**,** 571-81.

REFINETTI, R. 2006. *Circadian physiology,* Boca Raton, Fla., CRC ; London : Taylor & Francis [distributor].

REGHUNANDANAN, V. & REGHUNANDANAN, R. 2006. Neurotransmitters of the suprachiasmatic nuclei. *J Circadian Rhythms,* 4**,** 2.

REPPERT, S. M. & WEAVER, D. R. 2001. Molecular analysis of mammalian circadian rhythms. *Annu Rev Physiol,* 63**,** 647-76.

RICHTER, H. G., TORRES-FARFAN, C., ROJAS-GARCIA, P. P., CAMPINO, C., TORREALBA, F. & SERON-FERRE, M. 2004. The circadian timing system: making sense of day/night gene expression. *Biol Res,* 37**,** 11-28.

ROHLING, J. H., VANDERLEEST, H. T., MICHEL, S., VANSTEENSEL, M. J. & MEIJER, J. H. 2011. Phase resetting of the mammalian circadian clock relies on a rapid shift of a small population of pacemaker neurons. *PLoS One,* 6**,** e25437.

RUBY, N. F., BRENNAN, T. J., XIE, X., CAO, V., FRANKEN, P., HELLER, H. C. & O'HARA, B. F. 2002. Role of melanopsin in circadian responses to light. *Science,* 298**,** 2211-3.

SABBADINI, M. & YOST, C. S. 2009. Molecular biology of background K channels: insights from K(2P) knockout mice. *J Mol Biol,* 385**,** 1331-44.

SACK, R. L. 2009. The pathophysiology of jet lag. *Travel Med Infect Dis,* 7**,** 102-10.

SCHMIDT, T. M., CHEN, S. K. & HATTAR, S. 2011. Intrinsically photosensitive retinal ganglion cells: many subtypes, diverse functions. *Trends Neurosci,* 34**,** 572-80.

SCHMIDT, T. M. & KOFUJI, P. 2009. Functional and morphological differences among intrinsically photosensitive retinal ganglion cells. *J Neurosci,* 29**,** 476-82.

SCHMIDT, T. M. & KOFUJI, P. 2010. Differential cone pathway influence on intrinsically photosensitive retinal ganglion cell subtypes. *J Neurosci,* 30**,** 16262-71.

SCHWARTZ, W. J., TAVAKOLI-NEZHAD, M., LAMBERT, C. M., WEAVER, D. R. & DE LA IGLESIA, H. O. 2011. Distinct patterns of Period gene expression in the suprachiasmatic nucleus underlie circadian clock photoentrainment by advances or delays. *Proc Natl Acad Sci U S A,* 108**,** 17219-24.

SEMO, M., GIAS, C., AHMADO, A. & VUGLER, A. 2014. A role for the ciliary marginal zone in the melanopsin-dependent intrinsic pupillary light reflex. *Exp Eye Res,* 119**,** 8-18.

SHEARMAN, L. P., SRIRAM, S., WEAVER, D. R., MAYWOOD, E. S., CHAVES, I., ZHENG, B., KUME, K., LEE, C. C., VAN DER HORST, G. T., HASTINGS, M. H. & REPPERT, S. M. 2000. Interacting molecular loops in the mammalian circadian clock. *Science,* 288**,** 1013-9.

SKATCHKOV, S. N., EATON, M. J., SHUBA, Y. M., KUCHERYAVYKH, Y. V., DERST, C., VEH, R. W., WURM, A., IANDIEV, I., PANNICKE, T., BRINGMANN, A. & REICHENBACH, A. 2006. Tandem-pore domain potassium channels are functionally expressed in retinal (Muller) glial cells. *Glia,* 53**,** 266-76.

SNELLMAN, J., KAUR, T., SHEN, Y. & NAWY, S. 2008. Regulation of ON bipolar cell activity. *Prog Retin Eye Res,* 27**,** 450-63.

SOKOLOVE, P. G. & BUSHELL, W. N. 1978. The chi square periodogram: its utility for analysis of circadian rhythms. *J Theor Biol,* 72**,** 131-60.

SPOELSTRA, K., ALBRECHT, U., VAN DER HORST, G. T., BRAUER, V. & DAAN, S. 2004. Phase responses to light pulses in mice lacking functional per or cry genes. *J Biol Rhythms,* 19**,** 518-29.

SPOELSTRA, K. & DAAN, S. 2008. Effects of constant light on circadian rhythmicity in mice lacking functional cry genes: dissimilar from per mutants. *J Comp Physiol A Neuroethol Sens Neural Behav Physiol,* 194**,** 235-42.

STEPHAN, F. K. & ZUCKER, I. 1972. Circadian rhythms in drinking behavior and locomotor activity of rats are eliminated by hypothalamic lesions. *Proc Natl Acad Sci U S A,* 69**,** 1583-6.

SUJINO, M., MASUMOTO, K. H., YAMAGUCHI, S., VAN DER HORST, G. T., OKAMURA, H. & INOUYE, S. T. 2003. Suprachiasmatic nucleus grafts restore circadian behavioral rhythms of genetically arrhythmic mice. *Curr Biol,* 13**,** 664-8.

SUKUMARAN, S., ALMON, R. R., DUBOIS, D. C. & JUSKO, W. J. 2010. Circadian rhythms in gene expression: Relationship to physiology, disease, drug disposition and drug action. *Adv Drug Deliv Rev,* 62**,** 904-17.

TACHIBANAKI, S., SHIMAUCHI-MATSUKAWA, Y., ARINOBU, D. & KAWAMURA, S. 2007. Molecular mechanisms characterizing cone photoresponses. *Photochem Photobiol,* 83**,** 19-26.

TAHARA, Y., KURODA, H., SAITO, K., NAKAJIMA, Y., KUBO, Y., OHNISHI, N., SEO, Y., OTSUKA, M., FUSE, Y., OHURA, Y., KOMATSU, T., MORIYA, Y., OKADA, S., FURUTANI, N., HIRAO, A., HORIKAWA, K., KUDO, T. & SHIBATA, S. 2012. In vivo monitoring of peripheral circadian clocks in the mouse. *Curr Biol,* 22**,** 1029-34.

TALLEY, E. M., SIROIS, J. E., LEI, Q. & BAYLISS, D. A. 2003. Two-pore-Domain (KCNK) potassium channels: dynamic roles in neuronal function. *Neuroscientist,* 9**,** 46-56.

TALLEY, E. M., SOLORZANO, G., LEI, Q., KIM, D. & BAYLISS, D. A. 2001. Cns distribution of members of the two-pore-domain (KCNK) potassium channel family. *J Neurosci,* 21**,** 7491-505.

THOMPSON, S., FOSTER, R. G., STONE, E. M., SHEFFIELD, V. C. & MROSOVSKY, N. 2008. Classical and melanopsin photoreception in irradiance detection: negative masking of locomotor activity by light. *Eur J Neurosci,* 27**,** 1973-9.

TORTORA, G. J., DERRICKSON, B. & PREZBINDOWSKI, K. S. L. G. 2006. *Principles of anatomy and physiology, learning guide,* Hoboken, John Wiley & Sons.

VAN DER HORST, G. T., MUIJTJENS, M., KOBAYASHI, K., TAKANO, R., KANNO, S., TAKAO, M., DE WIT, J., VERKERK, A., EKER, A. P., VAN LEENEN, D., BUIJS, R., BOOTSMA, D., HOEIJMAKERS, J. H. & YASUI, A. 1999. Mammalian Cry1 and Cry2 are essential for maintenance of circadian rhythms. *Nature,* 398**,** 627-30.

VAN OOSTERHOUT, F., LUCASSEN, E. A., HOUBEN, T., VANDERLEEST, H. T., ANTLE, M. C. & MEIJER, J. H. 2012. Amplitude of the SCN clock enhanced by the behavioral activity rhythm. *PLoS One,* 7**,** e39693.

VANDERLEEST, H. T., ROHLING, J. H., MICHEL, S. & MEIJER, J. H. 2009. Phase shifting capacity of the circadian pacemaker determined by the SCN neuronal network organization. *PLoS One,* 4**,** e4976.

VEALE, E. L., KENNARD, L. E., SUTTON, G. L., MACKENZIE, G., SANDU, C. & MATHIE, A. 2007. G(alpha)q-mediated regulation of TASK3 two-pore domain potassium channels: the role of protein kinase C. *Mol Pharmacol,* 71**,** 1666-75.

VITATERNA, M. H., KO, C. H., CHANG, A. M., BUHR, E. D., FRUECHTE, E. M., SCHOOK, A., ANTOCH, M. P., TUREK, F. W. & TAKAHASHI, J. S. 2006. The mouse Clock mutation reduces circadian pacemaker amplitude and enhances efficacy of resetting stimuli and phase-response curve amplitude. *Proc Natl Acad Sci U S A,* 103**,** 9327-32.

VITATERNA, M. H., SELBY, C. P., TODO, T., NIWA, H., THOMPSON, C., FRUECHTE, E. M., HITOMI, K., THRESHER, R. J., ISHIKAWA, T., MIYAZAKI, J., TAKAHASHI, J. S. & SANCAR, A. 1999. Differential regulation of mammalian period genes and circadian rhythmicity by cryptochromes 1 and 2. *Proc Natl Acad Sci U S A,* 96**,** 12114-9.

VON GALL, C., NOTON, E., LEE, C. & WEAVER, D. R. 2003. Light does not degrade the constitutively expressed BMAL1 protein in the mouse suprachiasmatic nucleus. *Eur J Neurosci,* 18**,** 125-33.

WANG, J. S. & KEFALOV, V. J. 2011. The cone-specific visual cycle. *Prog Retin Eye Res,* 30**,** 115-28.

WANG, T. A., YU, Y. V., GOVINDAIAH, G., YE, X., ARTINIAN, L., COLEMAN, T. P., SWEEDLER, J. V., COX, C. L. & GILLETTE, M. U. 2012. Circadian rhythm of redox state regulates excitability in suprachiasmatic nucleus neurons. *Science,* 337**,** 839-42.

WISOR, J. P., PASUMARTHI, R. K., GERASHCHENKO, D., THOMPSON, C. L., PATHAK, S., SANCAR, A., FRANKEN, P., LEIN, E. S. & KILDUFF, T. S. 2008. Sleep deprivation effects on circadian clock gene expression in the cerebral cortex parallel electroencephalographic differences among mouse strains. *J Neurosci,* 28**,** 7193-201.

XUE, T., DO, M. T., RICCIO, A., JIANG, Z., HSIEH, J., WANG, H. C., MERBS, S. L., WELSBIE, D. S., YOSHIOKA, T., WEISSGERBER, P., STOLZ, S., FLOCKERZI, V., FREICHEL, M., SIMON, M. I., CLAPHAM, D. E. & YAU, K. W. 2011. Melanopsin signalling in mammalian iris and retina. *Nature,* 479**,** 67-73.

YAN, L., HOCHSTETLER, K. J., SILVER, R. & BULT-ITO, A. 2003. Phase shifts and Per gene expression in mouse suprachiasmatic nucleus. *Neuroreport,* 14**,** 1247-51.

YANG, J., NEMARGUT, J. P. & WANG, G. Y. 2011. The roles of ionotropic glutamate receptors along the On and Off signaling pathways in the light-adapted mouse retina. *Brain Res,* 1390**,** 70-9.

YOO, S. H., YAMAZAKI, S., LOWREY, P. L., SHIMOMURA, K., KO, C. H., BUHR, E. D., SIEPKA, S. M., HONG, H. K., OH, W. J., YOO, O. J., MENAKER, M. & TAKAHASHI, J. S. 2004. PERIOD2::LUCIFERASE real-time reporting of circadian dynamics reveals persistent circadian oscillations in mouse peripheral tissues. *Proc Natl Acad Sci U S A,* 101**,** 5339-46.

ZANZOURI, M., LAURITZEN, I., LAZDUNSKI, M. & PATEL, A. 2006. The background K(+) channel TASK-3 is regulated at both the transcriptional and post-transcriptional levels. *Biochem Biophys Res Commun,* 348**,** 1350-7.

Appendices

I. The $2^{-\Delta\Delta C_T}$ method for determination of relative mRNA concentration

In Polymerase Chain Reactions (PCR) the exponential amplification of target DNA can be defined by the equation:

$X_n = X_0 \times (E + 1)^n$

Where n is the number of cycles, E is the efficiency of the amplification (a value of 1 representing 100% amplification per cycle), X_n is the number of copies of target DNA in the final reaction and X_0 is the number of target DNA molecules in the initial reaction (Livak and Schmittgen, 2001).

This equation can be applied to the real-time PCR conducted in chapters 2 and 7.

Each amplification cycle by the LightCycler 480 (Roche, UK) ends with excitation of SYBR Green fluorescent dye at a wavelength of 483nm, and detection of emissions at 533nm. SYBR Green is a chelating agent which has the property of fluorescing only when intercalated with double-stranded DNA sequences. As the number of DNA products increase exponentially during successive reactions, the amount of intercalated SYBR Green increases proportionally. Therefore the level of SYBR Green emission directly correlates to number of DNA products.

The crossing threshold (C_T) is defined as the number of amplification cycles required for fluorescence to increase beyond a threshold level of accurate detection. This value is constant and therefore differences in C_T values between samples are due to variation in the number of target DNA copies in the initial reaction , X_0 .

Reactions with target DNA sequences of less than 150 base pairs and optimised reagent and primer concentrations efficiency, E, is considered to be close to 1.

Measurement of target gene relative to the reference gene, ΔC_T, is given by:

$$\Delta C_T = [C_{T\ Target\ gene} - C_{T\ Reference\ gene}]$$

Therefore relative quantification of mRNA during a time course, $\Delta\Delta C_T$, is given by the formula:

$$\Delta\Delta C_T = [C_{T\ Target\ gene} - C_{T\ Reference\ gene}]_{Time\ 0} - [C_{T\ Target\ gene} - C_{T\ Reference\ gene}]_{Time\ x}$$

Where $Time_0$ is the earliest time of sampling and $Time_x$ is sampling time point of interest.

II. Genotyping

Tissue retrieval

Tissue for genotyping was taken from the outer ear of the mouse as a punch biopsy or tag of approximately 2mm diameter and placed directly into labelled sterile micro-centrifuge tubes and stored at -80^{o}C until time of processing.

DNA extraction

Ear tissue was transferred into sterile micro-centrifuge tubes containing 100µL DirectPCR (Ear) tissue digest solution (Viagen Biotech, Bioquote, York, UK) with added Proteinase K (Sigma, Gillingham, UK) at a concentration of 0.3mg/mL. Tissue was fully submerged within the solution before being placed in a waterbath rack at 55°C for 4-6 hours. Tubes were vortex mixed every 2 hours to encourage tissue disruption, with digestion considered complete when tissue lumps were no longer observed. A further 45 minutes in the waterbath rack at 85°C, denatured the Proteinase K enzyme in preparation for subsequent stages.

Once digestion complete, tubes containing digest were centrifuged at 12,000 rpm for 5 minutes and genomic DNA-containing supernatant used for Polymerase Chain Reaction (PCR). Unused digest was stored at -80^{o}C for further confirmation of genotype, if required.

Polymerase chain reaction (PCR)

The DNA region of interest from the ear tissue digest was amplified by PCR to provide adequate yield for analysis. PCR tubes were prepared with the following reagents:

12.5µL Dreamtaq 2 x Mastermix (Fermentas ThermoFisher Scientific, Loughborough , UK)

1.0 µL DMSO (Sigma, UK)

4µL DNA extract (from digest, above)

7.5µL Primer mix containing forward and reverse primers* at a concentration of 10µM in nuclease-free water (Invitrogen, ThermoFisher Scientific, Loughborough, UK)

*Primers for PCR are as described by Brickley et al., 2007 (Supplemental Information) to give amplification of restriction fragments of 350 base pair (bp) length in Wild Type mice and 400 bp length in TASK-3 KO mice.

Forward Primer:

pL7S1: 5'- CTCTGTCCCGGCTACCGATCCTGC-3'

Reverse Primer:

P4TV2: 5'-TTCCGTGGGCGCAGCGGGTTCCGC-3'

PCR reactions were heated by thermal cycler for 5 minutes at 95°C, followed by 35 cycles of 95°C for 60s, 60°C for 60s, 72°C for 60s with a final step of 5 minutes at 72°C.

Gel Electrophoresis and Analysis

PCR DNA products were separated by electrophoresis on a 2% agarose gel (Sigma, UK) with 2μL of ethidium bromide (10mg/ml, Sigma, UK) in a running buffer of 0.5 x TAE (Tris-acetate-EDTA) buffer. Samples were run for 90 minutes at 85V alongside a DNA reference ladder (ThermoScientific, UK).

The electrophoresis gel was then removed from the running buffer, drained and viewed/photographed under UV illumination. Any double-stranded DNA present in the gel intercalates with the ethidium bromide, producing a fluorescent signal in the form of specific bands. The position of the bands is dependent on rate of migration according to number of base pairs present. Therefore restriction fragment bands can be compared to a DNA reference ladder for sizing. See Figure Appendix II, Figure 1.

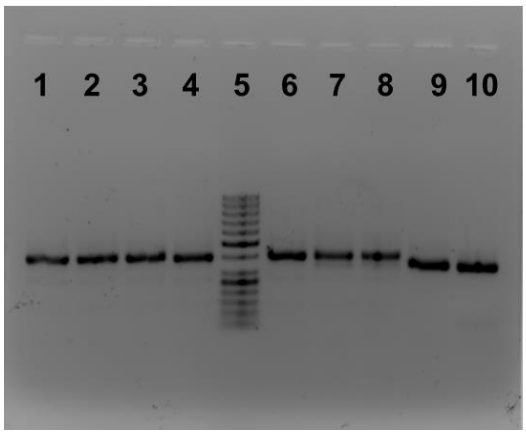

Appendix II, Figure 1: Example of genotyping electrophoresis gel.

An example electrophoresis gel demonstrating DNA bands from PCR genotyping of WT and TASK-3 KO mice. Lanes 1 to 4, 6 to 8 demonstrate 400bp TASK-3 KO bands, lanes 9 to 10 demonstrate 350bp WT bands. The DNA ladder is shown in lane 5.

III. Conversion of power to photon flux

Light intensity measured by optical power meter (Thorlabs, , UK) is given in Watts/cm^2. However irradiance is defined as the number of photons delivered per cm^2 per second.

If the energy of a photon, E_p ,is defined by:

$E_p = h \times f = h \times (c/\lambda)$

Where h is Plancks constant, 6.63×10^{-34} Js; c is the speed of light 2.998×10^8 m/s; f is the frequency and λ is the wavelength in m.

Then light intensity at a given wavelength can be converted into photon flux, ϕ_p, according to the formula:

$\phi_p = P / E_p = P \times \lambda / h \times c$

Where P is power in watts, E_p is the energy of a photon (as above), λ is the wavelength in m, h is Plancks constant, 6.63×10^{-34} Js and c is the speed of light 2.998×10^8 m/s

This simplifies to:

$\phi_p = P \times \lambda \times 5.03 \times 10^{15}$

Where P is power in Watts, λ is wavelength in m and ϕ_p is photon flux in photons/cm^2/s.

For monochromatic light, optical power measured at selected wavelength, for polychromatic white light, optical power measured at 500nm wavelength.

IV. Locomotor activity measurements in LD and DD

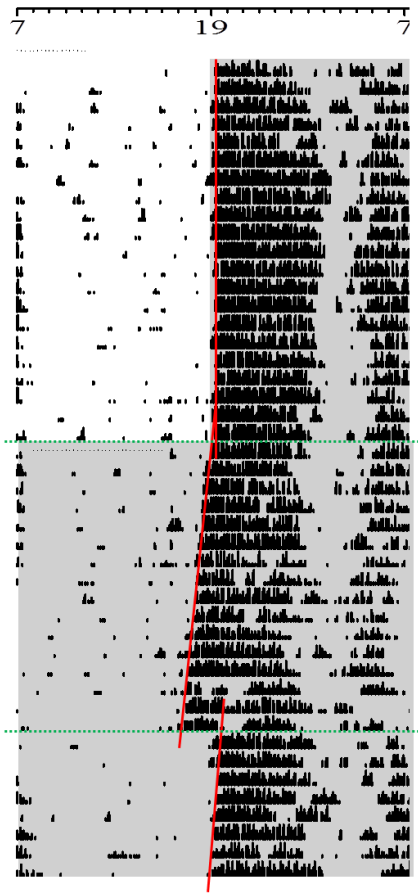

Phase angle of entrainment:
Distance from position of lights off to activity onset (mm converted to minutes, by convention onset after lights off is negative, onset prior to lights off is positive)

Tau:
24 hours - gradient of linear regression line (mm/day converted to hours/day)

Phase shift:
Distance between linear regression lines plotted through activity onsets prior to pulse and 3 days after pulse (extrapolated back to day of pulse, mm converted to minutes)

Tau values are calculated according to the following equations:

Where Tau is less than 24 hours (typically in DD)

Tau = gradient of linear regression line (hours/day) - 24

Where Tau is greater than 24 hours (typically in LL)

Tau = gradient of linear regression line (hours/day) + 24

V. Chi-square amplitude analysis

Chi-square periodogram analysis provides a measure of the stationarity of a time series through comparison of between-class and within-class variables by analysis of daily variance in mean levels and daily variance of variances. When applied to circadian rhythms it reflects the variance in period, mean and amplitude compared to a perfectly rhythmic series (Refinetti, 2004). Thus this analysis is a measure of robustness of the circadian rhythm.

Chi-square amplitude was performed by chronobiology kit software (Stanford Software Systems USA) on wheel-running locomotor activity data collected in 6-minute time bins over 10 days with no interventions.

Analysis of chi- square amplitude is derived from the formula for chi square periodogram, Q_P, by:

$$Q_P = KN \sum^{P}_{h=1} (M_h - M)^2 / \sum^{N}_{i=1} (X_i - M)^2$$

Where a data set has N values (X_i for i = 1 to N) which is broken down into K blocks ('days') of Period, P. M_h is the mean of K values for each unit of period length ($\sum X_i/K$, M is the mean of all N values($\sum X_i/N$) (Sokolove and Bushell, 1978).

The stronger the rhythmicity of a data set, the higher the value of Q_P. If it were possible to have a completely stationary time series, Q_P would be maximal (Refinetti, 2004).